UNIVERSITY OF SOUTHAMPTON

PORIN IN ITS' LIPID ENVIRONMENT

By

Aisling O' Keeffe

A thesis presented for the degree of
Doctor of Philosophy

Division of Biochemistry & Molecular Biology
School of Biological Sciences
U.K.

December 2000

UNIVERSITY OF SOUTHAMPTON

ABSTRACT

FACULTY OF SCIENCE
DIVISION OF BIOCHEMISTRY AND MOLECULAR BIOLOGY
SCHOOL OF BIOLOGICAL SCENCES

Doctor of Philosophy

PORIN IN ITS' LIPID ENVIRONMENT

by Aisling O' Keeffe

Porins are a family of proteins found in the outer membranes of Gram negative bacteria. These proteins form water-filled transmembrane pores which allow the influx of nutrients into the bacterial cell. The pore structure is formed by a closed β-barrel giving a highly stable structure. Interactions of this group of β-barrel proteins with its surrounding lipid were investigated. A method for reconstituting the *Escherichia coli* OmpF porin into membrane fragments of defined lipid composition was developed and this method was used in fluorescence quenching experiments with brominated phospholipids to assess the degree of lipid binding selectivity of the porins. Preferential binding was observed with phosphatidylcholines possessing fatty acyl chains with a length of 14 carbons. This is in contrast to α-helical proteins, such as the Ca^{2+}-ATPase, which show little lipid binding selectivity because they are less rigid and can adapt to different bilayer thickness by tilting in the membrane. The fluorescence properties of the two tryptophan residues in OmpF were studied independently by using recombinant techniques to yield single tryptophan and tryptophan-less mutants. These provided information regarding the environment of the tryptophan residues. Quenching with spin-labelled fatty acids was also carried out to determine the accessibility of the interface-located tryptophan. Functional studies were also performed to determine the effects of hydrophobic mismatch on the permeability rates of sugars through OmpF, and it was seen that permeability rates of monosaccharide sugars through OmpF are highest in dioleoylphosphatidylcholine.

ACKNOWLEDGEMENTS

I would like to take this opportunity to thank my supervisor Prof. Tony Lee for all his help throughout my project. Thanks also to Dr Jeremy Lakey and members of his group at the University of Newcastle for providing me with strains, plasmids and friendly advise. I am also grateful to Prof. Jurg Rosenbusch and Dr Gaby Rummel for providing me with their unpublished purification protocol. Within the department I'd like to thank Drs Malcolm East and David O' Connor for their help, Bob Broadbridge for opening his cache of glasswear and doing the mass spectrometry for me, and the secretaries Maureen and Bridget. Thanks to everyone in the AGL and JME groups for being such good fun to work with. I'd particularly like to thank Wendy, Sue, the lardy boys Ian and Sanjay, and of course Mel for endless banter. I'd also like to thank my old housemates Suzie, John, Jo and Andrew, some of whose love of football could only inspire me to go to my room and write-up.

Big thanks are extended to my family who've been very supportive and made sure my baked bean stocks were always ample. Lastly I'd like to thank Andy who's been a star throughout.

CONTENTS

CHAPTER 3: RECONSTITUTION OF OMPF

CHAPTER 4: CHARACTERISATION OF TRYPTOPHAN RESIDUES IN OMPF

CHAPTER 5: RELATIVE PHOSPHOLIPID BINDING AFFINITIES OF OMPF

REFERENCES

ABBREVIATIONS

Ca^{2+}–ATPAse	Ca^{2+} and Mg^{2+} activated ATPase
BCA	bichoninic acid
BSA	sovine serum albumin
cmc	Citical micellar concentration
$C_{12}E_8$	Dodecylpoly(ethyleneglycolether)$_8$
di(Br_2C18:0)PC	1,2-di(9,10-dibromostearoyl) phosphatidylcholine
di(Br_2C14:0)PC	1,2-di(9,10-dibromomyristoyl) phosphatidylcholine
di(Br_2C18:0)PE	1,2-di(9,10-dibromostearoyl) phosphatidylethanolamine
di(C12:0)PC	Dilaurylphosphatidylcholine
di(C14:1)PC	Dimyristoylphosphatidylcholine
di(C16:1)PC	Dipalmitoylphosphatidylcholine
di(C18:1)PC	Dioleoylphosphatidylcholine
di(C20:)PC	Dieicosenoylphosphatidylcholine
di(C22:1)PC	Dieurcylphosphatidylcholine
di(C24:1)PC	Dinervonylphosphatidylcholine
EDTA	Ethylenediamine tetraacetic acid
EGTA	Ethyleneglycol-bis(β-aminoethylether)-N,N,N',N'-tetraacetic acid
HEPES	N-(2-hydroxyethyl)piperazine-N'-(2-ethyanesulphonic acid)
kDa	kilo Daltons
LPS	Lipopolysaccharide
LUV	large unilamellar vesicles
MDO	Membrane-derived oligosaccharide
MLV	Multilamellar vesicles
OG	n-Octyl β-D-glucopyranoside
Omp	Outer membrane protein
PAGE	Polyacrylamide gel electrophoresis
PC	Phosphatidylcholine
PE	Phosphatadylethanolamine
PG	Phosphatidylglycerol

PIPES	Piperazine-N, N'-bis(2-ethanesulfonic acid)
POE	polyoxyethylene
SDS	Sodium dodecyl sulphate
SR	Sarcoplasmic reticulum
SUV	Small unilamellar vesicles
TLC	Thin-layer chromatography
Tris	Tris(hydroxymethyl)aminomethane
Triton X-100	Octylphenolpoly(ethyleneglycoether)$_8$

Standard one and three letter amino acid abbreviations were used throughout.

Standard element abbreviations were used throughout.

CHAPTER 1
GENERAL INTRODUCTION

1.1 Overview

Biological membranes provide cells with highly selective permeability barriers that allow the composition of the intracellular medium to be regulated. Membranes are approximately 60 Å thick and consist primarily of lipid and protein, with some carbohydrate. The structure of membrane is summarised in the 'fluid-mosaic' model of Singer and Nicholson (1972), which describes a fluid, polar lipid bilayer in which integral membrane proteins are embedded (Singer & Nicholson, 1972). The precise composition of membranes varies among species, cell types and organelles and can alter in response to environmental influences.

1.2 Membrane Lipids

Membrane lipids are an extraordinarily diverse group of molecules. This diversity suggests that membrane lipids do more than simply provide a permeability barrier. The lipid composition of a membrane affects a number of its physical properties including the fluidity, the hydrophobic thickness, the polarity, the membrane charge and the curvature of the membrane (Epand, 1998). The roles of membrane lipids can include:

1) providing second messengers for signal cascade pathways, e.g., inositol triphosphate from phosphatidyl inositols, and arachidonic acid (Lambeth & Ryu, 1996; Johnson & Cornell, 1999).
2) forming lipid 'rafts', which are involved in targeting of membrane proteins (Simons & Ilkonen, 1997)

Pages 2 - 4
are
missing from
the volume

Lipid molecules have a tendency to self-associate in aqueous media because of the energetic cost of exposing the hydrocarbon tails to water. The structure of the molecular assembly will depend on physical properties of the lipid. Biological membranes are organised as a lamellar lipid bilayer but a significant fraction of the lipid that makes up biological membranes can also form non-lamellar lipid structures.

The ability of lipids to form lamellar phases is dependent on the ratio of the cross-sectional areas of the head group and fatty acyl chain (Epand, 1998). A phospholipid whose headgroup area matches that of the two fatty acyl chains assumes an overall cylindrical shape, which will readily pack into a lamellar or bilayer phase, an example being phosphatidylcholine. Bilayer formation is a spontaneous process driven by the requirement to shield the hydrophobic fatty acyl chains from the aqueous phase (Van Voorst & de Kruijff, 2000). Van der Waals attractive forces between the hydrocarbon tails, and electrostatic and hydrogen bonding attractions between the polar head groups and water stabilise the bilayer structure.

Lipids with a smaller headgroup than acyl chain area adopt a conical shape, which would introduce curvature stress into a bilayer (de Kruijff, 1987). These lipids (see Figure 1.5) instead adopt a curved non-lamellar phase. Where the head group area is smaller than the tail area, as is the case with phosphatidylethanolamine, an inverted hexagonal (H_{II}) phase will be adopted (Lee, 1983). This phase is characterised by a cylindrical arrangement of lipids, the core consisting of the lipid head groups surrounding an aqueous interior (de Kruijff, 1987). Non-bilayer phases are also adopted by those lipids, which have a larger headgroup than acyl chain area. The shape adopted by such lipids is normal, hexagonal (H_I), however, with the lipid head groups exposed rather than buried in the interior as with the inverted hexagonal lipids. The surface area occupied by lipids will also be influenced by the head group charge because charge repulsion between lipid head groups will increase the effective surface area of the head group. Phosphatidic acid, for example, has a small head group, which carries a negative charge. The overall shape therefore, adopted by this lipid is cylindrical. Some lipids

also adopt cubic lipid phases. These phases are complex three-dimensional assemblies that can be continuous or non-continuous with the polar and non-polar components.

Within a biological membrane, lipids are stabilised in a lamellar state. Those lipids, which favour non-bilayer phases, can be stabilised in a bilayer by those lipids, which readily form bilayers (Cullis *et al.*, 1996). Non-bilayer forming lipids are proposed to exert a strong effect on the lateral pressure of a bilayer, which could influence membrane protein assembly and functioning (Booth *et al.*, 1997; Booth & Curran, 1999). The lateral pressure across a membrane bilayer could, for example, have a strong effect on membrane proteins whose functioning requires conformational changes (Van Voorst & de Kruijff, 2000).

An important feature of biological membranes is their fluidity, which supports the lateral mobility of the membrane components (Lee, 1983). The gel-to-liquid crystalline phase transition changes the membrane from a highly ordered, low temperature solid (gel) phase to a high temperature liquid crystalline (fluid) phase. Lipids in the gel state will only be found in the lamellar phase, where interactions between the fatty acyl chains are maximised (Cullis *et al.*, 1996). Lipids in a fluid state have considerable rotation about C-C bonds and fast lateral diffusion in the membrane. A number of factors can influence the membrane fluidity. Nearly all naturally occurring double bonds in fatty acids are of the cis-conformation. This produces a kink in the molecule that disrupts the ordered packing of chains in the bilayer. The greater the degree of unsaturation the lower the transition temperature (T_m) of a phospholipid. Conversely the longer the fatty acyl chains the higher the T_m. The fluidity of membranes can be altered by organisms in response to environmental conditions. In prokaryotes the fluidity can be altered by varying the number of double bonds and the length of the fatty acyl chains (Cronan, 1978). Eukaryotes, in addition, can vary the content of cholesterol, which is a key regulator of membrane fluidity (Stubbs, 1983; Lee, 1983). The hydroxyl group of cholesterol forms hydrogen bonds with phospholipid head groups and the hydrocarbon tail resides in the membrane interior (see Figure 1.1 for the structure of cholesterol). At concentrations above the phase transition

cholesterol decreases the lipid order, which is a measure of the extent of motion of the lipid fatty acyl chain, but the order will be increased at concentrations below the phase transition.

1.3 Membrane Proteins

The protein content of membranes varies according to the cellular and organellar location. Myelin membranes, for example, can have as little as 18 % protein by weight because myelin simply has to act as an electrical insulator. A typical plasma membrane will contain 50 % protein, and the inner mitochondrial membrane can contain as much as 75 % protein by weight (Stryer, 1995).

Peripheral membrane proteins can be attached to membranes via a combination of some or all of the following, including electrostatic, hydrophobic and hydrogen bond interactions, as well as by calcium bridges (White & Wimley, 1998; Yau *et al.*, 1998; Johnson & Cornell, 1999; Buckland & Wilton, 2000). These interactions can be dissipated by altering the pH or salt concentration across the membrane. Integral membrane proteins, however, span the bilayer and removal therefore requires complete disruption of the membrane. Integral membrane proteins that are involved in the movement of molecules across membranes can be classified as either pumps or channels. Pumps are active transporters that require the input of energy to transport substances across the membrane. This energy can be provided in the form of ATP, light or as an electrochemical gradient. Examples of pumps include the Ca^{2+}-ATPase and bacteriorhodopsin. Channels are passive transporters that can exist in an open or closed state. The gating mechanism can be initiated upon ligand binding, as is the case of the nicotinic acetylcholine receptor, or when the voltage across the membrane exceeds a certain threshold (Stryer, 1995). An example of the later is the voltage-gated Na^{+} channel. Another example of channels is the family of porins found in the outer membrane of Gram-negative bacteria. A gating mechanism in porins has been observed

in reconstituted bilayer lipid membranes, but the *in vivo* relevance of this phenomenon is uncertain (Lakey *et al.*, 1985; Bainbridge *et al.*, 1998).

1.3.1 Structure of Membrane Proteins

1.3.1.1 Structure of α-helical Membrane Proteins

The hydrophobic core of biological membranes is approximately 30 Å thick (Lewis & Engelman, 1983). Proteins embedded in the membrane require a non-polar surface to make favourable interactions with this interior. Many transmembrane proteins have α-helical structures that consist of a transmembrane region of approximately 20 hydrophobic amino acid residues (Seshadri *et al.*, 1998). Examples where the high resolution structures are known include the Ca^{2+}-ATPase (Toyoshima *et al.*, 2000), bacteriorhodopsin (Luecke *et al.*, 1999), and the potassium channel, KcsA (Doyle *et al.*, 1998). The proteins of the outer membranes of Gram-negative bacteria have β-barrel structures (Jap & Walian, 1996), as do several bacterial toxins, such as α-hemolysin, produced by *Staphylococci* (Buchanan, 1999). The sequence patterns of these β-barrel proteins were initially puzzling, as all membrane proteins characterised to that date were α-helical, which are easily recognised as a long span of hydrophobic amino acid residues. The β-sheet, however, is a more extended conformation requiring only 11-14 amino acids to span the bilayer. Predictions of β-sheet sequences are more difficult as alternate residues face the membrane, but the internal residues may be hydrophobic or hydrophilic (Seshadri *et al.*, 1998).

Residues found in transmembrane α-helices are predominantly hydrophobic, the most common being Leu (Landolt-Marticorena *et al.*, 1993). Ile, Val and Thr are also frequently encountered. Some polar groups that are required in proteins such as transporters and ion channels will be shielded from direct contact with the lipid bilayer by the α-helices. The positional preferences of amino acid residues in transmembrane α-helices (Landolt-Marticorena *et al.*, 1993) are shown in Figure 1.6. An Ile-rich region followed by a Val-rich region can be seen at the N-terminus of the transmembrane

domain, which is located at the external face of the membrane (Landolt-Marticorena *et al.*, 1993). The boundary regions of the transmembranous region are predominantly filled by aromatic residues, which are thought to play a role in anchoring the protein in the membrane (Killian & von Heijne, 2000). Trp can be located at either end of the transmembrane domain but Tyr and Phe will be found only at the C-terminus of the transmembrane domain (Landolt-Marticorena *et al.*, 1993). Phe can also be found in the hydrophobic segments (Landolt-Marticorena *et al.*, 1993). Figure 1.7 shows the clustering of Trp residues at the interfacial regions in the potassium channel KcsA (Doyle *et al.*, 1998). Similar, although less well defined arrangements of aromatic residues are seen in the bacterial photosynthetic reaction centre (von Heijne, 1996) and the Ca^{2+}-ATPase (Toyoshima *et al.*, 2000), as shown in Figures 1.8 and 1.9, respectively. The C-terminus of the transmembrane α-helix is rich in Leu residues (Landolt-Marticorena *et al.*, 1993). The extramembrane regions can include polar residues like Arg and Lys at the C-terminus, and Asn, Ser, and Pro at the N-terminus. The presence of positively charged residues at the C-terminus is thought to be important for membrane insertion, and is referred to as the 'positive inside' rule (von Heijne, 1996).

The position of residues in the transmembranous regions of β-barrel proteins is less well defined, as there is only a strict requirement that the alternate residues that are lipid exposed are hydrophobic. Those residues on the inside of the β-barrel can therefore be hydrophobic or hydrophilic. There is a notable arrangement of aromatic residues at the interfacial region in all of the porin structures that have been resolved to a high resolution (Jap & Walian, 1996).

1.3.1.2 Structure of Members of the Porin Family

Proteins of the outer membrane of *E. coli* were initially identified using sodium dodecyl sulphate (SDS) – polyacrylamide electrophoresis (PAGE) (Lugtenberg *et al.*, 1975; Nakamura & Mizushima, 1976). These proteins include a class of

transmembrane pores called porins, which can be classified into general or specific diffusion pores (Jap & Walian, 1996). The former display low selectivity and allow the diffusion of nutrients up to a relative molecular mass of approximately 600 Da. The general porins of *E. coli* include OmpF and OmpC, which are weakly cation selective and are regulated by osmotic pressure and temperature, and PhoE, a phosphoporin that is weakly anion selective and derepressed under phosphate starvation. Approximately 60 % homology exists between the primary sequences of these three proteins (Todt *et al.*, 1992; Schulz, 1993; Nikaido, 1994; Jap & Walian, 1996). The specific group of porins, including the maltodextran porin, LamB found in *E. coli* (Schirmer *et al.*, 1995), and the sucrose porin, ScrY, found in Salmonella species (Forst *et al.*, 1998), provide specialised translocation pathways necessary for larger solutes, as passage through the general porins would be too slow. Many porins also serve as receptor sites for binding of phages and bacteriocins (Jap & Walian, 1996).

The amino acid composition of porins is more hydrophilic than water-soluble proteins and the porins contain no long consecutive stretches of hydrophobic residues (Schulz, 1993). Spectroscopic studies (Rosenbusch, 1974; Nakamura & Mizushima, 1976; Vogel & Jahnig, 1986) have revealed the structure to consist predominantly of β-sheet (65 +/- 8 %). In this type of structure the polypeptide chain is almost fully extended and is stabilised by H-bonds between –NH and –CO groups in different polypeptide chains to yield a β-sheet structure. β-strands can cross the thickness of a 30 Å thick bilayer in 11-12 residues (Eppens *et al.*, 1997).

High resolution crystal structures are available for several of the porins and have revealed the basic structural motif to be a closed β-barrel cylinder (36-45 kDa). Although there is a low homology between the primary sequences of the *E. coli* general porins (OmpC, OmpF and PhoE), and those of *Rhodobacter blastica* and *capsulatus* species and the specific porins ScrY and LamB, similar quaternary structures are evident from the high resolution structures (Weiss *et al.*, 1990; Weiss *et al.*, 1991; Weiss & Schulz, 1992; Cowan *et al.*, 1992; Forst *et al.*, 1993; Kreusch & Schulz, 1994; Schirmer *et al.*, 1995; Forst *et al.*, 1998).

The cylinder is composed of 16 β-strands in the general porins and 18 β-strands in the specific porins. The strands tilt at an angle of approximately 45 ° to the membrane plane (Jap & Walian, 1996). The functional unit is a homotrimer with three distinct pores, as can be seen for the OmpF trimer (Cowan *et al.*, 1992) shown in Figure 1.10. The loops (L1-L8 in OmpF) that connect adjacent β-sheets are longer on the extracellular face (5-44 residues) of the membrane than the loops (T1-T8 in OmpF) on the cytoplasmic face (2-5 residues) (Jap & Walian, 1996). In addition the lipid-exposed β-barrel wall is higher (approximately 38 Å) than the wall at the trimer interface (approximately 35 Å) to create a molecular 'awning' over the pore entrance. This can be seen in the crystal structure of the OmpF monomer (Cowan *et al.*, 1992) shown in Figure 1.11. The external loop 3, between β5 and β6, is particularly long in the general porins (34-43 residues) and folds into the pore to create a 'constriction zone', where the diameter of the pore is at its narrowest (Cowan *et al.*, 1992; Todt *et al.*, 1992; Nikaido, 1994; Jap & Walian, 1996). This region is thought to have a role in the ion selectivity and size exclusion limits of the pore (Bainbridge *et al.*, 1998).

The pore diameter of this constriction region in OmpF is approximately 7 x 11 Å (Cowan *et al.*, 1992). Figure 1.13 provides a schematic view of the important residues in this region. Mutation of residues, particularly charged residues, in the constriction zone can alter the ion selectivity and molecular weight cut-off of the pores (Harwood & Russel, 1984; Phale *et al.*, 1997; Bainbridge *et al.*, 1998). Deletions within loop 3 can also alter the pore diameter (Jeanteur *et al.*, 1994; Schmid *et al.*, 1998). A strong transverse electric field is created across the constriction zone by basic residues on the barrel wall (Lys16, Arg42, Arg82 and Arg132 in OmpF) and acidic residues (Asp113 and Glu117 in OmpF) and peptide carbonyl groups on loop 3 (Van Gelder *et al.*, 1997). The electrostatic forces that exist across this region force maximal extension of the side chains of the charged residues. This produces a rigid, well-defined pore that excludes larger solutes from the pore (Jap & Walian, 1996). The electrostatic potential of the constriction zone is amplified by the dielectric boundary between water in the pore and the low dielectric matrix of the β-pleated sheets of the barrel walls (Gutman *et al.*, 1992). Theoretical models to study the electrostatic properties of porins have shown

that the electrostatic field that exists takes on a screw-like form in the channel and shows increased amplitude in the constriction zone (Jap & Walian, 1996). Estimations of the electrostatic potentials of OmpF and PhoE have revealed differences at the constriction zone and extracellular mouth, with a potential of approximately zero for OmpF and a positive potential for PhoE (Karshikoff, 1994).

The constriction zone in the specific porins is created by three internal loops (Schirmer, 1998). High resolution structures of the ScrY sucrose porin from *S. typhimurium*, and the maltose porin LamB from E. coli show that the diameter of this region is only 8.5 x 11 Å in ScrY and is 7 x 10 Å in LamB (Forst *et al.*, 1998). The structure of the LamB porin is shown in Figure 1.12. In contrast to the general porins there is no obvious segregation of charge at this region in the specific porins (Schirmer *et al.*, 1995; Forst *et al.*, 1998). The two extra β-sheets that make up the β-barrel structure of the specific porins are instead thought to contribute towards additional features that provide solute selectivity. These additional features include a 'greasy slide' and 'ionic tracks'. The greasy slide is a left-handed helical arrangement of aromatic amino acid residues that extends along the pore lining, thereby providing a hydrophobic path for the glucosyl moieties of the sugar residues that pass through the pore (Schirmer *et al.*, 1995). Additionally ionic tracks are found either side of the greasy slide through the constriction zone, providing suitable hydrogen-bonding arrangements for the sugars. A low affinity binding site is thus provided at the pore entrance, which extends into the pore lining to orientate the solute on its passage through the pore. The wider pore diameter in ScrY is created by substitution of some of the larger constriction zone residues of LamB with smaller residues, thereby allowing transport of the relatively bulky sucrose molecule (Forst *et al.*, 1998).

In the general porins 12 strands of each barrel are in contact with the hydrocarbon chains of the bilayer and the remaining 4 strands are involved in interactions at the interface between monomeric units (Cowan *et al.*, 1992). The interface regions of the three subunits form a trimeric core, which consists of 270 residues in OmpF. The interactions at this interface are very strong and can only be

disrupted by heating the trimers to temperatures above 70 °C (Garavito & Rosenbusch, 1985). Intersubunit interactions are mainly hydrophobic and include numerous Phe side chains interdigitating with neighbouring subunits. Loop 2 (L2) contributes to trimer stability through hydrophilic interactions in the gap between L2* and L4* of a neighbouring monomer (where * denotes the loops of a neighbouring monomer). L2 forms H-bonds with residues from L2*, L3* and L4* and a strong salt bridge is made between a glutamyl residue on L2 and Arg residues on L3* (Karshikoff, 1994; Jap & Walian, 1996). Similarly tight intersubunit binding is seen in the specific porins (Schirmer *et al.*, 1995). Deletion of the highly conserved Phe in the C-terminus that has been found in all porins sequenced so far, decreases stability and deletion of the sixteenth strand abolishes trimer formation (Fourel *et al.*, 1994).

The nonpolar membrane-spanning region of porins (approximately 25 Å thick) is bordered by a ring of aromatic amino acids at each end, which mark the interface between the polar head groups and fatty acyl chains of the surrounding phospholipids (Cowan *et al.*, 1992). The C_β-C_γ bonds of the Phe side chains point towards the non-polar outer surface and those of Tyr and Trp point away. These residues are thought to play a role in anchoring the protein in the membrane and protecting the non-polar surfaces from interactions with the polar moiety of the membrane (Pattnaik *et al.*, 1997). Alternatively polarizable aromatic amino acids may be energetically favourable at interfaces between media of vastly different dielectric constant (Cowan *et al.*, 1992).

An enrichment of charged, mostly acidic residues is seen in the hydrophilic portions of the protein, where interactions with LPS are probably formed through divalent cation bridges (Nikaido, 1994). The rough periplasmic face of porin that is exposed to the external media is approximately 20 Å high and displays a less uniform distribution of charge than the smooth face. Residues conserved in this region include anionic side chains H-bonded to Tyr residues in the aromatic boundary and a cluster of carboxyl groups that may be involved in the cation bridges (Cowan *et al.*, 1992). The structural basis for the distinct pore characteristics of different general porins arise from

differences in the external loops at the rough face of the barrel where most insertions and deletions between OmpF and PhoE have been observed (Cowan *et al.*, 1992; Jap & Walian, 1996).

1.3.2 Function and Mechanism of the Porins

The general diffusion porins contain large, open, water-filled channels that nonspecifically mediate the passive penetration of ions and small hydrophilic nutrient molecules with a molecular mass up to 600 Da (Cowan *et al.*, 1992). Initial screening of solutes is performed at the mouth of the pore (Jap & Walian, 1996). A number of charged residues are found here, which can vary between porins that play an important role in the initial selection process. Mutation of Lys-64 found at the pore mouth in PhoE, for example, to a glutamic acid abolishes its preference for anions (Bauer *et al.*, 1989). After solute molecules enter the pore mouth they encounter a wider pore region before the ultimate size selection at the constriction zone is performed.

The high electric field that exists across the constriction zone makes entry of non-polar molecules energetically unfavourable, as entry into the pore requires the displacement of water molecules to minimise their potential energy (Schulz, 1993). The diffusion of polar molecules through the channel is proposed to be facilitated by orientation of solute dipoles within the screw-like electric field to avoid collisions with the barrel wall. Once the solute molecules have passed through the constriction zone they again encounter a wide region of the pore and can move relatively freely into the periplasmic space (Jap & Walian, 1996).

Maltoporin (LamB) facilitates the diffusion of maltodextrins across the outer membrane of *E. coli*. The passage of sucrose is impeded through LamB and is instead facilitated through ScrY in *Salmonella typhimurium*, which has a larger pore size (Forst *et al.*, 1993; Forst *et al.*, 1998). Passage of solutes through the specific porins begins with binding of the solute molecule to aromatic residues at the mouth of the pore

(Schirmer *et al.*, 1995). Subsequently formation of hydrogen bonds between the sugars and the ionic tracks occurs. Entry of sugars into the pore therefore also requires shedding of the hydration shell of solute molecules, as with the general porins (Schirmer *et al.*, 1995). In the absence of bound ligand the constriction zone is filled with tightly bound water molecules, which are displaced upon binding of solutes. Bound sugar residues can be visualised in the pores with their reducing ends facing the periplasmic space (Jap & Walian, 1998).

1.3.3 Voltage Gating

Voltage gating has been observed in several porins *in vitro*, where the opening/closing of channels occurs in response to changes in the transmembrane potential (Lakey *et al.*, 1985). Channel closure is symmetrical, i.e., it occurs in response to both positive and negative applied potentials. The mechanism of this closure has been studied in some detail because until recently, with the emergence of the high resolution crystal structure of the KcsA channel (Doyle *et al.*, 1998), porins were the only voltage-gated channels whose structure was known at a high resolution. The sensitivity of voltage gating can be altered by mutation of the Arg residues in the constriction zone (Lakey *et al.*, 1991; Saint *et al.*, 1996). The sensitivity is increased in the cationic porins OmpF and OmpC, but decreased in the anionic porin PhoE (Lakey *et al.*, 1991; Saint *et al.*, 1996; Van Gelder *et al.*, 1997). Substitution of negatively charged residues in PhoE, however, increased the sensitivity to voltage gating, which led to the proposal that the voltage sensors are positive residues in the anion-selective porins and are negative residues in the cation-selective porins (Van Gelder *et al.*, 1997). Mutagenesis studies that have tethered loop 3 to the barrel wall with disulphide bonds at the constriction zone in PhoE and OmpF have shown that gating is not due to any gross conformational change of loop 3 (Phale *et al.*, 1997; Eppens *et al.*, 1997; Bainbridge *et al.*, 1998).

The relevance of this voltage sensitivity *in vivo* has not been ascertained, as the potential, which exists across the outer membrane, is low due to the permeability of the outer membrane. This low membrane potential is known as the Donnan potential (30 mV) and is insufficient to cause channel closure (Klebba & Newton, 1998). This potential is largely due to the presence of negatively charged membrane-derived oligosaccharides (MDO's) in the periplasmic space. It has been postulated that a combination of factors such as pressure, pH and the presence of MDO's may lower the threshold that would make a voltage gating mechanism possible (Delcour *et al.*, 1992; Todt *et al.*, 1992; Le Dain *et al.*, 1996). An alternative proposal has been that voltage gating is important for those porins that are misrouted to the inner cytoplasmic membrane, where a sufficient membrane potential exists to cause channel closure (Eppens *et al.*, 1997).

1.3.4 Membrane Sorting and Regulation of Synthesis

All proteins targeted to bacterial outer membranes seem to have β-barrel structures. This includes the general and specific porins and additionally a group of proteins found in the outer membrane that are responsible for the active transport of iron and vitamins (Buchanan, 1999). All outer membrane proteins are synthesised in the cytoplasm as precursor proteins with an N-terminal extension (Eppens *et al.*, 1997). Signal sequences are typically 15-25 residues long and have one or more positive residues at the N-terminus, followed by a stretch of approximately 8-12 hydrophobic amino acids (Freudl *et al.*, 1988). This signal sequence is cleaved once the protein has been translocated, via the Sec machinery, across the inner membrane (Eppens *et al.*, 1997).

The precise mechanism of folding and insertion into the outer membrane has yet to be elucidated. Access to the outer membrane may be achieved via fusion sites between the inner and outer membranes or alternatively may involve passage through the periplasm where folding may occur prior to insertion (Cowan *et al.*, 1992). The

discovery of several periplasmic proteins that have potential roles in outer membrane protein folding has supported the notion that outer membrane proteins will pass through the periplasm before inserting into its target membrane (Bernstein, 2000). The amphipathic nature of the β-barrel structure may have been adapted for this pathway. Formation of the native state of outer membrane proteins in the outer membrane is believed to require LPS (Buchanan, 1999; Bernstein, 2000). Phosphatidylethanolamine is also postulated to play a chaperone role (Dowhan, 1998; Bogdanov & Dowhan, 2000; Van Voorst & de Kruijff, 2000).

Regulators tightly control the synthesis of porins in order that the permeability of the outer membrane can be altered by changing the number and type of porin species present (Jap & Walian, 1996). The diversity that is achieved amongst porins, by variations in the pore geometry, distribution of charged, polar and aromatic residues, and through the use of selective substrate binding sites, ensures that a wide range of permeabilities can be achieved. Environmental influences on the outer membrane permeability include osmolarity, ionic strength, and composition of the culture medium and temperature. EnvZ is an environmental sensor that phosphorylates the transcription factor, OmpR, to regulate the transcription of porin genes (Schulz, 1993). High osmolarity and high temperature for instance inhibit the expression of OmpF (Buehler *et al.*, 1991). These conditions that prevail in the environment of the intestine favours the production of the OmpC porin probably because it has a smaller pore diameter than OmpF, thereby limiting the entry of bile salts into the bacteria. Decreased OmpF expression also makes bacteria more resistant to antimicrobial compounds and to various antibiotics.

1.4 Fluorescence

1.4.1 Principles of Fluorescence Spectroscopy

The techniques of fluorescence spectroscopy were used in the studies reported in this thesis, to define the way that porins interact with a lipid bilayer.

Fluorescence is the emission of light when a molecule returns from an excited electronic state to the ground state and is best illustrated by the Jablonski diagram, as shown in Figure 1.14 (Lakowicz, 1983). Compounds containing conjugated double bonds absorb light of an appropriate wavelength to form the short-lived excited state of the molecule. Absorption occurs in less than 10^{-15} seconds and results in the excitation of an electron from the ground state (S_0) to a higher energy level (S_1, S_2, etc.). After absorption, energy can be lost very quickly by non-radiative processes (e.g., as heat) so that the energy of the excited molecules falls to the lowest vibrational energy of the excited state (S_1 V_0). Fluorescence is the emission of light that occurs on return from this excited state to the ground state. The lower energy of the emitted light relative to the absorbed light is seen as a shift to a longer wavelength, and is called the Stokes shift (Lakowicz, 1983). Because the relaxation to the lowest vibrational level of S_1 occurs so rapidly (i.e., in 10^{-12}seconds) emission spectra are generally independent of the excitation wavelength.

For Trp-containing proteins, fluorescence is dominated by the Trp residues (Lakowicz, 1983). In part this is because of the strong absorbance by the Trp residues and a relatively high quantum yield for Trp (typically about 0.2). In Trp-free proteins, Tyr fluorescence is observed; Tyr fluorescence is usually not seen in Trp-containing proteins because of efficient energy transfer between Tyr and Trp residues.

1.4.2 Fluorescence Quenching

The indole nucleus of Trp is extremely sensitive to solvent effects (Lakowicz, 1983). Fluorescence can therefore be used as a tool to investigate the environment surrounding these residues. Trp residues are particularly sensitive to quenching by a variety of substances. Fluorescence quenching is a process of deactivation of the excited state, which results in a diminishing of the fluorescence intensity. Quenching can occur by one of two processes:

1) by dynamic quenching which results from collisional encounters between the fluorophore and the quencher, or
2) by static quenching which is due to complex formation between the fluorophore and the quencher (Jones & Cossins, 1990).

The former is time-dependent and can be described by the Stern-Volmer equation (Lakowicz, 1983):

$$F_o/F = 1 + k_q\tau_0[Q] = 1 + K_D[Q] \qquad \text{Equation 1.1}$$

where F_o and F are the fluorescence intensities in the absence and presence of quencher, respectively, k_q is the bimolecular quenching constant, τ_0 is the lifetime of the fluorophore in the absence of quencher, [Q] is the concentration of quencher, and $K_D = k_q\tau_0$ is the Stern-Volmer quenching constant.

Dynamic quenching results in a decrease in the fluorescence lifetime of the fluorophore as it presents another process by which the excited state can be deactivated (Lakowicz, 1983). Static quenching follows from the formation of a non-fluorescent ground-state complex, which is immediately returned to the ground state upon absorption of light. Static quenching therefore removes the fluorescence contribution of those Trp residues that are accessible to the quencher, leaving only the fluorescence from those residues that cannot be complexed with quencher (Lakowicz, 1983; Jones & Cossins, 1990).

Examples of quenchers include halogens, spin labels, molecular oxygen, xenon and acrylamide (Lakowicz, 1983). Brominated lipids are efficient quenchers of Trp fluorescence and can be used to study membrane proteins (East & Lee, 1982; Webb *et al.*, 1998). Bromines can be introduced across the C-C double bonds of unsaturated fatty acyl chains to produce phospholipid species, which act essentially identically to the nonbrominated species (East & Lee, 1982). This is because the presence of bulky bromine groups on the fatty acyl chains have a similar effect on the phase transition

temperature as the presence of a cis double bond. Lateral exchange of phospholipids in a bilayer occurs at a rate of approximately 10^8 per second, which is slower than the fluorescence decay time of Trp residues, which occurs in the ns time scale (East & Lee, 1982). Quenching by phospholipids is thus considered a static process and can therefore be used to measure the relative affinities of membrane proteins for various phospholipids, that differ in fatty acyl chain length and alcohol head group (East & Lee, 1982; Webb *et al.*, 1998).

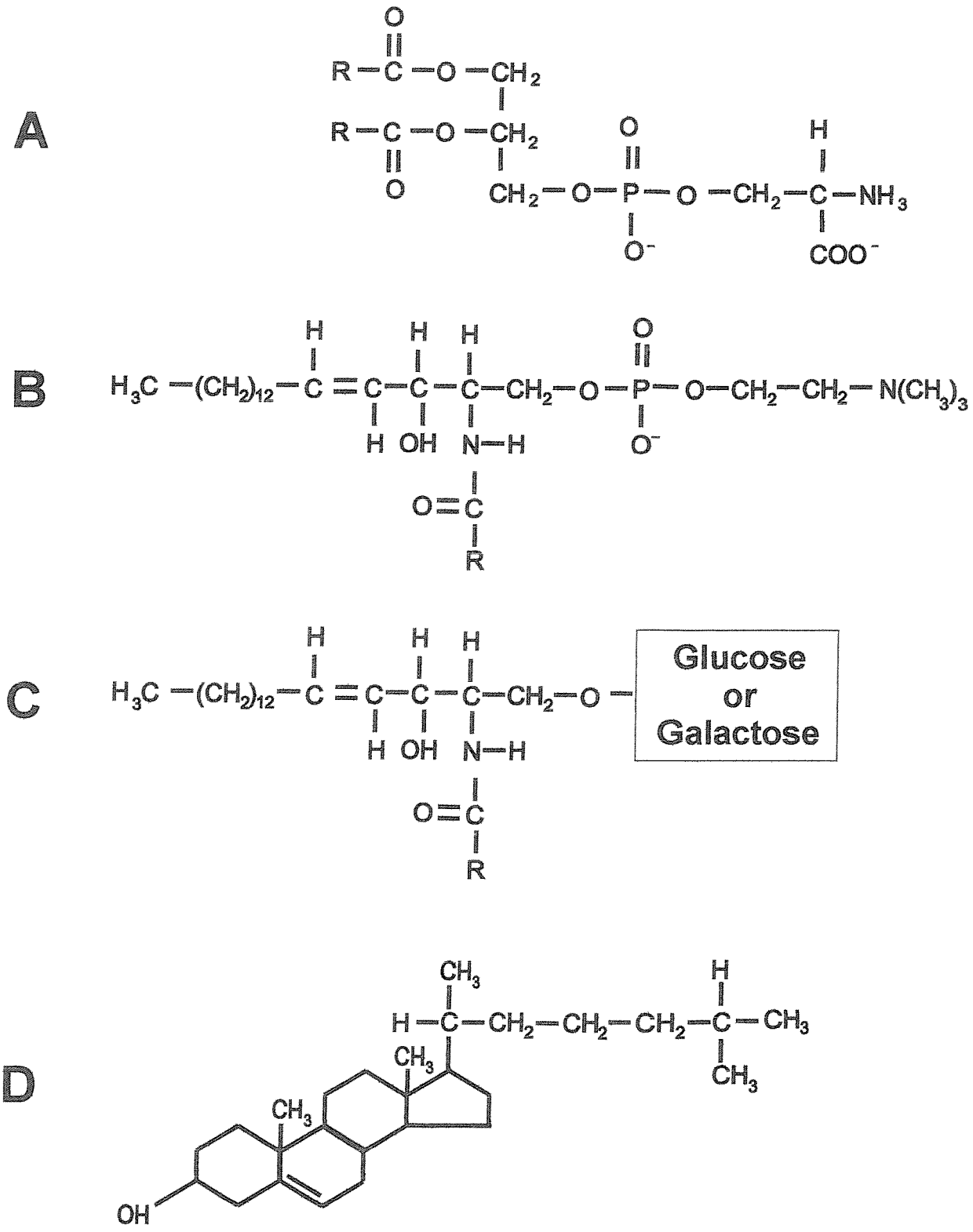

Figure 1.1: The structures of the different membrane lipid classes

A. Phosphatidylserine, B. sphingomyelin, C. cerebroside, and D. cholesterol (adapted from Stryer (1995)).

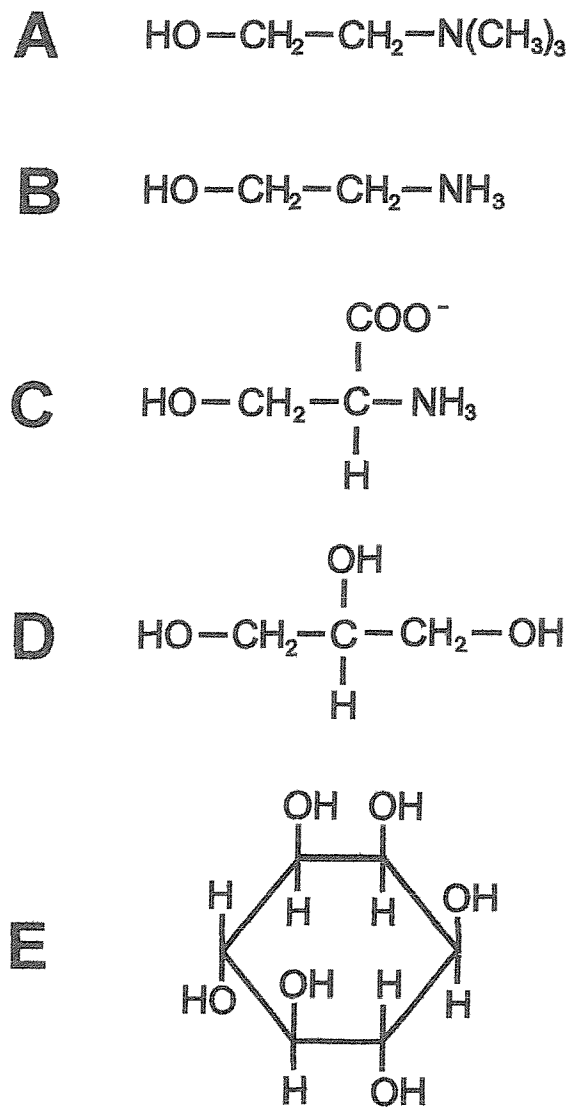

Figure 1.2: The structure of the head groups for different classes of phospholipids (adapted from (Cullis *et al.*, 1996)).

A: choline; B: ethanolamine; C: serine; D: glycerol; and E: myo-inositol.

Number of Carbon Atoms	Structure	Common Acid Name
	Saturated fatty acids	
12	$CH_3(CH_2)_{10}COOH$	Lauric
14	$CH_3(CH_2)_{12}COOH$	Myristic
16	$CH_3(CH_2)_{14}COOH$	Palmitic
18	$CH_3(CH_2)_{16}COOH$	Stearic
20	$CH_3(CH_2)_{18}COOH$	Arachidic
24	$CH_3(CH_2)_{22}COOH$	Lignoceric
	Unsaturated fatty acids	
16	$CH_3(CH_2)_5CH=CH(CH_2)_7COOH$	Palmitoleic
18	$CH_3(CH_2)_5CH=CH(CH_2)_7COOH$	Oleic
20	$CH_3(CH_2)_4CH=CHCH_2CH=CHCH_2CH=CH$ $CH_2CH=CH(CH_2)_5COOH$	Arachidonic

Figure 1.3: Structure of fatty acids commonly found in phospholipids (adapted from (Lehninger, 1982)).

Pages 24 - 26
are
missing from
the volume

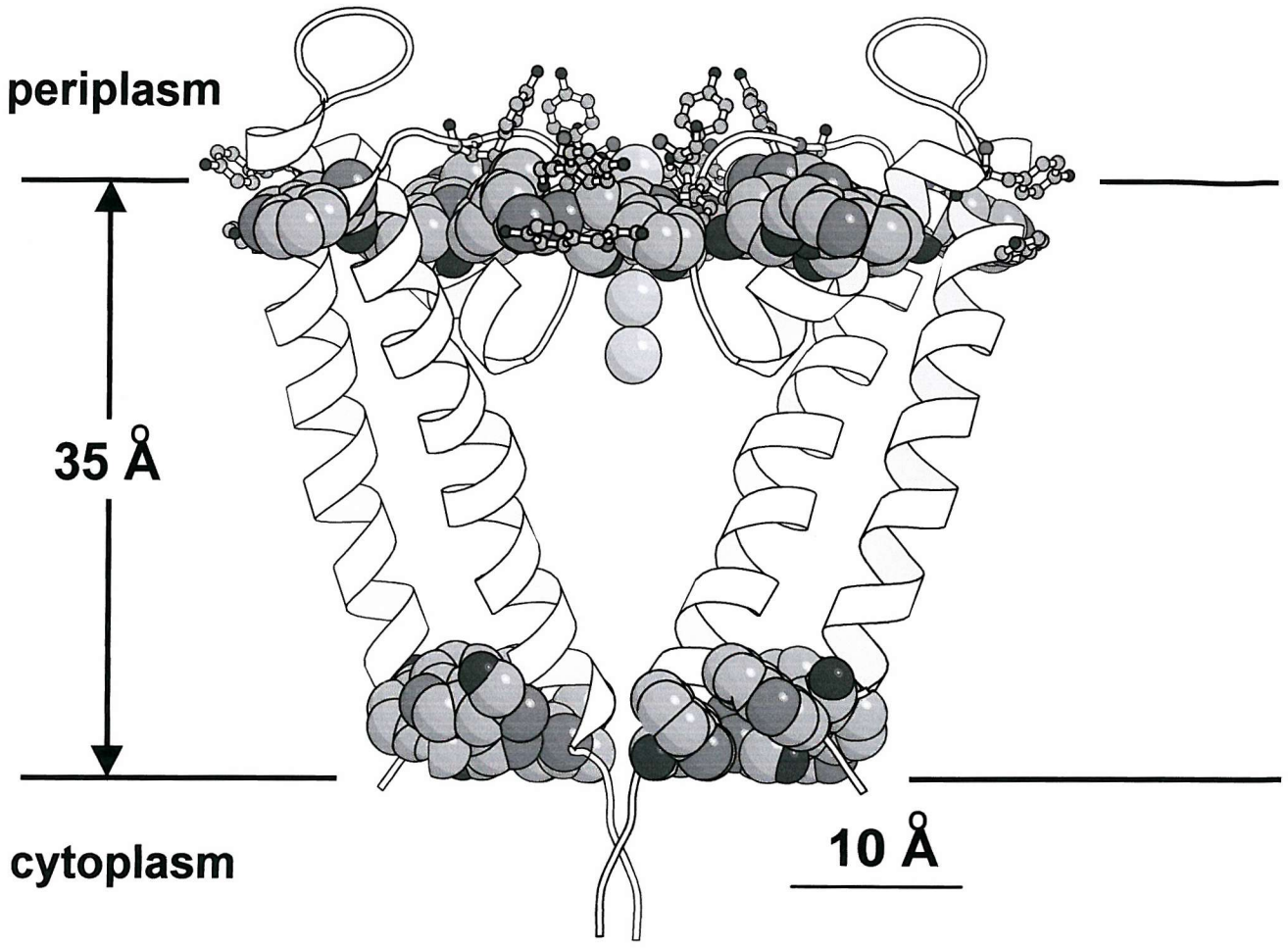

Figure 1.7: Crystal structure of the potassium channel, KcsA from *Streptomyces lividnas.*

Two of the four identical subunits are shown at a cross-sectional view, with Trp residues represented in space-fill and Tyr residues shown in ball-and-stick representation (PDB file 1b18).

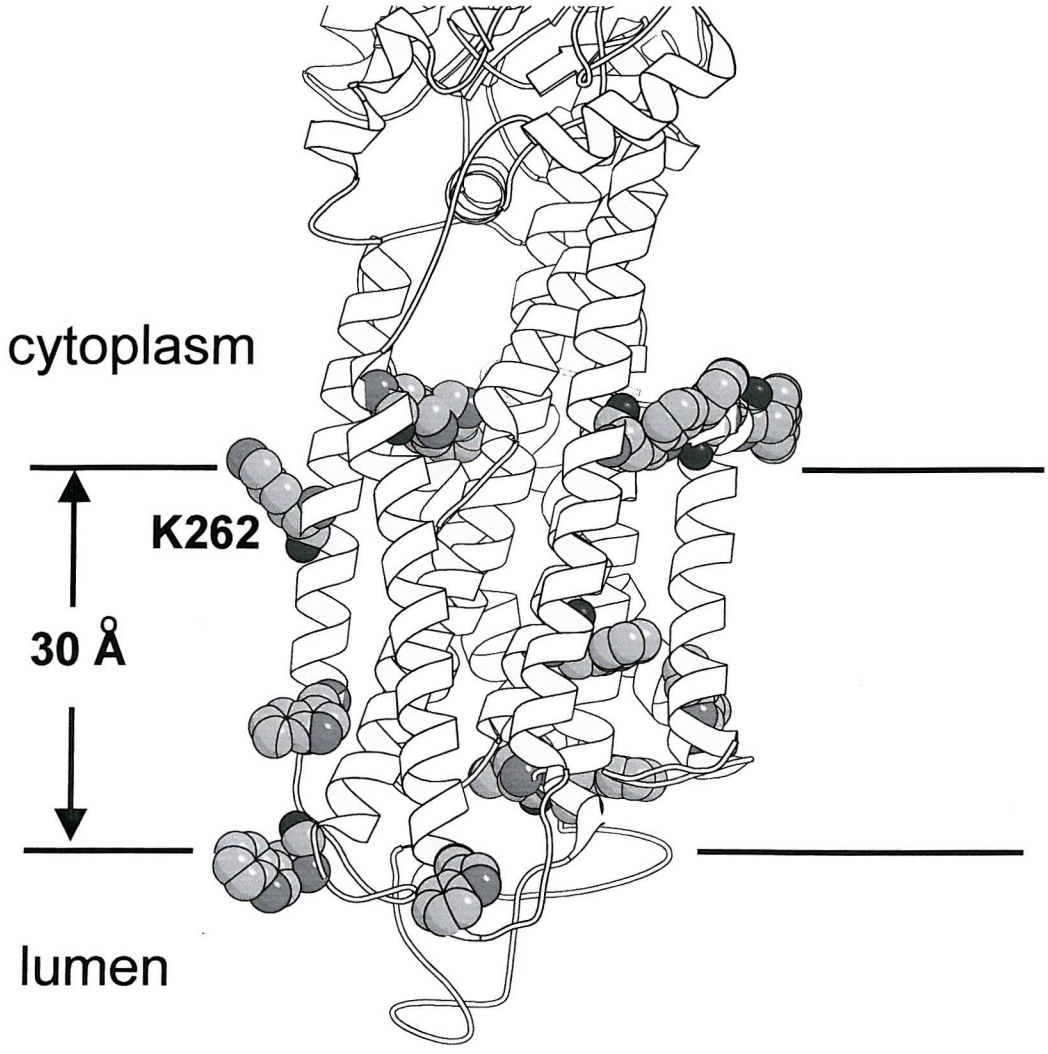

Figure 1.8: Crystal structure of the transmembrane region of the Ca^{2+}-ATPase of skeletal muscle SR.

The transmembranous region of the Ca^{2+}-ATPase has a ring of aromatic residues at the cytoplasmic interface of the membrane. The distribution of aromatics at the lumenal interface is less well-defined (PDB file1eul).

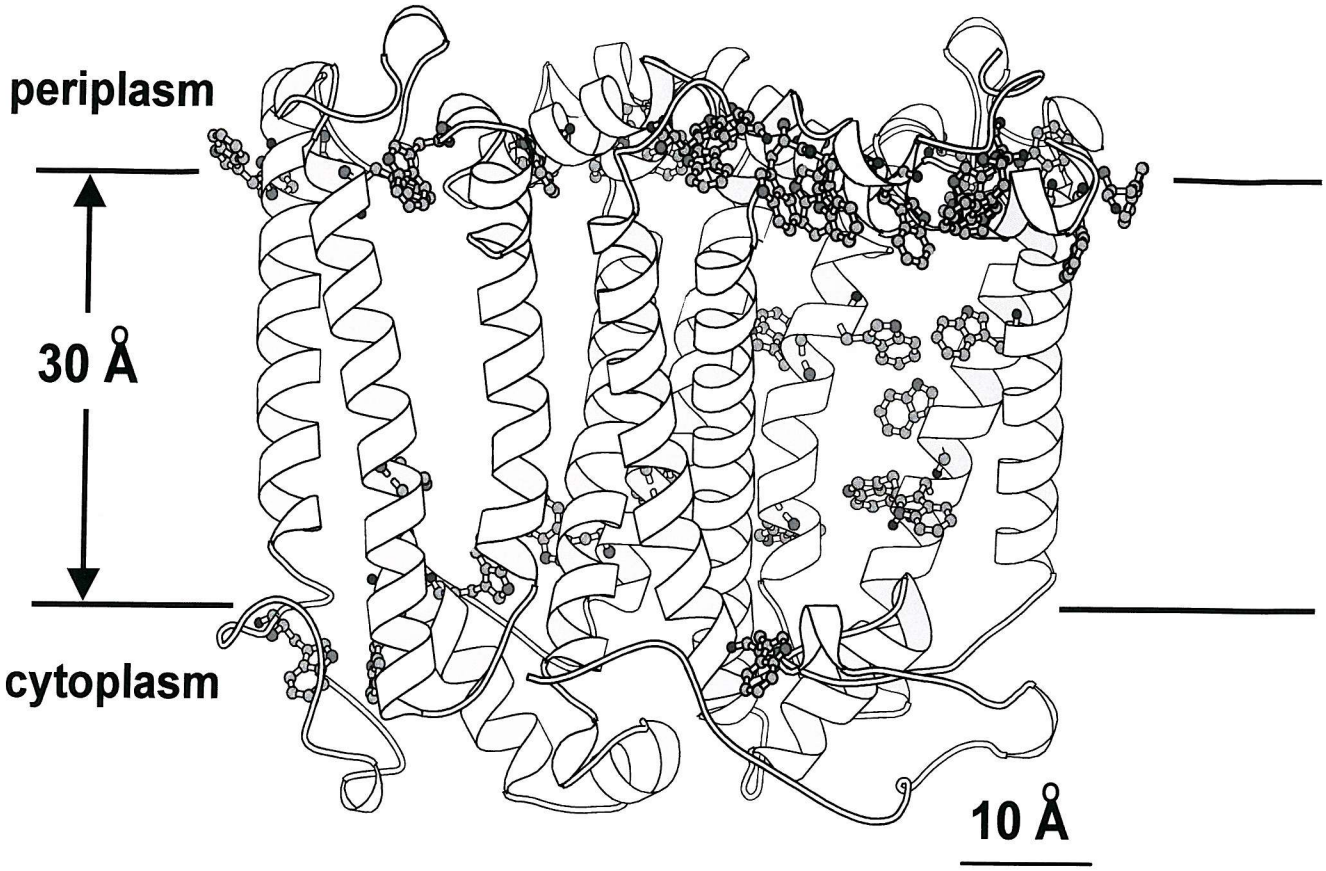

Figure 1.9: Crystal structure of the L and M subunits of the photosynthetic reaction centre of *Rhodobacter spaeroides.*

Trp residues are shown in ball-and-stick representation (PDB file Iaij).

Figure 1.10: The structure of the OmpF trimer.

Each monomer is shown in a different colour to highlight the interactions between monomers (PDB file 1OMPF).

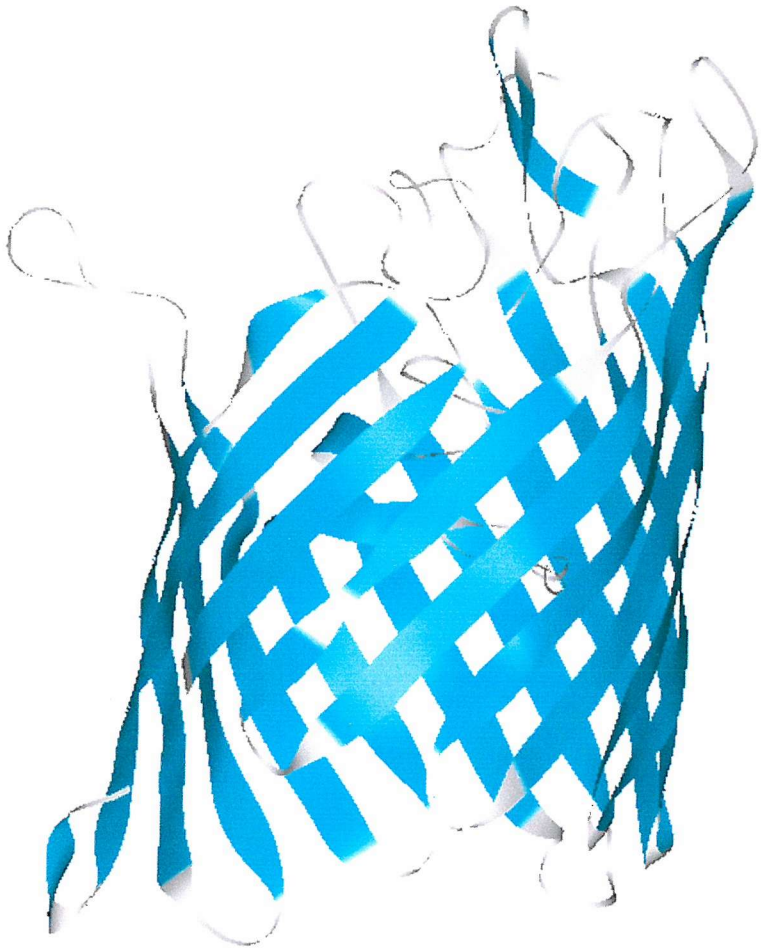

Figure 1.11: Sideview of the OmpF monomer.

The β-sheet structure is illustrated by the blue ribbon (adapted from PDB file 1OMPF).

Figure 1.12: Structure of the LamB porin from *E. coli*.

Each monomer of Lamb is shown in a different colour (adapted from PDB file 1AF6).

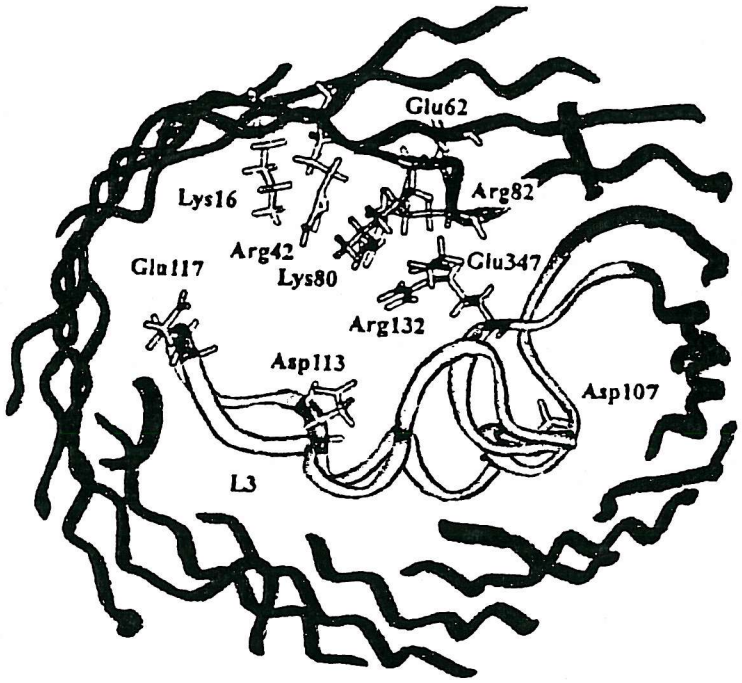

Figure 1.13: **View of the pore constriction in OmpF, illustrating the important residues (adapted from Nikaido, 1994).**

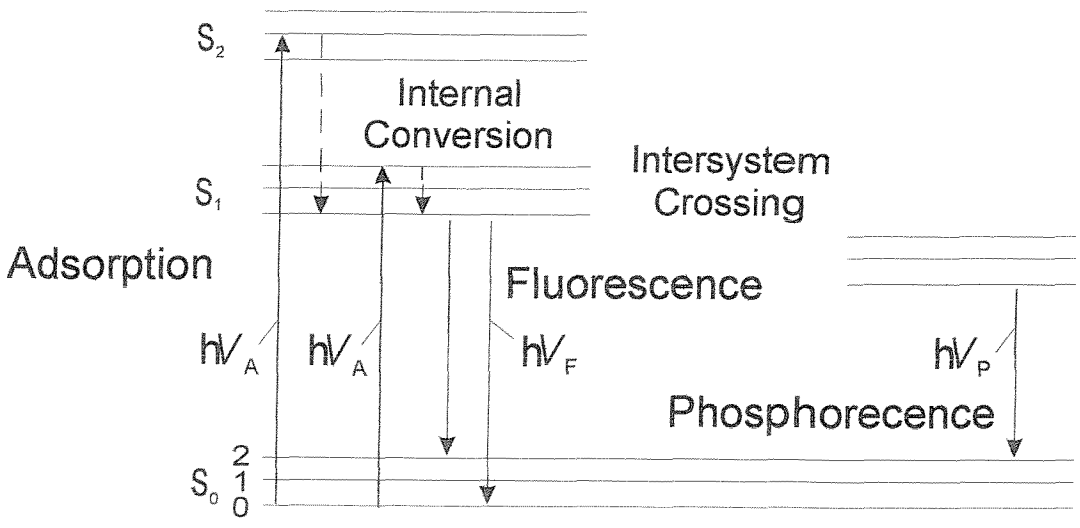

Figure 1.14: Jablonski diagram (Lakowicz, 1983).

S_o, S_1, and S_2 represent the ground, first and second electronic states respectively. The fluorophores can exist in a number of different vibrational levels (0, 1 , 2, etc.) at each of these electronic energy levels. Transitions between the various electronic levels are vertical.

CHAPTER 2
GENERAL MATERIALS AND METHODS

2.1 Materials

All chemicals were obtained from Sigma or BDH. Exceptions were:

Avanti Polar Lipids

1,2-dimyristoleoyl-sn-glycero-3-phosphatidylcholine (di(C14:1)PC)

1,2-dipalmitoleoyl-sn-glycero-3-phosphatidylcholine (di(C16:1)PC)

1,2-dioleoyl-sn-glycero-3- phosphatidylcholine (di(C18:1)PC)

1,2-dieicosenoyl-sn-glycero-3- phosphatidylcholine (di(C20:1)PC)

1,2-dierucoyl-sn-glycero-3- phosphatidylcholine (di(C22:1)PC)

1,2-dinervonyl-sn-glycero-3- phosphatidylcholine (di(C24:1)PC)

1,2-dioleoyl-sn-glycero-3-phosphatidylglycerol (di(C18:1)PG)

1,2-dioleoyl-sn-glycero-3-phosphatidyethanolamine (di(C18:1)PE)

Bachem

Octyl-polyoxyethylene (octyl-POE)

Difco

Bactotryptone

Bacto Yeast Extract

Bacto-agar

Pharmacia

Agarose (NA Grade)

Calbiochem

Hepes

Tris

Dodecylpoly(ethyleneglycolether)$_8$ ($C_{12}E_8$)

National Diagnostics

ProtoGel (30 % (w/v) acrylamide: 0.8 % (w/v) Bisacrylamide stock solution)

2.2 Methods

2.2.1 Microbiological Techniques

2.2.1.1 Sterilisation

Growth media, solutions, microfuge tubes and pipette tips were sterilised by autoclaving at 120 °C, 15 lbs.sq.inch for 20 minutes. Antibiotic stock solutions (ampicillin 100 mg/ml and kanamycin 10 mg/ml) were sterilised by filtration through sterile 0.22 μm Millipore filters.

2.2.1.2 Strains and Vectors Used

Escherichia coli strain BZB1107 was used for the preparation of biologically active OmpF. BZB1107 is an *E. coli* B^E strain (Bainbridge *et al.*, 1998). This strain only expresses the OmpF general porin, unlike other *E. coli* strains, which encode three different general porin proteins (Buehler *et al.*, 1991). A Tn5 insertion mutation knocks out the *ompF* gene, and provides the cells with kan resistance (Buehler *et al.*, 1991). The expression of the *ompF* gene was placed under the control of a *tac* operon in a pBR322-derived vector, pMS119 (Bainbridge *et al.*, 1998), which is shown in Figure 2.1(Prilipov *et al.*, 1998). The pMS119 vector containing the *ompF* gene insert is known as pGBF96 (Bainbridge *et al.*, 1998; Prilipov *et al.*, 1998). As this vector carries the *bla* gene that encodes the protein for ampicillin resistance, selection for pGBF96-containing cells can be performed on ampicillin-containing media.

Selection on kan-containing media was also performed to ensure that the cells did not revert to the wild type phenotype by eviction of the Tn5 transposon element. Expression of the specific porin, LamB, was inhibited by catabolite repression in a glucose-containing media (Bainbridge *et al.*, 1998). The cells and vector were a generous gift from Dr Lakey, Department of Biochemistry, University of Newcastle.

2.2.1.3 Media Used

Luria Broth Medium (LB)

10 g Bactotryptone

5 g Bacto Yeast Extract

10 g NaCl

The solution was made to a final volume of 1 l with distilled water and the pH was adjusted to 7.2 before autoclaving.

LB Agar

1.5 % Bacto-agar was added to 1 l of LB medium before being autoclaved. Growth media was left to cool to 50 °C before adding sterile antibiotics solutions. Final concentrations were 60 μg/ml of ampicillin and 10 μg/ml kan.

SOC Medium

20 g Bactotryptone

5 g Bacto Yeast Extract

0.5 g NaCl

Approximately 950 mls of analar water and 10 ml of 250 mM KCl solution was added. The pH was adjusted to 7.0 with NaOH and then made up to final volume of 1 l with distilled water before autoclaving. The media was left to cool to approximately 60 °C before adding 20 ml of 1 M sterile-filtered glucose.

2.2.2 DNA Techniques

2.2.2.1 Small-Scale Preparation of Plasmid DNA

10 ml of antibiotic-containing LB media were inoculated with single bacterial colonies, and grown for 12-16 hours at 37 °C. Plasmid DNA was prepared from these cultures using the Promega's modified Wizard™ Miniprep procedure as recommended by the manufacturer.

2.2.2.2 Restriction Enzyme Digest

All digests were performed in 20 µl or 50 µl volumes according to the manufacturer recommendations. The digest products were separated by agarose gel electrophoresis as described in Section 2.2.2.3 and visualised under UV light.

2.2.2.3 Agarose Gel Electrophoresis

50x TAE
Tris 242 g
glacial Acetic Acid 57.1 ml
Na EDTA 1.9 g
Distilled water was added to 1 l and the solution was diluted 1:50 to use.

Loading Buffer
3 ml glycerol
30 mg bromophenol blue
1 ml 10x TE buffer
Distilled water was added to 10 ml

Ethidium Bromide
100 mg ethidium bromide
Distilled water was added to 10 ml

1 % agarose (in 1X TAE) was melted to which 0.2 % ethidium bromide was added before pouring in a horizontal gel tank. 2 µl of a 1 kB ladder was separated in lanes beside the DNA samples that had been mixed 4:1 with sample buffer. Gels were run at 100 V for approximately 60 minutes in 1X TAE.

2.2.2.4 Preparation of Electrocompetent *E. coli* Cells

10 ml of antibiotic-containing LB cultures were grown for 12-16 hours at 37 °C and were used to inoculate 500 ml of LB-kanamycin. Cells were grown at 37 °C in an orbital shaker to an absorbance at 600 nm of between 0.5 and 1.0. Cells were harvested by centrifugation at 4,500 x g in a Sorvall RC3B at 4 °C and the cell pellet was resuspended in 500 ml of cold sterile distilled water. The cells were centrifuged as before and the pellet was resuspended in sterile 20-30 ml of 10 % glycerol and again centrifuged as before. The pellet was finally suspended in 2-3 ml of 10 % sterile glycerol and aliquoted into 60 µl fractions. These cells were snap-frozen in liquid nitrogen and stored at –70 °C.

2.2.2.5 Transformation of *E. coli* cells by Electroporation

50 µl of electrocompetent cells were mixed with 1 -10 ng of DNA in a sterile electroporation cuvettte, and left to stand on ice for 1 minute. Transformation was performed using a voltage of 2.5 kV. 1 ml of SOC medium was immediately added and the cells were then left to recover at 37 °C for 60 minutes. The transformed cells were aliquoted onto antibiotic-containing LB agar plates in the following volumes: 10 µl, 100 µl, and 1000 µl. The cells were spread on the plates using a sterile spreader and then incubated for 12-16 hours at 37 °C. The transformation efficiency was determined by counting the number of cells for each dilution.

2.2.3 Overexpression and Purification of OmpF from *E. coli*

2.2.3.1 Overexpression of OmpF in BZB1107 Cells

5 ml of antibiotic containing LB cultures were grown for 12-16 hours at 37 °C from single BZB1107 colonies, and were used to inoculate 500 ml of antibiotic containing LB, supplemented with 0.2 % glucose. The cells were grown to an absorbance at 600 nm of approximately 0.6 and then induced with 1 ml of 100 mg/ml isopropyl-β,D-thiogalactopyranoside (IPTG). Late exponential phase cells were harvested by centrifugation at 4,500 x g for 20 minutes at 4 °C in a Sorvall RC3B. The cell pellet was resuspended in 20 mM phosphate buffer, pH 7.3 before snap-freezing the cells with liquid nitrogen and storing at –70 °C.

2.2.3.2 Purification of OmpF

Cells were broken at 60 °C by homogenisation for 60 minutes in a glass Teflon homogeniser in 20 mM Tris-HCl, pH 7.2, 2 % SDS. The envelope fraction was extracted from this suspension by centrifugation at 100,000 x g for 45 minutes at 4 °C. The cell envelope pellet was washed in 20 mM NaH_2PO_4, pH 7.3 to remove any residual SDS. A pre-extraction was performed on the pellet by homogenising in 20 mM NaH_2PO_4, pH 7.3 containing 0.125 % octyl-POE at 37 °C for 60 minutes to remove the majority of contaminants. The peptidoglycan-associated proteins were isolated by centrifuging at 100,000 x g for 45 minutes at 4 °C. The porin was freed from the pellet by shaking at 37 ° C for 60 minutes in 20 mM NaH_2PO_4, pH 7.3 containing 3.0 % octyl-POE. This step allows solubilisation of the outer membrane proteins, which were isolated by centrifuging at 100,000 x g for 45 minutes at 25 °C. The supernatant containing the purified porin was dialysed for 2 x12 hours against 20 mM NaH_2PO_4 containing 1 % octyl-POE, pH 7.3, and then aliquoted and stored at –20 °C. The dialysis tubing used had a molecular weight cut-off of between 12,000 and 14,000.

2.2.2.3 Determination of the Protein Concentration by the Bichoninic Acid Assay

This method was performed as described (Smith *et al.*, 1985) using bovine serum albumin protein standards (0.1-1.0 mg/ml). 10 µl of each sample was mixed with 200 µl of bichoninic acid (BCA) reagent in a microtitre plate and left at 37 °C for 30 minutes. A purple complex is formed with protein, which has an absorbance maximum of 562 nm. The concentration of protein was read using a Dynatech MR5000 micro-ELISA auto reader.

2.2.2.4 SDS-PAGE

Resolving Gel	3.3ml acrylamide
	1.7 ml 1.5 M Tris-HCl, pH 8.8
	0.1 ml 10 % SDS
	3.6 ml analar water
	0.3 ml 10 % ammonium persulphate (APS)
	5 µl TEMED
Stacking Gel	0.65 ml acrylamide
	1.25 ml 0.5 M Tris-HCl, pH 6.8
	0.1 ml 10 % SDS
	2.85 ml distilled water
	0.15 ml 10 % APS
	5 µl TEMED
Coomassie Blue	0.5 g Coomassie blue
	800 ml methanol
	140 ml acetic acid
	distilled water was added to 2 l.

Destain Solution	400 ml methanol
	70 ml acetic acid
Sample Buffer	2.5 ml 0.5 M Tris-HCl, pH 6.8
	4 ml 10 % SDS
	2ml glycerol
	0.2 mg bromophenol blue

Separation of the protein products of the porin purification was performed according to the method of (Laemmli, 1970) using 12 % polyacrylamide separating gels. Gels were cast and run on a BioRad mini-gel system. Samples (5-15 μg) were denatured by boiling for several minutes in sample buffer. Nondenatured samples were prepared in the same way but without the heat treatment. Electrophoresis was carried out at a constant current of 20 mAmps and bromophenol blue was used as a dye front marker. The gels were stained using coomassie blue and destained in a destain solution until the protein bands were clearly visible.

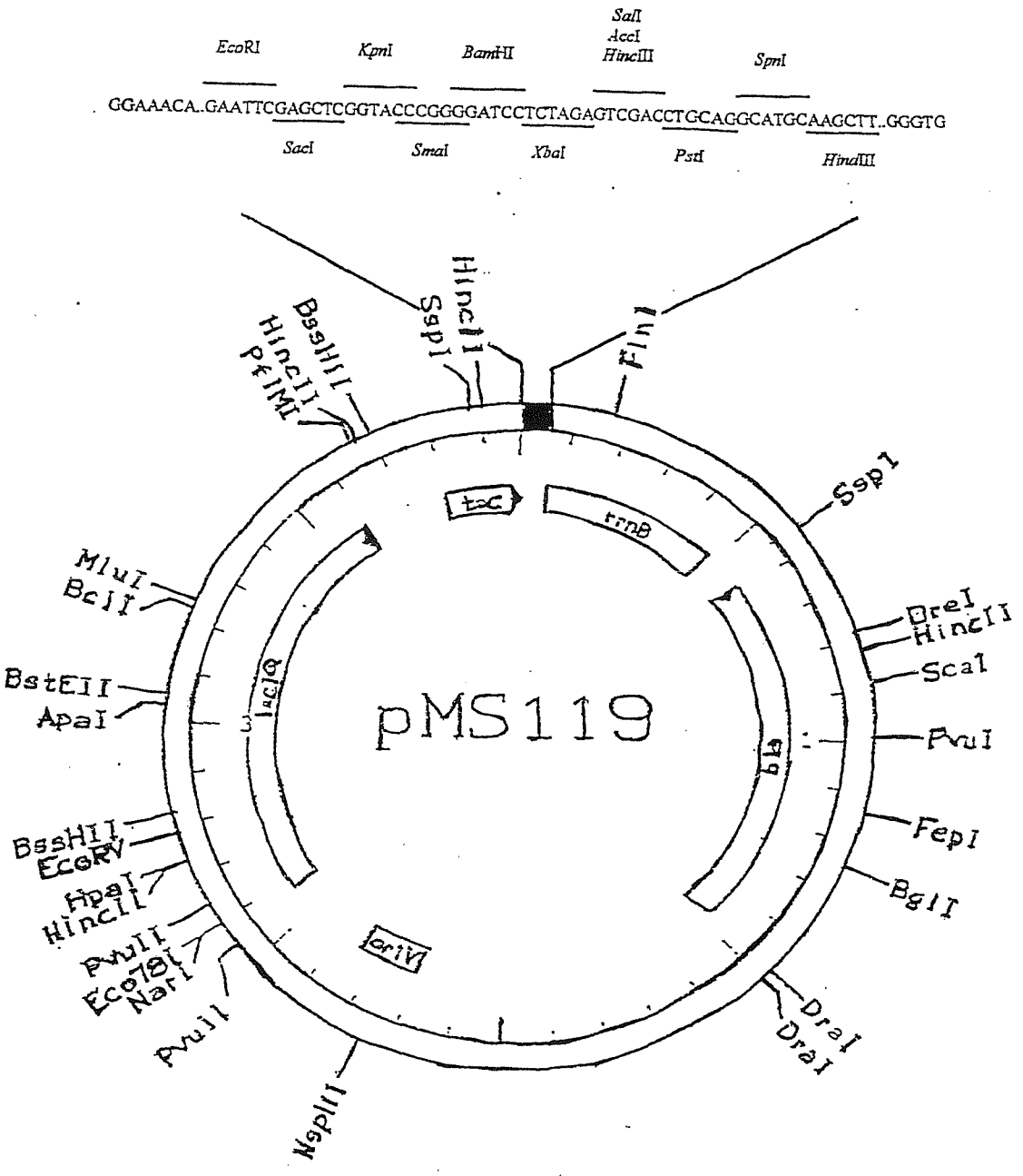

Figure 2.1: Diagram illustrating the features of the expression vector pGBF96.

The *ompF* gene was cloned into the vector as an *Eco*RI-*Hind*III fragment, behind the *tac* promoter. pGBF96 can be selected for on ampicillin-containing media, as it contains the bla gene that encodes a protein for ampicillin resistance.

CHAPTER 3
RECONSTITUTION OF OMPF

3.1 INTRODUCTION

The composition of biological membranes is complex which makes functional and structural studies of individual membrane components difficult. The task is simplified, however, if the components to be studied can be isolated and reconstituted into model membrane systems. Such models have improved our knowledge of many membrane-associated functions including energy transduction, transport of nutrients and transmission of external signals. Several techniques have been developed for producing model membranes involving the use of organic solvents, mechanical means and detergents (Rigaud *et al.*, 1995). Prolonged exposure of membrane proteins to organic solvents and long sonication times can lead to denaturation in many cases, making detergent-mediated reconstitution the most common method employed to reconstitute membrane proteins.

3.1.1 Detergents

Successful detergent-mediated reconstitution requires solubilisation of the membrane protein and lipid components under study without irreversible loss of protein activity and reassembly of the solubilised components to form a reconstituted functioning system after removal of the detergent (Silvius, 1992). Detergents are amphipathic, having both a hydrophilic and hydrophobic region. The hydrophobic groups are generally hydrocarbon and have poor solubility in water. The hydrophilic group may be charged or uncharged, but polar (Lichtenberg *et al.*, 1983). Detergents are frequently classified on the basis of the charge and/or the nature of the polar and hydrophobic portions (Moller *et al.*, 1986; Yanagita & Kagawa, 1986). These groups are summarised below, and some examples are shown in Figure 3.1.

1) the nonionic detergents that consist of a nonpolar hydrocarbon chain and a polar headgroup. The head group can consist of a sugar residue (e.g., glucose in n-octyl β-D-glucopyranoside (OG) and maltose in dodecyl maltoside (DM)), or alternatively can be derived from polyoxyethylene glycol. The structure of polyoxyethylene glycol-based detergents is represented as C_xE_y, where C refers to an alkyl chain with x number of C atoms, and y refers to the average number of polyoxyethylene glycol units (E).
2) the ionic detergents that consist of a nonpolar hydrocarbon chain and a charged headgroup region. Some examples include the anionic detergent SDS that is highly denaturing and 3-[(3-chloramidopropyl)dimethylammonio]-1-propane-sulfonate (CHAPSO), a zwitterionic detergent.
3) the bile salts or steroid-based detergents which are relatively rigid (Yanagita & Kagawa, 1986). The hydrophobic and polar regions in the bile salts are not as clearly discernible as the other detergent classes.

A number of parameters are used to describe the physicochemical properties of each detergent. In the aqueous phase detergent monomers will associate to form micelles, in which the hydrophobic portions of the detergents are shielded from the environment and the hydrophilic moieties are exposed (Helenius & Simons, 1975). This micellar state is energetically more favourable due to the low solubility of the hydrophobic portions in water. There is an equilibrium between the detergent molecules in the aqueous and micellar phases, the position of which is indicated by a parameter called the critical micellar concentration (cmc). The cmc of a detergent is the minimum concentration of detergent at which micelles are formed. The aggregation number reveals the number of monomers of a particular detergent that come together to form a micelle. The hydrophilic-lipophilic balance compares the partitioning of the detergent between the aqueous and lipidic phases, where the more hydrophobic detergents have a greater tendency to form micelles (Helenius & Simons, 1975). These detergents will

become incorporated into the micelle more readily and will therefore have low cmc values.

The ionic detergents generally have high cmc values and form relatively small micelles, but can denature proteins at concentrations below their cmc (Moller *et al.*, 1986; Yanagita & Kagawa, 1986). In contrast the nonionic detergents are usually mild but can have low cmc values. The bile salts have high cmc values but are pH-sensitive and will precipitate at values less than pH 7.0.

3.1.2 Solubilisation

The solubilisation of membrane components by detergents is frequently described by a three-stage model (Rigaud *et al.*, 1995). Upon addition of a detergent to a membrane suspension the detergent monomers will become incorporated into the lipid bilayer or will remain in solution (Helenius & Simons, 1975; Rigaud *et al.*, 1995). Although the lipid bilayer structure remains, at the sub-solubilising detergent concentrations in stage I, structural changes are evident from the observed increase in membrane permeability (Rigaud *et al.*, 1995; Paternostre *et al.*, 1988). When the lipid bilayer becomes saturated with detergent and the concentration of detergent in solution approaches the cmc the bilayer structure becomes unstable. In stage II the transition from the bilayer to the micellar phase occurs. Mixed micelles of detergent-lipid and detergent-protein-lipid will gradually form (Moller *et al.*, 1986; Yanagita & Kagawa, 1986). In the final stage of solubilisation an isotropic solution of detergent-lipid and detergent-protein-lipid micelles will exist. These detergent mixed micelles will be in equilibrium with the detergent monomer at concentrations equal to the cmc.

To develop a detergent-mediated reconstitution procedure for a particular membrane protein the first step is to find a detergent that will dissolve the protein of interest. This can be tested by measuring the turbidity of the protein suspension as a function of detergent concentration. The addition of detergent to a membrane

suspension results in the formation of small micelles that scatter light to a far lesser extent than the original suspension. Thus it is possible to measure the extent of solubilisation of a membrane suspension by a detergent and hence gain an indication of the effectiveness of that detergent under a particular set of conditions (Hirata, 1986).

3.1.3 Reconstitution

Detergent micelles can mimic the lipid bilayer and provide an environment that is suitable for the hydrophobic portions of membrane proteins and lipids. Upon reduction of the detergent concentration bilayer fragments or vesicles will form spontaneously by a mechanism that is the mirror image of the solubilisation process (Rigaud *et al.*, 1995). As the concentration of detergent decreases the number of detergent molecules in the mixed micelles are reduced such that micelle-micelle interactions become energetically favourable. As the concentration of detergent is further decreased transformation from the micellar phase will occur and lipid bilayers will reform to minimize exposure of hydrophobic regions to the aqueous milieu.

The ease with which a detergent can be removed from a solution is dictated by the cmc. A high cmc indicates the position of equilibrium of detergent monomers is shifted towards the bulk aqueous phase. Several options exist for those detergents with a high cmc - dilution or dialysis or removal by gel-filtration (Silvius, 1992). The detergent concentration will be reduced to a value below its cmc so that the detergent will no longer exist as micelles but as monomers in aqueous solution. There are, however, fewer choices for those detergents with low cmc values. They may be exchanged by dialysis for a detergent with a high cmc which can subsequently be removed by one of the methods mentioned above or alternatively detergents with a low cmc can be removed with detergent absorbing beads, such as Biobeads-SM2 or Amberlite (Silvius, 1992; Rigaud *et al.*, 1995). These polystyrene beads will effectively reduce the detergent concentration without absorbing the lipid or protein. The beads are

believed to adsorb both the monomer and micellar form of the detergent. Adsorption is also efficient for those detergents with a high cmc (Rigaud *et al.*, 1995).

Once a suitable detergent is found the next factor to be examined is the mixing of the protein and lipid in solution. One method employed to characterise reconstituted systems is to apply the sample to a sucrose density gradient. This technique allows separation of macromolecules on the basis of density. Lipid being less dense will float on top of the gradient, whereas protein will be found in the lower, denser layers. Reconstituted protein-lipid complexes will, however, be found at an intermediate density, and so if the lipid and protein components of a reconstitution are mixing properly they should be found at a region of intermediate density (Levy *et al.*, 1992).

Another important factor in detergent-mediated reconstitution is that the protein of interest is stable in the detergent used. For enzymes this can be established by measuring enzyme activity and for ion channels or transporters the activity may be checked in reconstituted vesicle systems. Spectroscopic methods, such as circular dichroism and fluorescence spectroscopy, may also be employed to check that the protein remains in a functional state. Some detergents are known to be very 'harsh' on proteins and are therefore unsuitable for reconstitution studies. An example includes SDS. The structure of porins, however, is extremely stable and requires boiling for several minutes in SDS buffer before denaturation will occur (Garavito & Rosenbusch, 1985). The denaturing action of some detergents is therefore not a problem when dealing with a stable protein like porin.

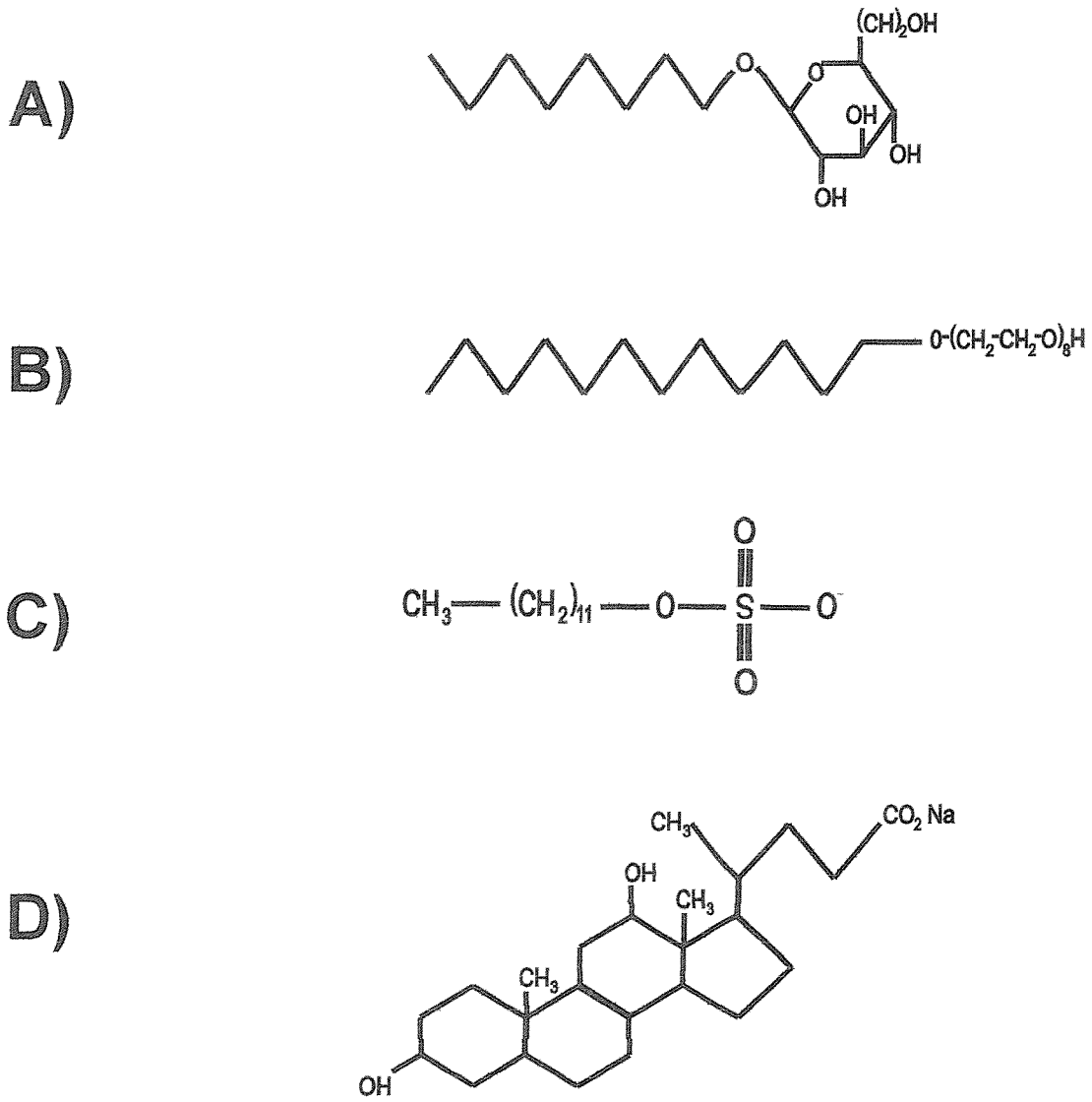

Figure 3.1: The structure of some commonly used detergents.

A) OG, B) $C_{12}E_8$, C) SDS, and D) deoxycholate (derived from (Moller *et al.*, 1986)).

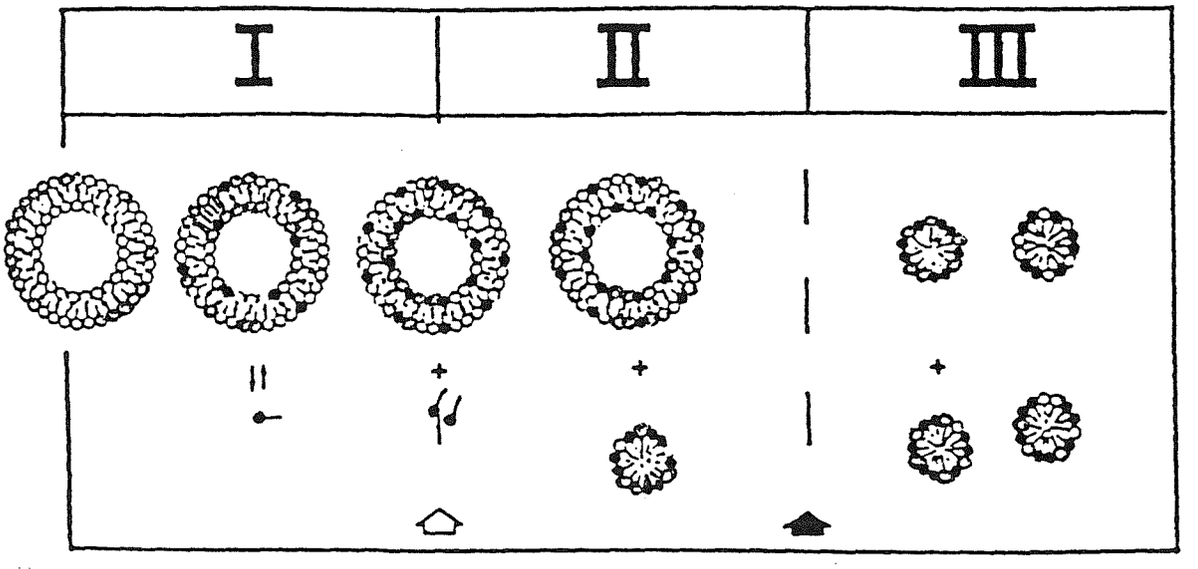

Figure 3.2: **The three-stage model of solubilisation of lipid vesicles (derived from Rigaud *et al.*, 1995)).**

3.2 Methods

3.2.1 Light Scatter Studies

3.2.1.1 Purification of OmpF

To determine the effects of a variety of detergents on the turbidity of OmpF the protein was required in a purified form in a detergent-free solution. The purification method of Lakey was employed (Lakey *et al.*, 1985).

A suspension of cells in 20 mM NaH_2PO_4, pH 7.3 were sonicated at 4 °C using a probe sonicator for 15 cycles, 15 seconds on, 15 seconds off. Unbroken cells were removed by centrifugation at 6,000 x g for 15 minutes at 4 °C. The cell-free supernatant was centrifuged, at 100,000 x g for 40 minutes at 4 °C, to isolate the membrane fraction. The pellet was shaken at 55 °C in 10 mM Tris-HCl, pH 7.4, 2 % SDS until solubilised. This suspension was centrifuged at 100,000 x g for 40 minutes at 20 °C. These solubilisation-centrifugation steps were repeated three times on the pellet. The porin was then freed from the pellet by shaking at 37 °C in the same buffer containing 0.5 M NaCl and 0.7 M β-mercaptoethanol. The sample was then centrifuged at 100,000 x g for 40 minutes at 20 °C. The supernatant was dialysed for 2 x 12 hour periods at room temperature in 5 mM $NaHCO_3$, pH 7.2, 0.1 % SDS. Porin was then precipitated from this solution with 90 % acetone, for 2 hours at 4 °C. The porin was pelleted by centrifugation in polypropylene tubes at 20,000 x g for 10 minutes at 4 °C. The pellet was washed twice in acetone and then in water, before finally resuspending in 10 mM Tris-HCl, pH 7.4. Protein aliquots were stored at -20 °C.

3.2.1.2 Preparation of Potassium Cholate and Potassium Deoxycholate

Potassium cholate for the solubilisation of OmpF was prepared by dissolving equimolar quantities of cholic acid and potassium hydroxide in a minimal volume of methanol. The potassium cholate was precipitated from the methanol by adding an excess of diethyl ether and leaving at 4 °C overnight. The solvent was filtered

off and the solid dried under vacuum for about 12 hours. 5 % (w/v) solutions were made in 20 mM Hepes, pH 7.2, 1 mM EGTA.

Potassium deoxycholate was prepared in a similar manner, using deoxycholic acid.

3.2.1.3 Light Scatter Measurements.

The light scatter of 0.25 nmols of OmpF was measured in 2.5 ml of 20 mM Hepes, pH 7.2, 1 mM EGTA using an SLM 8000C fluorimeter with an excitation and emission wavelength of 400 nm. Slit widths of 4 nm were used for excitation and emission. All solutions were made in 20 mM Hepes, pH 7.2, 1 mM EGTA. The detergents tested were DM, octyl-POE, dodecylpoly(ethyleneglycolether)$_8$ ($C_{12}E_8$), OG, cholate and deoxycholate. The concentrations of the detergents tested were raised in increments and the absorbance was continuously recorded until no further changes were observed. The degree of light scatter of the OmpF suspension was plotted as a function of the detergent concentration. Samples without protein were subtracted to correct for light scatter contributed by buffer and detergent. Comparisons were made under identical conditions with the sarcoplasmic reticulum (SR) of rabbit skeletal muscle, which consists predominantly of the Ca^{2+}-ATPase, a typical α-helical protein

3.2.2 Reconstitution of OmpF

3.2.2.1 Preparation of Brominated Lipids

Lipids were obtained from Avanti Polar Lipids. The synthesis of 1,2-bis (9,10-dibromostearoyl)-sn-glycero-3-phosphorylcholine (di(Br_2C18:0)PC) was as outlined by Dawidowicz & Rothman (1976). 100 mg of (di(C18:1)PC) in 5 ml of chloroform was reacted with 14 µl of bromine at –20 °C. The reaction was left for 30 minutes. Excess bromine was removed by rotary evaporation. The di(Br_2C18:0)PC was

stored in chloroform (100 mg/ml) under nitrogen at –20 °C. Homogeneity of the solution was verified by thin-layer chromatography (TLC) using chloroform: methanol: 25 % ammonia (14:16:1 v/v/v).

3.2.2.2 Reconstitution into Lipid Bilayers using the Dilution Method

The detergent octyl-POE was used to reconstitute OmpF into bilayers of di(C18:1)PC or di(Br_2C18:0)PC. The concentration of octyl-POE required for this purpose was estimated by measuring the level of fluorescence quenching in di(Br_2C18:0)PC as a function of the detergent concentration used. In brief the method involved initially solubilising the phospholipid in octyl-POE and then mixing the lipid with OmpF that has also been solubilised in octyl-POE.

2.5 μmols of di(C18:1)PC or di(Br_2C18:0)PC) were dried onto the walls of a 10 ml glass scintillation vial in a vacuum dessicator. The lipid was resuspended in 200 μl reconstitution buffer (10 mM Hepes, pH 8.0, 15 % w/v sucrose) containing:

68.4 mM octyl-POE (samples a, b, e and f)
34.2 mM octyl-POE (samples c and g) or
17.1 mM octyl-POE (samples d and h)

Samples were sonicated to clarity using an Ultrawave bath sonicator and 150 μl of a 1.0 mg/ml (4.05 nmols) OmpF solution, purified according to the method of Rummel (personal communication, Section 2.4.2), was then added. The concentration of octyl-POE used to solubilise OmpF was:

85.6 mM octyl-POE (samples a and e)
28.5 mM octyl-POE (samples b, c, d, f, g and h)

The suspension was left at room temperature for 15 minutes, followed by incubation on ice for a further 60 minutes before measuring the fluorescence. 10 μl of sample (0.12 nmols of OmpF) was diluted into a 3 mls of 20 mM Hepes, pH 7.2, 1 mM EGTA, for fluorescence measurements.

To verify that the dilution factor being used was sufficient to reduce the octyl-POE to a concentration well below its cmc, the level of dilution was increased from 300- to 1500-fold. This was performed by adding 2 μl of the reconstituted samples (0.023 nmols OmpF) to a final volume of 3 ml. Samples d and h were used and the level of quenching was compared for the two dilution factors.

The detergent concentrations chosen for further experiments were 17.1 mM in the reconstitution buffer to solubilise the lipid and 28.5 mM (equivalent to a 1 % w/v octyl-POE solution) to solubilise the OmpF. Combined, these give an octyl-POE concentration of 22.0 mM, which after a 300-fold dilution is reduced to 0.07 mM.

3.2.2.3 Reconstitution into Lipid Bilayers using the Biobeads Method

5 g of Bio-Beads SM-2 (Biorad) were stirred in 200 ml of methanol for 15 minutes. The beads were collected on a sintered glass funnel and washed with a further 100 ml of methanol and subsequently with 10 mM Pipes, pH 7.1, 100 mM K_2SO_4. The beads were then slowly washed in a column with approximately 400 ml of the same buffer. The beads were stored in this buffer at 4 °C for a maximum of 2 weeks.

OmpF was reconstituted with di(C18:1)PC or di(Br_2C18:0)PC using the same conditions to those used in Section 3.2.2.2 but the detergent was removed using Biobeads instead of by dilution. After the 15 minute incubation at room temperature 57 mg of Biobeads-SM2 was added to the sample. An additional 57 mg of Biobeads-SM2 were added after 1 hour, 2 hours and 3 hours. The sample was separated from the Biobeads, by pipetting, 5 minutes after the final Biobead addition was made. The protein

concentration of the sample was determined using the BCA assay and the fluorescence of the sample was then recorded as described in Section 3.2.2.5.

3.2.2.4 Reconstitution into Lipid Bilayers using the Dialysis Method

OmpF was reconstituted with di(C18:1)PC or di(Br_2C18:0)PC identically to section 3.2.2.2 but the detergent was removed by dialysis. After the 15 minute incubation at room temperature the sample was dialysed against 500 ml 10 mM Pipes, pH 7.1, 100 mM K_2SO_4 for 2 x 3 hour periods at room temperature with one change of buffer. The dialysis tubing used had a molecular weight cut off of 12-14000 Da. The protein concentration of the sample was determined using the BCA assay and the fluorescence of the sample was then recorded as in Section 3.2.2.5.

3.2.2.5 Fluorescence Measurements

All fluorescence measurements were performed using an SLM8000C fluorimeter at 25 $^{\circ}$C using an excitation wavelength of 280 nm. Fluorescence emission spectra were recorded between 300 and 400 nm and slit widths of 4 nm were used for both excitation and emission. All experiments were performed in 20 mM Hepes, pH 7.2, 1 mM EGTA and were corrected for light scattering by subtracting the spectra of a sample of reconstituted phospholipid lacking OmpF. Fluorescence spectra were not corrected for wavelength shifts between samples.

3.2.2.6 SDS-PAGE of Reconstituted OmpF

Samples of approximately 8.0 μg samples of OmpF reconstituted into di(C18:1)PC or di(Br_2C18:0)PC, prepared by detergent dilution and using Biobeads, were analysed by SDS-PAGE using 15 % polyacrylamide to ascertain whether the trimer structure was maintained after reconstitution.

3.2.2.7 Sucrose Density Centrifugation

10 μmols of di(C18:1)PC containing 0.1 nmols of ^{3}H-PC were dried onto the walls of a glass vial and then resuspended in 0.8 ml of reconstitution buffer (10 mM Hepes, pH 8.0, containing 0.6 % octyl-POE). The vial was sealed under nitrogen, mixed and sonicated to clarity in an Ultrawave bath sonicator. 600 μg (16.2 nmols) of OmpF was added and the reconstitution was left at room temperature for 15 minutes and then left on ice for a further 45 minutes. The suspension was then dialysed at room temperature in 10 mM Pipes, pH 7.1, 100 mM K_2SO_4 for 5 hours. 0.75 ml of the dialysate was loaded onto a gradient containing the following concentrations of sucrose in 10 mM Pipes, pH 7.1, 100 mM K_2SO_4: 2.5, 5.0, 10.0, 15.0, 20.0 and 30.0 % w/v at 4 °C. The 30.0 % sucrose solution was supplemented with 0.05 % Triton X-100. Tubes were centrifuged in a swing-out rotor at 80,000 x g for 18 hours. 1.5 ml fractions were pipetted carefully from the gradients and the protein and lipid content of each was quantified using a modified Lowry assay (Sigma Diagnostics) and scintillation counting respectively.

To determine whether the same level of quenching of OmpF was obtained in di(Br_2C18:0)PC lipid bilayers after separation on sucrose gradients as in the fluorescence reconstitutions (Sections 3.2.2.2 – 3.2.2.4), the same method was followed but using 10 μmols of di(Br_2C18:0)PC instead of di(C18:1)PC. Following separation on a sucrose gradient the fluorescence of 0.12 nmols of OmpF, from the most concentrated protein fraction, was recorded, as described inn Section 3.2.2.5.

3.3 Results

3.3.1 Purification of OmpF

OmpF purification was achieved by the method of Lakey et al for the light scatter studies (Lakey *et al.*, 1985). Protein yield was approximately 1.5 mg per litre of BZB1107 cells. Heat-denatured OmpF displayed an apparent M_r of 37 k on SDS-PAGE, as shown in Figure 3.3.

The purification method of Rummel (personal communication) was employed for all OmpF reconstitution studies, and yielded 3-4 mg of pure OmpF per litre of BZB1107 cells. Figure 3.4 shows purified OmpF as a 37 k monomer after heat denaturation, and as a trimer of approximately 90 k without denaturation.

3.3.2 Solubilisation of OmpF

The solubility of purified OmpF in a variety of detergents was assessed by light scatter and comparisons were made with the SR of rabbit skeletal muscle, which consists predominantly of the Ca^{2+}-ATPase, a typical α-helical protein. The results obtained are shown in Figures 3.5 to 3.10, with turbidity of OmpF and the SR plotted as a function of the detergent concentration. Table 3.1 provides a summary of the detergents studied (Moller *et al.*, 1986).

DM is a non-ionic detergent and the results in Figure 3.5 show that total solubilisation of SR is achieved with DM concentrations of approximately 0.3 mM, a concentration just above the cmc value (See Table 3.1). Concentrations as high as 2 mM, however, are ineffective in solubilising OmpF. Octyl-POE, another non-ionic detergent, solubilises both OmpF and the SR at a concentration of approximately 7 mM, as can be seen in Figure 3.6. This concentration is comparable to the cmc of octyl-POE (see Table 3.1). The non-ionic detergent $C_{12}E_8$ was ineffective in solubilising OmpF as shown in Figure 3.7. Complete solubilisation was seen with concentrations less than 1.0

mM for SR, but no change in the light scatter of OmpF was seen with the concentrations used. Another non-ionic detergent that solubilised both proteins was OG, shown in Figure 3.8. Light scatter was fully reduced at 40 mM for both SR and OmpF, a concentration above the cmc of OG, i.e., 25 mM. The detergents cholate and deoxycholate were both unsuccessful in solubilising OmpF, but completely solubilised the SR Ca^{2+}-ATPase at concentrations of approximately 15 mM and 5 mM, respectively (Figures 3.9 and 3.10).

3.3.4 Reconstitution into di(C18:1)PC or di(Br_2C18:0)PC using the Dilution Method

The light scatter results suggest that octyl-POE is a suitable detergent for studies on OmpF. This detergent was initially used in OmpF studies by Rosenbusch for solubilisation and crystallisation work (Garavito & Rosenbusch, 1985). OmpF was therefore reconstituted into lipid bilayers using the non-ionic detergent octyl-POE. The minimum concentration of detergent required for reconstitution of OmpF into membranes of a desired lipid was ascertained by reconstituting the protein with a fluorescence quenching lipid species, di(Br_2C18:0)PC. Quenching by bromine requires an intimate contact between the fluorophore, in this case the Trp residues, and the quencher (East & Lee, 1982; Webb *et al.*, 1998), thus a reduction in the fluorescence intensity indicates the brominated lipid is in close contact with Trp residues in OmpF and that reconstitution has taken place (Webb *et al.*, 1998). The positions of the two Trp residues found in each OmpF monomer are shown in Figure 3.11. Trp 214 is found on the outer wall of the barrel, in contact with the lipid membrane. Trp 61 is, however, found at the trimer interface, where it is probably shielded from interaction with the lipid milieu (Cowan *et al.*, 1992). Using this quenching approach it is assumed that the bromine will quench the fluorescence of those Trp residues in contact with the lipid when the lipid and protein are mixing efficiently.

Samples of lipid and OmpF were mixed at 600:1 molar ratio, respectively, in octyl-POE, incubated at room temperature for 15 minutes and then at 4 °C for 45 minutes before being diluted 300-fold into a 3 ml volume. Since the sample was to be reconstituted by dilution it was essential to use a low concentration of octyl-POE for the initial solubilisation so that the dilution would be sufficient to lead to reformation of membranes. In the reconstitution the lipid was initially solubilised with octyl-POE and dispersed by sonication before mixing with the octyl-POE-solubilised OmpF. In calculating the concentration of octyl-POE used during the reconstitution, therefore, the amount of octyl-POE in the protein sample as well as that added to solubilise the lipid need to be taken into account.

The fluorescence spectra of OmpF reconstituted in bilayers of di(C18:1)PC and di(Br_2C18:0)PC are shown in Figure 3.12. The fluorescence intensities of OmpF reconstituted in di(C18:1)PC bilayers were essentially identical for different concentrations of octyl-POE used in the reconstitution buffers as shown by spectra a-d. In samples a and d 85.59 mM (3.0 %) octyl-POE was used to solubilise OmpF. An additional 68.45 mM octyl-POE was used to solubilise the phospholipids. The OmpF and lipid samples were mixed at a 600:1 molar ratio of lipid to protein to give a final octyl-POE concentration of 75.81 mM. After a 300-fold dilution into the cuvette this concentration was reduced to 0.253 mM. The level of quenching of the fluorescence intensity of this sample in di(Br_2C18:0)PC was approximately 30 %. Reduction of the octyl-POE concentration in the OmpF buffer from 85.59 mM to 28.53 mM (1.0 %) by dialysis, while using the same lipid-solubilising concentration gave a final octyl-POE concentration of 51.35 mM in the reconstituted samples b and f. After dilution the concentration of octyl-POE was 0.171 mM and resulted in an increased quenching as shown by spectrum f relative to spectrum e. A further increase in the level of quenching was seen when the octyl-POE concentration used to solubilise the lipid was reduced. When octyl-POE concentrations of 34.24 mM and 17.12 mM were used to solubilise the lipid and the concentration of octyl-POE in the OmpF buffer was kept at 28.53 mM, the combined octyl-POE concentrations were 31.79 mM and 22 mM, respectively. The dilution reduced the detergent concentration to 0.107 mM and 0.073 mM respectively,

and the level of quenching seen in di(Br_2C18:0)PC was essentially identical (plots g and h). The maximum level of quenching achieved when OmpF was reconstituted into bilayers of di(Br_2C18:0)PC is 50 ± 2 %.

To verify that the sample was being diluted sufficiently, the sample which achieved maximal fluorescence quenching (i.e., using an octyl-POE concentration of 22 mM in the lipid-protein-detergent mixture) was further diluted to see if the same level of quenching was observed. A 1500-fold dilution was performed, that effectively reduces the final detergent concentration in the cuvette to 0.0147 mM. The fluorescence was detectable when the slit widths were increased to 8nm and is shown if Figure 3.13. The fluorescence intensity of OmpF reconstituted in di(Br_2C18:0)PC was 54 % of that of the same sample reconstituted in di(C18:1)PC compared to a value of 50 % when a 300-fold dilution was used (Table 3.2).

3.3.5 Effect of the Method of Detergent Removal on the Level of Quenching in di(Br_2C18:0)PC

Removing the octyl-POE by dialysis or using Biobeads-SM2 followed by dilution gave levels of 54 % and 50 % quenching, respectively, in di(Br_2C18:0) (Table 3.2). These results confirm that reconstitution can be achieved by dilution, dialysis or using Bio-Beads.

3.3.6 SDS-PAGE of Reconstituted OmpF

OmpF reconstituted in di(C18:1)PC or di(Br_2C18:0)PC has an approximate M_r of 90 k by SDS-PAGE as shown in Figures 3.14 and 3.15. It is apparent therefore that reconstitution of OmpF with non-native lipids, using 22 mM octyl-POE is seen not to interfere with the native trimer structure, when the detergent is removed by either dilution or with Bio-Beads.

3.3.7 Sucrose Density Centrifugation

Figure 3.16 shows that if OmpF and lipid are mixed in the absence of detergent and subjected to sucrose gradient centrifugation, the lipid and protein separate to the top (fractions 1-3), and bottom (fractions 9-10) of the gradients, respectively. However, when reconstituted the majority of protein and lipid were found together in fractions 3 to 5 at lipid-to-protein molar ratios of between 300 and 700:1 after detergent removal by dialysis (see Figure 3.17).

The fluorescence spectra of OmpF were recorded after separation of samples reconstituted in di(C18:1)PC or di(Br_2C18:0)PC on sucrose gradients. The fluorescence of 0.12 nmols of OmpF from fraction 4 of the sucrose gradients is shown in Figure 3.18. As can be seen the fluorescence of OmpF reconstituted in di(Br_2C18:0)PC was 52 % that of OmpF reconstituted in di(C18:1)PC. This is comparable to the results shown in Table 3.2.

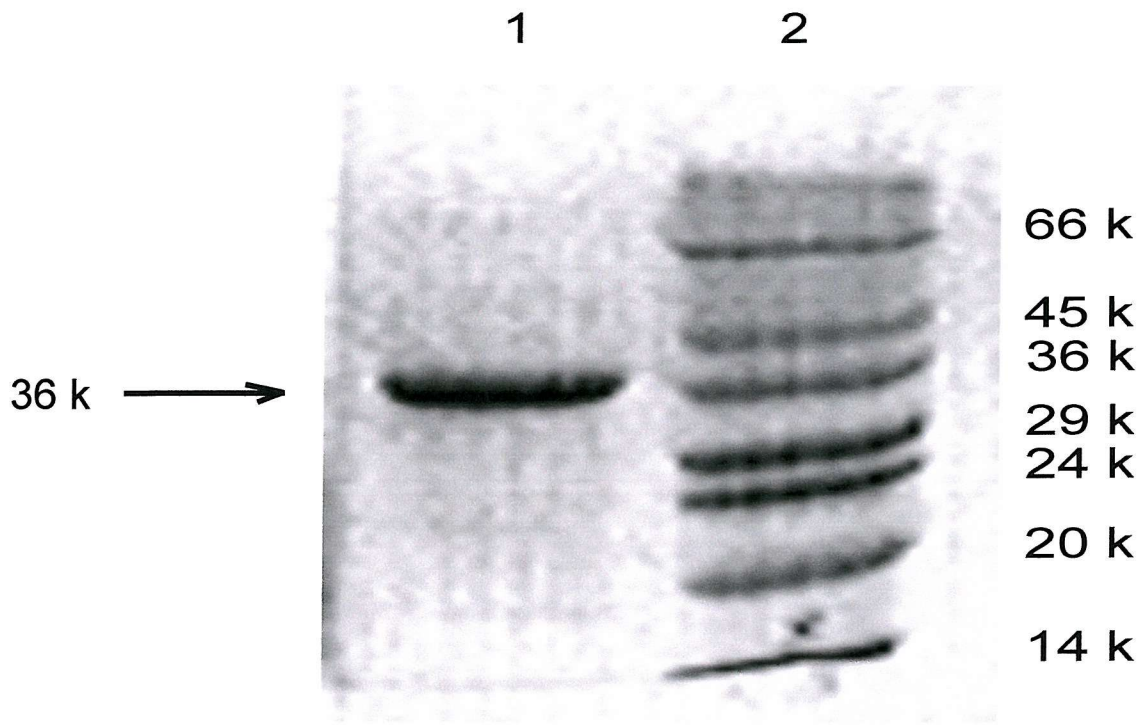

Figure 3.3: 15 % SDS-polyacrylamide gel stained with Coomassie brilliant blue showing OmpF purified by the method of Lakey (Lakey *et al.*, 1985).

Lane 1 contains 6.0 μg of OmpF, purified by the method of Lakey (Lakey *et al.*, 1985) which has been heat-denatured at 100 °C for 5 minutes to produce monomer, showing an apparent M_r of 37 k. Lane 2 contains low M_r Sigma marker.

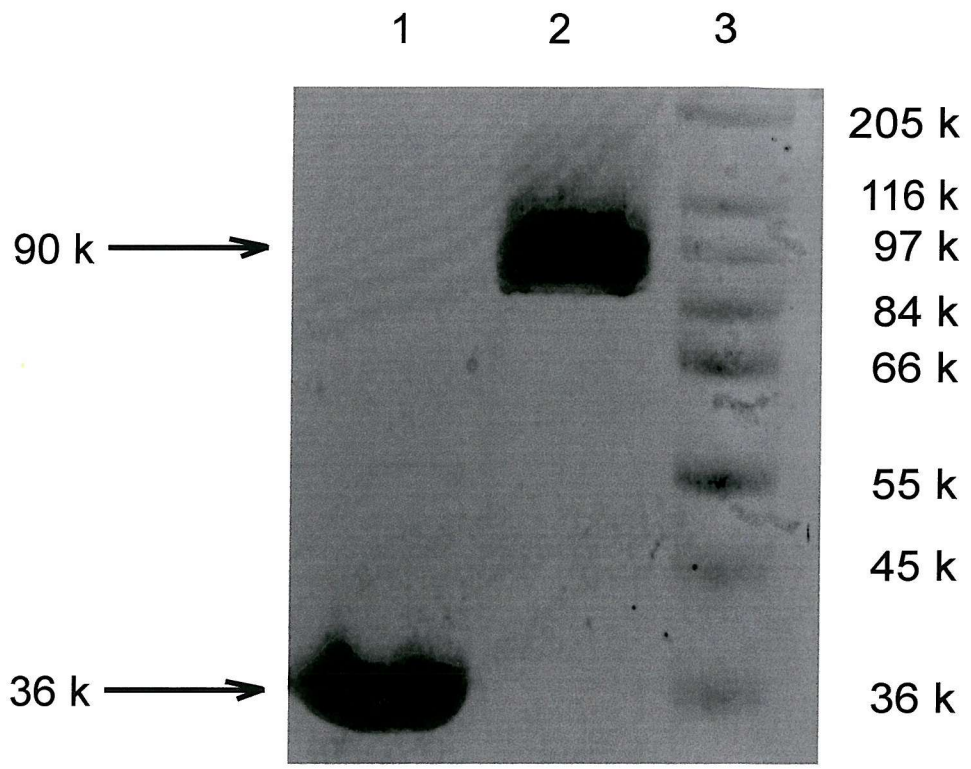

Figure 3.4: 15 % SDS-polyacrylamide gel stained with Coomassie brilliant blue showing OmpF purified by the method of Rummel (personal communication). Lane 1 contains 10.0 μg of OmpF, purified by the method of Rummel et al (personal communication), which has been heat-denatured at 100 °C for 5 minutes to produce monomer, showing an apparent M_r of 37 k. Lane 2 contains 10.0 μg of OmpF, purified by the same method, which has not had heat-treatment, and shows an apparent M_r of approximately 90 k. Lane 3 contains high M_r Sigma marker.

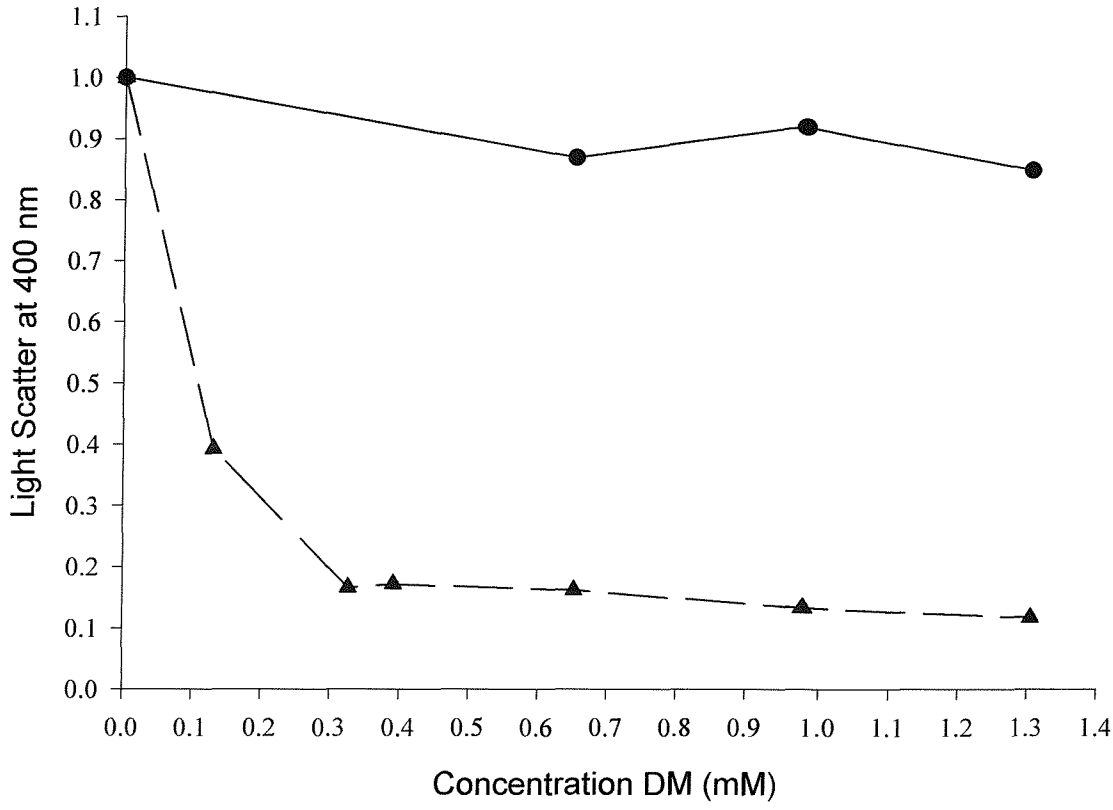

Figure 3.5: Effect of the non-ionic detergent DM on the turbidity of OmpF and on rabbit SR ATPase.

The turbidity of 0.25 μM of the proteins OmpF (—●—) and rabbit SR ATPase (—▲—) were monitored as a function of increasing DM concentrations. The buffer used was 200 mM Hepes, pH 7.2, 1 mM EGTA. The light scatter was recorded using excitation and emission wavelengths of 400nm.

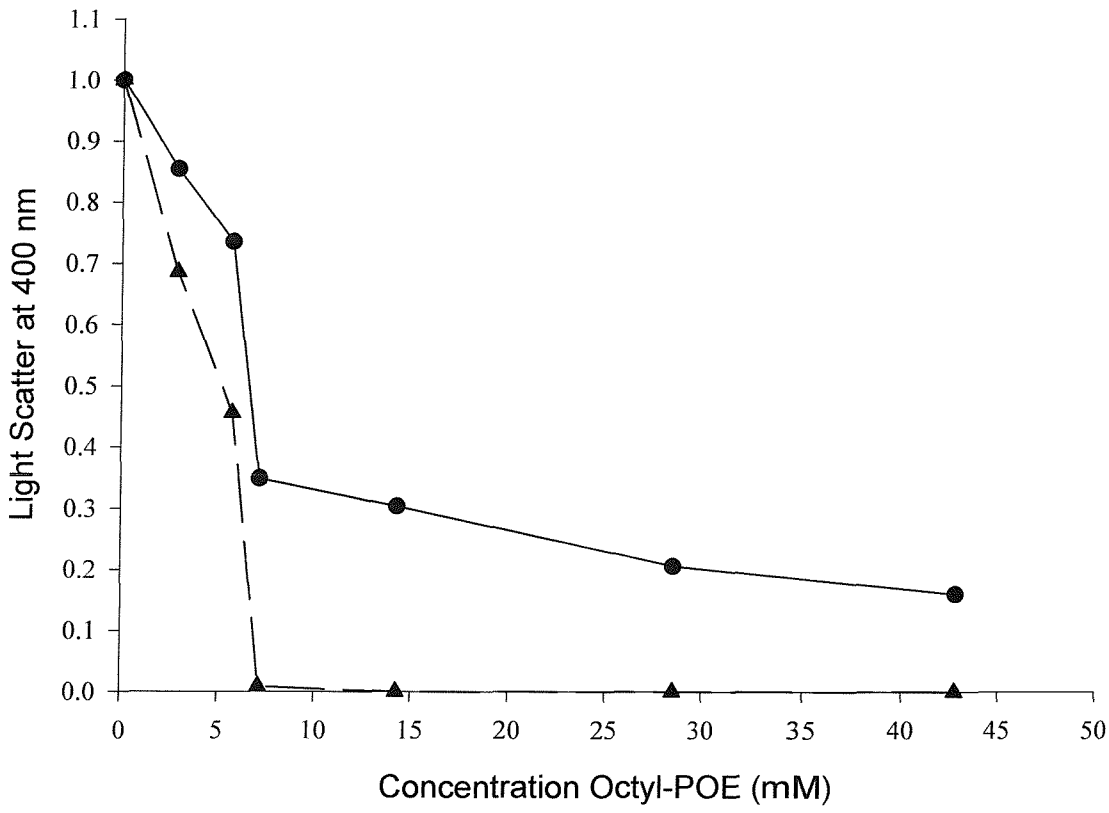

Figure 3.6: Effect of the non-ionic detergent octyl-POE on the turbidity of OmpF and on rabbit SR ATPase.

The turbidity of 0.25 μM of the proteins OmpF (—●—) and rabbit SR ATPase (—▲—) were monitored as a function of increasing octyl-POE concentrations. The buffer used was 200 mM Hepes, pH 7.2, 1 mM EGTA. The light scatter was recorded using excitation and emission wavelengths of 400nm.

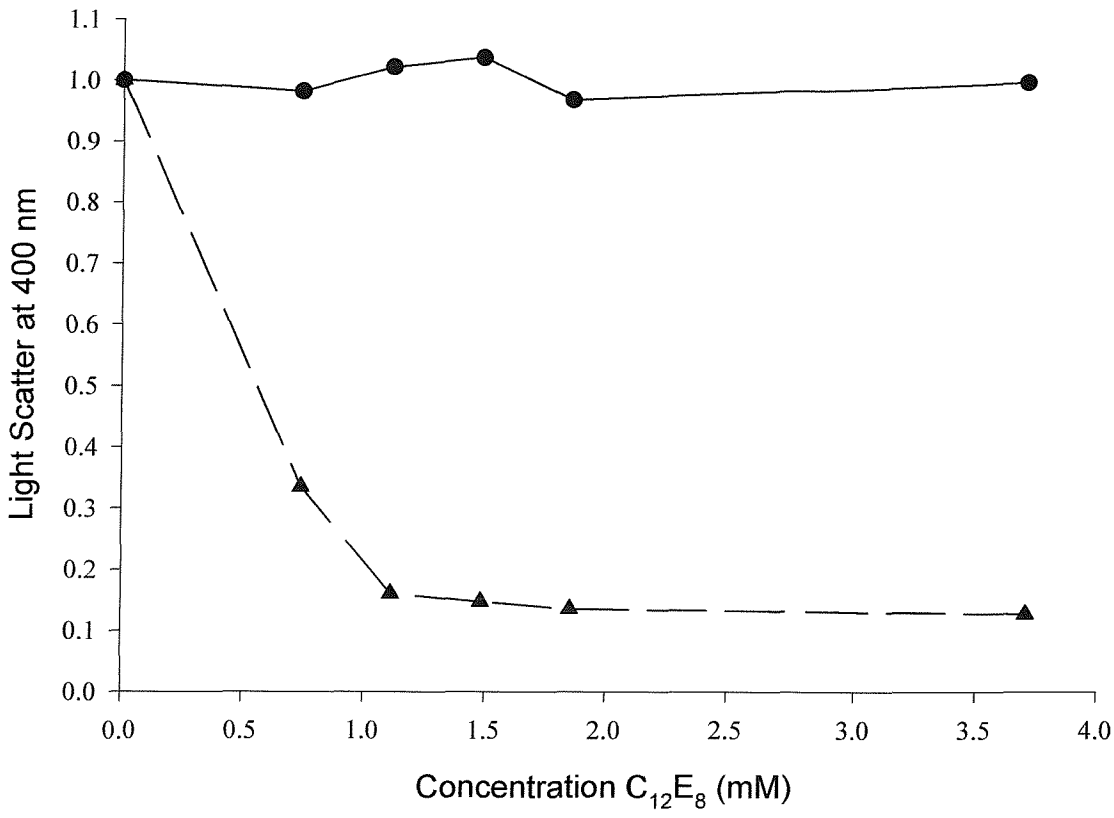

Figure 3.7: Effect of the non-ionic detergent $C_{12}E_8$ on the turbidity of OmpF and on rabbit SR ATPase.

The turbidity of 0.25 μM of the proteins OmpF (—●—) and rabbit SR ATPase (—▲—) were monitored as a function of increasing $C_{12}E_8$ concentrations. The buffer used was 200 mM Hepes, pH 7.2, 1 mM EGTA. The light scatter was recorded using excitation and emission wavelengths of 400nm.

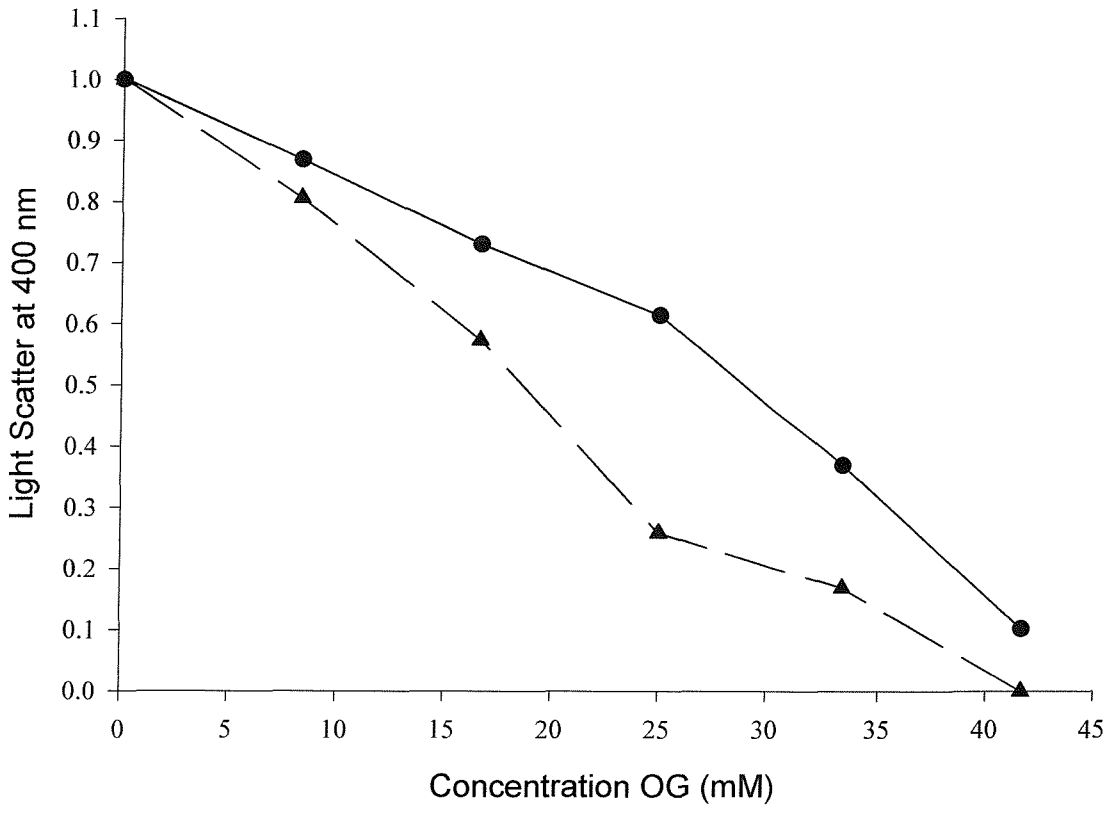

Figure 3.8: Effect of the non-ionic detergent OG on the turbidity of OmpF and on rabbit SR ATPase.

The turbidity of 0.25 μM of the proteins OmpF (—●—) and rabbit SR ATPase (—▲—) were monitored as a function of increasing OG concentrations. The buffer used was 200 mM Hepes, pH 7.2, 1 mM EGTA. The light scatter was recorded using excitation and emission wavelengths of 400nm.

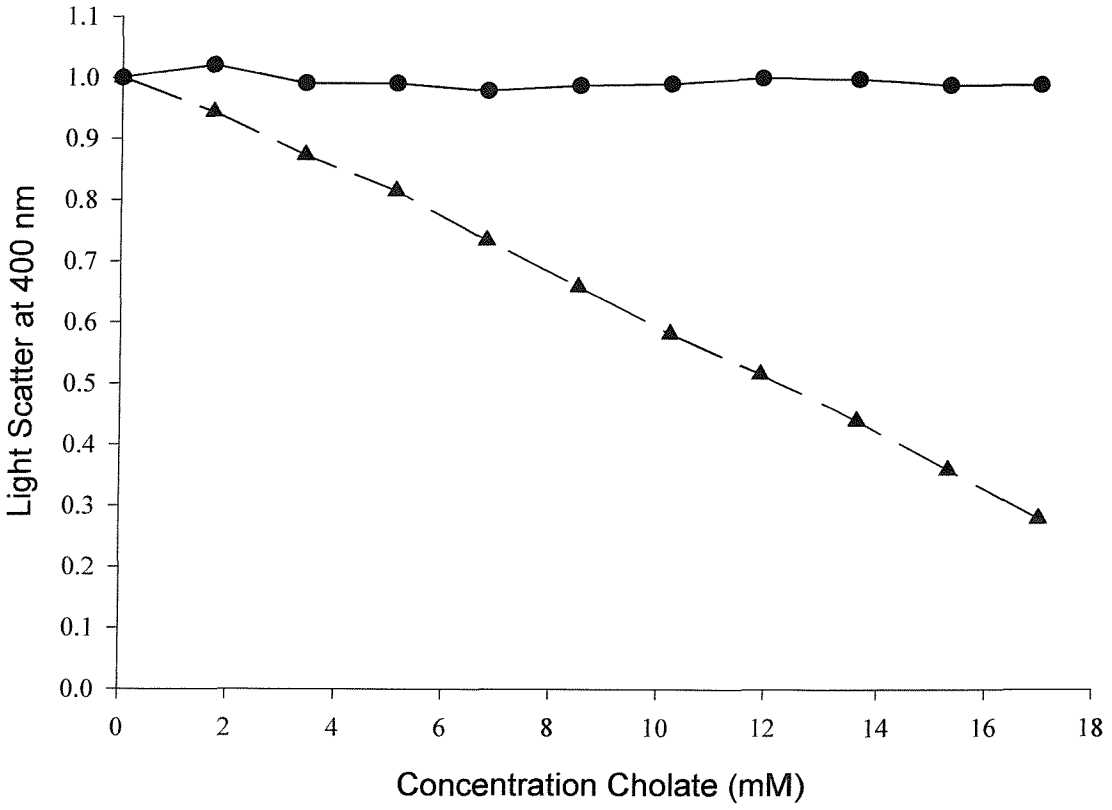

Figure 3.9: Effect of the detergent cholate on the turbidity of OmpF and on rabbit SR ATPase.

The turbidity of 0.25 μM of the proteins OmpF (—●—) and rabbit SR ATPase (—▲—) were monitored as a function of increasing cholate concentrations. The buffer used was 200 mM Hepes, pH 7.2, 1 mM EGTA. The light scatter was recorded using excitation and emission wavelengths of 400nm.

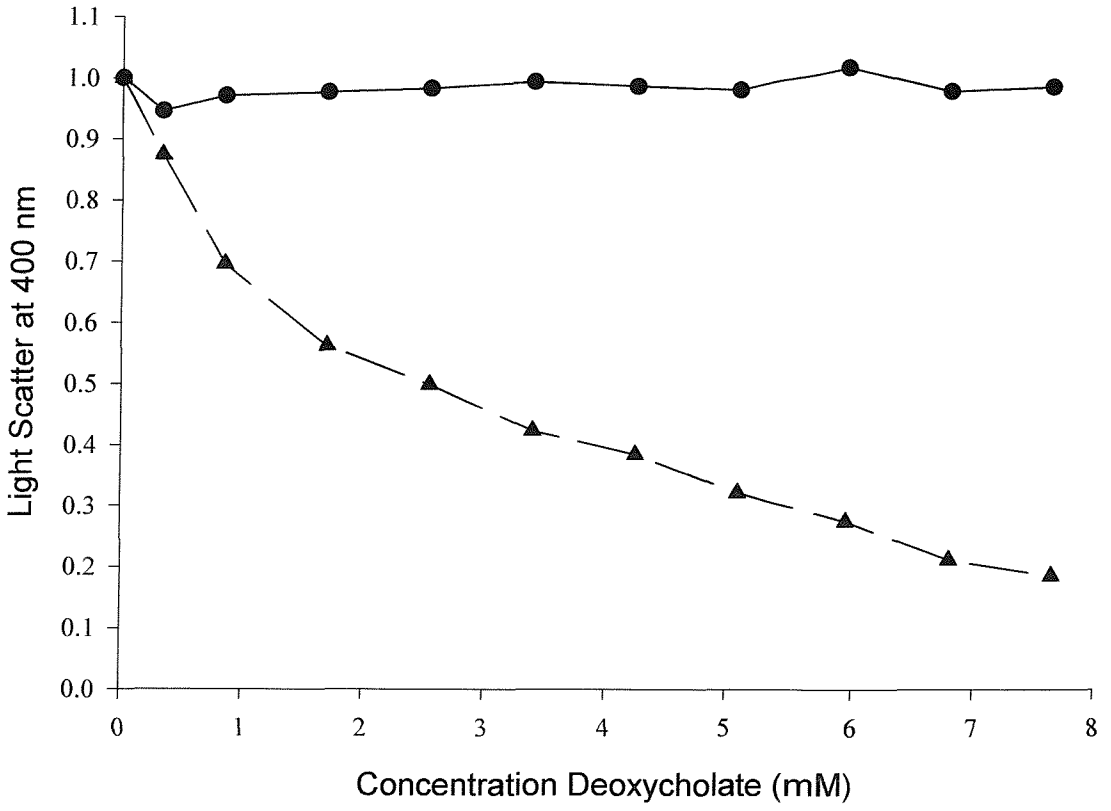

Figure 3.10: Effect of the detergent deoxycholate on the turbidity of OmpF and on rabbit SR ATPase.

The turbidity of 0.25 μM of the proteins OmpF (—●—) and rabbit SR ATPase (—▲—) were monitored as a function of increasing deoxycholate concentrations. The buffer used was 200 mM Hepes, pH 7.2, 1 mM EGTA. The light scatter was recorded using excitation and emission wavelengths of 400nm.

Figure 3.11: Position of Trp residues in OmpF

There are two Trp residues per OmpF monomer: Trp 61 is found at the trimer interface of OmpF and Trp 214 is found on the outer wall of OmpF, which is in contact with the lipid bilayer (PDB file 1OMPF).

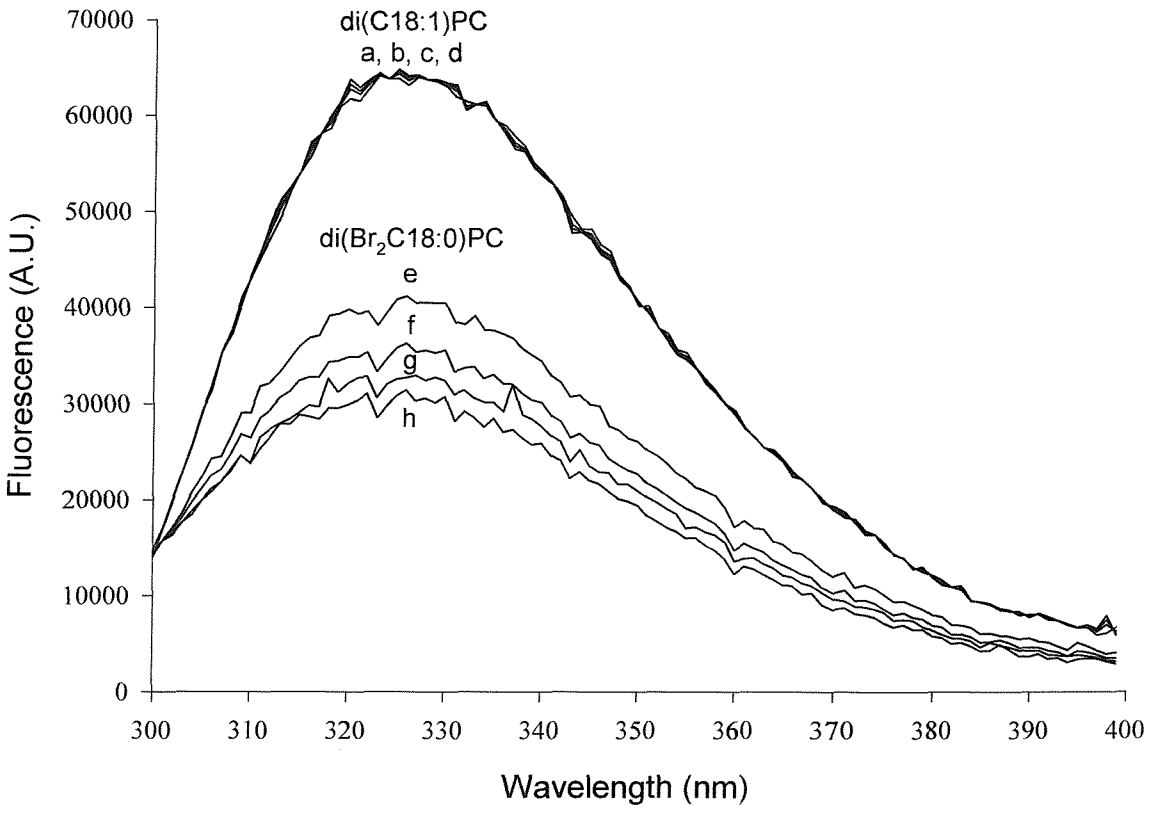

Figure 3.12: Effect of the detergent concentration on the level of quenching achieved when OmpF is reconstituted into bilayers of di(Br_2C18:0)PC.

OmpF was reconstituted into di(C18:1)PC (a-d) or di(Br_2C18:0)PC (e-h), at a 600:1 mole ratio of lipid-to-protein, using varying concentrations of the detergent octyl-POE. The fluorescence of 0.12 nmols of OmpF from each reconstitution was recorded by diluting 10 µl of each sample 300-fold into 200 mM Hepes, pH 7.2, 1 mM EGTA. The fluorescence was measured at 25 °C, using an excitation wavelength of 280 nm. The final concentrations of octyl-POE in the assay cuvette following dilution were: 0.253 mM in plots a and e; 0.171 mM in plots b and f; 0.107 mM in plots c and g; 0.073 mM in plots d and h.

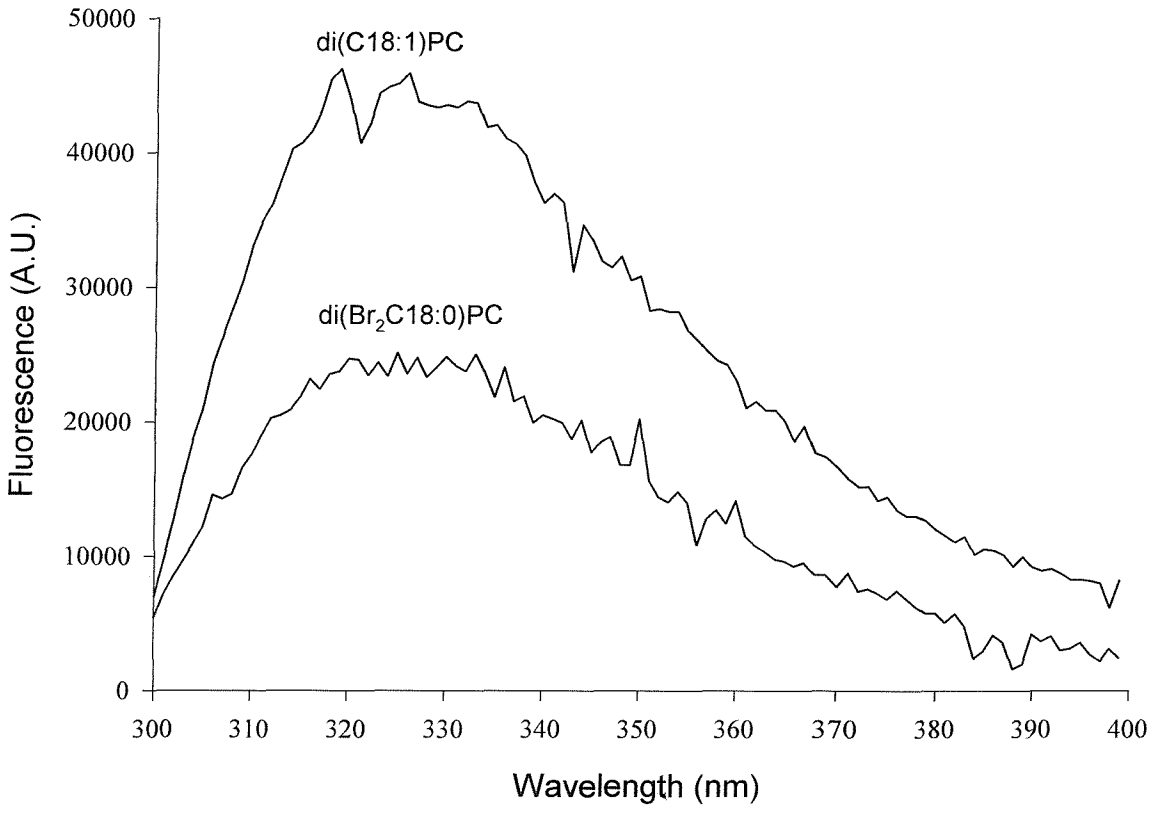

Figure 3.13: Effect of detergent dilution on the level of quenching in di(Br_2C18:0)PC.

OmpF was reconstituted into di(C18:1)PC or di(Br_2C18:0)PC, at a 600:1 mole ratio of lipid to protein, using 22.0 mM of the detergent octyl-POE. The fluorescence of 0.023 nmols of OmpF was recorded by diluting 2 µl of sample 1500-fold into 200 mM Hepes, pH 7.2, 1 mM EGTA. The fluorescence was measured at 25 °C, using an excitation wavelength of 280 nm. The final concentration of octyl-POE in the assay cuvette following dilution was 0.0147 mM.

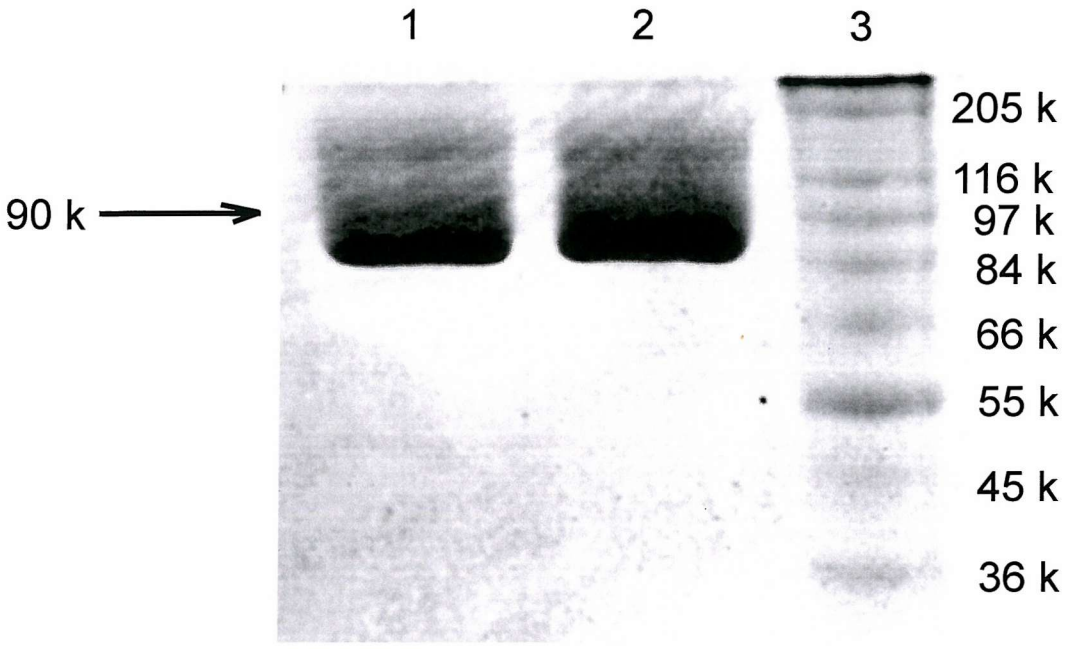

Figure 3.14: 15 % SDS-polyacrylamide gel stained with Coomassie brilliant blue showing OmpF reconstituted by the dialysis method.

Lane 1 shows 8.0 μg of OmpF that has been reconstituted in di(C18:1)PC and lane 2 contains OmpF that has been reconstituted in di(Br_2C18:0)PC. Both samples have a lipid-to-protein molar ratio of 600:1 and were reconstituted using the detergent octyl-POE, which was subsequently removed by dialysis. Lanes 3 contains high M_r Sigma marker.

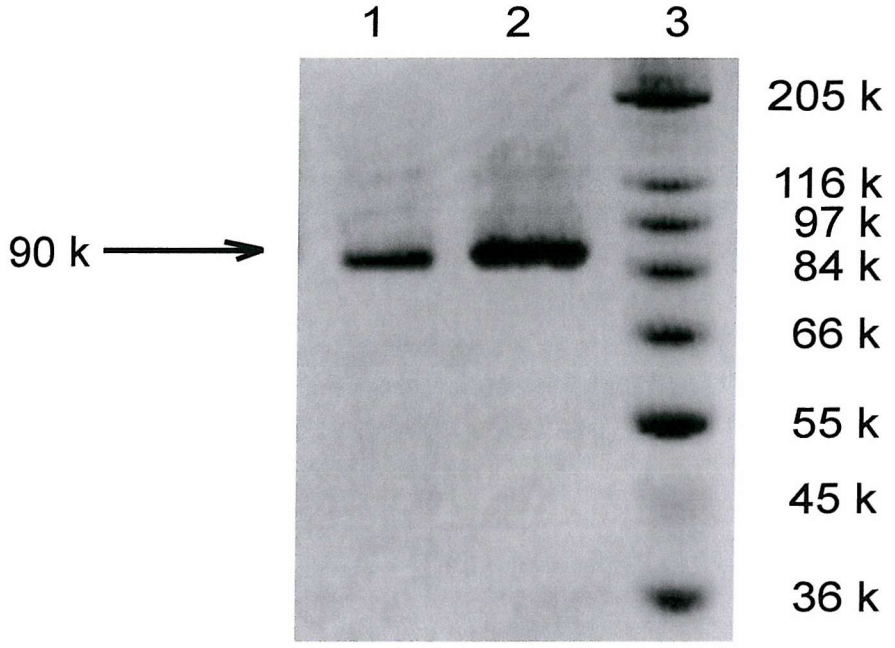

Figure 3.15: 15 % SDS-polyacrylamide gel stained with Coomassie brilliant blue showing OmpF reconstituted using the Biobeads method.

Lane 1 shows 8.0 μg of OmpF that has been reconstituted in di(C18:1)PC and lane 2 contains OmpF that has been reconstituted in di(Br_2C18:0)PC. Both samples have a lipid-to-protein molar ratio of 600:1 and were reconstituted using the detergent octyl-POE, which was subsequently removed using Biobeads. Lane 3 contains high M_r Sigma marker.

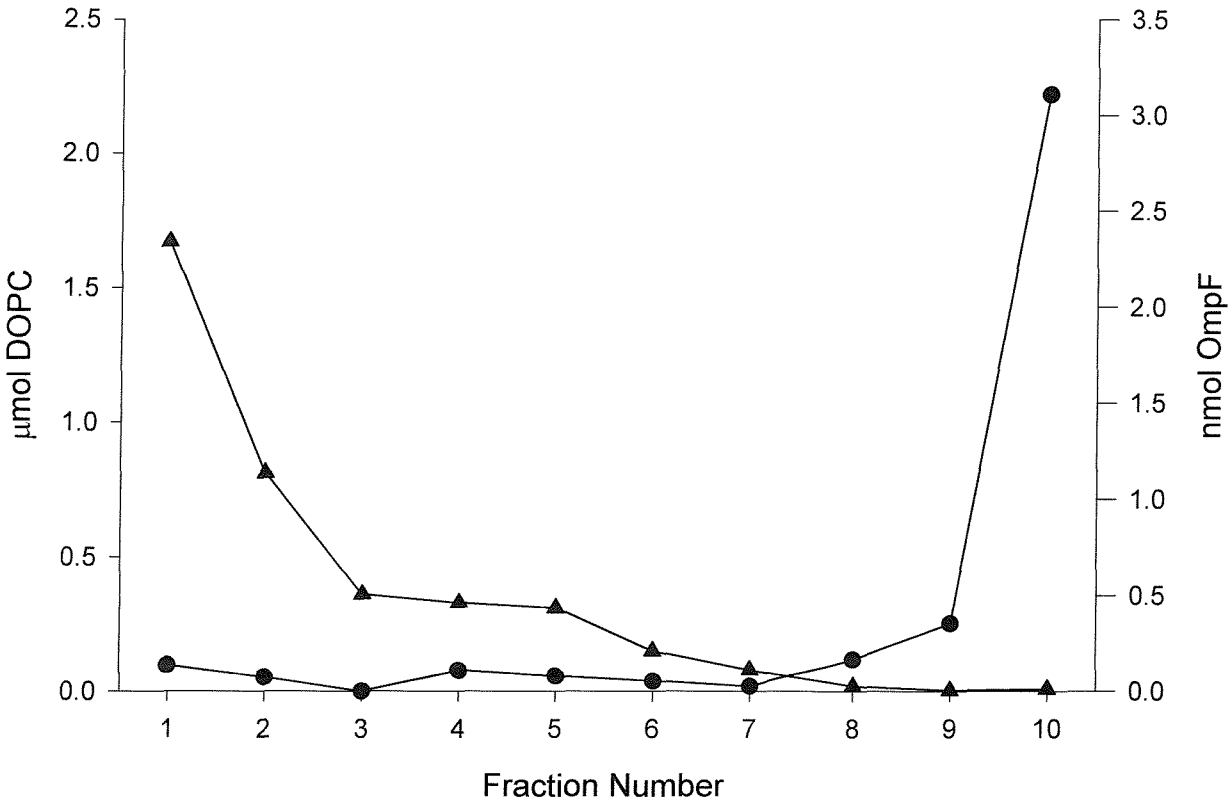

Figure 3.16: Sucrose gradient analysis of OmpF and di(C18:1)PC controls.

Controls were separated on a discontinuous sucrose gradient from 30 to 2.5 % sucrose. 1.5 ml fractions were taken and analysed for lipid (—▲—) and OmpF (—●—) content.

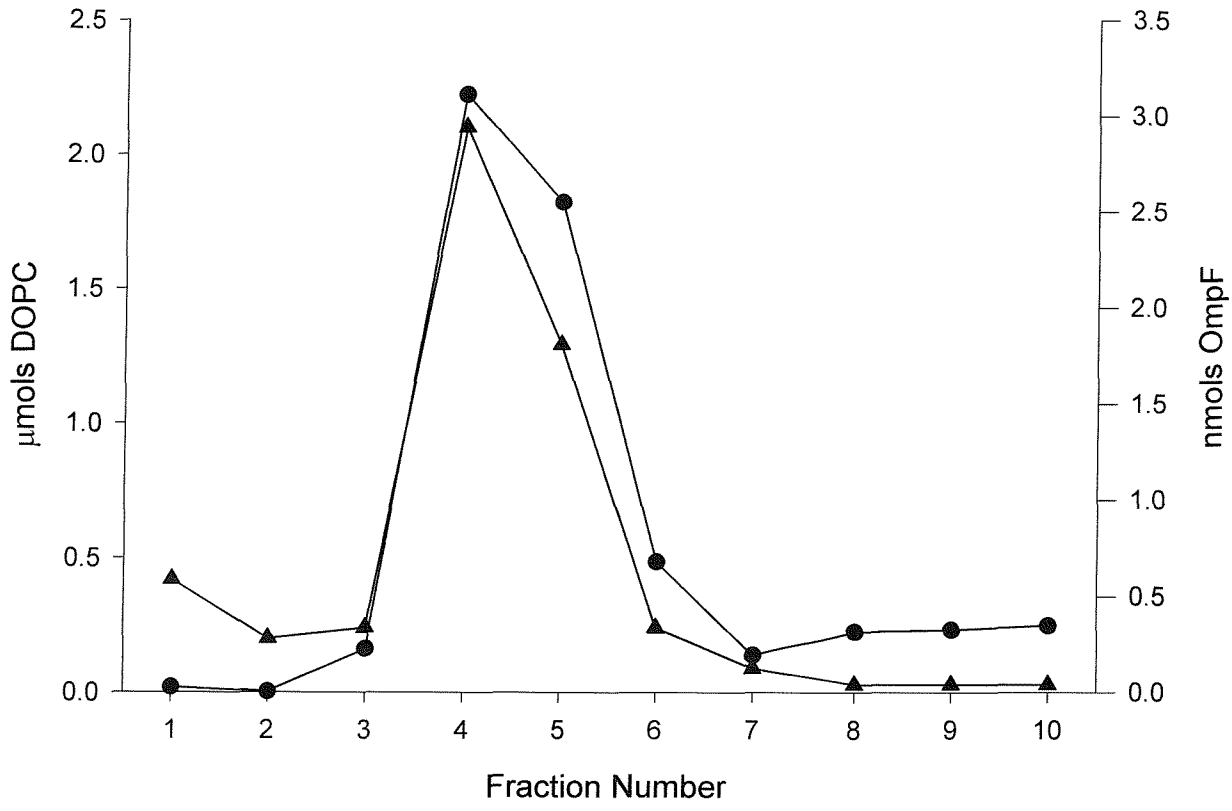

Figure 3.17: Sucrose gradient analysis of OmpF reconstituted by the dialysis method.

A sample of OmpF reconstituted by the dialysis method in di(C18:1)PC at a lipid-to-protein mole ratio of 600:1, was separated on a discontinuous sucrose gradient from 30 to 2.5 % sucrose. 1.5 ml fractions were taken and analysed for lipid (—▲—) and OmpF (—●—) content.

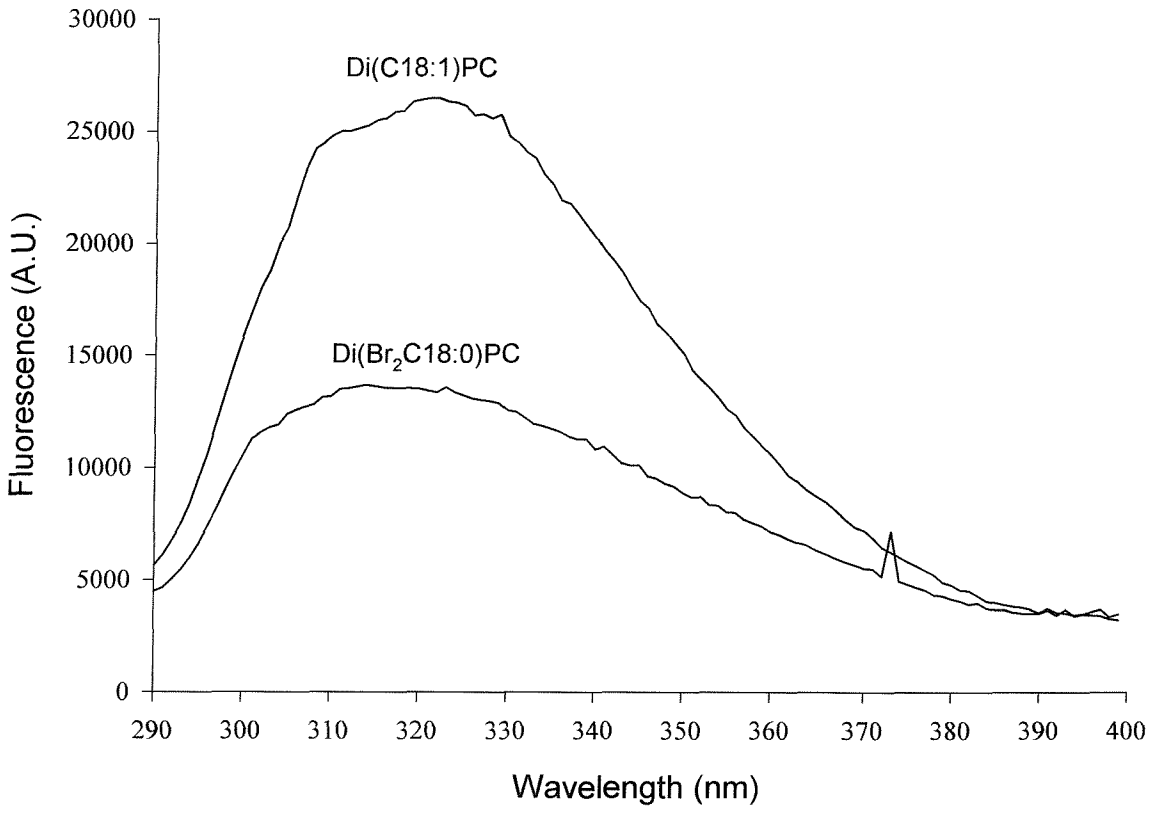

Figure 3.18: Fluorescence emission of OmpF samples fractionated from sucrose gradients.

The fluorescence of 0.12 nmols of OmpF from fraction 4 extracted from a sucrose gradient were measured for samples that had been reconstituted in either di(C18:1)PC or di(Br_2C18:0)PC.

Detergent	Properties	cmc (mM)	Monomer M_R	Ability to solubilise OmpF
OG	Nonionic	25	292.4	Yes
Na Cholate	Anionic	13 - 15	431	No
Na Deoxycholate	Anionic	4-6	415	No
Octyl-POE	Nonionic	6.6	Approx. 350	Yes
$C_{12}E_8$	Nonionic	0.087	539.1	No
DM	Nonnionic	0.17	510.6	No

Table 3.1: Properties of detergents used in solubility studies of OmpF (Moller *et al.*, 1986).

Method	F/F_o
Dialysis	0.54 ± 0.02
Dilution (300-fold)	0.50 ± 0.02
Dilution (1500-fold)	0.54 ± 0.02
Biobeads-SM2	0.50 ± 0.02

Table 3.2: Effect of method of reconstitution on fluorescence quenching of OmpF by di(Br_2C18:0)PC.

F and F_o are the fluorescence intensities for OmpF reconstituted in di(Br_2C18:0)PC and di(C18:1)PC, respectively. The fluorescence of 0.12 nmols of OmpF was excited at 280 nm and emission was monitored at 318 nm.

3.4 DISCUSSION

Influx of nutrient molecules across the outer membrane of Gram negative bacteria is achieved through water-filled porin channels. In this project the OmpF porin from *E. coli* has been successfully overexpressed and purified from *E. coli* strain BZB110. The outer membrane of most Gram negative cells usually contains multiple species of porin, and separation of one porin from another is difficult (Nikaido, 1983). However the B^E – derived strain that was used only expresses the OmpF porin. Expression of the native protein was prevented by insertion of a Tn5 transposon element into the ompF gene, thus allowing production of OmpF to be solely under the control of a *tac* promoter in the vector pMS119 (Bainbridge *et al.*, 1998). Expression of the lamB gene that codes for the maltodextran-specific porin was repressed catabolically by including glucose in the media.

Purification of OmpF for light scatter studies was achieved by the method of Lakey (Lakey *et al.*, 1985). In this method late-exponential phase cells were broken by sonication and a crude cell envelope fraction was obtained by centrifugation. A peptidoglycan-associated fraction was then separated with SDS buffer. OmpF was freed from this fraction with SDS in a high salt buffer. The protein was acetone extracted and stored in Tris buffer. The final protein yield was approximately 1.5 mg of OmpF per litre of LB. OmpF purified by this method is shown in Figure 3.3.

Purification of OmpF for all reconstitutions was achieved using the purification method of Rummel (personal communication), which utilises the porin-solubilising property of the non-ionic detergent octyl-POE. After cell disruption with SDS breaking buffer and recovery of the envelope fraction, unrelated proteins were extracted with 0.125 % octyl-POE to yield a fraction enriched in peptidoglycan-associated proteins. A further extraction with 3 % octyl-POE solubilises outer membrane proteins and yields a fraction enriched in OmpF. SDS-PAGE analysis of the purified fraction revealed a single band at 37 k in the denatured sample and a single band at approximately 90 k in the non-denatured trimeric form (Figure 3.4). OmpF is

very stable in its trimeric form and therefore denaturation usually caused by the action of SDS on proteins is not observed. Hence, it is not necessary to run non-denaturing gels to observe the native form of this protein. The stability of the native trimeric form of OmpF has been mainly attributed to hydrophobic interactions between adjacent monomers (Cowan *et al.*, 1992). Protein yield, determined by the BCA assay, was approximately 3 mg per litre of LB. Purification using both methods was simplified with OmpF being the only porin expressed in the particular strain used (Bainbridge *et al.*, 1998).

The effectiveness of a variety of detergents in solubilising OmpF was assessed by measuring the light scatter. The detergents DM, $C_{12}E_8$, cholate and deoxycholate were very effective in solubilising the SR Ca^{2+}-ATPase, a typical α-helical membrane protein, but did not solubilise OmpF (Figures 3.5, 3.7 3.9 and 3.10). However the detergents OG and octyl-POE were seen to be highly effective in solubilising OmpF as well as the SR Ca^{2+}-ATPase (Figures 3.6 and 3.8). Octyl-POE was synthesised by Rosenbusch to provide a detergent with a high cmc and that forms well-defined micelles, for purification and crystallisation of OmpF (Garavito & Rosenbusch, 1985).

SDS is a highly denaturing ionic detergent that is widely used for these properties in polyacrylamide gel electrophoresis. These same properties prevent its use in reconstitutions. The non-ionic detergents are, however, less invasive to the native protein structure and are popular choices for reconstitutions. Some of the commonly employed nonionic detergents are derivatives of polyoxyethyleneglycol, which are easily manufactured on a large scale (Helenius & Simons, 1975). The nature of the polymerisation process means the products are heterogeneous, unless fractionated (Moller *et al.*, 1986). A limitation to their use is that many members of this group have low cmc values. Octyl-POE, however, has a relatively high cmc as shown in Table 3.1, which makes it a useful detergent in reconstitution studies. The polyoxyethylene glycol chain of octyl-POE is replaced by a glucose residue in OG (Moller *et al.*, 1986). OG is homogeneous and has an exceptionally high cmc (see Table 3.1), which has made it a

popular choice in membrane work (Helenius *et al.*, 1979). The concentrations of both detergents required to solubilise OmpF were higher than the cmc, i.e., results showed almost complete solubilisation with concentrations of 7 mM and 40 mM for octyl-POE and OG, respectively (Figures 3.6 and 3.8). Both octyl-POE and OG have high cmc values and are therefore relatively easy to remove when used in reconstitution systems.

Octyl-POE was chosen for further reconstitution studies with OmpF, because of its ability to solubilise OmpF, as seen in the light scatter studies, its commercial availability and also its use in the purification of OmpF (Garavito & Rosenbusch, 1985). Fluorescence quenching by bromine-containing lipids was used to demonstrate that reconstitution had occurred. OmpF was reconstituted into lipid bilayers at a 600:1 mole ratio of lipid-to-protein, using various concentrations of the octyl-POE. Each OmpF monomer contains two Trp residues: Trp 61 is found at the trimer interface and Trp 214 is found at the outer wall, in contact with the lipid matrix (Figure 3.10) (Cowan *et al.*, 1992). Quenching of the fluorescence emission from one or both of these Trp residues, when OmpF is reconstituted into bilayers of di(Br_2C18:0)PC, would indicate contact between the fluorophore, Trp, and the quencher, di(Br_2C18:0)PC (East & Lee, 1982). Thus a reduction in the fluorescence of OmpF reconstituted in di(Br_2C18:0)PC, relative to the fluorescence emission from OmpF reconstituted in di(C18:1)PC, can be taken as evidence that the protein and lipid components of the reconstitution are mixing.

The formation of membranes after detergent removal has been described as the mirror image of the solubilisation process (Rigaud *et al.*, 1995). Membranes are reformed upon removal of detergents because the hydrophobic regions of proteins and lipids are no longer protected from the aqueous environment by detergent molecules. Exposure to the aqueous surroundings is energetically unfavourable and so the hydrophobic moieties of lipids and proteins will associate (Helenius & Simons, 1975). Where there is incomplete removal of detergent the efficiency of reconstitution will be reduced.

In these reconstitutions octyl-POE was used to solubilise both the lipid and the protein. Octyl-POE has a high cmc, therefore, detergent removal can be achieved most simply by sample dilution. This requires that the concentration of octyl-POE be sufficiently low following dilution to allow membranes to reconstitute. As shown in Table 3.2 when the concentration of octyl-POE in the reconstitution mix was low, a 50 ± 2 % quenching of fluorescence was seen following a dilution of 300-fold. The maximal quenching levels were obtained using 31.79 mM and 22.0 mM octyl-POE in the reconstitution mixture (Figure 3.12). At these concentrations it was presumed that after a 300-fold dilution into the assay cuvette the detergent was not interfering with the reconstitution process and that a further reduction in the octyl-POE concentration used would not alter this result. Support for this was obtained by increasing the dilution factor for the same sample from 300-fold to 1500-fold (Figure 3.13). The same level of quenching was obtained in this experiment (Table 3.2). The reconstitution of OmpF was subsequently performed by solubilising a 600:1 mole ratio of lipid-to-protein with a final octyl-POE concentration of 22.0 mM and removing the detergent with a 300-fold dilution.

To determine whether the method of detergent removal had an effect on the reconstitution of OmpF detergent removal was also performed by dialysis and using Bio-Beads SM-2. Biobeads are composed of a large number of highly crosslinked microspheres and adsorb organics from aqueous solution. The fluorescence quenching level in di(Br_2C18:0)PC was similar for dilution, dialysis or using Bio-Beads (Table 3.2).

SDS-PAGE analysis was used to determine if the native trimeric structure of OmpF was intact after reconstitution. Interactions between monomers are very stable and mean the protein can withstand temperatures up to 70 °C in SDS buffer without denaturation (Garavito & Rosenbusch, 1985). The aromatic residues lining the protein barrel walls will interdigitate with small aliphatic residues from opposite walls (Cowan *et al.*, 1992). Numerous hydrogen bonds are also made between loop 2 of one monomer and loops 2, 3, and 4 of the adjacent monomer. In addition, strong salt bridges are made

between loop 2 and the Arg residues in loop 3 of an adjacent monomer. As detergent removal by dilution would leave the sample too dilute to analyse by SDS-PAGE, only those reconstituted protein samples that had the detergent removed by dialysis or using Biobeads were analysed. The samples, which were not subjected to heat-denaturation, had an apparent M_r of 90 k, corresponding to that previously seen for OmpF trimers (Figure 3.14 and 3.15). It was therefore concluded that the native trimeric structure of OmpF is not altered by octyl-POE-mediated reconstitution in non-native lipids. As the maximum level of quenching seen was 50 %, and it is seen that the native structure is not denatured by reconstitution, it was presumed that only Trp 214 is in contact with the lipid and that Trp 61 found at the trimer interface is not in contact with the lipid.

The reconstituted samples were also analysed on sucrose density gradients. The samples were loaded onto gradients after detergent removal by dialysis. The majority of the reconstituted samples were found in the intermediate fractions 3-5 (10-15 % sucrose) (Figure 3.17). The lipid-to-protein molar ratio in these fractions was between 300 and 700:1. The lipid control, being less dense, was found in the upper fractions containing the lower concentrations of sucrose. The protein controls, however, were found in the lower more dense fractions (Figure 3.16). The fluorescence emission spectra of 0.12 nmols of di(C18:1)PC- and di(Br_2C18:0)PC -reconstituted OmpF that were fractionated from the sucrose gradients were measured and showed a 48 % reduction in the fluorescence when reconstituted in di(Br_2C18:0)PC (Figure 3.18). This was comparable to the quenching levels seen for the different reconstitution methods that were looked at (Table 3.2).

CHAPTER 4

CHARACTERISATION OF TRYPTOPHAN RESIDUES IN OMPF

4.1 Introduction

4.1.1 Aromatic Residues in Membrane Proteins

The interfacial region between the hydrophobic fatty acyl chains and the polar head groups of membrane lipid presents a complex environment to the lipid-exposed surfaces of integral membrane proteins. Amino acids, which are commonly found at this interface, have been termed 'anchoring' residues and include the aromatic amino acids – Trp and Tyr, and positively charged amino acids, such as Lys residues (Landolt-Marticorena *et al.*, 1993; Yau *et al.*, 1998; Koeppe *et al.*, 1998; Killian & von Heijne, 2000). Phe residues can additionally be found in the hydrophobic segments (Landolt-Marticorena *et al.*, 1993). Studies using Trp analogues have shown them to bind in the glycerol backbone and lipid headgroup region of the bilayer (Yau *et al.*, 1998). Killian *et al* suggest that Trp are preferentially located near the carbonyl group of surrounding lipids, with the indole imino moiety positioned near the centre of the lipid carbonyl region and the fused aromatic rings in contact with the lipid acyl chains (Killian & von Heijne, 2000). In contrast, Yau *et al* have defined the preferential localisation of Trp residues at the interface to be a balance between the hydrophobic effect that keeps it out of the aqueous phase, complex electrostatic interactions that favours residing in the hydrated headgroup region, and cohesive interactions between the fatty acyl chains that repel it (Yau *et al.*, 1998). The position of Lys residues is thought to be more flexible but it is thought that the long aliphatic side chain will be positioned in the hydrophobic bilayer where they will 'snorkel' up the interfacial region where the positively charged amine moiety will be preferentially located near the phosphate groups (Killian & von Heijne, 2000).

The hydrophobic band of amino acids encircling the porin trimer is bordered at each end by rings of aromatic residues (Cowan *et al.*, 1992), as shown in Figure 4.1.

Similar arrangements are seen in other membrane proteins including the light harvesting centre and bacteriorhodopsin (von Heijne, 1996). It is believed that more rigid membrane proteins, such as porin, requiring very little structural changes to function, will have Trps (and Tyrs) as anchoring residues. Those membrane proteins, however, whose functioning requires conformational changes will employ more flexible membrane anchors (Killian & von Heijne, 2000).

4.1.2 Studying Trp Residues

The sensitivity of the fluorescence of Trp residues to quenching agents allows the accessibility to aqueous and organic quenchers to be determined (Lakowicz, 1983). This sensitivity has been attributed to the propensity of the indole ring to donate electrons (Lakowicz, 1983). Detailed analysis of individual Trp residues, however, can be made difficult by the existence of multiple Trp residues in a protein and because the emission from each is dependent on solvent effects. Polarity has a large influence on the emission of Trp residues (Lakowicz, 1983). The emission maxima of Trp residues in water occurs at 348 nm. In a protein, however, the emission maxima are generally blue-shifted with respect to Trp residues in water, because the Trp will be shielded to varying extents from the aqueous environment in the protein. Upon denaturation of proteins in urea or guanidium hydrochloride the emission spectra of proteins will be red-shifted, as all the Trp residues are exposed. The emission from a multitryptophan protein will therefore be composed of the overlapping spectral contributions from each individual Trp (Lackowicz, 1983).

Another complication in analysing Trp fluorescence is the spectral contribution of Tyr residues (Lakowicz, 1983). The adsorption at 280 nm is due to both Tyr and Trp residues. Tyr residues have an emission maximum centred around 303 nm and unlike Trp they are relatively insensitive to solvent polarity. Tyr emission is, however, absent in many proteins when excited at 280 nm because of energy transfer from the Tyr residues to the Trp and also because of Tyr fluorescence quenching.

Energy transfer between Tyr and Trp residues is a highly efficient process, occurring at distances of up to 14 Å (Lakowicz, 1983). Tyr emission can usually be avoided by exciting at wavelengths longer than 295 nm where Trp residues are selectively excited.

4.1.3 Making Recombinant Proteins

The structural and functional characterisation of proteins has been greatly accelerated by advances made in the field of molecular biology. These techniques enable specific alterations to protein structure via changes in the gene sequence. Proteins with primary sequences differing by only a single amino acid can now be easily constructed. There are several methods to choose from in the construction of a recombinant protein. The polymerase chain reaction (PCR), for example, is a powerful technique that allows quick and easy modification of DNA fragments. High fidelity is assured with thermostable proof-reading enzymes like *Pfu* polymerase.

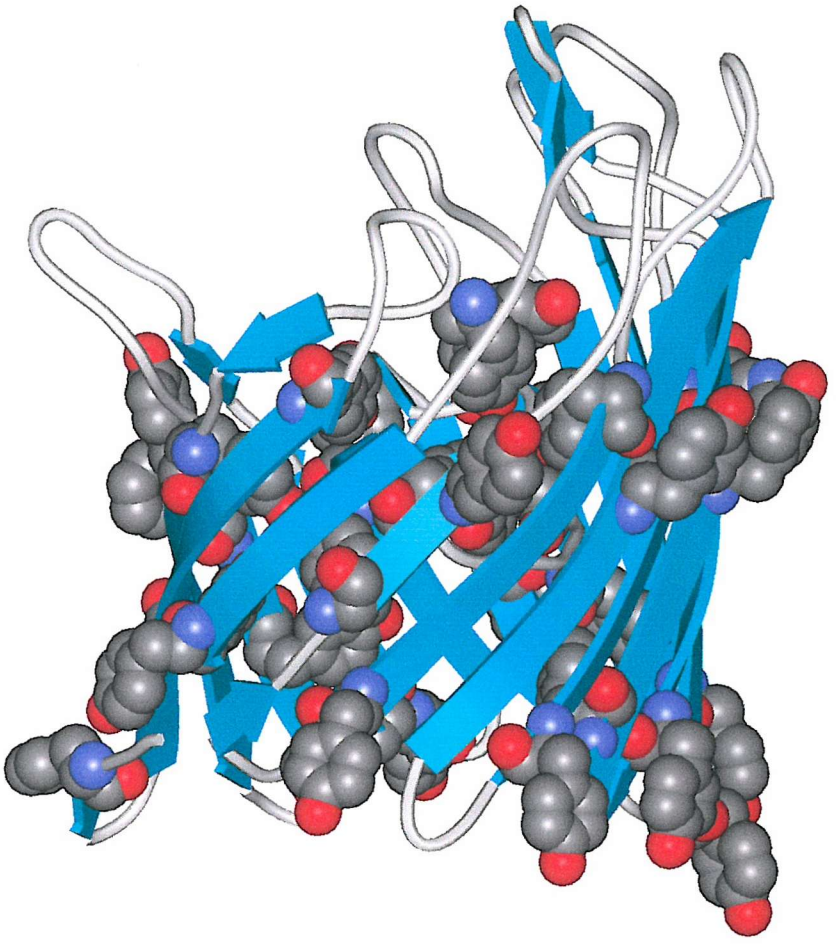

Figure 4.1: Crystal structure of the OmpF monomer showing the arrangement of aromatic residues

Aromatic residues are presented in spacefill format and can be seen to form two distinct belts at either side of the transmembranous hydrophobic band (PDB file 1OMPF).

4.2 Materials and Methods

4.2.1 Materials

Promega

Cloned *Pfu* polymerase
Wizard DNA clean-up system
Wizard PCR clean-up system

Boehringer

T4 DNA Ligase

Amersham
T7 Sequenase™ Version 2.0

Millipore
Nitrocellulose filters

New England Biolabs
1.0 kb DNA ladder
*Sal*I
*Eco*RI
*Hind*III

4.2.2 Methods

4.2.2.1 Mutation of Trp Residues in OmpF by Recombinant PCR

Mutants were made from the *ompF* template, shown in Figure 4.2, held in the high-copy number DNA plasmid pUC18. This was cloned into the vector as an

*Eco*RI-*Hind*III fragment and was kindly supplied by Dr Lakey, Department of Biochemistry, University of Newcastle. The strategies used to construct W61F and W214F are shown in Figures 4.3 and 4.4 respectively, and the primers used are detailed in Table 4.1.

The thermostable *Pfu* polymerase was used for all reactions because of its proofreading activity. Reactions included 125 ng of each primer, 5 µl of 10 x reaction buffer, 1 µl of *Pfu* polymerase, 0.8µl of dNTP mix (25 mM each), and 5-50 ng of DNA template. PCR conditions used were 1 cycle at 95 °C for 45 seconds, 25 cycles at 95 °C for 45 seconds, T_m (melting temperature of primer) - 5 °C for 45 seconds and 72 °C for a time period allowing 2 minutes/kilobase (kb). A holding temperature of 4 °C was used. All products were analysed on 1 % agarose gels and purified using Promega PCR DNA clean-up kits. The final 1.089 kb products were digested with *Eco*RI and *Hind*III prior to ligation with pUC18 and pGBF96.

4.2.2.2 Extraction of DNA from Agarose Gels

Wild-type *ompF* was digested from pUC18 and pGBF96 with *Eco*RI and *Hind*III restriction enzymes. The vectors pUC18 (2.96 kb) and pMS119 (3.97 kb) were excised from 1 % agarose gels with sterile scalpels and the excised agarose bands were snap-frozen in liquid nitrogen. The frozen agarose was then placed in 0.5 ml thick-walled tube that had been plugged with siliconised glass wool. A hole was made in the base of these tubes, using a 23 g hypodermic needle, and they were placed in 1.9 ml microfuge tubes, followed by centrifugation at 6,000 x g for 5 minutes. The eluted DNA was isolated using the Wizard DNA clean-up system.

4.2.2.3 Ligation Reactions

Ligations were carried out using T4 DNA ligase enzyme and buffers according to manufacturer instructions. Controls included samples with vector alone, insert alone or no DNA. Reactions were carried out at 16 °C overnight, and were dialysed in 10 % glycerol using 0.025 μm nitrocellulose dialysis membranes (Millipore) for 30 minutes prior to electroporation.

4.2.2.4 Small-Scale Preparation of Plasmid DNA by Alkaline Lysis

This cheap and efficient method was used for screening multiple transformants.

Solution 1	50 mM glucose
	25 mM Tris (pH 8.0)
	10 mM EDTA (pH 8.0)
Solution 2	0.2 M NaOH
	1 % SDS
Solution 3	60 % 5 M potassium acetate

10 ml antibiotic-containing LB cultures were inoculated with single colonies and were grown for 12-16 hours at 37 °C. The cells were centrifuged on a Heraeus Labofuge 400e, and the pellets were suspended by vortexing in 100 μl of ice-cold solution 1. 200 μl of freshly prepared solution 2 was added, followed by 150 μl of ice-cold solution 3, before leaving to stand on ice for 5 minutes. Samples were then centrifuged at 14,000 x g on a bench top microfuge for 5 minutes. The supernatant was vortexed with an equal volume of phenol/chloroform and then centrifuging at 14,000 x g for 2 minutes. DNA was precipitated from the supernatant by mixing with 2 volumes of ethanol at room temperature. Samples were left to stand for 2 minutes at room temperature before centrifuging at 14,000 x g for 5 minutes. Pellets were washed in 1

ml of ice-cold 70% ethanol and re-centrifuged. These pellets were left to dry for 3 minutes in a vacuum dessicator, before redissolving in 50 µl of TE buffer, pH 8.0, containing 20 µg/ml RNAase. To check whether the selected colonies contained the recombinant insert, restriction enzyme digests were performed on all samples with *Eco*RI and *Hind*III, in final volumes of 10 µl, according to manufacturers instructions. Products were visualised after separation by electrophoresis on agarose gels, as described in Section 2.2.2.3.

4.2.2.5 DNA Sequencing

DNA sequencing was carried out using the T7 Sequenase™ Version 2.0 sequencing kit. This kit employs a chain-termination DNA sequencing method. All steps were performed according to manufacturer instructions. Plasmid DNA of high purity is required for this method so all samples were prepared using Promega miniprep kits. Approximately 0.4 kb can be sequenced by this method. The DNA sequences were analysed for both mutants in the vectors pGBF96 and pUC18. The DNA containing the mutation at residue 61 was sequenced using the 5' end (+) primers pUC Start and pMS Start in the vectors pUC18 and pGBF96, respectively. The mutation at residue 214 was sequenced in both vectors with the (-) primer 829 that binds at 0.829 kb in the *ompF* insert.

4.2.2.6 Construction of the Double mutant W61F/W214F using restriction enzymes.

The double mutant W61F/W214F was produced by combining DNA fragments from W61F and W214F. The wild-type ompF DNA sequence, shown in Figure 4.2, has a *Sal*I restriction site at 0.508 kb, located between the two Trp codons. 50 µl restriction digests were performed with the enzymes *Eco*RI and *Sal*I on the mutants W61F and W214F in the vector pGBF96. The following restriction products

were extracted from 1 % agarose gels as described in Section 4.2.2.2: 0.513 kb fragment from W61F and the 4.551 kb fragment from W214F. The extracted DNA fragments were isolated with a Promega DNA clean-up kit and ligated as described in Section 4.2.2.3, before being transformed by electroporation into BZB1107 cells.

4.2.2.7 Mutant Purification

All mutants were purified as described for wild-type OmpF in Section 2.2.3.2.

4.2.2.8 Fluorescence Characterisation

4.2.2.8.1 Reconstitution into di(Br_2C18:0)PC and di(C18:1)PC

W61F, W214F and W61F/W214F were reconstituted by the dilution method into di(Br_2C18:0)PC and di(C18:1)PC as outlined in Section 3.2.2.2. Wild-type OmpF was included as a positive control. Fluorescence spectra of 0.12 nmols of protein in 3mls of 20 mM Hepes, pH 7.2, 1 mM EGTA were recorded and were corrected for light scattering by subtracting the spectra of a sample of reconstituted phospholipid lacking protein. Fluorescence measurements were performed on an SLM8000C fluorimeter at 25 ^{o} C using an excitation wavelength of 280 nm. Fluorescence emission spectra were recorded between 300 and 400 nm and slit widths of 4 nm were used for both excitation and emission.

The level of fluorescence quenching in di(Br_2C18:0)PC was studied as a function of the excitation wavelength under identical conditions. Excitation wavelengths between 270 and 290 nm were used.

Reconstituted samples of the mutants were also prepared using the dialysis method as described in Section 3.2.2.4 to allow for SDS-PAGE analysis.

4.2.2.8.2 Quenching with Spin Labelled Fatty Acid

0.1 mM 5-doxyl stearic acid (Figure 4.5) made up in dimethyl sulfoxide (DMSO) was titrated into a cuvette containing 0.12 nmols OmpF. OmpF that had been reconstituted in di(Br_2C18:0)PC or purified, native OmpF (i.e., OmpF in 20 mM NaH_2PO_4, pH 7.2, 1 % octyl-POE) were used. Fluorescence spectra were recorded for each in 20 mM Hepes, pH 7.2, 200 mM KCl, or in 20 mM Hepes, pH 7.2, 1 mM EGTA, using an excitation wavelength of 280 nm.

4.3 Results

4.3.1 Recombinant PCR

Figures 4.6 and 4.7 show the PCR products used in the construction of W61F and W214F. The two fragments generated for W61F were 0.278 and 0.872 kb, and for W214F were 0.730 and 0.408 kb. The two PCR products for each mutant have a double-stranded overlapping fragment of 34 and 22 base pairs at the site of the mutation in W61F and W214, respectively. When the single-stranded PCR products are combined heteroduplexes form between the complementary regions as schematised in Figures 4.2 and 4.3. Using the end primers pUC Start and pUC End, the full-length sequences for each mutant were produced (shown in Figure 4.8) from those heteroduplexes with free 3'-OH.

4.3.2 Analysis of DNA Products for Ligation Reactions

pUC18 and pGBF96 that had been digested with *Eco*RI and *Hind*III were separated by agarose gel electrophoresis are shown in Figure 4.9. The extracted vectors (see Figure 4.10) were isolated using Promega's DNA clean-up kit before ligating with the PCR products, which had also been digested with *Eco*RI and *Hind*III.

4.3.3 Purification and Sequencing of Recombinant DNA.

BZB1107 cells were transformed with the recombinant *ompF* DNA held in the vector pGBF96, to be used for protein expression. DH5α cells were transformed with the recombinant DNA held in pUC18, to be used for any further DNA manipulations. The control ligation products were also transformed into these two *E. coli* strains. All transformants selected from LB-Amp and LB-Amp-Kan agar plates contained recombinant ompF at 1.089 kb and the vectors at 2.96 and 3.97 kb for pUC18

and pGBF96 respectively. Figure 4.11 and 4.12 respectively show pUC18 and pGBF96 plasmid DNA holding W61F and W214F that were used for sequencing reactions.

Figures 4.13 and 4.14 show the sequence near the mutation sites of W61F and W214F, respectively, in the vector pGBF96. The sequences show the presence of the codon TTT, which codes for Phe, in place of the Trp codon, TGG, for Trp 61 (at 0.247 kb) and Trp 214 (at 0.706 kb). Identical results were seen for both mutants in the pUC18 vector.

4.3.4 W61F/W214F Production

To produce the Trp-less mutant, W61F/W214F, the *omp*F gene's internal *Sal*I restriction site was utilised. The products of a restriction digest of W61F and W214F with *Sal*I and *Eco*RI were separated on 1 % agarose gels as shown in Figure 4.15A. The 0.513 kb fragment of W61F and the 4.551 kb fragment from W214F were extracted from the agarose gel by the squeeze-freeze method and isolated using Promega DNA clean-up kits (seen in Figure 4.15B). The 0.513 kb fragment of W61F was ligated with the 4.551 kb fragment from W214F to provide a Trp-less mutant in the pGBF96 vector. The vector was transformed into the BZB1107 cells by electroporation. The plasmid was purified from the transformed cells and the 1.089 kb recombinant insert was visualised after digesting with *Eco*RI and *Hind*III, as shown in Figure 4.16.

4.3.5 Purification of OmpF Mutants

The mutant proteins were purified according to the method of Rummel (personnel communication) and are shown beside the wild-type OmpF in Figure 4.17. Samples of each were denatured by boiling at 100 °C for 5 minutes, and show an apparent M_r of 36 k. Native samples of each were also analysed and show an apparent M_r of 90 k.

4.3.6 Fluorescence Studies

4.3.6.1 Reconstitution in di(C18:1)PC and di(Br_2C18:0)PC

Using the mutants described enabled the fluorescence spectra of the two Trp to be studied independently - Trp 61 in the W214F mutant, and Trp 214 in the W61F mutant. Figure 4.18 shows that the fluorescence intensities of W61F and W214F reconstituted in di(C18:1)PC are approximately half that of the wild-type OmpF. W214F emission is more blue-shifted than that of wild type and W61F. As Trp emission wavelengths generally decrease with decreasing environmental polarity (Lakowicz, 1983), this would suggest that Trp 61 at the trimer interface is in a more hydrophobic environment than Trp 214. The non-quenchable fluorescent moiety of the wild-type OmpF in di(Br_2C18:0)PC is also blue-shifted with respect to that of wild type OmpF in di(C18:1)PC (Figure 4.18B). These data would point to Trp 61 being the nonquenchable moiety. The Trp-less mutant W61F/W214F has a high fluorescence emission that is centred at 305 nm due to the 29 Tyrs in OmpF. The lack of extensive Tyr fluorescence in the spectra of wild type and single Trp proteins suggest that Tyr fluorescence is quenched by energy transfer to the Trp.

In di(Br_2C18:0)PC quenching of 50 ± 2 % of the fluorescence intensity of wild type OmpF is seen, 35 % of the fluorescence of W214F and 64 % of W61F, using an excitation wavelength of 280 nm (Figure 4.18B). Quenching of the fluorescence of the Trp-less mutant is approximately 44 %. The effect of varying the excitation wavelength on the level of quenching in di(Br_2C18:0)PC is shown in Table 4.2. The level of quenching is expressed as F/F_o, where F is the fluorescence emission in di(C18:1)PC and F_o is the intensity of fluorescence emission in di(Br_2C18:0)PC. The results show the quenching levels of the wild-type and W61F proteins to be almost independent of the excitation wavelength. The quenching of W214F, however, is seen to decrease as the excitation wavelength is increased from 270 to 290 nm. At 290 nm the Trp fluorescence will be directly excited through the Trp residues, but at 270 nm significant excitation by energy transfer from Tyrs can occur. This suggests that the

quenching of W214F, excited at 280 nm, (seen in Figure 3.16) is due to quenching of the Tyr residues, and that di(Br_2C18:0)PC is unable to bind near Trp 61.

Reconstituted samples, prepared by the dialysis method, are shown on SDS-PAGE in Figure 4.19. All four proteins show an apparent M_r of 90 k, indicating that the trimeric structure of each is retained after reconstitution. Thus mutation of the Trp residues does not lead to disruption of trimer formation.

4.3.6.2 Quenching with 5-Doxyl Stearic Acid

Figures 4.20 shows the effect of addition of the fluorescence quencher 5-doxyl stearic acid on the fluorescence spectra of wild-type OmpF in 20 mM Hepes, pH 7.2 containing 1 mM EGTA. 5-doxyl stearic acid is clearly a very effective quencher of the Trp fluorescence of OmpF as the fluorescence of OmpF is quenched by up to 62 %, compared to only 50 ± 2 % by di(Br_2C18:0)PC. Fatty acids will be present predominately in the anionic form at pH 7.2, therefore, binding of fatty acids to lipid bilayers will be expected to result in a build-up of negative charge on the membrane, limiting further binding of the fatty acid. The experiment was therefore repeated at high ionic strength to reduce any charge effects. As shown in Figure 4.21 quenching is slightly more extensive in the presence of 200 mM KCl and is increased to 67 %. The level of quenching is plotted as a function of the spin-label concentration in Figure 4.22.

Figures 4.23 and 4.24 show the fluorescence spectra of W61F and W214F in the presence of increasing concentrations of 5-doxyl stearic acid. The maximum level of quenching achieved was 73 % and 45 % for W61F and W214F, respectively. In Figure 4.25 the level of quenching of the mutants are compared to the wild type by plotting as a function of the spin-label concentration. As seen with di(Br_2C18:0)PC a higher level of quenching is seen with W61F than with W214F, presumably because the accessibility of the Trp 61 at the trimer interface is more limited than the lipid-exposed Trp 214.

5-doxyl stearic acid was also titrated into samples of OmpF that had been reconstituted in di(Br_2C18:0)PC to determine whether further quenching could be achieved. The fluorescence spectra for wild-type, W61F and W214F in di(Br_2C18:0)PC are shown in Figures 4.26 to 4.28, respectively. It can be seen that a further 33 ± 2 % quenching is achieved for both W61F and wild type OmpF, on addition of 5-doxyl stearic acid. However, only an additional 25 % quenching of W214F is seen upon addition of the fatty acid quencher. In Figure 4.29 these results are compared as the level of quenching plotted as a function of the spin-label concentration. The fluorescence remaining in W61F, after exposure to di(Br_2C18:0)PC and 5-doxyl stearic acid is 0.13, compared to 0.24 for W214F, and 0.33 for wild type OmpF. These results suggest that 5-doxyl stearic acid may be able to bind to sites from which phospholipid is excluded.

Figure 4.2: DNA Sequence of the *ompF* gene, showing restriction enzyme sites.

This sequence was kindly presented by Dr Bainbridge, Biochemistry Department, University of Newcastle. The restriction sites *Eco*RI, *Hind*III, and *Sal*I are indicated on the 1.089 kb *ompF* gene.

```
                                                                                GAATTC
      Start                                                                     EcoRI
1     ATGATGAAGC  GCAATATTCT  GGCAGTGATC  GTCCCTGCTC  TGTTAGTAGC  AGGTACTGCA
61    AACGCTGCAG  AAATCTATAA  CAAAGATGGC  AACAAAGTAG  ATCTGTACGG  TAAAGCTGTT
121   GGTCTGCATT  ATTTTTCCAA  GGGTAACGGT  GAAAACAGTT  ACGGTGGCAA  TGGCGACATG
181   ACCTATGCCC  GTCTTGGTTT  TAAAGGGGAA  ACTCAAATCA  ATTCCGATCT  GACCGGTTAT
            Trp 61
241   GGTCAGTGGG  AATATAACTT  CCAGGGTAAC  AACTCTGAAG  GCGCTGACGC  TCAAACTGGT
281   AACAAAACGC  GTCTGGCATT  CGCGGGTCTT  AAATACGCTG  ACGTTGGTTC  TTTCGATTAC
321   GGCCGTAACT  ACGGTGTGGT  TTATGATGCA  CTGGGTTACA  CCGATATGCT  GCCAGAATTT
381   GGTGGTGATA  CTGCATACAG  CGATGACTTC  TTCGTTGGTC  GTGTTGGCGG  CGTTGCTACC
441   TATCGTAACT  CCAACTTCTT  TGGTCTGGTC  GACGGCCTGA  ACTTCGCTGT  TCAGTACCTG
                              SalI
501   GGTAAAAACG  AGCGTGACAC  TGCACGCCGT  TCTAACGGCG  ACGGTGTTGG  CGGTTCTATC
561   AGCTACGAAT  ACGAAGGCTT  TGGTATCGTT  GGTGCTTATG  GTGCAGCTGA  CCGTACCAAC
                                                          Trp 214
621   CTGCAAGAAG  CTCAACCTCT  TGGCAACGGT  AAAAAAGCTG  AACAGTGGGC  TACTGGTCTG
681   AAGTACGACG  CGAACAACAT  CTACCTGGCA  GCGAACTACG  GTGAAACCCG  TAACGCTACG
741   CCGATCACTA  ATAAATTTAC  AAACACCAGC  GGCTTCGCCA  ACAAAACGCA  AGACGTTCTG
801   TTAGTTGCGC  AATACCAGTT  CGATTTCGGT  CTGCGTCCGT  CCATCGCTTA  CACCAAATCT
                                                                    XbaI
881   AGAGCGAAAG  ACGTAGAAGG  TATCGGTGAT  GTTGATCTGG  TGAACTACTT  TGAAGTGGGC
941   GCAACCTACT  ACTTCAACAA  AAACATGTCC  ACCTATGTTG  ACTACATCAT  CAACCAGATC
1021  GATTCTGACA  ACAAACTGGG  CGTAGGTTCA  GACGACACCG  TTGCTGTGGG  TATCGTTTAC
1081  CAGTTCTAAT  AGAAGCTT
            Stop    HindIII
```

Figure 4.3: Recombinant PCR strategies for production of W61F.

W61F was constructed by recombinant PCR using 4 primers: pUC Start, pUC End, 233 and 266 (details on Table 4.1). The *ompF* template DNA was held in the vector pUC18 as an *Eco*RI-*Hind*III fragment. Using the primers pUC Start and 266, PCR reaction 1 produced the predicted 0.278 kb fragment. The second reaction, using the primers pUC End and 233, produced the predicted 0.872 kb fragment. To produce the full-length sequence, heteroduplexes were formed in a reaction between the 0.278 kb and 0.872 kb products. These heteroduplexes were amplified with the end primers pUC Start and pUC End to produce the mutated ompF sequence. All reactions were performed using cloned *Pfu* polymerase.

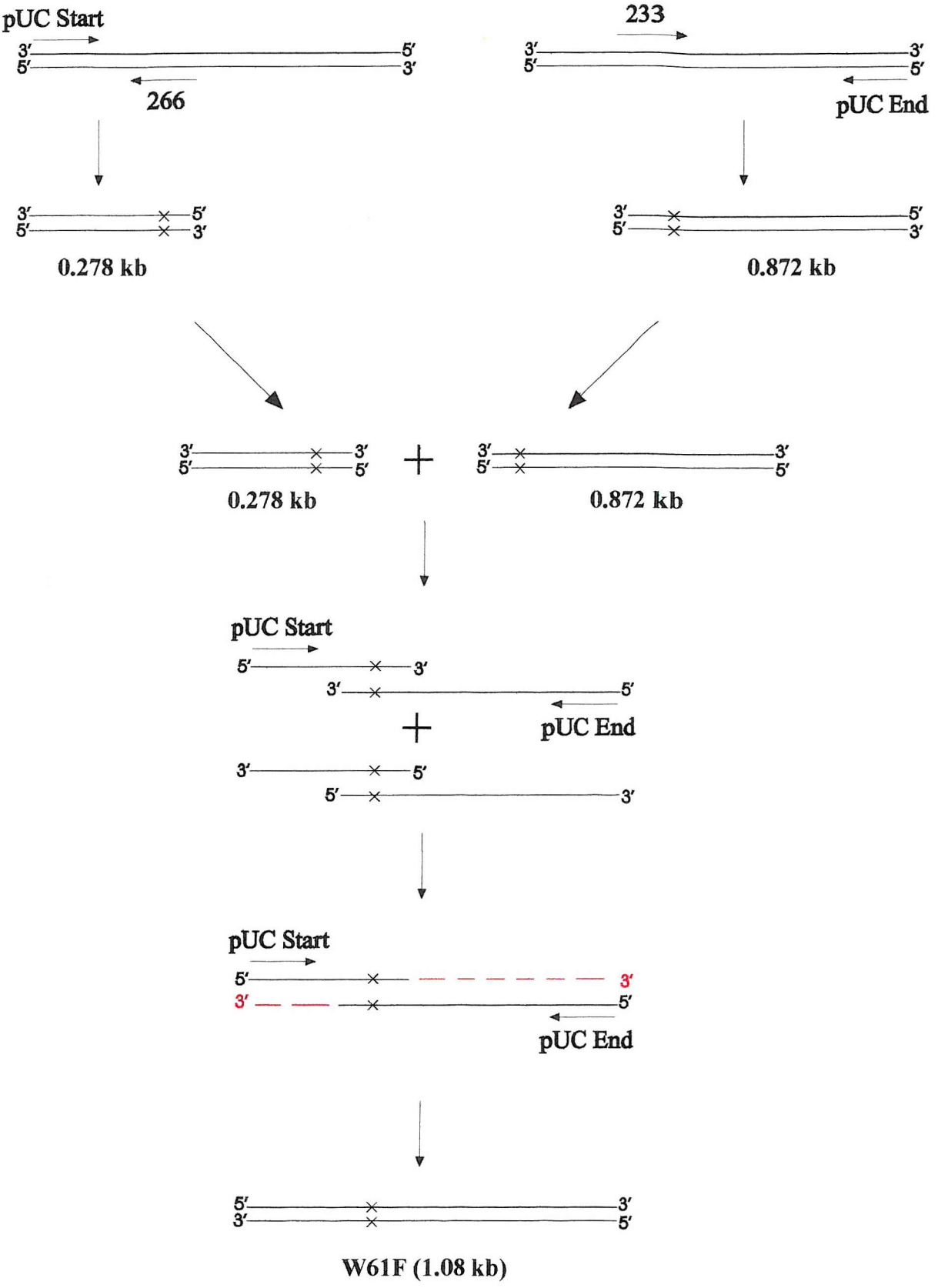
pUC Start
3′
5′
5′
3′
266
233
3′
5′
3′
5′
pUC End
3′
5′
5′
3′
0.278 kb
3′
5′
5′
3′
0.872 kb
3′
5′
3′
5′
0.278 kb
3′
5′
3′
5′
0.872 kb
pUC Start
5′
3′
3′
5′
pUC End
3′
5′
5′
3′
pUC Start
5′
3′
3′
5′
pUC End
5′
3′
3′
5′
W61F (1.08 kb)

Figure 4.4: Recombinant PCR strategies for production of W214FF.

W214F was constructed by recombinant PCR using 4 primers: pUC Start, pUC End, 697 and 718 (details on Table 4.1). The *ompF* template DNA was held in the vector pUC18 as an *Eco*RI-*Hind*III fragment. Using the primers pUC Start and 718, PCR reaction 1 produced the predicted 0.730 kb fragment. The second reaction, using the primers pUC End and 697, produced the predicted 0.408 kb fragment. To produce the full-length sequence, heteroduplexes were formed in a reaction between the 0.730 kb and 0.408 kb products. These heteroduplexes were amplified with the end primers pUC Start and pUC End to produce the mutated *ompF* sequence. All reactions were performed using cloned *Pfu* polymerase.

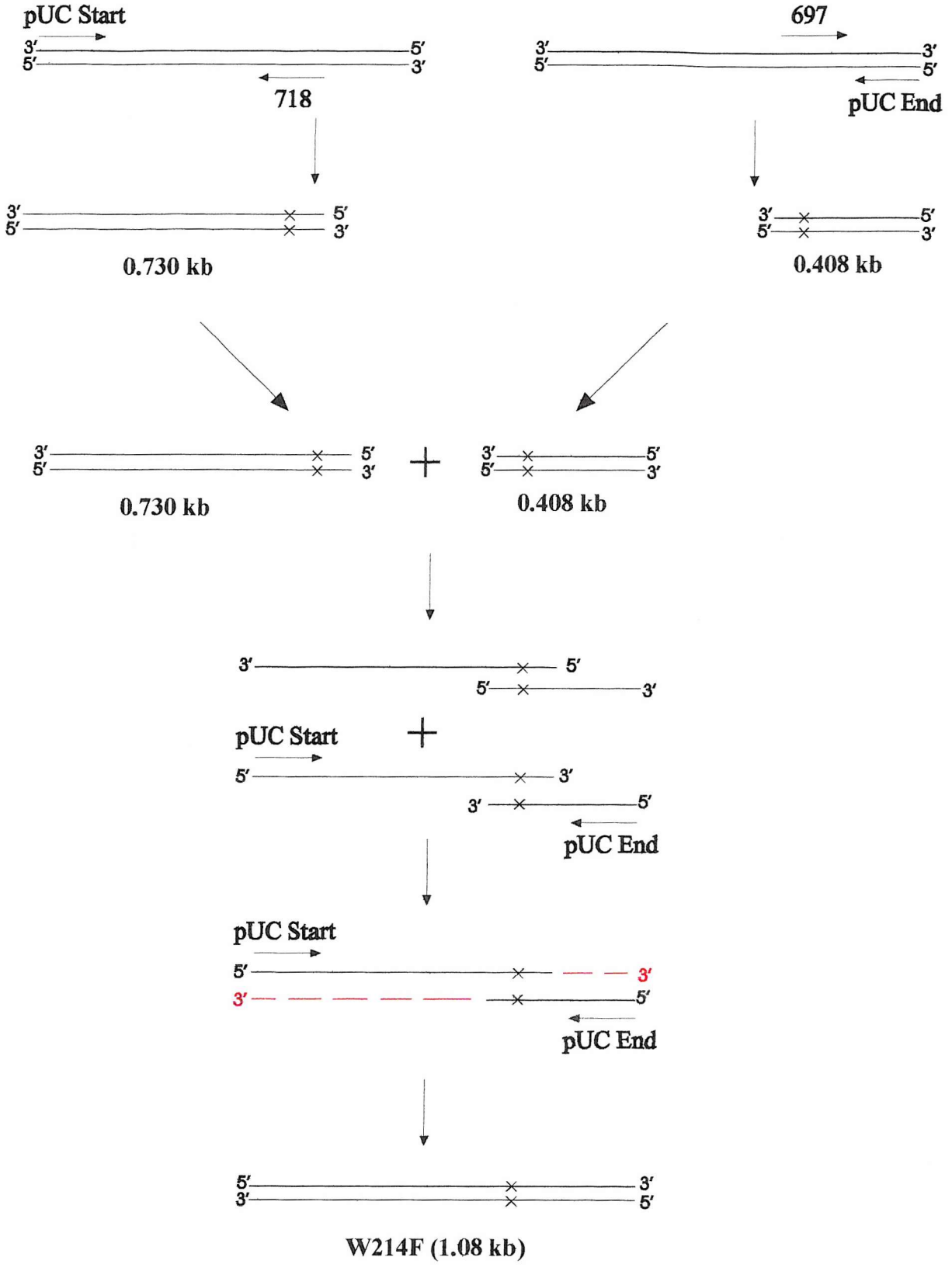
pUC Start
3′
5′
5′
3′
718
697
3′
5′
3′
5′
pUC End
3′
5′
5′
3′
0.730 kb
3′
5′
5′
3′
0.408 kb
3′
5′
5′
3′
0.730 kb
3′
5′
5′
3′
0.408 kb
3′
5′
5′
3′
pUC Start
5′
3′
3′
5′
pUC End
pUC Start
5′
3′
3′
5′
pUC End
5′
3′
3′
5′
W214F (1.08 kb)

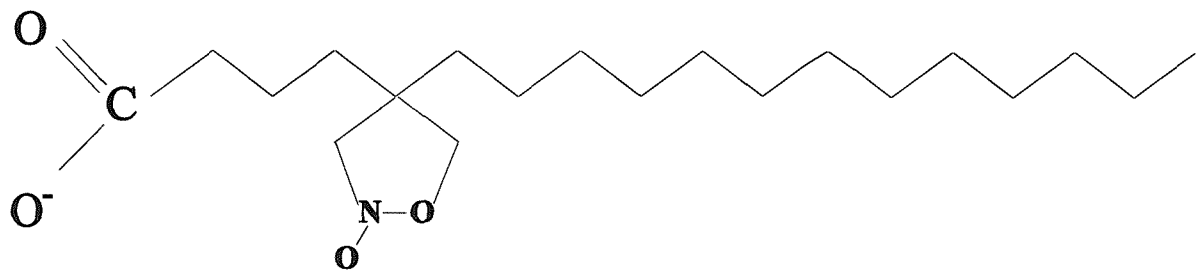

Figure 4.5: Structure of 5-Doxyl Stearic Acid

This figure was adapted from (Knowles *et al.*, 1976) and was drawn using CorelDraw. The doxyl group is attached to C-5 of the stearic acid chain.

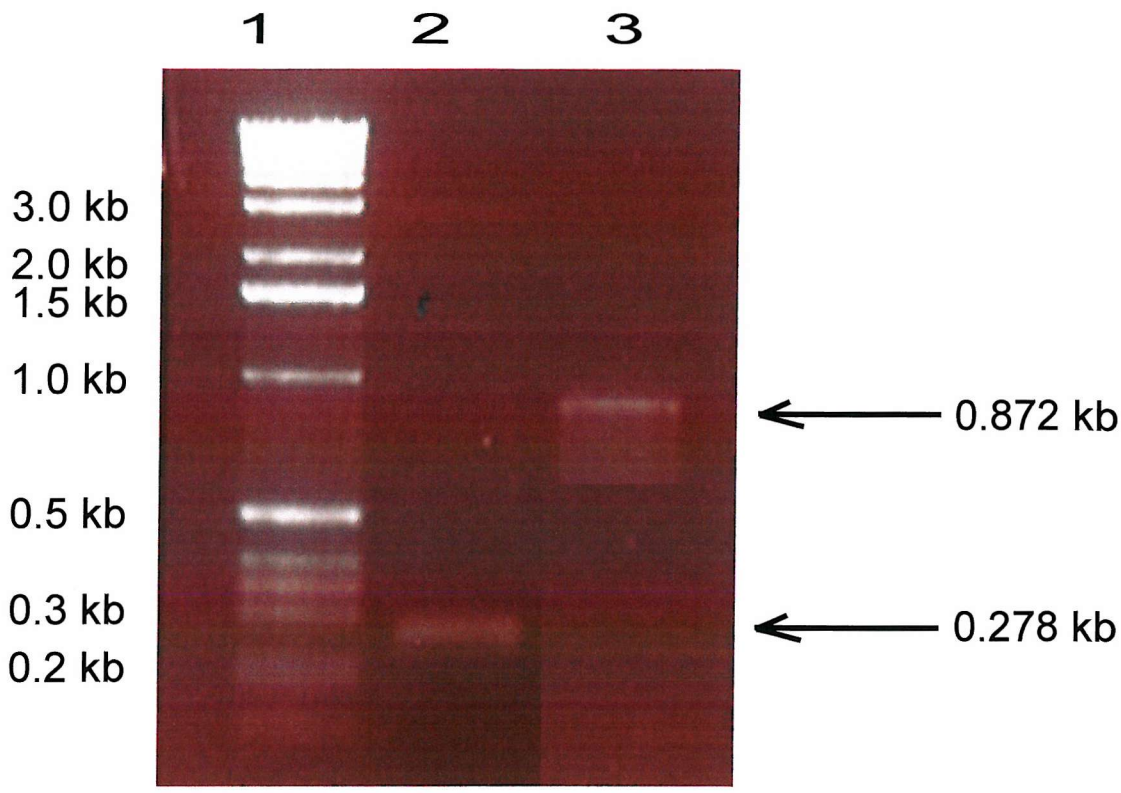

Figure 4.6: Products from W61F PCR reactions

Lane 1 contains a 1.0 kb ladder (New England Biolabs). Lanes 2 and 3 contain the PCR products of 0.278 kb and 0.872 kb from reactions 1 and 2, respectively. These DNA fragments were synthesised in 2 separate reactions by *Pfu* polymerase using the *ompF* gene held in pUC18 as a template. Reaction 1 used the primers pUC Start and 266 to produce a 0.278 kb fragment. Reaction 2 used the primers pUC End and 233 to produce a 0.872 kb fragment.

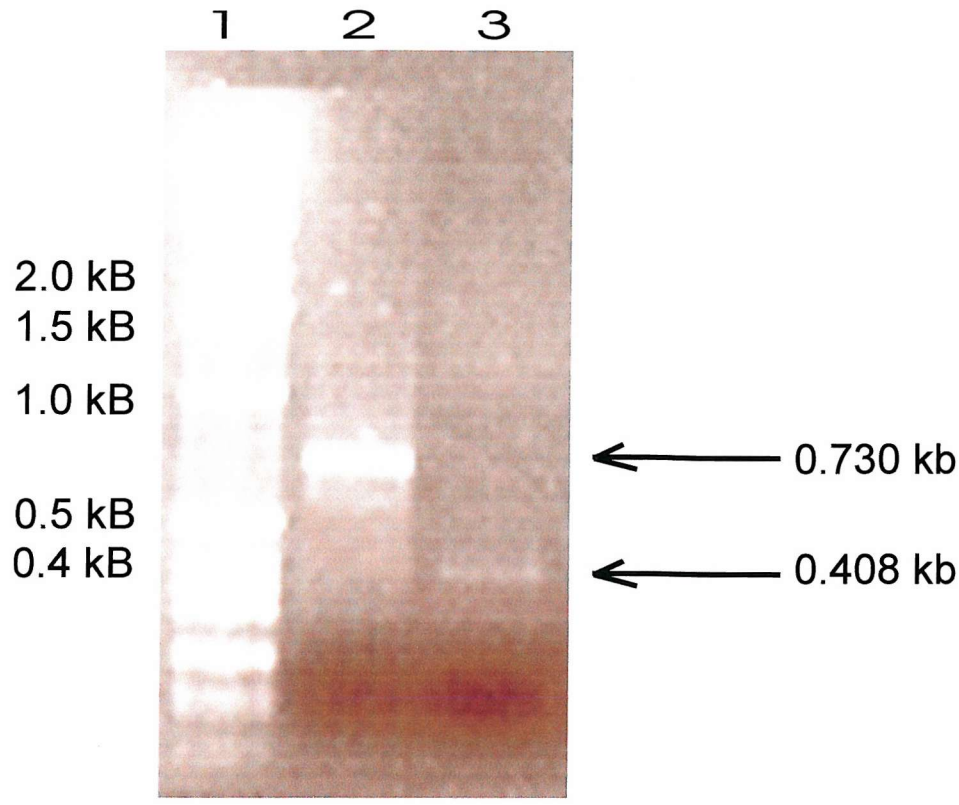

Figure 4.7: Products from W214F PCR reactions.

Lane 1 contains a 1.0 kb ladder. Lanes 2 and 3 contain the PCR products of 0.730 and 0.408 kb from reactions 1 and 2, respectively. These fragments were synthesised in 2 separate reactions by *Pfu* polymerase using the *ompF* gene held in pUC18 as a template. Reaction 1 used the primers pUC Start and 718 to produce a 0.730 kb fragment. Reaction 2 used the primers pUC End and 697 to produce a 0.408 kb fragment.

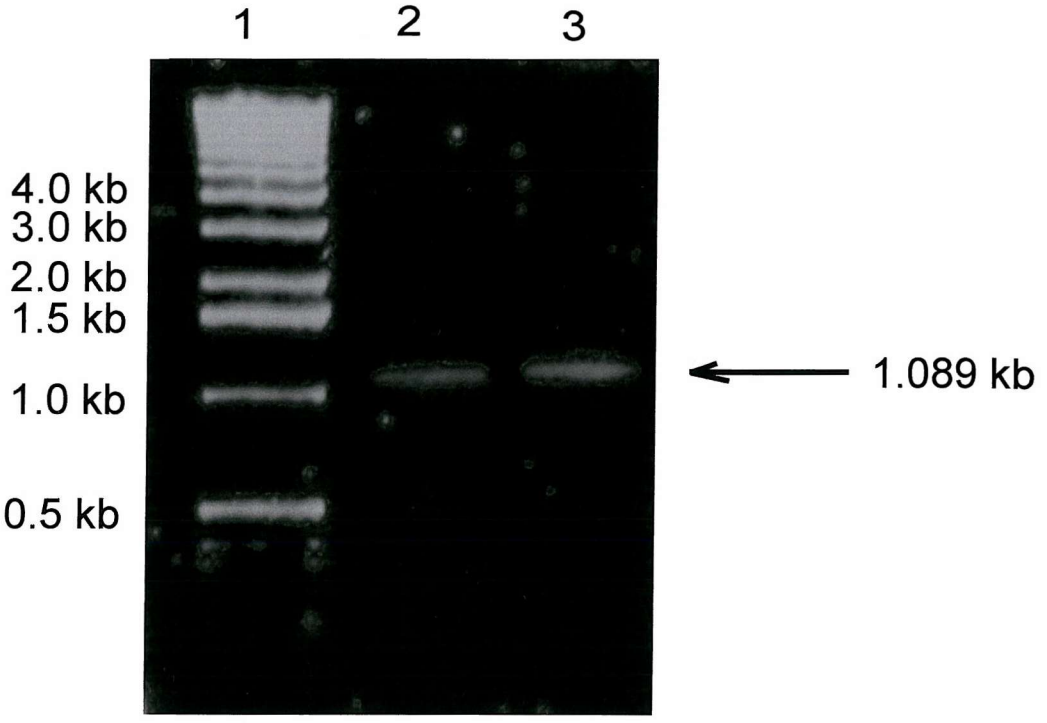

Figure 4.8: Full-length recombinant DNA for W61F andW214F.

Lanes 1 contains a 1.0 kb ladder. Lanes 2 and 3 contain the final PCR products of 1.089 kb coding for the recombinant *ompF* genes encoding the proteins W61F and W214F, respectively.

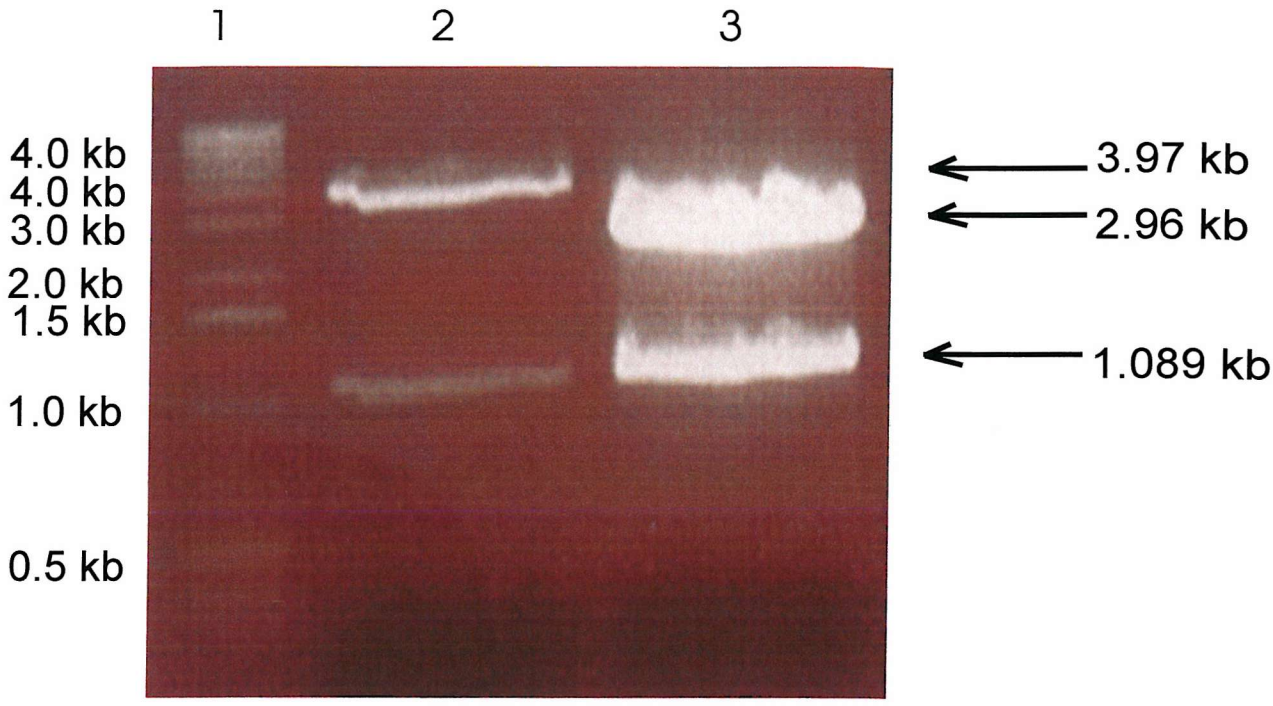

Figure 4.9: Digestion of vectors pUC18 and pGBF96 for gel extraction

pUC18 and pGBF96 were digested with *Eco*RI and *Hind*III in final volumes of 50 µl. Lane 1 contains 1.0 kb DNA ladder. Lanes 2 and 3 contain the *ompF* gene at 1.089 kb from digested pGBF96 and pUC18, respectively. Lane 2 has the vector pMS119 at 3.97 kb and lane 3 shows the pUC18 vector at 2.96 kb.

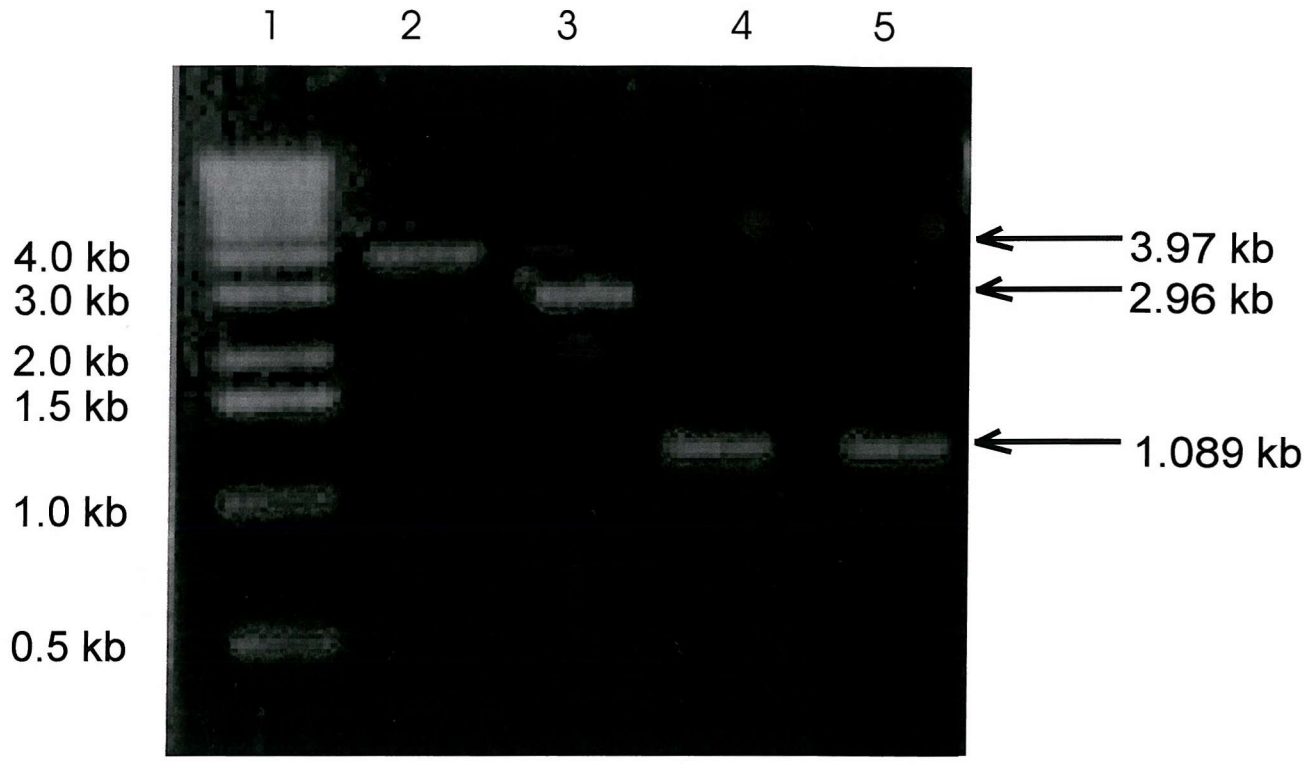

Figure 4.10: Extracted vectors and PCR inserts for ligation reactions

Lanes 1 contains 1.0 kb DNA ladder, lane 2 and 3 contain the vectors pMS119 (3.97 kb) and pUC18 (2.96 kb), respectively, and lanes 4 and 5 hold the DNA (1.089 kb) coding for W61F and W214F, respectively.

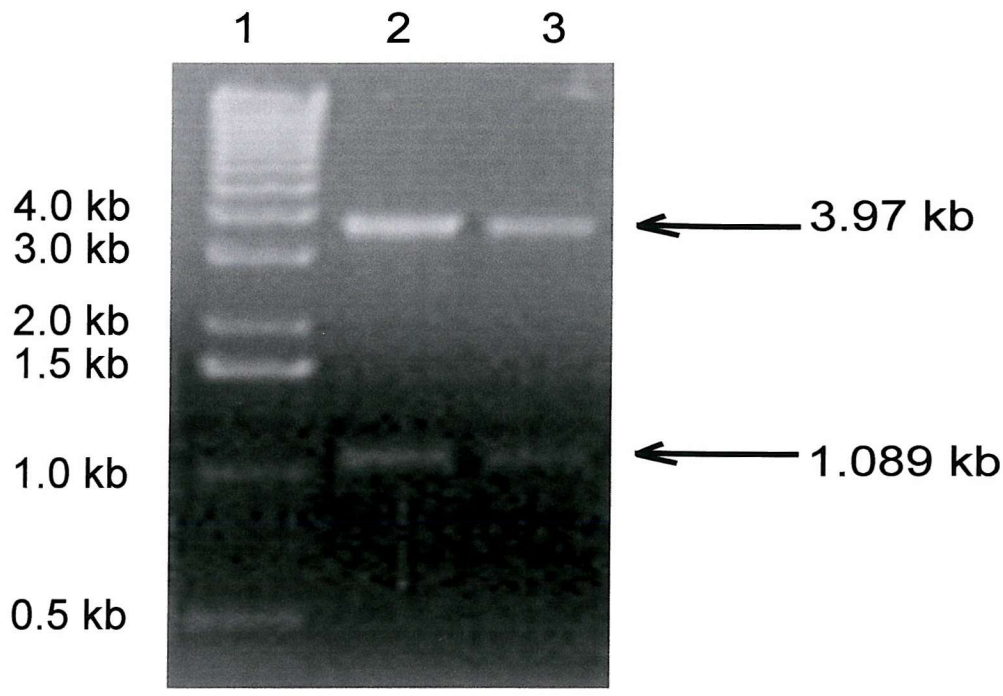

Figure 4.11: Recombinant pGBF96 DNA isolated from transformed *E. coli* cells.

Lane 1 contains a 1.0 kb DNA ladder, lanes 2 and 3 contain recombinant pGBF96 plasmid DNA selected from LB-Amp-Kan agar plates for the mutants W61F and W214F, respectively. Restriction digests of plasmid DNA purified from transformed colonies of each with *Eco*RI and *Hind*III show the *ompF* inserts of 1.089 kb and the vector pMS119 at 3.97 kb. Both DNA preparations were further analysed by DNA sequencing.

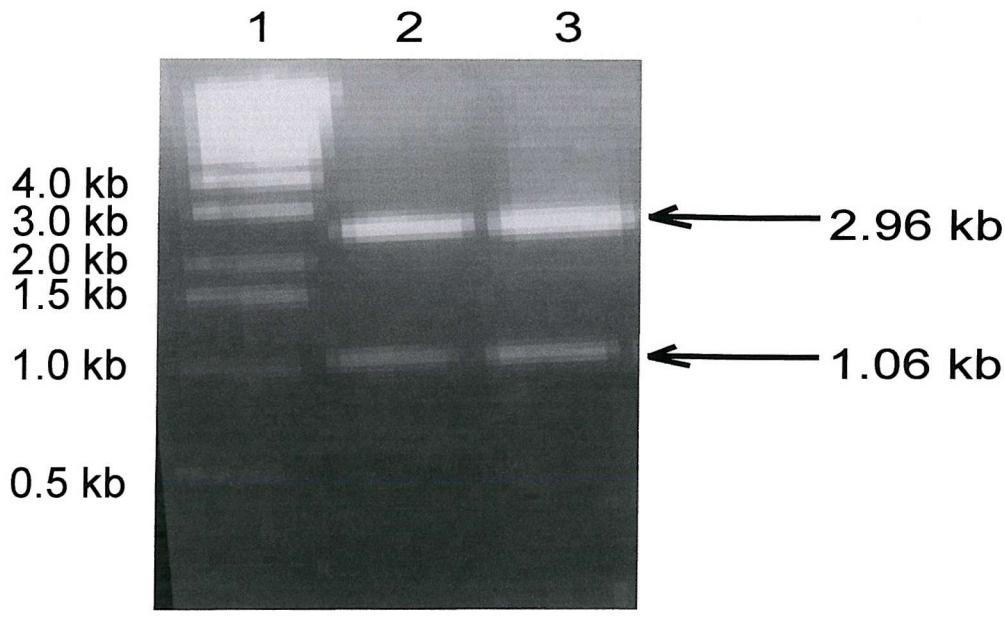

Figure 4.12: Recombinant pUC18 DNA isolated from transformed *E. coli* cells. Lane 1 contains a 1.0 kb DNA ladder, lanes 2 and 3 contain recombinant pUC18 plasmid DNA selected from LB-Amp agar plates for the mutants W61F and W214F, respectively. Restriction digests of plasmid DNA purified from transformed colonies of each with *Eco*RI and *Hind*III show the *ompF* inserts of 1.089 kb and the vector pUC18 at 2.96 kb. Both DNA preparations were further analysed by DNA sequencing.

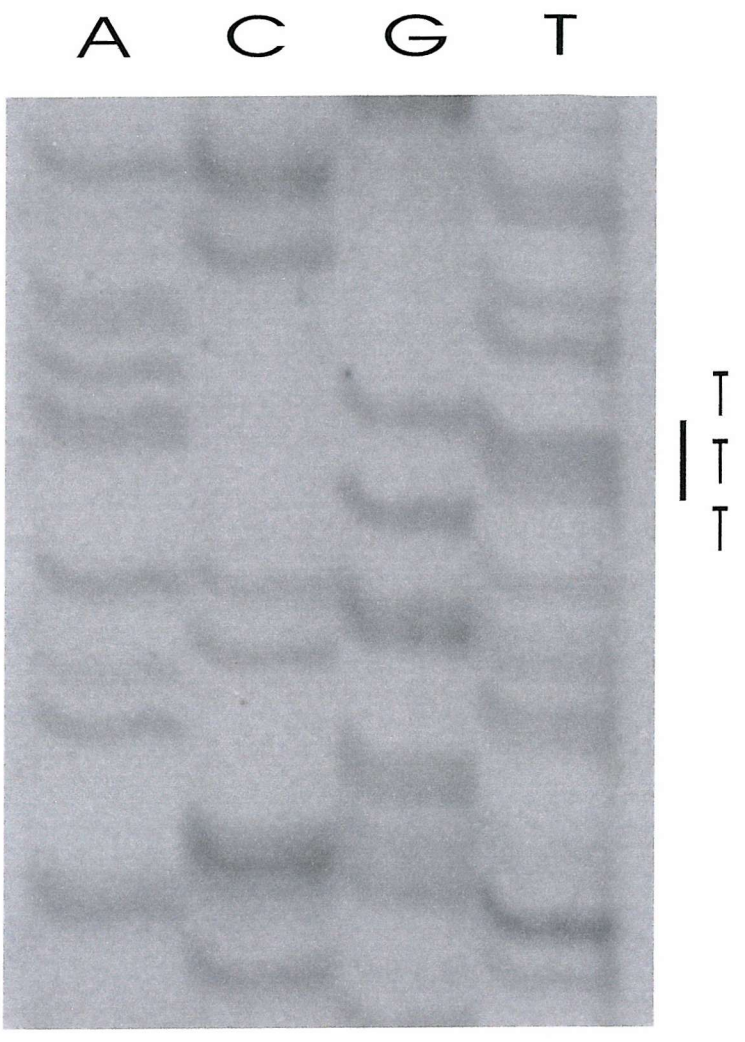

Figure 4.13: Sequences of W61F.

DNA coding for W61F held in the pGBF96 vector was sequenced using T7 sequenase The primer pMS Start (see table 4.1) was used to read over the site of the mutation in the forward direction. Sequences of up to 0.4 kb can be read with this method. The position of the mutant Phe codon, TTT is indicated at 0.247 kb.

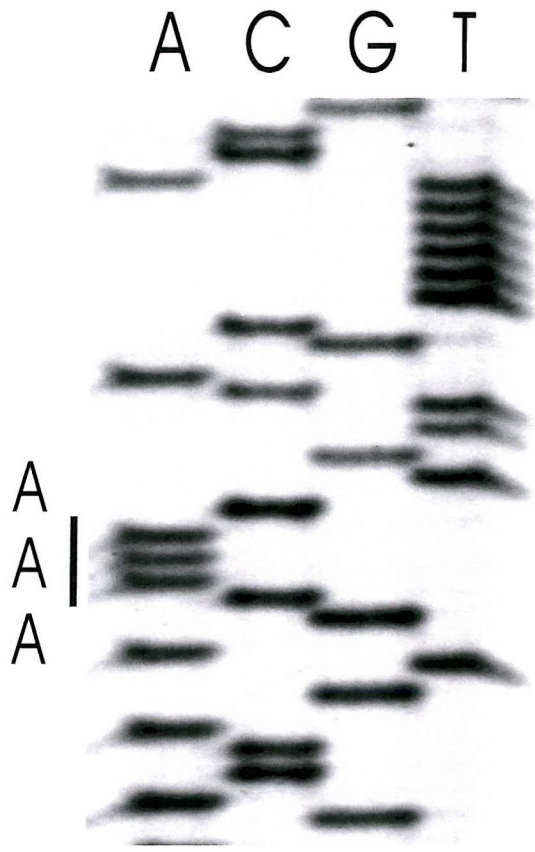

Figure 4.14: Sequences of W214F.

DNA coding for W214F that was held in the pGBF96 vector was sequenced using T7 sequenase. The reverse primer 829 was used to read over the site of the mutation. Sequences of up to 0.400 kb can be read with this method. The figure shows the sequence between bases 683 and 714. The position of the triplet AAA at 0.706 kb marks the site of the complementary recombinant Phe codon, TTT.

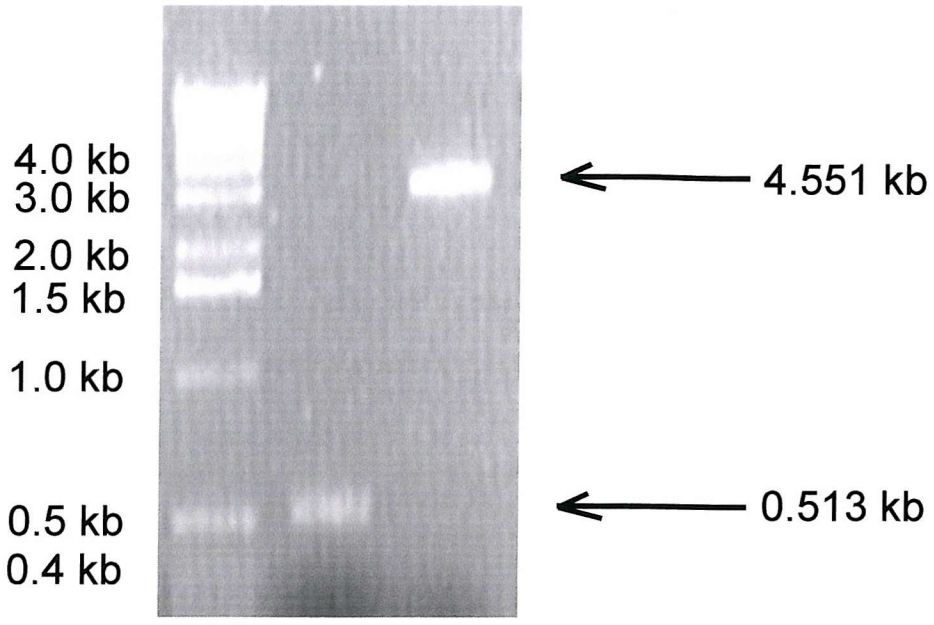

Figure 4.15: Digestion of the DNA coding for W61F and W214F with *Sal*I and *Eco*RI.

Lane 1 contains 1.0 kb DNA ladder. Lane 2 shows the isolated 0.513 kb product from W61F and lane 3 shows the isolated 4.551 kb product from W214F.

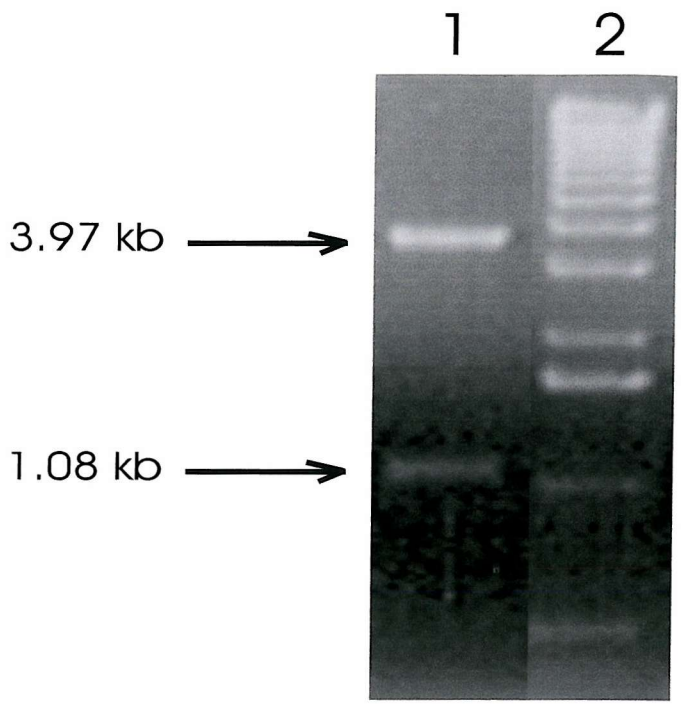

Figure 4.16: Recombinant *ompF* DNA coding for W61F/W214F

Lane 1 shows pGBF96 containing the recombinant DNA insert encoding W61F/W214F that was prepared from transformants selected off LB-Amp-Kan agar plates. After digestion of pGBF96 with *Eco*RI and *Hind*III the insert was seen at 1.089 kb and the vector at 3.97 kb. Lane 2 contains 1.0 kb marker.

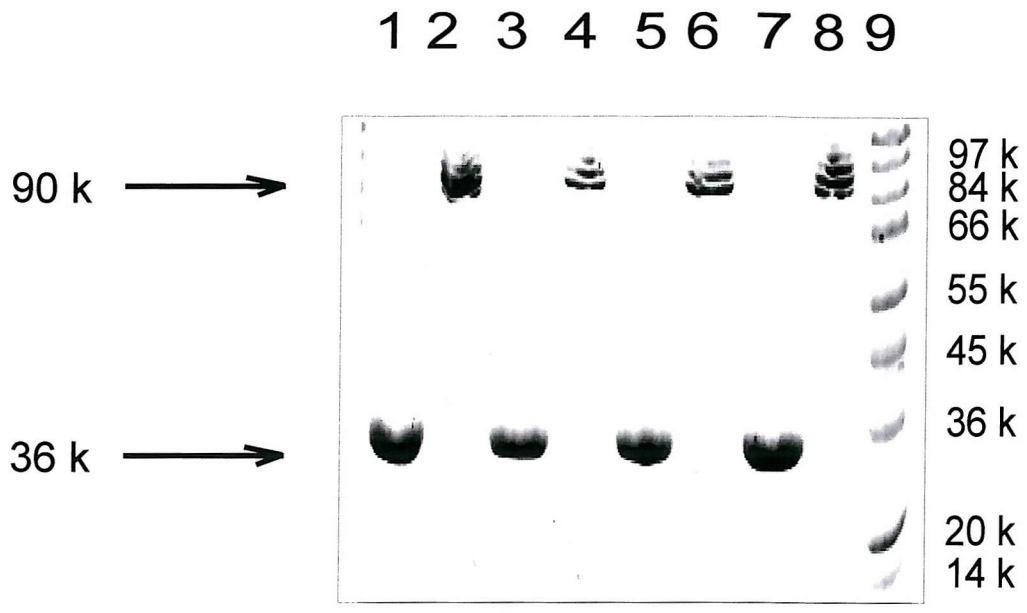

Figure 4.17: SDS-PAGE of Recombinant OmpF Proteins

Lanes 2, 4, 6 and 8 contain 8 μg of native trimeric proteins with an apparent M_r of approximately 90 k: wild type, W61F, W214F and W61F/W214F OmpF, respectively. Lanes 1, 3, 5, and 7 contain 8 μg of protein that has been boiled at 100 °C for 5 minutes to produce monomer, showing an apparent M_r of 37 k for wild type, W61F, W214F and W61F/W214F OmpF, respectively. Lane 9 contains high M_r Sigma marker.

Figure 4.18: Fluorescence emission spectra of native and mutant OmpF reconstituted in di(C18:1)PC.

The fluorescence emission spectra of wild type OmpF and the mutants W61F (a), W214F (b) and W61F/W214F (c) reconstituted in di(C18:1)PC are shown in (A) or in di(Br_2C18:)PC (B). For all spectra the fluorescence of 0.12 nmols of protein was measured by exciting at 280 nm. The molar ratio of lipid-to-protein was 600:1. The buffer was 20 mM Hepes, pH 7.2, mM EGTA.

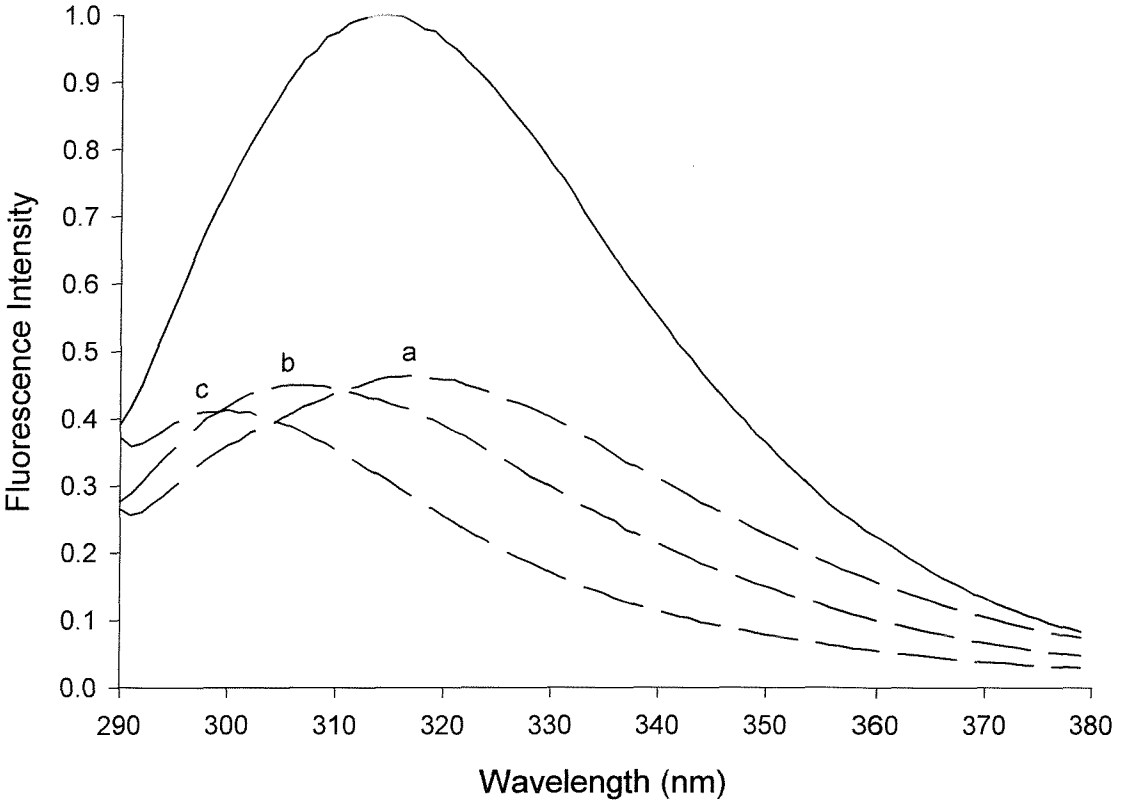
Fluorescence Intensity
1.0
0.9
0.8
0.7
0.6
0.5
0.4
0.3
0.2
0.1
0.0
290
300
310
320
330
340
350
360
370
380
Wavelength (nm)
a
b
c

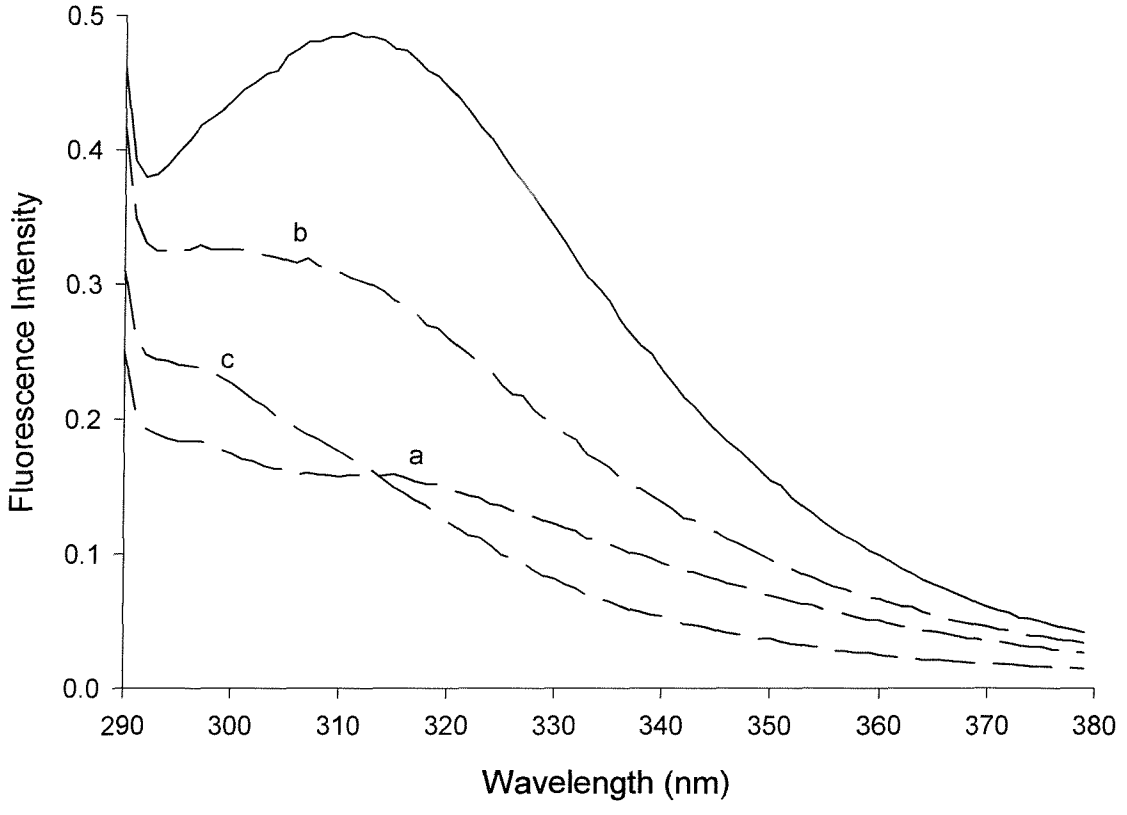
Fluorescence Intensity
0.5
0.4
0.3
0.2
0.1
0.0
290
300
310
320
330
340
350
360
370
380
Wavelength (nm)
a
b
c

Figure 4.19: SDS-PAGE of Reconstituted W61F and W214F

Lane 1 contains high M_r Sigma marker. Lanes 2, 3, 4 and 5 contain the following proteins reconstituted in di(C18:1)PC: wild type, W61F, W214F and W61F/W214F OmpF, respectively. All the proteins show an apparent M_r of 90 k after reconstitution by dialysis into di(C18:1)PC at a lipid-to-protein molar ratio of 600:1.

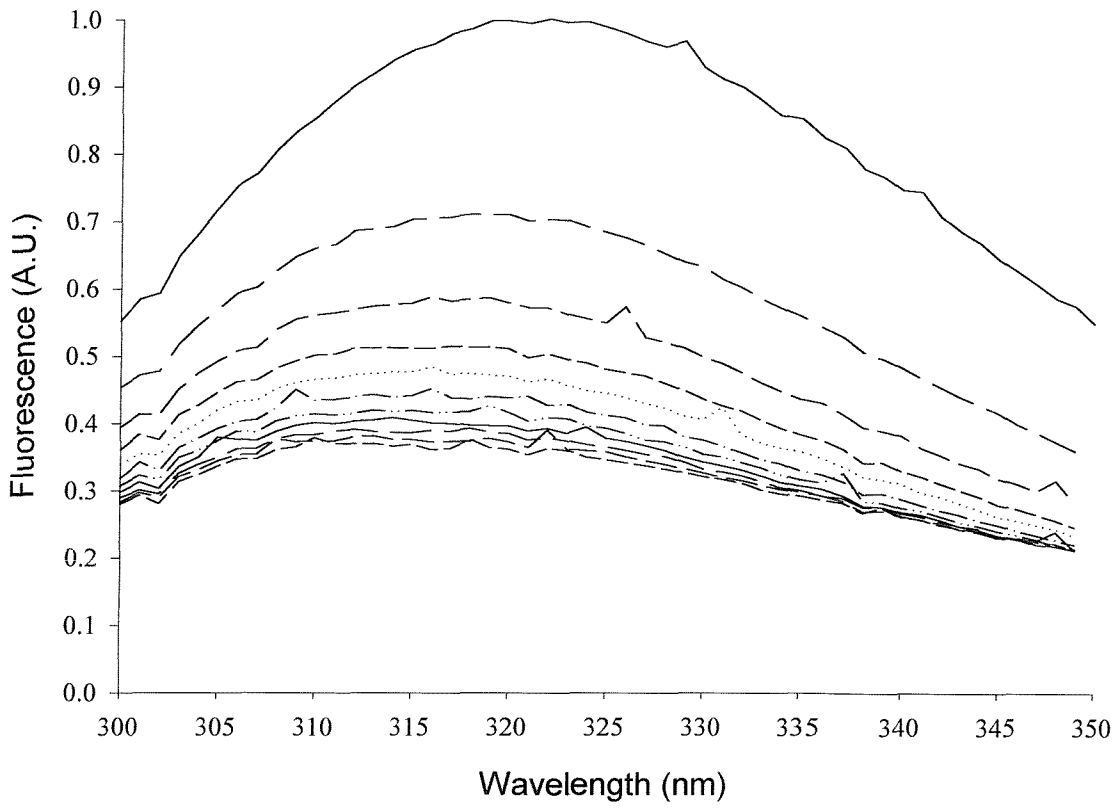

Figure 4.20: Quenching of the fluorescence intensity of wild-type OmpF by 5-doxyl stearic acid in 20 mM Hepes, pH7.2, 1 mM EGTA.

The fluorescence emission spectra of 0.12 nmols of wild type OmpF were recorded in the presence of 5-doxyl stearic acid. Increasing concentrations of the fatty acid were titrated into the cuvette and the fluorescence spectra recorded. The concentrations of 5 doxyl stearic acid from the top spectra down are: 0.0, 3.3, 6.7, 10.0, 13.3, 16.6, 20.0, 23.3, 26.6, 30.0 and 33.3 μM. All spectra were recorded in 20 mM Hepes, pH 7.2, 1 mM EGTA with an excitation wavelength of 280 nm.

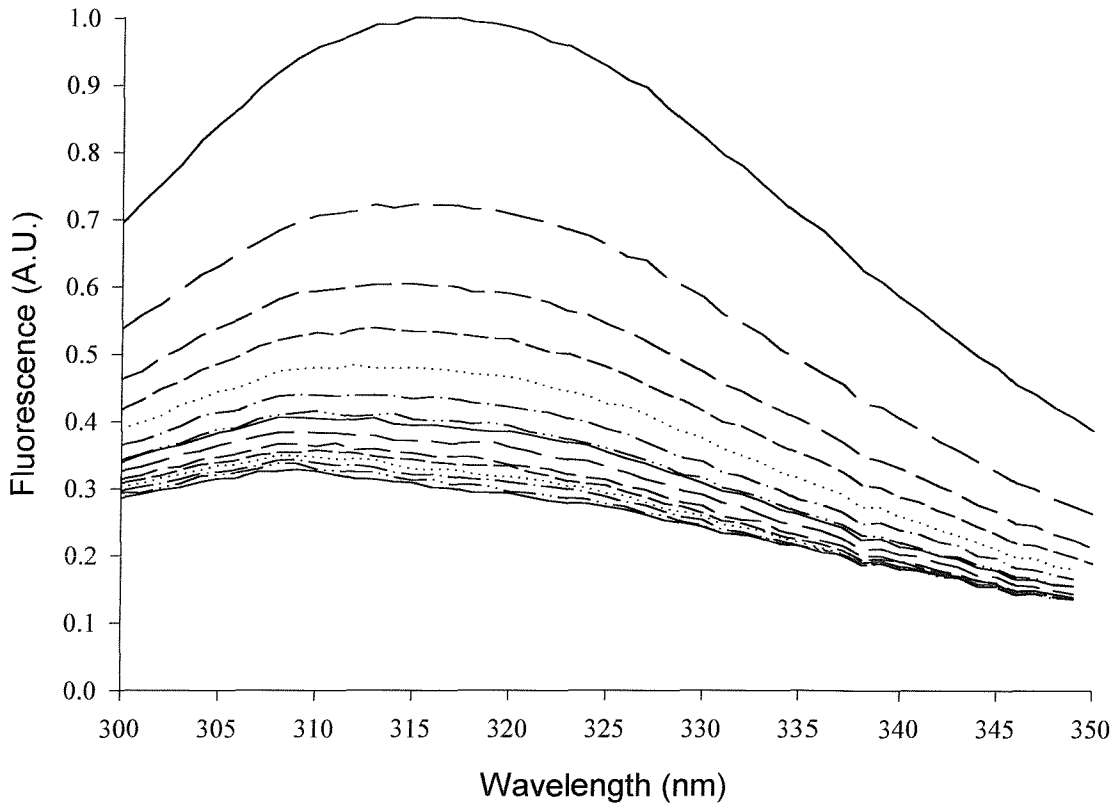

Figure 4.21: Quenching of the fluorescence intensity of wild-type OmpF by 5-doxyl stearic acid in 20 mM Hepes, pH 7.2, 200 mM KCl buffer.

The fluorescence emission spectra of 0.12 nmols of wild type OmpF were recorded in the presence of 5-doxyl stearic acid. Increasing concentrations of the fatty acid were titrated into the cuvette and the fluorescence spectra recorded. The concentrations of 5-doxyl stearic acid from the top spectra down are: 0.0, 1.7, 3.3, 5.0, 6.6, 8.3, 10.0, 11.6, 13.3, 14.9, 16.6, 18.3, 21.6, 24.9 and 31.5 μM. All spectra were recorded in 20 mM Hepes, pH 7.2, 200 mM KCl with an excitation wavelength of 280 nm.

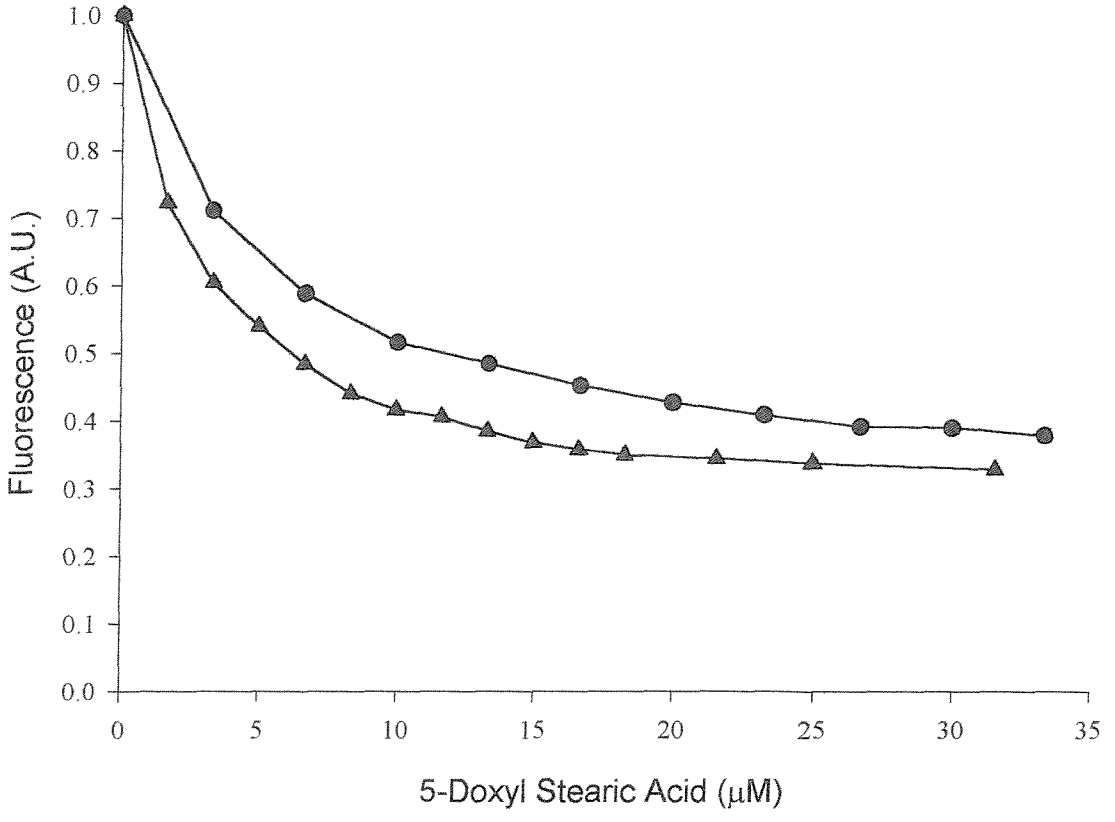

Figure 4.22: Effects of the buffer ionic strength on the level of fluorescence quenching of wild-type OmpF by 5-doxyl stearic acid.

Fluorescence quenching of 0.12 nmols of OmpF by 5-doxyl stearic acid is plotted as a function of the quencher concentration. The buffer used was 20 mM Hepes, pH 7.2 containing either 1 mM EGTA (—●—), or 200 mM KCl (—▲—).

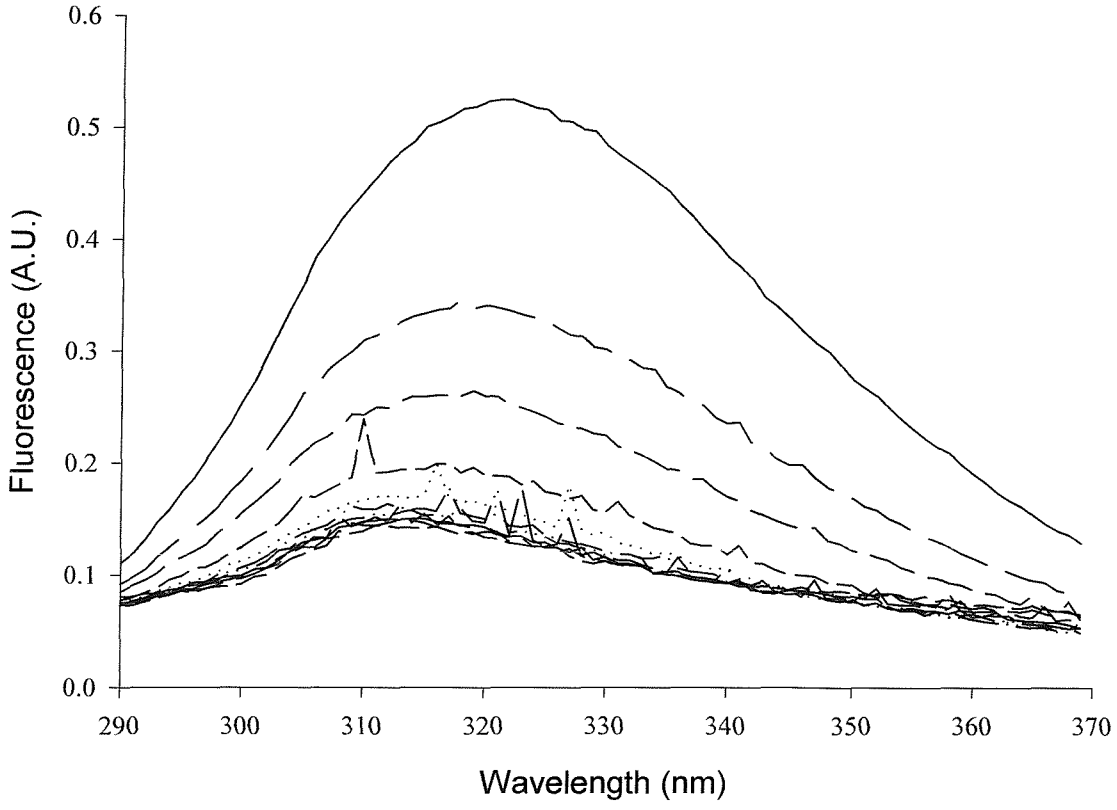

Figure 4.23: Quenching of the fluorescence intensity of W61F by 5-doxyl stearic acid.

The fluorescence emission spectra of 0.12 nmols of W61F were recorded in the presence of 5-doxyl stearic acid. Increasing concentrations of the fatty acid were titrated into the cuvette and the fluorescence spectra recorded. The concentrations of 5-doxyl stearic acid from the top spectra down are: 0.0, 3.5, 6.9, 13.9, 20.8, 27.7, 34.7, 41.6, 48.5, 55.5 and 62.4 μM. All spectra were recorded in 20 mM Hepes, pH 7.2, 200 mM KCl with an excitation wavelength of 280 nm.

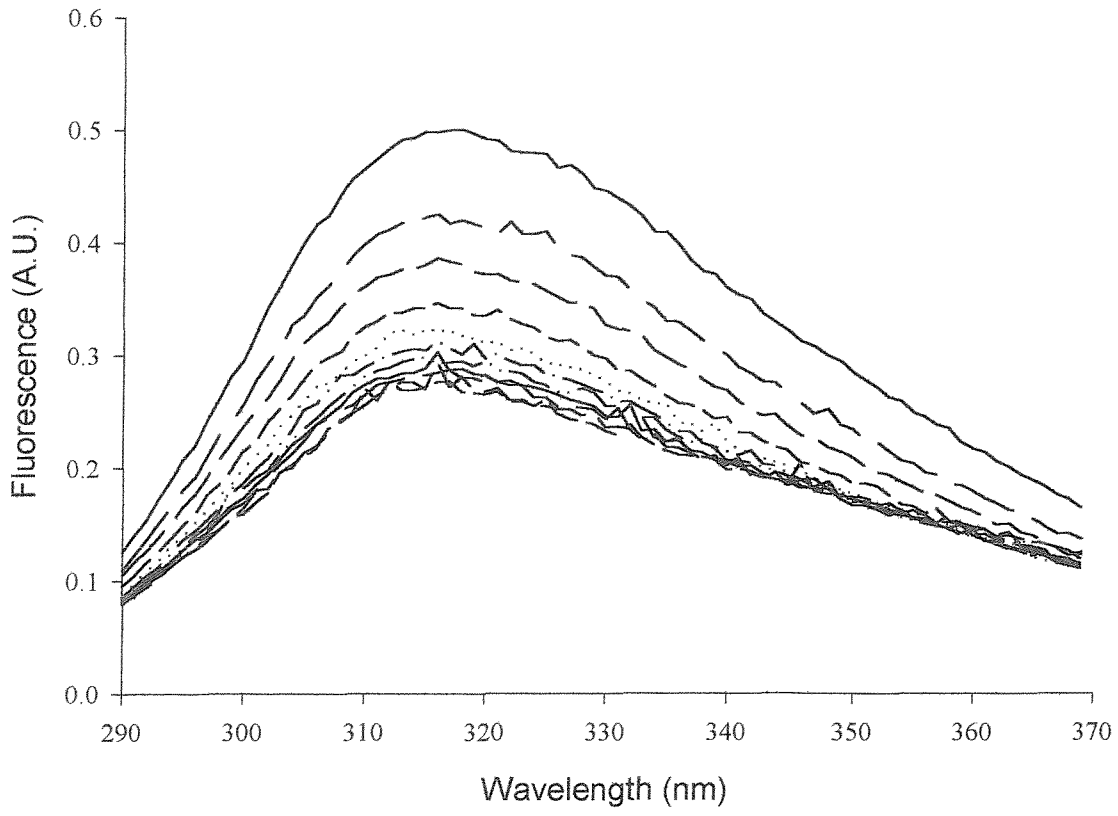

Figure 4.24: Quenching of the fluorescence intensity of W214F by 5-doxyl stearic acid.

The fluorescence emission spectra of 0.12 nmols of wild type OmpF were recorded in the presence of 5-doxyl stearic acid. Increasing concentrations of the fatty acid were titrated into the cuvette and the fluorescence spectra recorded. The concentrations of 5-doxyl stearic acid from the top spectra down are: 0.0, 3.5, 6.9, 13.9, 20.8, 27.7, 34.7, 41.6, 48.5, 55.5 and 62.4 μM. All spectra were recorded in 20 mM Hepes, pH 7.2, 200 mM KCl with an excitation wavelength of 280 nm.

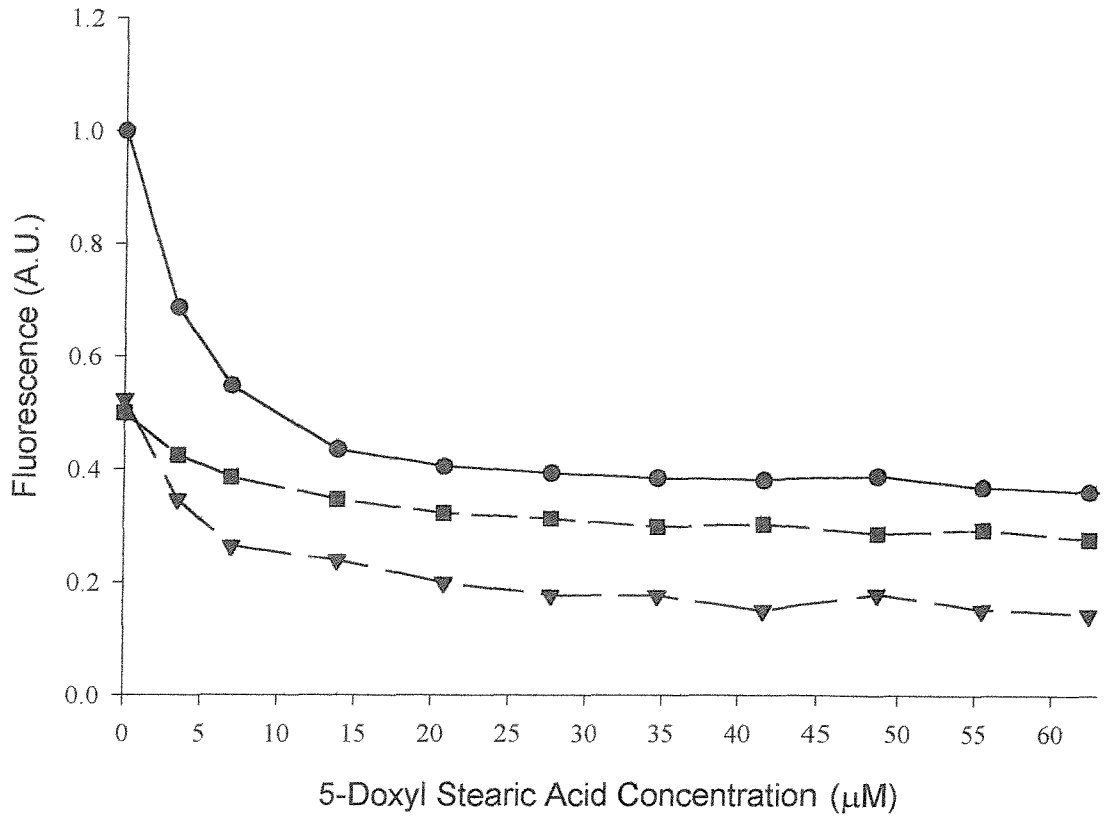

Figure 4.25: Quenching of the fluorescence intensity of wild-type, W61F and W214F by 5-doxyl stearic acid.

Fluorescence quenching by 5-doxyl stearic acid of the three proteins - wild type (—●—), W61F (—▲—) and W214F (—■—), are compared as a function of the 5-doxyl stearic acid concentration. The fluorescence of 0.12 nmols of protein was recorded in 20 mM Hepes buffer, pH 7.2, 200 mM KCl.

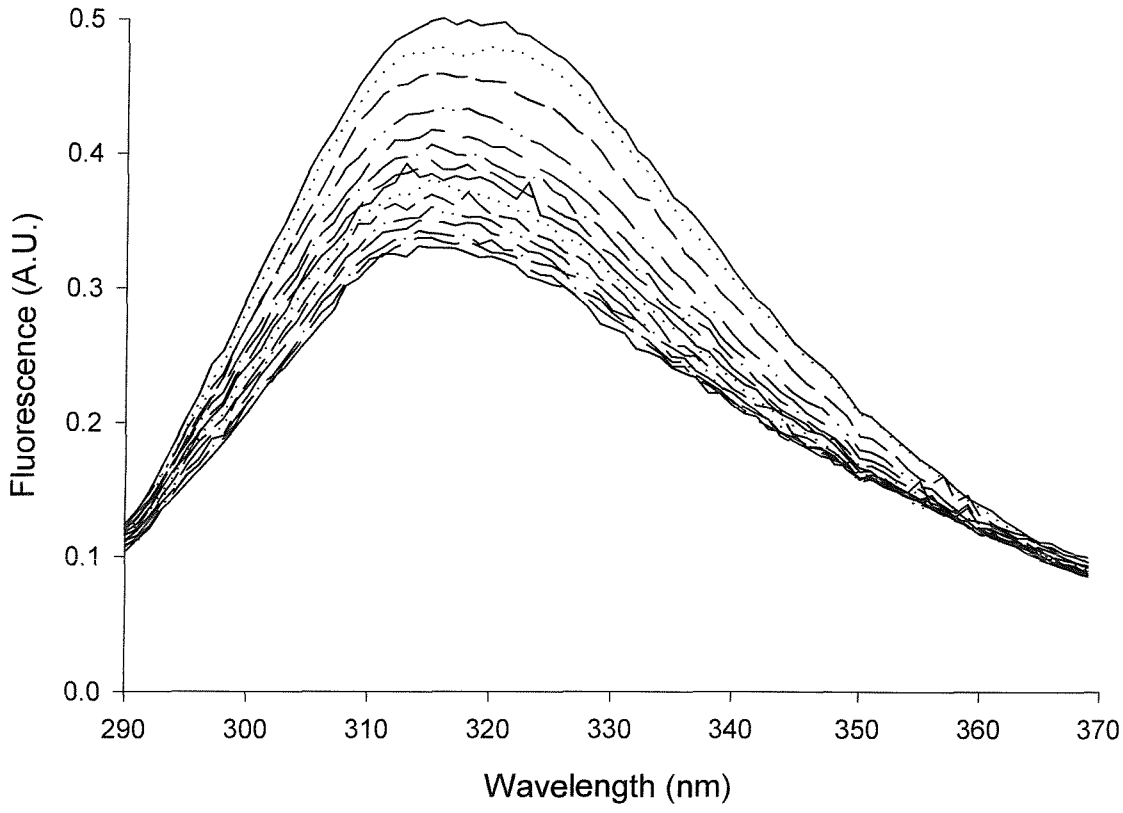

Figure 4.26: Quenching of the fluorescence intensity of wild-type OmpF reconstituted in di(Br_2C18:0)PC by 5-doxyl stearic acid.

The fluorescence emission spectra of 0.12 nmols of wild type OmpF reconstituted in di(Br_2C18:0)PC were recorded in the presence of 5-doxyl stearic acid. Increasing concentrations of the fatty acid were titrated into the cuvette and the fluorescence spectra recorded. The concentrations of 5-doxyl stearic acid from the top spectra down are: 0.0, 3.5, 6.9, 13.9, 20.8, 27.7, 34.7, 41.6, 48.5, 55.5, 62.4, 69.3, 76.3, 83.2, 90.0, 94.0 and 100.0 μM. All spectra were recorded in 20 mM Hepes, pH 7.2, 200 mM KCl with an excitation wavelength of 280 nm.

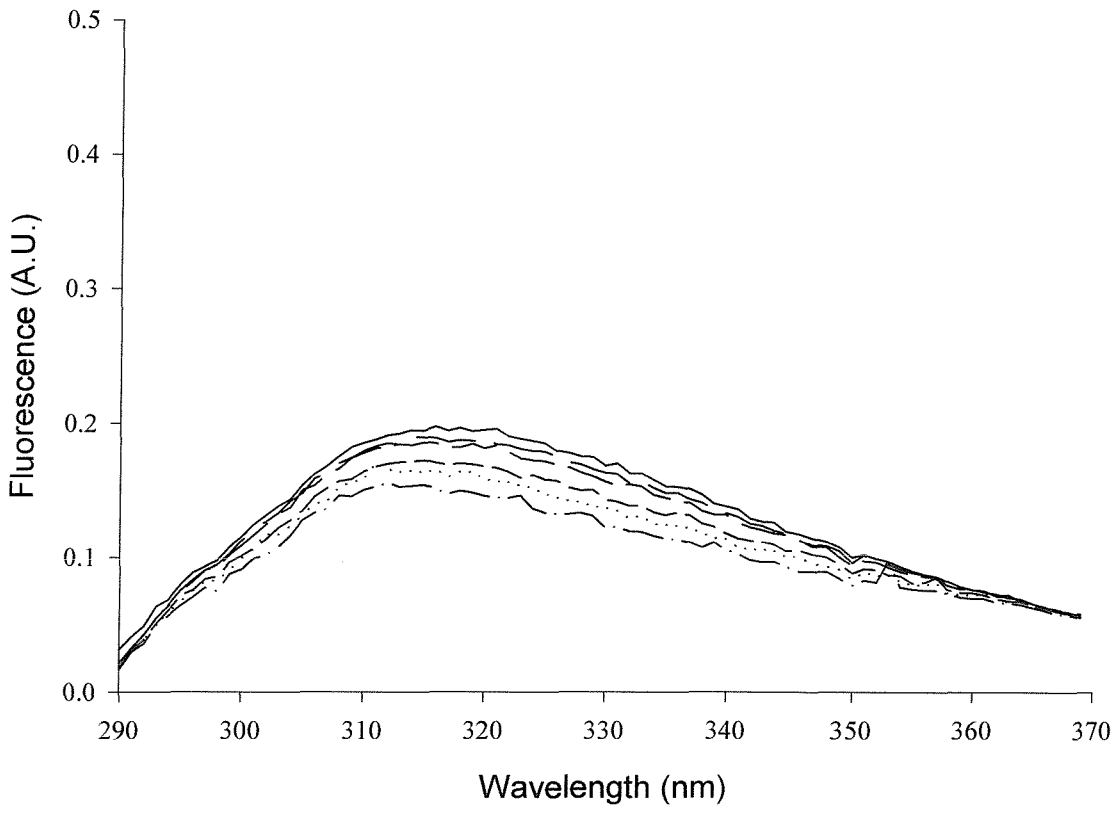

Figure 4.27: Quenching of the fluorescence intensity of W61F reconstituted in di(Br_2C18:0)PC by 5-doxyl stearic acid.

The fluorescence emission spectra of 0.12 nmols of W61F reconstituted in di(Br_2C18:0)PC were recorded in the presence of 5-doxyl stearic acid. Increasing concentrations of the fatty acid were titrated into the cuvette and the fluorescence spectra recorded. The concentrations of 5-doxyl stearic acid from the top spectra down are: 0.0, 3.5, 6.9, 13.9, 20.8, 31.0, 41.6, 52.0, 62.4, 73.1, 76.3, 83.2, 90.0, 94.0 and 100.0 μM. All spectra were recorded in 20 mM Hepes, pH 7.2, 200 mM KCl with an excitation wavelength of 280 nm.

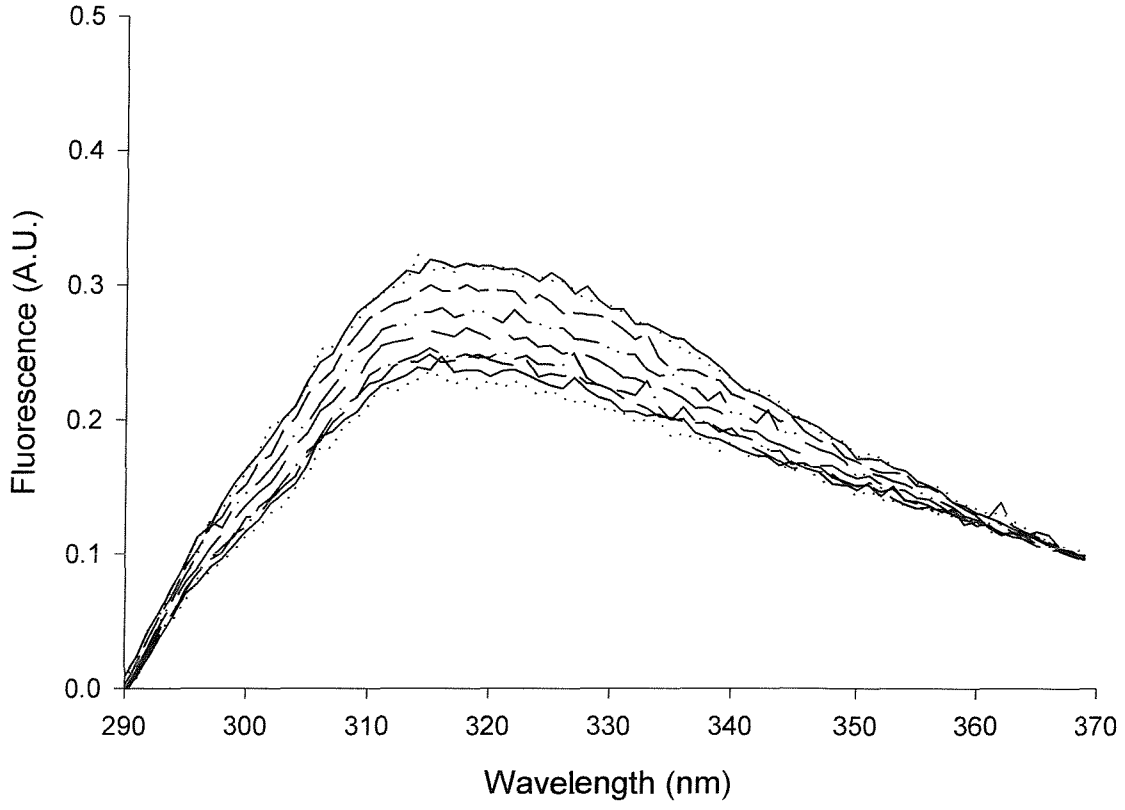

Figure 4.28: Quenching of the fluorescence intensity of W214F reconstituted in di(Br_2C18:0)PC by 5-doxyl stearic acid.

The fluorescence emission spectra of 0.12 nmols of W214F reconstituted in di(Br_2C18:0)PC were recorded in the presence of 5-doxyl stearic acid. Increasing concentrations of the fatty acid were titrated into the cuvette and the fluorescence spectra recorded. The concentrations of 5-doxyl stearic acid from the top spectra were: 0.0, 3.5, 6.9, 13.9, 20.8, 31.0, 41.6, 52.0, 62.4, 73.1, 76.3, 83.2, 90.0, 94.0 and 100.0 μM. All spectra were recorded in 20 mM Hepes, pH 7.2, 200 mM KCl with an excitation wavelength of 280 nm.

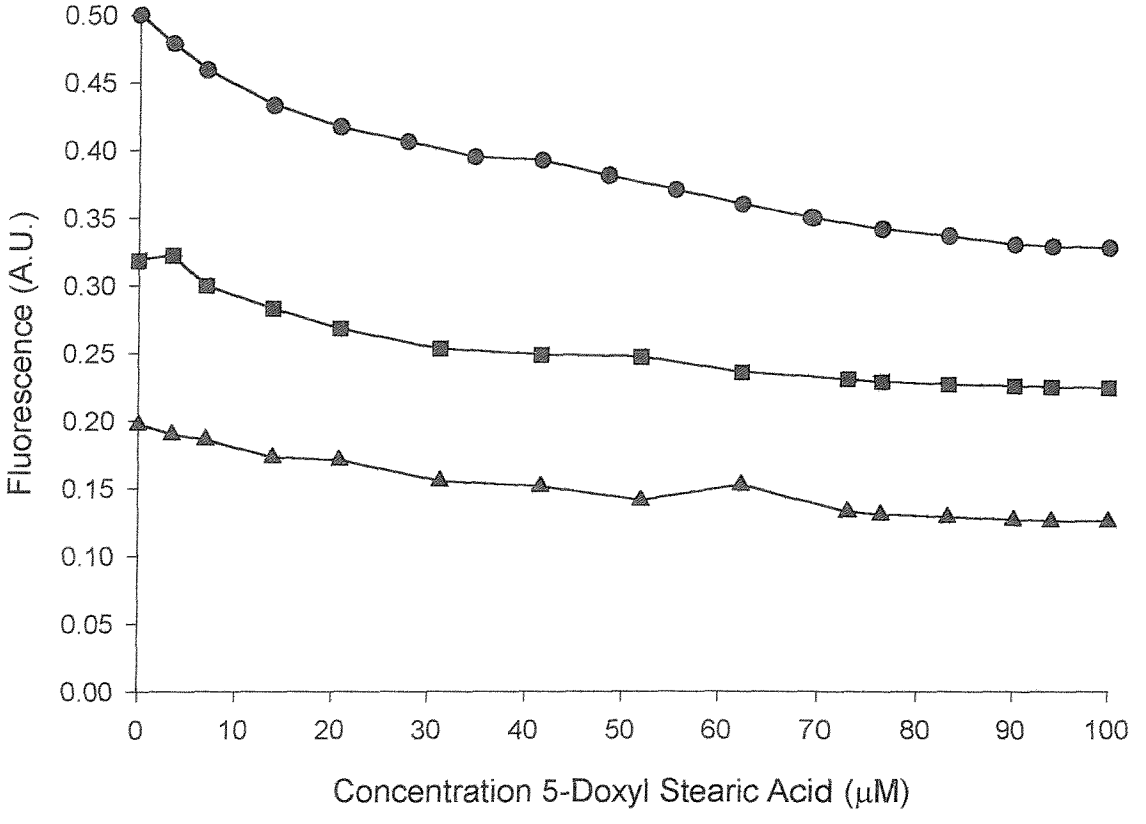

Figure 4.29: Quenching of the fluorescence intensity of wild-type, W61F and W214F OmpF reconstituted in di(Br_2C18:0)PC by 5-doxyl stearic acid.

Fluorescence quenching of the three proteins - wild type (—●—), W61F (—▲—) and W214F (—■—), reconstituted in di(Br_2C18:0)PC are compared as a function of the 5-doxyl stearic acid concentration. The fluorescence of 0.12 nmols of protein was recorded in 20 mM Hepes buffer, pH 7.2, 200 mM KCl.

Primer	Sequence
pUC Start	GATTACGAATTCATGATGAAGCGC
pUC End	AGTGCCAAGCTTCTATTAGAACTG
233	CCGGTTATGGTCAGTTTGAATATAACTTCCAGGG
266	CCCTGGAAGTTATATTCAAACTGACCATAACCGG
697	GCTGAACAGTTTGCTACTGGTC
718	GACCAGTAGCAAACTGTTCAGC
829	GCGTTTTGTTGGCGAAGCCGC
pMS Start	ATAACAATTTCACACAGG

Table 4.1: Primers used in the construction and sequencing of W61F and W214F.

All primers were obtained from Oswel.

System	F/F_0 270 nm	F/F_0 280 nm	F/F_0 290 nm
Wild Type	0.48	0.49	0.54
W61F	0.35	0.37	0.42
W214F	0.80	0.76	0.96

Table 4.2: Effect of excitation wavelength on the level of fluorescence quenching of OmpF in di(Br_2C18:0)PC.

F and F_0 are fluorescence intensities for OmpF reconstituted in di(Br_2C18:0)PC and di(Br_2C18:1)PC, respectively. Fluorescence was excited at the given wavelength and emission was monitored at 320 nm.

4.4 Discussion

Recombinant PCR provided a very quick and efficient method of producing OmpF mutants varying in the content of Trp residues. Phe appeared to be a successful replacement for Trp, as the native trimeric structure, seen on SDS-PAGE, was not disrupted (Figure 4.17). Trp residues in membrane proteins have been identified as 'anchoring' residues, because of their location at the polar/apolar interface near the lipid carbonyl groups (Allen *et al.*, 1980). The stability of Trps at this location has been attributed to dipolar interactions, interactions of the π-electrons and hydrogen bonding of the imino group (Killian *et al.*, 1996). The other aromatic amino acids Tyr and Phe also possess π-electrons and have a dipole moment and can therefore play a similar role in membrane proteins (Braun & von Heijne, 1999). It is clear that Trp residues are not essential for OmpF structure or for correct insertion into the membrane, since the mutant with two Trp residues replaced by Phe is produced normally. In α-helical membrane proteins, Phe is found at all positions in the transmembrane helices whereas Tyr and Trp are concentrated at the ends of the transmembranous regions (Braun & von Heijne, 1999). It is possible that Phe can act as an 'anchor' in the absence of Tyr or Trp, as studies with model α-helices have suggested (Mall *et al.*, 2000). It would be of interest to see if mutants with the Trp residues replaced by residues such as Ala were stable, although it is possible that in OmpF that the 29 Tyr residues are sufficient to maintain the native structure in the absence of Trp residues.

Using these mutants enabled the emission spectra of the two Trp residues to be studied independently. The low wavelength of the emission maxima show that both Trps reside in hydrophobic environments, particularly Trp 61 at the trimer interface. The trimer interface may be more hydrophobic than the lipid-protein interface, but fluorescence also blue-shifts if the fluorescent group is immobile (Lakowicz, 1983). Therefore the blue-shift may reflect immobilisation rather than a hydrophobic environment. In molecular dynamics studies Trp 61 is completely immobile near the trimer axis (Tielman *et al.*, 1998).

The Trp emission in the wild-type and single Trp mutants predominates over Tyr emission, which is undetectable upon excitation at 280 nm (Figure 4.18A). However, after removal of both Trp residues by mutagenesis a relatively high emission is seen centred at 305 nm due to the 29 Tyr residues found in OmpF, when exciting at 280 nm (Figure 4.18A plot c). The lack of extensive Tyr fluorescence in the spectra of the wild type and single Trp proteins suggest that Tyr fluorescence is quenched by energy transfer to the Trp residues. The diameter of OmpF is approximately 20 Å, and is therefore within the distance required for efficient Tyr-to-Trp transfer to occur (Lakowicz, 1983).

Quenching of the wild type by brominated lipid gives fluorescence emission spectra similar to that of the W214F mutant (Figure 5.18). This confirms that di(Br_2C18:0)PC quenches the lipid-exposed Trp 214. When the spectra is excited at 280 nm there appears to be some quenching of the Trp 61 (in W214F), but this may arise indirectly from quenching of Tyr residues. At higher excitation wavelengths, where Trp residues are directly excited, quenching levels of W214F in di(Br_2C18:0)PC were close to zero (Table 4.2). This would indicate that di(Br_2C18:0)PC cannot quench Trp 61 and that phospholipids are excluded from the trimer interface. The crystal structure of the FhuA porin has revealed the presence of an LPS molecule at the trimer axis, with the glucosamine moiety of the LPS positioned just above the aromatic belt (Ferguson *et al.*, 1998; Ferguson *et al.*, 2000). X-ray diffraction studies on OmpF suggest there is no room at this site for the binding of a large LPS molecule (Cowan *et al.*, 1992). Electron microscopy and biochemical studies, however, present evidence for the presence of a tightly bound LPS at the OmpF trimer axis (Cowan *et al.*, 1992; Jap & Walian, 1996). It is therefore possible that di(Br_2C18:0)PC cannot bind at the trimer interface because it is unable to displace the tightly bound LPS molecule.

5-doxyl stearic acid quenched the fluorescence of OmpF to a higher level than brominated lipid. Higher spin-label quenching was seen in ionic buffer when charge repulsion between carboxyl groups was neutralised. Quenching of W214F by spin-labelled fatty acid is presumably limited by the accessibility of Trp 61 to the fatty

acid. A high baseline was again seen with quenched W61F, where total quenching was expected. This may again be due to fluorescence contribution from other aromatic residues in OmpF. Additional quenching of OmpF by 5-doxyl stearic acid suggests that the fatty acid may be able to bind to sites from which di(Br_2C18:0)PC is excluded.

CHAPTER 5

RELATIVE PHOSPHOLIPID BINDING AFFINITIES OF OMPF

5.1. INTRODUCTION

5.1.1 Hydrophobic Matching

The thickness of the hydrophobic core of biological membranes is determined by the length of the fatty acyl chains of membrane lipids and is approximately 30 Å. Amino acids found in the membrane-spanning region of membrane proteins are generally hydrophobic because the cost of burying a charged or polar residue in a hydrophobic environment is high (if charged or polar amino acids are found in the membrane-spanning region, they are generally assumed to be part of a binding site like that of calcium in the transmembrane region of the Ca^{2+}-ATPase, or to line aqueous pores across the membrane). The transmembrane region of membrane proteins are arranged to maximise the formation of hydrogen bonds in the peptide backbone because in water, peptides with amine groups can hydrogen bond to the surrounding water but in the hydrocarbon interior of the lipid bilayer, hydrogen bonding to the solvent (hydrocarbon) is no longer possible. The cost of transferring a peptide bond from water to a non-polar environment has been estimated to be about 25 kJ mol^{-1} when not hydrogen bonded but only about 2.4 kJ mol^{-1} when hydrogen bonded (Roseman, 1988). Optimal hydrogen bonding arrangements can be achieved for transmembrane peptides in α-helical or β-sheet structures. A typical α-helix will have 3.6 residues per turn and a translation per residue of 1.5 Å (Creighton, 1993). The membrane-spanning region of an α-helix will therefore require approximately 20 amino acid residues to span a bilayer. The β-sheet is a more extended conformation, however, requiring only 11-14 amino acids to span the bilayer. The majority of proteins found in membranes are α-helical structures. A family of proteins, called porins, that span the membrane as β-sheets are found in the outer membrane of Gram negative bacteria.

Page 138 is missing from the volume

preference between di(C14:0)PC in the gel phase and di(C18:1)PC in the fluid phase (Piknova *et al.*, 1997). Fluorescence quenching studies with the sarcoplasmic reticulum Ca^{2+}-ATPase, however, found that the relative binding affinities were independent of the lipid chain length (London & Feigenson, 1981; East & Lee, 1982). These results suggest that in fluid lipid bilayers, α-helical membrane proteins can distort in the lipid bilayer to match the thickness of the membrane's hydrocarbon core. Studies on single α-helical peptides have shown that the tilt angle adopted by the peptide can vary in response to changes in the lipid chain thickness, as the protein conforms to match the bilayer thickness (Webb *et al.*, 1998).

A number of hydrophobic matching models are now available that allow the interaction free energy between a membrane protein and the surrounding lipid bilayer to be calculated. These models treat the protein as a rigid solute around which the flexible lipid chains will deform (Mouritsen & Bloom, 1984; Fattal & Ben-Shaul, 1993; Nielson *et al.*, 1998). The integral membrane protein can be characterised by a hydrophobic length, d_P, and a lipid bilayer by a hydrophobic length, d_L. The greater the level of matching between the hydrophobic regions of the lipid and protein, the lower the free energy of the membrane. The free energy of a membrane can be calculated using a number of terms (Fattal & Ben-Shaul, 1993; Nielson *et al.*, 1998), the concept of some of which are illustrated in Figure 5.2:

1) compression/expansion energy of the fatty acyl chains as these molecules must stretch or compress to match the hydrophobic region of the protein,
2) loss of conformational entropy, because the fatty acyl chains at the lipid-protein interface become more ordered
3) surface energy changes occur due to changes in the area occupied by a lipid head group following from stretching/compression of the fatty acyl chains, and
4) splay energy due to changes in the cross-sectional area available to the chains along their length, resulting from curvature of the monolayer

surface near the protein, i.e., the splay term accounts for changes in the average lipid chain tilt.

In the model of Fattal and Ben-Shaul (1993) the energy required to deform the lipid acyl chains is expressed as a sum of the contributions from the fatty acyl chain and membrane surface regions (Fattal & Ben-Shaul, 1993). The resulting profile of energy of interaction as a function of hydrophobic mismatch was fairly symmetrical about the point of zero mismatch. The calculated lipid perturbation energy, F (in units of kT $Å^{-1}$ of protein circumference) fits the equation

$$F = 0.37 + 0.005 (d_p - d_L)^2 \qquad \text{Equation 5.1}$$

where d_p and d_L are the hydrophobic thickness of the protein and lipid bilayer, respectively, and the unperturbed bilayer thickness is 24.5 Å. The hydrophobic thickness of a bilayer of phosphatidycholine in the liquid crystalline phase is given by

$$d_L = 1.75 (N_c - 1) \qquad \text{Equation 5.2}$$

where N_c is the number of carbon atoms in the fatty acyl chain (Lewis & Engelman, 1983). Assuming that all of the lipid perturbation energy is concentrated in the first shell of lipids around the protein and that each lipid occupies 6 Å of a protein's circumference, the energy difference (ΔF) for a hydrophobic mismatch of 7 Å, compared to a perfect hydrophobic match ($d_p = d_L$) is

$$0.005 \times 7^2 = 0.245 \text{ kT } Å^{-1}$$

$$= 1.47 \text{ kT per lipid molecule (i.e., multiplying by 6 Å)}$$

where the Boltzmann's constant, $k = 1.381 \times 10^{-23}$ J K^{-1}, and the temperature t = 298 °K.

$$\text{therefore } \Delta F = 1.47 \times 1.381 \times 10^{-23} \times 298$$

$$= 6.05 \times 10^{-21} \text{ J per lipid}$$

and multiplying by Avogrado's Number (6.022×10^{23}) to calculate the energy change per mole of lipid gives $\Delta F = 3.6$ kJ mol^{-1}.

The change in the lipid binding constant (k) can be calculated from the energy change using the equation

$$\Delta G^\circ = -RT \log_e k \qquad \text{Equation 5.3}$$

where ΔG° is equivalent to ΔF, and R is the gas constant (1.98×10^{-3} cal mol^{-1} K^{-1}). Therefore for a mismatch of 7 Å, the lipid perturbation energy will be 3.6 kJ mol^{-1}, corresponding to a decrease in the lipid binding constant by a factor of 4.3. For a mismatch of 14 Å, the lipid perturbation energy would be 14.6 kJ mol^{-1}, and the lipid binding constant would change by a factor of 360. The effects of hydrophobic mismatch would be reduced if the changes in the lipid-protein interaction energy were to affect lipids beyond the first shell.

The approach of Nielson et al. (1998) analyses the free energy of the deformation as the sum of three contributions: compression-expansion, splay distortion and surface tension (Nielson *et al.*, 1998). The mattress model of Mouritsen and Bloom (Mouritsen & Bloom, 1984) calculates the free energy of the lipid-protein system as a sum of two terms - the first pertains to the free energy associated with exposure of the hydrophobic surface of the protein or lipid to the aqueous media and the second regards the contact area between the fatty acyl chains and the hydrophobic surface of the protein. Although all of these models calculate the lipid-protein perturbation energy from combinations of different parameters, they reach similar conclusions regarding the effects of hydrophobic mismatch in the membrane.

5.1.2 Measuring Lipid Binding Affinity

The relative binding constants of a membrane protein for different phospholipids can be calculated from the changes in the Trp fluorescence intensity of the protein seen when that protein is reconstituted in mixtures of brominated and nonbrominated lipid. Quenching of Trp fluorescence by brominated molecules occurs by a process of heavy atom quenching that requires an intimate collision between the Trp and the bromine-containing molecule. Because the time taken for two lipids to exchange positions in the membrane (10^{-8} seconds) is considerably slower than the fluorescence lifetime of Trp (10^{-9} seconds), quenching is considered a static process (East & Lee, 1982). The lattice model of quenching can therefore be used to analyse fluorescence quenching of membrane proteins by brominated lipids. The degree of quenching in the lattice model is proportional to the probability that a brominated lipid occupies a lattice site close enough to the Trp residues in the protein to cause quenching. For a random distribution of lipids, the probability that any lattice site is not occupied by a brominated lipid is $1 - x_{Br}$ where x_{Br} is the mole fraction of brominated lipid in the bilayer. The probability that any particular Trp residue will give rise to fluorescence is proportional to the probability that none of the lattice sites close enough to the Trp residue to cause quenching is occupied by a brominated lipid. This is illustrated in Figure 5.3. The fluorescence can be described by

$$F = F_{min} + (F_o - F_{min})(1 - x_{Br})^n \qquad \text{Equation 5.4}$$

where, F_o and F_{min} are the fluorescence intensities for the protein in nonbrominated and brominated lipids, respectively and n is the number of lattice sites. F is the fluorescence intensity in the phospholipid mixture when the mole fraction of lipid is x_{Br}. Figure 5.4 shows how the level of fluorescence quenching is dependent on the number of lattice sites surrounding a Trp residue. It can be seen from this diagram that the higher the number of lattice sites, the higher is the probability of a lattice site being occupied by brominated lipid. When all of the fluorescence of the protein is quenched,

$$F = F_o(1 - x_{Br})$$

However, if only a fraction of the fluorescence of the protein is quenched, then

$$F = F_{min} + (F_o - F_{min})(1 - x_{Br})^n$$

The lattice model can also be used to describe fluorescence quenching of a protein in a mixture of lipids, with different affinities for the protein. At each lattice site an equilibrium will exist, where

$$PQ + L \Leftrightarrow PL + Q$$

where PQ and PL are complexes of the protein (P) with brominated (Q) and non-brominated lipid (L) respectively. The equilibrium can be described by an equilibrium constant, K, given by

$$K = [PL][Q]/[PQ][L] \qquad \text{Equation 5.5}$$

where K is the binding constant of the non-brominated lipid relative to the brominated lipid. If the L binds more strongly than the Q (i.e., K is large), the sites around the protein will tend to be occupied by the nonbrominated lipid and so fluorescence will be high. Conversely if the L binds less strongly than the Q (i.e., K is small), the sites around the protein will tend to be occupied by the brominated lipid and so fluorescence will be low. The effect of K on the level of quenching is shown in Figure 5.5.

Fluorescence quenching can then be fitted to an equation analogous to Equation 5.4, in which

$$F = F_{min} + (F_o - F_{min})(1 - f_{Br})^n \qquad \text{Equation 5.6}$$

where the fraction of sites at the lipid-protein interface that are occupied by brominated lipid is f_{Br} (East & Lee, 1982). The value of f_{Br} can be calculated from Equation 5.5, as follows. It is assumed that the amount of lipid is much greater than the amount of

protein, so that the fraction of lipid bound to the protein is negligible. In Equation 5.5, [L] and [Q] can be put equal to the mole fraction of L and Q in the total lipid mixture, so that,

$$[Q] = x_{Br}$$

$$[L] = 1 - x_{Br}$$

$$[PQ] = f_{Br}$$

$$[PL] = 1 - f_{Br}$$

Hence, $K = ((1 - f_{Br})(x_{Br}))/ ((f_{Br}) (1 - x_{Br}))$

$= (x_{Br} - f_{Br} x_{Br})/(f_{Br} - f_{Br} x_{Br})$

and $f_{Br} = x_{Br}/(x_{Br} + K(1 - x_{Br})$ Equation 5.7.

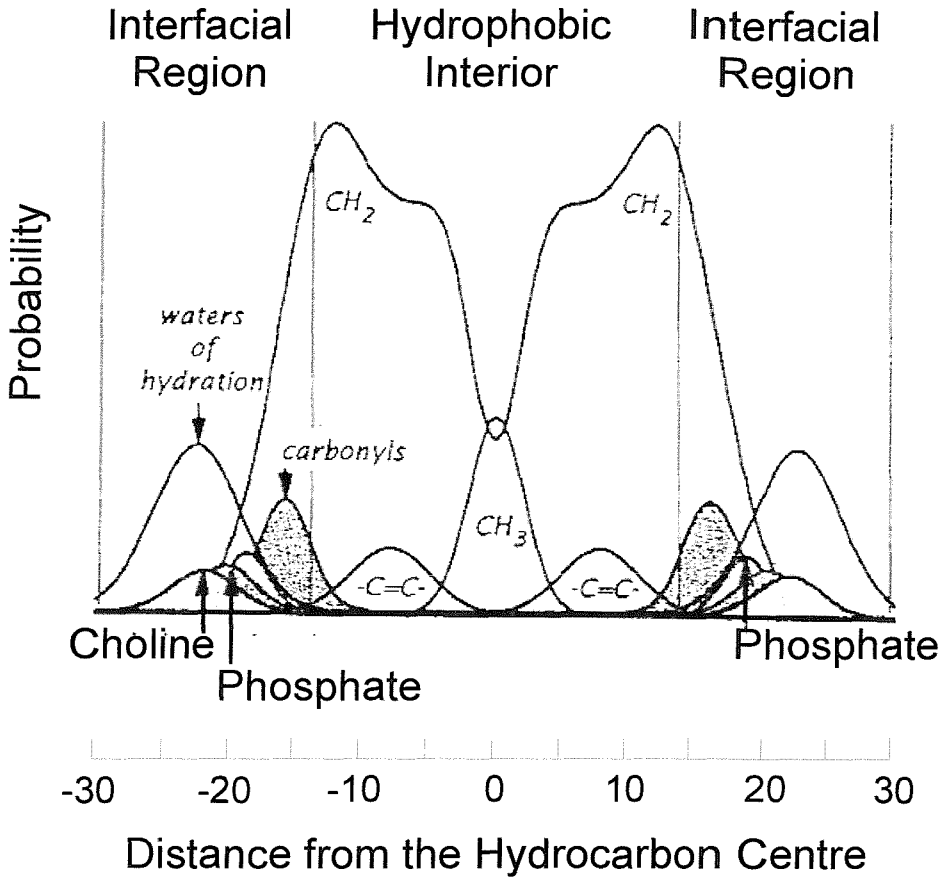

Figure 5.1: The structure of a fluid di(C18:1)PC bilayer determined from x-ray and neutron diffraction data (derived from White & Wimley, 1999)).

The structure consists of the time-averaged distribution of the principal lipid groups and water of hydration. The distributions are Gaussian distributions and represent the probability of finding a structural group at a particular location in the membrane.

Figure 5.2: The result of a mismatch between the hydrophobic length of a peptide and the hydrophobic thickness of a lipid bilayer (adapted from (Fattal & Ben-Shaul, 1993; Nielson *et al.*, 1998)).

1) compression (a) or expansion (b) of a lipid bilayer in response to a negative ($d_P < d_L$) or a positive ($d_P > d_L$) hydrophobic mismatch.

2) loss of the conformational entropy of lipid chains in the vicinity of a rigid membrane protein.

3) surface energy changes, as the area occupied by the lipid head group is increased or decreased in response to expansion or compression of the lipid chains, respectively.

1) Compression/Expansion

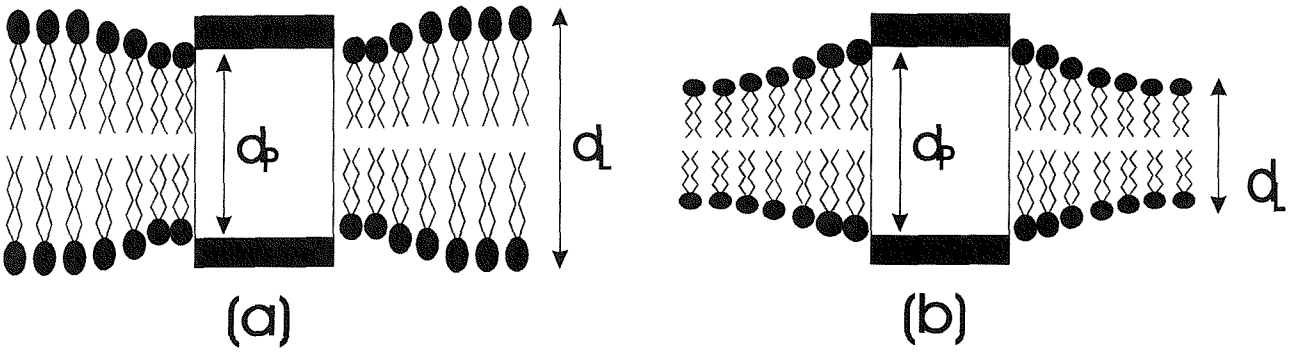

2) Loss of Conformational Entropy

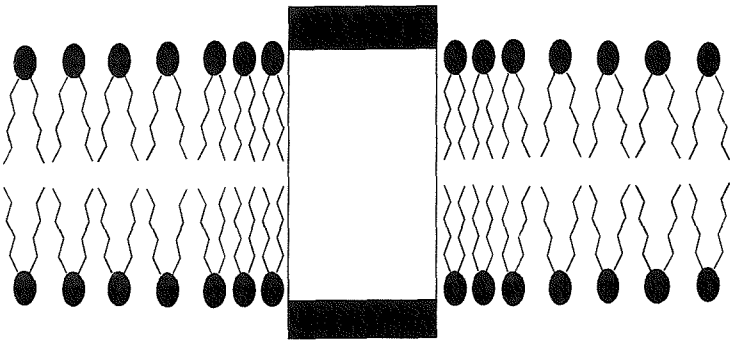

3) Surface Changes

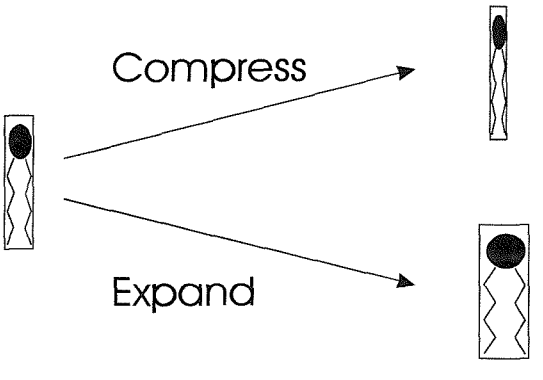

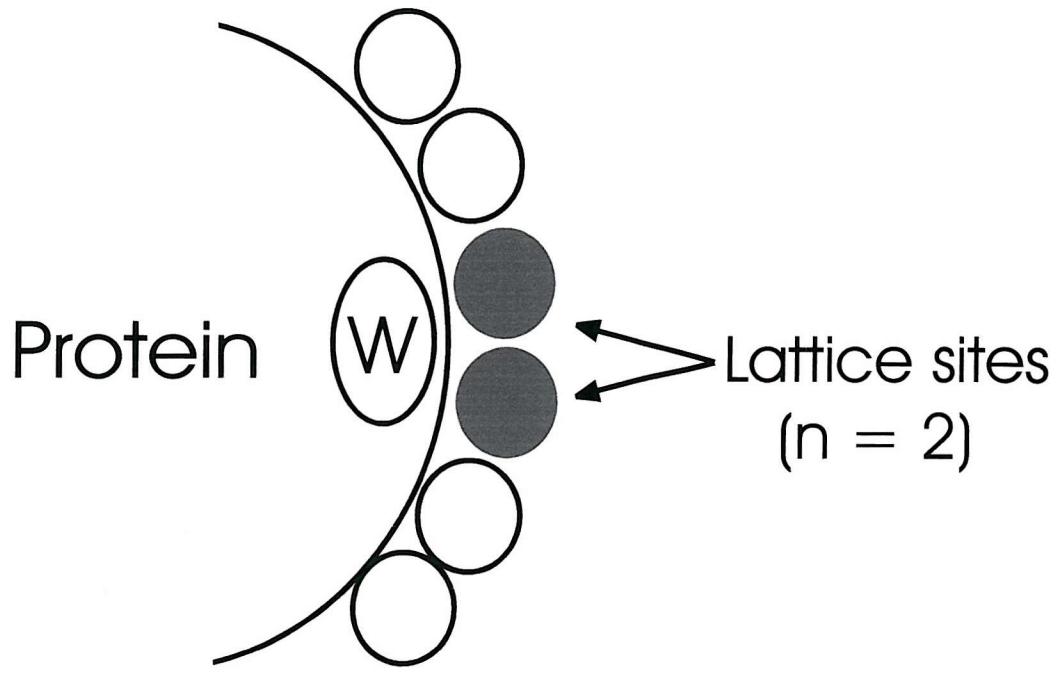

Figure 5.3: Schematic diagram of the lattice sites surrounding a membrane protein.

The lattice sites close enough to the Trp residue (represented by W) of the protein are filled in grey. There are two lipid sites that are close enough to the Trp to cause fluorescence quenching, if these sites were occupied by brominated lipid.

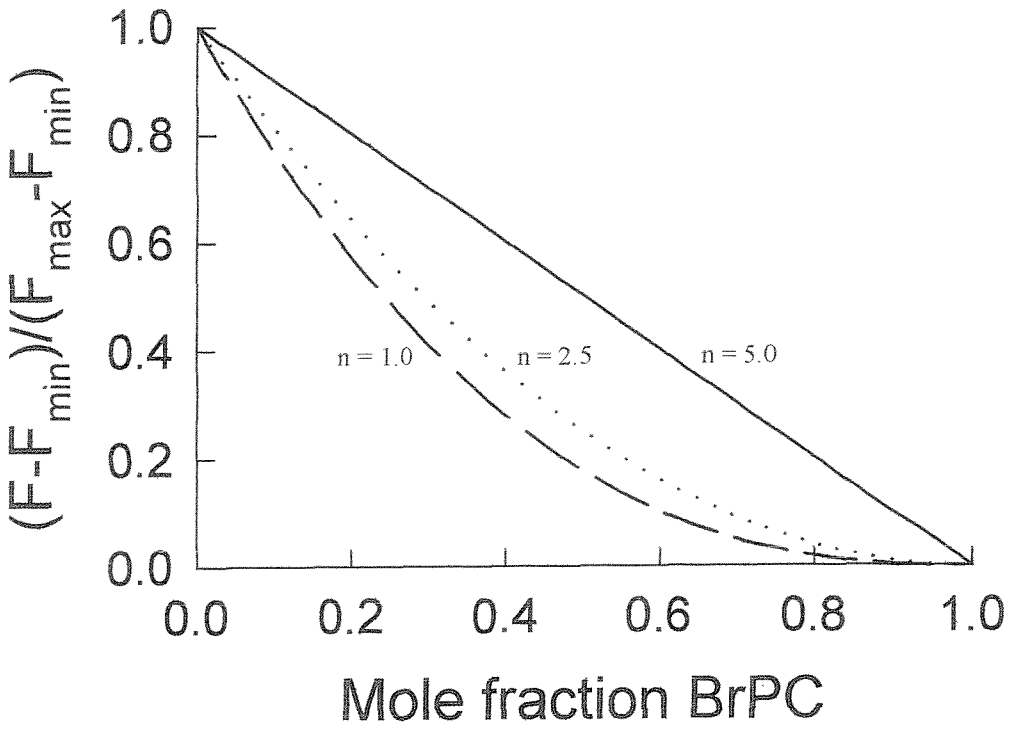

Figure 5.4: Diagram showing how the probability of a lattice site being occupied by a brominated lipid is dependent of the number of lattice sites (n).

The fluorescence of a protein in mixtures of brominated and non-brominated lipids is plotted as a function of the mole fraction of the brominated lipid. The level of quenching of the protein is seen to be dependent on the number of lattice sites (n) surrounding the Trp residues, where the number of sites is indicated on the graph for each line.

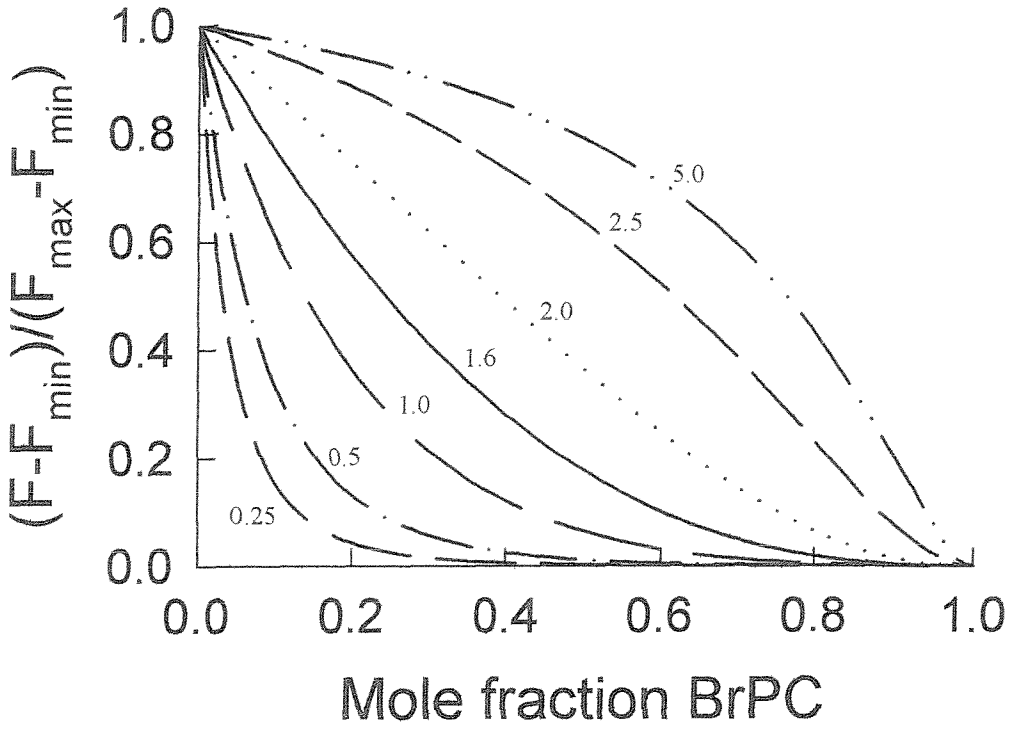

Figure 5.5: Diagram showing how the level of fluorescence quenching of a protein by a brominated lipid in mixtures of brominated and non-brominated lipid is dependent on the relative binding affinity of the protein for the non-brominated lipid species.

The fluorescence of a protein in mixtures of brominated and non-brominated lipids is plotted as a function of the mole fraction of the brominated lipid. The level of quenching of the protein is seen to be dependent on the relative lipid binding affinity (K) of the protein for the non-brominated lipid, where the K value is indicated on the graph for each line.

5.2 Methods

5.2.1 Preparation of Di(C14:1)PE

Dimyristoleoylphosphatidylethanolamine (di(C14:1)PE) can be prepared from di(C14:1)PC by phospholipase D (PLD) catalysed transphosphatidylation in the presence of ethanolamine (Dawson, 1967). The site of action of PLD is illustrated in Figure 5.6.

50 mg of di(C14:1)PC was dissolved in 10 mls of diethyl ether in a round-bottom flask. A 400-fold molar excess of ethanolamine at pH 5.6 in 5 mls of 0.1 M sodium acetate, pH 5.6, containing 0.1 M calcium chloride was added to the flask and mixed vigorously at 30 °C. 2000 units of PLD, extracted from cabbage (Sigma), was dissolved in 0.5 ml of 0.1 M sodium acetate and added in 166 µl aliquots at times, t = 0, 30 and 60 minutes. The reaction was followed by thin-layer chromatography (TLC) using a chloroform: methanol: acetic acid: water solvent system (25:65:4:2 v/v/v/v). The reaction was terminated after 7 hours by addition of 2.5 mls of 0.1 M EGTA. All of the lipid was extracted from the biphasic mixture by adding approximately 50 mls of diethyl ether in a separating funnel. The solvent was then removed by rotary evaporation, and the weight of the lipid product was determined, before resuspending in 1 ml of the chloroform: methanol: acetic acid: water solvent mixture. A slurry of silicic acid was prepared in the same solvent, and this was used to prepare a silicic acid column. The lipid product was purified on the column with the chloroform: methanol: acetic acid: water solvent mixture. 1 ml fractions were collected and analysed on TLC. The di(C14:1)PE-containing fractions were pooled and the solvent was removed to determine the yield. The product was resuspended in chloroform to a final concentration of 20 mg/ml, and was analysed by electrospray ionisation mass spectrometry in negative ionisation mode.

5.2.2 Preparation of Brominated Lipids

The brominated lipids 1,2-bis(9,10-dibromomyristoyl)-sn-glycero-3-phosphorylcholine (di(Br_2C14:0)PC) and 1,2-bis(9,10-dibromostearoyl)-sn-glycero-3-phosphorylethanoamine (di(Br_2C18:0) PE) were prepared by the method of Dawidowicz & Rothman (Dawidowicz & Rothman, 1976), as described in Section 3.2.2.1.

5.2.3 Reconstitution of Wild-type OmpF into Mixtures Containing Brominated Lipids

To determine the relative binding constant of OmpF for phospholipids varying in the length of their fatty acyl chains OmpF was reconstituted into mixtures of the brominated lipid, di(Br_2C18:0)PC and various non-brominated phosphatidylcholine species. The following non-brominated lipids were used: dilauroylphosphatidylcholine (di(C12:0)PC), di(C14:1)PC, di(C16:1)PC, di(C18:1)PC, di(C20:1)PC, di(C22:1)PC, and di(C24:1)PC. Reconstitution followed the dilution method described in Section 3.2.2.2 using a total of 2.5 μmols of lipid. The fluorescence was recorded as in Section 3.2.2.5 and samples reconstituted by the dialysis method were run on SDS-PAGE. OmpF was also reconstituted into mixtures of di(Br_2C14:0)PC and di(C18:1)PC.

To determine the effect of different head groups on the OmpF binding affinity, OmpF was reconstituted into mixtures of di(Br_2C18:0)PE with di(C18:1)PE and di(Br_2C18:0)PC with di(C18:1)PG, di(C18:1)PE or di(C14:1)PE.

5.2.4 Reconstitution of W61F into Mixtures containing Brominated Lipids

The OmpF mutant W61F was also reconstituted into mixtures of di(Br_2C18:0)PC with the following: di(C14:1)PC, di(C18:1)PC, or di(C24:1)PC.

5.2.5 Analysis of LPS binding by SDS-PAGE

To determine if LPS bound to native OmpF was displaced during reconstitution, OmpF samples were analysed before and after reconstitution. OmpF was reconstituted into di(C18:1)PC by the dialysis method, described in a Section 3.2.4, at a mole ratio of 600:1 protein-to-lipid. The sample was separated by sucrose density centrifugation as described in Section 3.2.2.7. 6.0 μg of OmpF from the most concentrated protein fraction (i.e., fraction 4, Section 3.15) was analysed on 15 % SDS-PAGE beside 6.0 μg of non-reconstituted OmpF, as described in Section 2.2.2.4.

5.3 Results

5.3.1 Preparation of Di (C14:1)PE

Di(C14:1)PE was prepared by headgroup exchange using phospholipase D. As can be seen from TLC analysis, shown in Figure 5.7, a single spot of the product was seen, running at the same position as the species di(C18:1)PE. Mass spectrometry analysis showed the presence of a single product with a M_r = 630. This value corresponds to the expected molecular weight for di(C14:1)PE (See Figure 5.8).

5.3.2 Relative Phospholipid Binding Affinities

OmpF was reconstituted by the dilution method established in chapter 3 (Section 3.2.2.2) using the detergent octyl-POE, at a lipid-to-protein molar ratio of 600:1. Figure 5.9 shows the results of an experiment in which OmpF was reconstituted into mixtures of di(C18:1)PC and di(Br_2C18:0)PC. As can be seen, fluorescence intensity decreases with increasing di(Br_2C18:0)PC content; at 100 % di(Br_2C18:0)PC the fluorescence intensity being 50 ± 2 % relative to the fluorescence intensity for OmpF reconstituted in di(C18:1)PC.

In Figure 5.10 the fluorescence intensity excited at 280 nm is plotted as a function of the mole fraction of di(Br_2C18:0)PC in the mixture. The fluorescence intensity is plotted as the fraction of the quenchable fluorescence, $(F - F_{min})/(F_o - F_{min})$, where F_o and F_{min} are the fluorescence intensities when the mole fraction of di(Br_2C18:0)PC is 0 and 1, respectively, and F is the fluorescence intensity at intermediate mole fractions of di(Br_2C18:0)PC. This plot was fitted to Equation 5.3 (see Section 5.1.2) by applying the nonlinear least squares programme in Sigmaplot. The data fit to the equation with a value for n, the number of 'sites' from which Trp fluorescence can be quenched, of 2.54 ± 0.25. The quenching data for mixtures of di(Br_2C18:0)PC and phosphatidylcholine with fatty acyl chain lengths between C12 and C24 are presented in Figures 5.11 to 5.16. The data for the di(Br_2C18:0)PC mixtures

with di(C14:1)PC, di(C18:1)PC and di(C24:1)PC are compared in Figure 5.17. It can be seen from this figure that OmpF in phosphatidylcholine mixtures with shorter fatty acyl chains have higher fluorescence intensities at molar ratios of di(Br_2C18:0)PC between 0.2 and 0.8 than the OmpF in phosphatidylcholine with longer fatty acyl chains. These shorter fatty acyl chain length phosphatidylcholine molecules are therefore less easily displaced from OmpF by di(Br_2C18:0)PC than PC with chain lengths C20 to C24.

The data for each phosphatidylcholine was fitted to Equation 5.5 using n = 2.54, thereby providing a binding constant (K) for each lipid relative to that for di(C18:1)PC. The mean binding constants for each fatty acyl chain length are shown in Figure 5.18 (see also Table 5.1), where they are compared to those previously obtained for the Ca^{2+} -ATPase, a typical α-helical membrane protein (East & Lee, 1982). The results show that OmpF has a higher affinity for di(C14:1)PC than for di(C18:1)PC, whereas the Ca^{2+}-ATPase displays no such selectivity for any particular fatty acyl chain length. The relative binding constants of OmpF decrease for phosphatidylcholine with fatty acyl chain lengths longer or shorter than C14, particularly those with fatty acyl chains longer than C18.

This conclusion that OmpF selectively binds to di(C14:1)PC was confirmed in experiments using di(Br_2C14:0)PC as the quenching lipid instead of di(Br_2C18:0)PC. OmpF was reconstituted into mixtures of di(Br_2C14:0)PC and di(C18:1)PC. Fitting the data shown in Figure 5.19 to Equation 5.5 gave a value for K of 0.75 ± 0.03. In this case, K refers to the binding constant of di(C18:1)PC relative to di(Br_2C14:0)PC, since the quenching lipid was di(Br_2C14:0)PC in this case. Thus the binding constant of di(Br_2C14:0)PC relative to di(C18:1)PC can be calculated from 1/K, which is equal to 1.33. This compares to 1.67, the relative binding constant of di(C14:1)PC calculated from quenching in mixtures of di(Br_2C18:0)PC and di(C14:1)PC (Figure 5.12). Thus OmpF has a higher binding affinity for phosphatidylcholine with fatty acyl chain lengths of C14 than for C18.

These experiments were repeated with the mutant W61F. In this case reconstitution with di(Br_2C18:0)PC leads to 64 ± 2 % quenching of the fluorescence intensity (see Figure 4.18). The relative binding constant of the OmpF mutant W61F for phosphatidylcholines with varying chain lengths was determined. This was done in an identical manner to those with the wild type OmpF, by reconstituting W61F in mixtures of di(Br_2C18:0)PC and one of the following non-brominated lipids: di(C14:1)PC, di(C18:1)PC or di(C24:1)PC. The results are presented in Figure 5.20 as the level of quenching as a function of the di(Br_2C18:0)PC content. A similar trend is seen to that of the wild type protein (see Figure 5.17) where the protein has higher fluorescence intensities in phosphatidylcholine mixtures with shorter fatty acyl chains at molar ratios of di(Br_2C18:0)PC between 0.2 and 0.8, than the protein in phosphatidylcholine with longer fatty acyl chains. The number of sites, n was calculated from the fluorescence data of W61F in mixtures of di(Br_2C18:0)PC and di(C18:1)PC to be 2.61 ± 0.26. The K values were calculated relative to di(C18:1)PC (K = 1.0) and gave mean values of 1.6214 ± 0.18 for di(C14:1)PC and 0.61 ± 0.09 for di(C24:1)PC.

The relative binding affinity of native OmpF for phospholipids with different head groups was also measured by reconstituting OmpF in mixtures of di(Br_2C18:0)PC with di(C18:1)PE or di(C18:1)PG. To ensure that the n value attained for the phosphatidylcholine data was suitable for analysis of data for other phospholipids the n value for OmpF reconstituted in mixtures of di(C18:1)PE and di(Br_2C18:0)PE was calculated. These data (Figure 5.21) gave an n value of 2.32 ± 0.15, which is similar to the n value, 2.54, obtained from mixtures of di(Br_2C18:0)PC and di(C18:1)PC (Figure 5.10). Figure 5.22 showed that similar quenching of OmpF by di(Br_2C18:0)PC is seen in mixtures with di(C18:1)PE and with di(C18:1)PC. In mixtures of di(Br_2C18:0)PC with di(C18:1)PG, however, OmpF is quenched more readily between the di(Br_2C18:0)PC mole fraction 0.2 to 0.8. The K value of di(C18:1)PE, relative to di(C18:1)PC, was 0.87 ± 0.09. The K value for di(C18:1)PG relative to di(C18:1)PC was 0.56 ± 0.07, approximately half that of the zwitterionic phospholipids.

5.3.3 SDS-PAGE Analysis of Reconstituted OmpF

To ensure that the state of oligomery of OmpF does not change when it is reconstituted into bilayers varying in their hydrophobic thickness and charge properties, SDS-PAGE analysis was performed. SDS-PAGE gels for OmpF that had been reconstituted by the dialysis method into di(C14:1)PC, di(C24:1)PC, di(C18:1)PE, and di(C18:1)PG are shown in Figure 5.23. The apparent M_r of all the samples is 90 k showing that reconstitution into the afore mentioned lipids does not disrupt the trimer structure of OmpF.

5.3.4 Analysis of LPS Binding by SDS-PAGE

The result of SDS-PAGE analysis of OmpF binding before and after reconstitution is shown in Figure 5.24. As can be seen in lanes 2 and 3 the OmpF appears as a trimer with an apparent M_r of approximately 90 K. Several diffuse bands can be observed in each sample, where each band represents OmpF with different amounts of LPS bound to it. The lower band in each of the two lanes is OmpF devoid of bound LPS. As the amount of bound LPS increases the apparent M_r increases, so that the highest bands show those OmpF trimers with the highest amounts of bound LPS. Upon close examination it can be seen that the proportion of LPS-free OmpF is relatively higher in lane 3, containing reconstituted OmpF, than in lane 2, containing non-reconstituted OmpF.

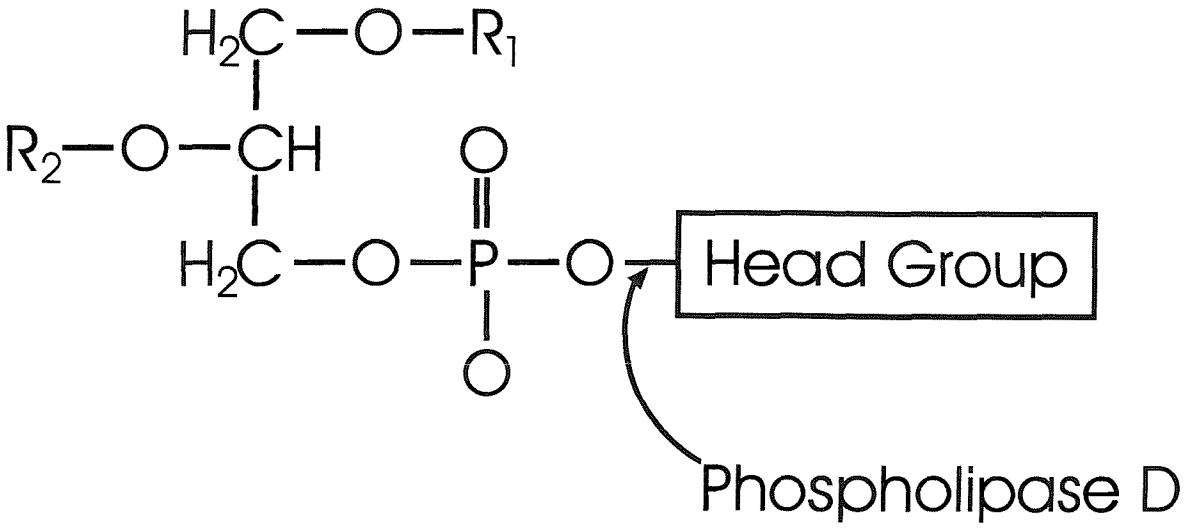

Figure 5.6: Site of action of PLD on phospholipids.

PLD hydrolyses phospholipids at the head group ester bond. In addition to the hydrolase activity PLD also acts as a transferase in the presence of a primary alcohol (Martin, 1983).

Figure 5.7: TLC of di(C14:1)PE prepared by transphosphatidylation using phospholipase D.

Purified di(C14:1)PE was spotted onto a TLC plate beside commercial di(C18:1)PE from Avanti Lipid Products. The solvent system used was chloroform: methanol: acetic acid: water (25:65:4:2 v/v/v/v). di(C18:1)PE and di(C14:1)PE are shown in 1 and 2, respectively.

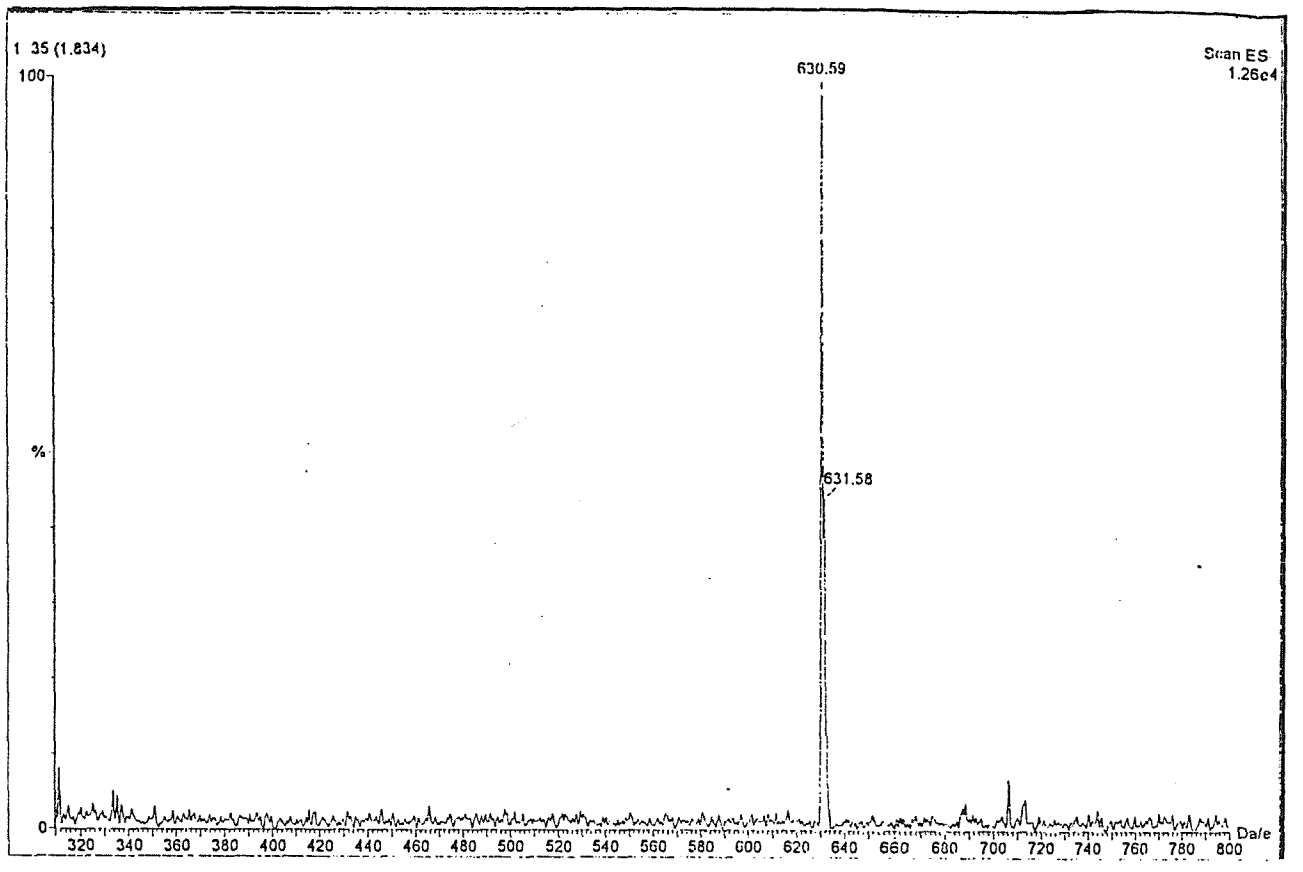

Figure 5.8: Mass spectrometry of purified di(C14:1)PE.

Purified di(C14:1)PE suspended in methanol was analysed by negative ionisation electrospray mass spectrometry. A single peak was seen at a mass-to-charge ratio of 630 which corresponds to the molecular weight of di(C14:1)PE.

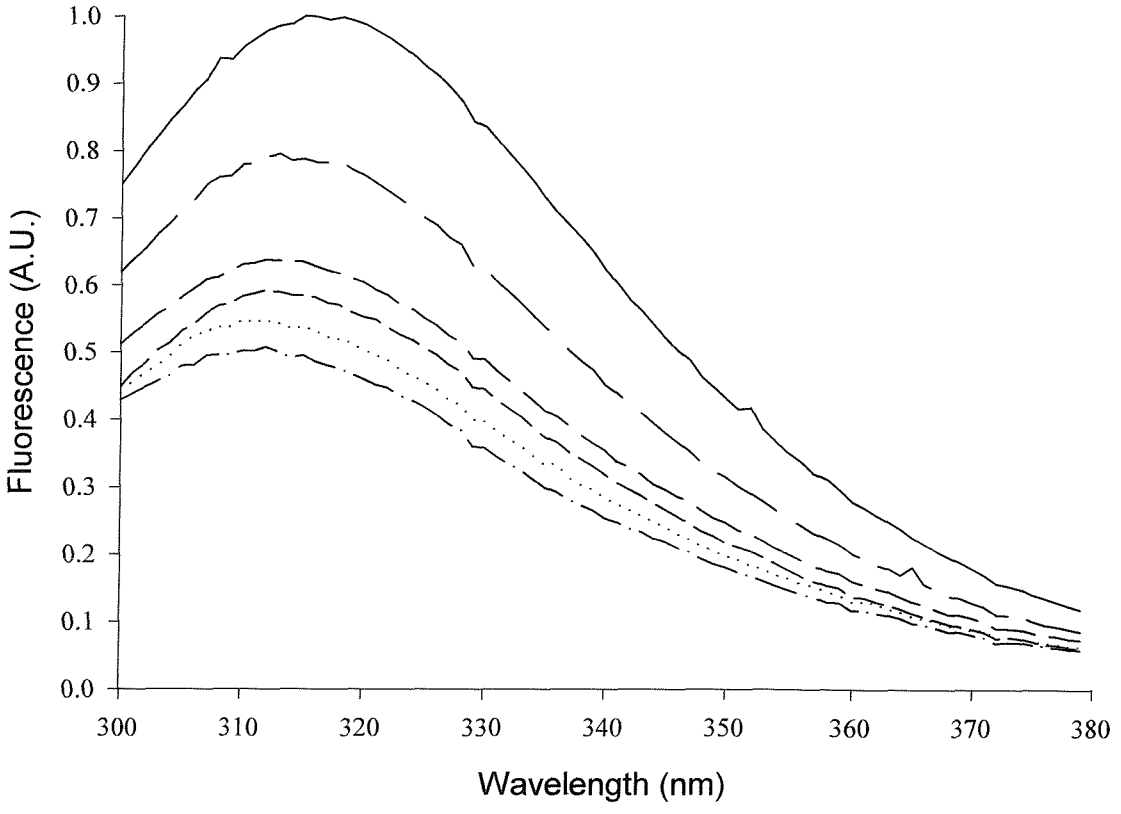

Figure 5.9: Fluorescence spectra of OmpF reconstituted in mixtures of di(C18:1)PC and di(Br_2C18:0)PC.

OmpF was reconstituted by the dilution method into mixtures of di(C18:1)PC and di(Br_2C18:0)PC at increasing molar fractions of brominated lipid. The lipid-to-protein molar ratio in all reconstitutions was 600:1 and for all emission spectra the fluorescence of 0.12 nmols of OmpF was excited at 280 nm in 20 mM Hepes, pH 7.2, 1 mM EGTA. The emission spectra in descending order correspond to mole fractions of di(Br_2C18:0)PC of 0.0, 0.2, 0.4, 0.6, 0.8 and 1.0.

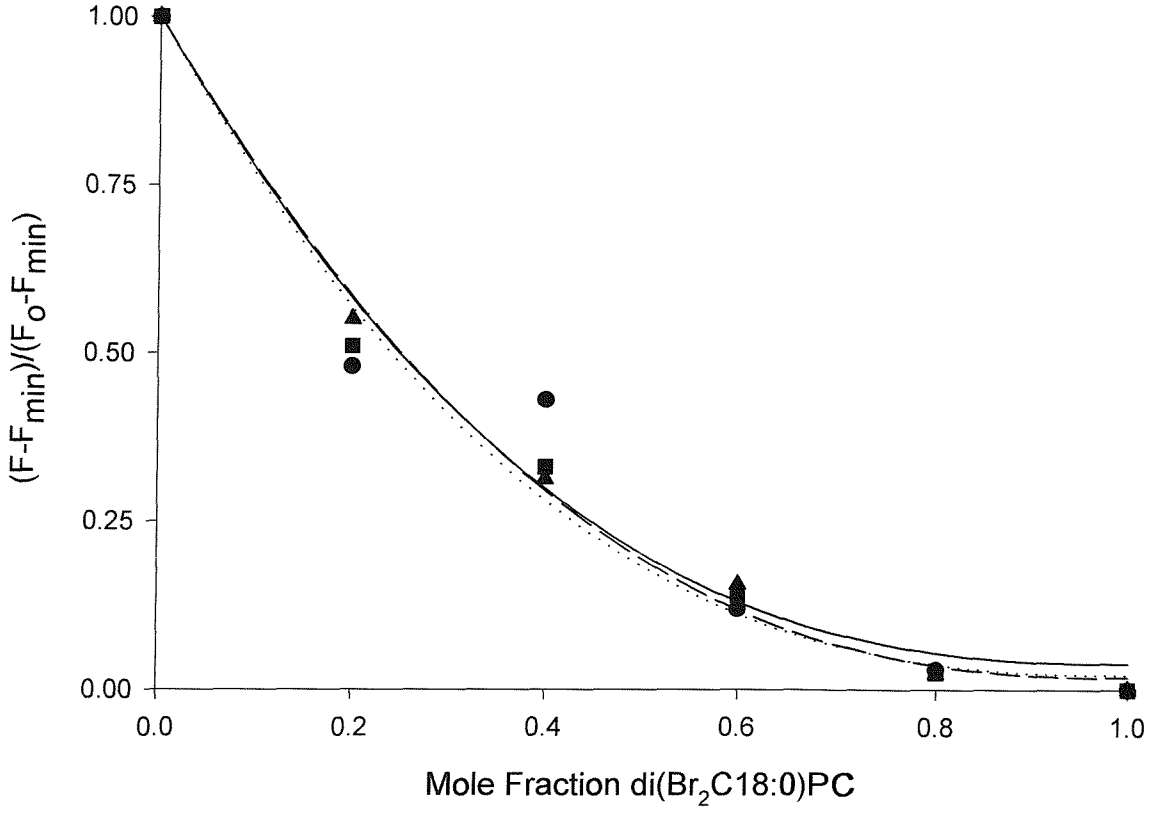

Figure 5.10: Relative fluorescence intensities for OmpF in mixtures of di(C18:1)PC and di(Br_2C18:0)PC.

OmpF was reconstituted in mixtures of di(C18:1)PC and di(Br_2C18:0)PC at the given mole fraction of brominated lipid. The fluorescence intensity is expressed as the fraction of the quenchable fluorescence $(F-F_{min})/(F_o-F_{min})$, where F_o and F_{min} are the fluorescence intensities when the mole fraction of di(Br_2C18:0)PC is 0 and 1, respectively, and F is the maximum fluorescence intensity at intermediate mole fractions of di(Br_2C18:0)PC. In all spectra the fluorescence of 0.12 nmols of OmpF was excited at 280 nm in 20 mM Hepes, pH 7.2, 1 mM EGTA. The symbols represent the fluorescence results presented in triplicate, and the lines are the best-fit curves giving n values of 2.56 ± 0.23 (—●—), 2.38 ± 0.22 (—▲—), 2.67 ± 0.32 (—■—).

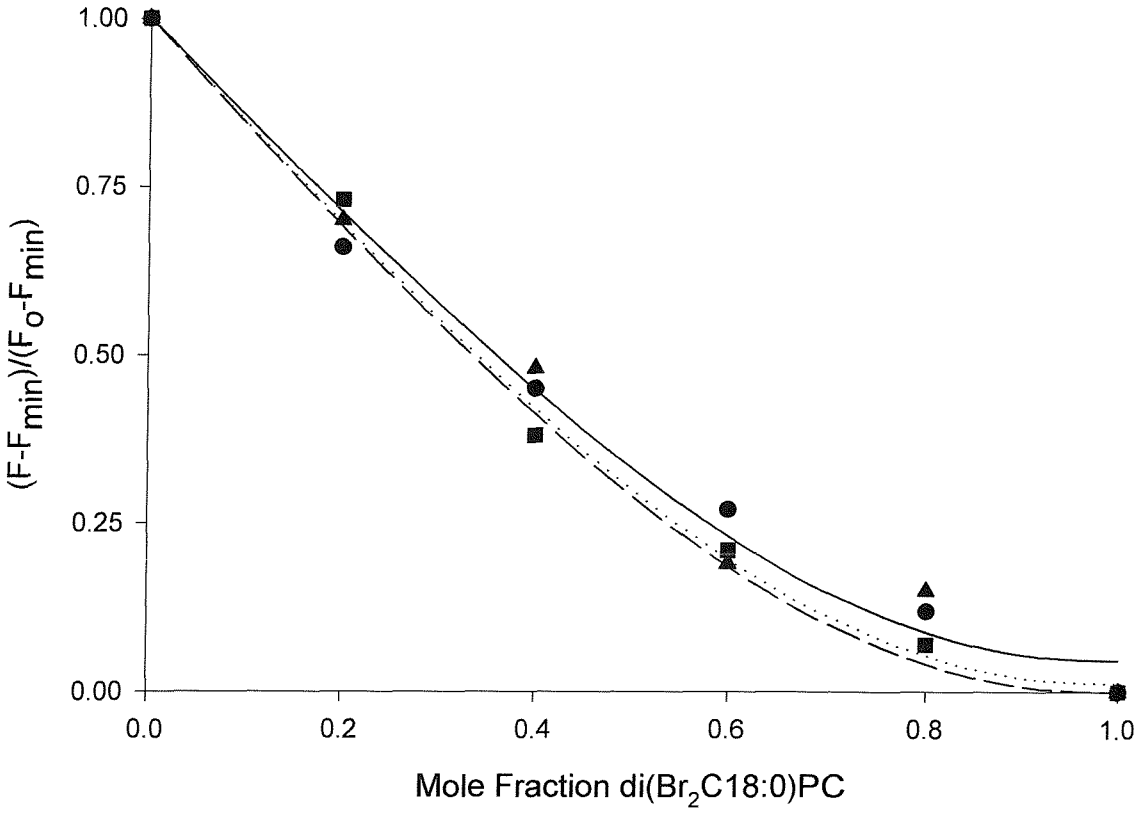

Figure 5.11: Relative fluorescence intensities for OmpF in mixtures of di(C12:1)PC and di(Br_2C18:0)PC.

OmpF was reconstituted in mixtures of di(C12:1)PC and di(Br_2C18:0)PC at the given mole fraction of brominated lipid. For experimental conditions see Figure 5.10. The symbols represent fluorescence results presented in triplicate, and the lines are fitted using an n value of 2.54 to give K values of 1.09 ± 0.28 (—●—), 1.043 ± 0.09079 (—▲—), and 0.98 ± 0.13 (—■—).

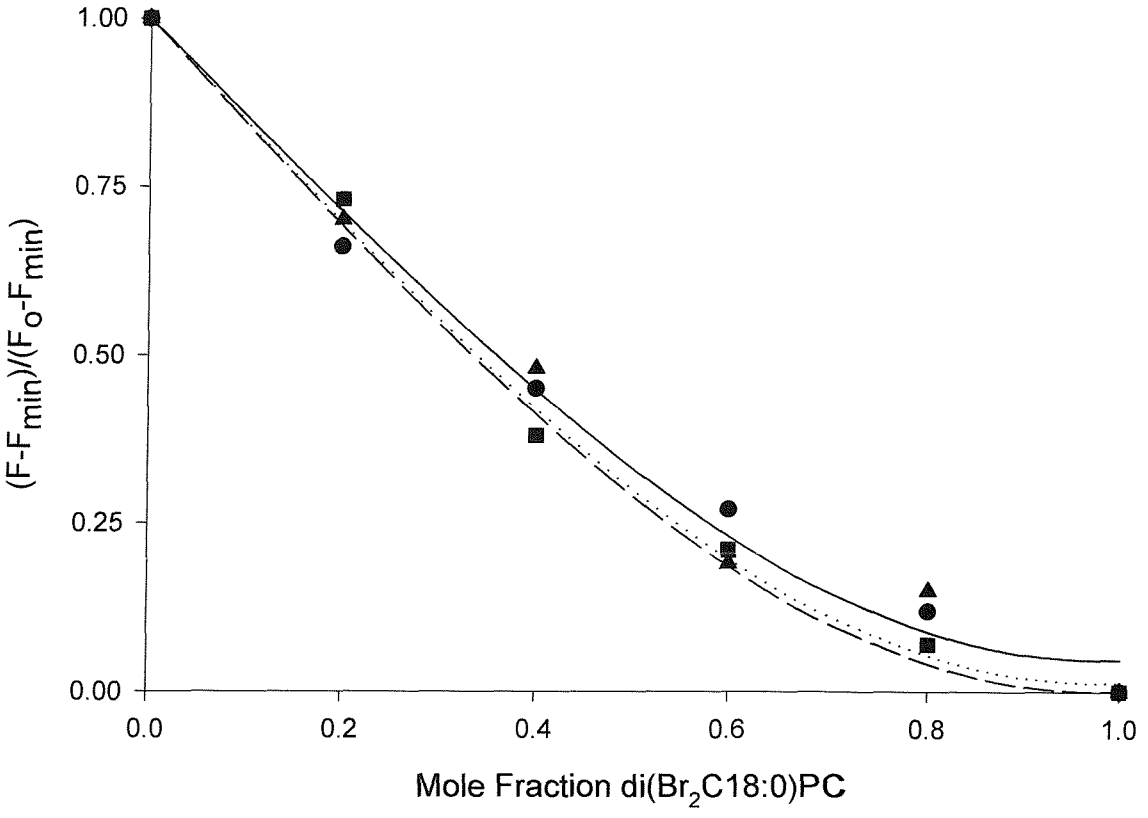

Figure 5.12: Relative fluorescence intensities for OmpF in mixtures of di(C14:1)PC and di(Br_2C18:0)PC.

OmpF was reconstituted in mixtures of di(C14:1)PC and di(Br_2C18:0)PC at the given mole fraction of brominated lipid. For experimental conditions see Figure 5.10. The symbols represent fluorescence results presented in triplicate, and the lines are fitted using an n value of 2.54 to give K values of 1.66 ± 0.22 (—●—), 1.66 ± 0.25 (—▲—), and 1.68 ± 0.17 (—■—).

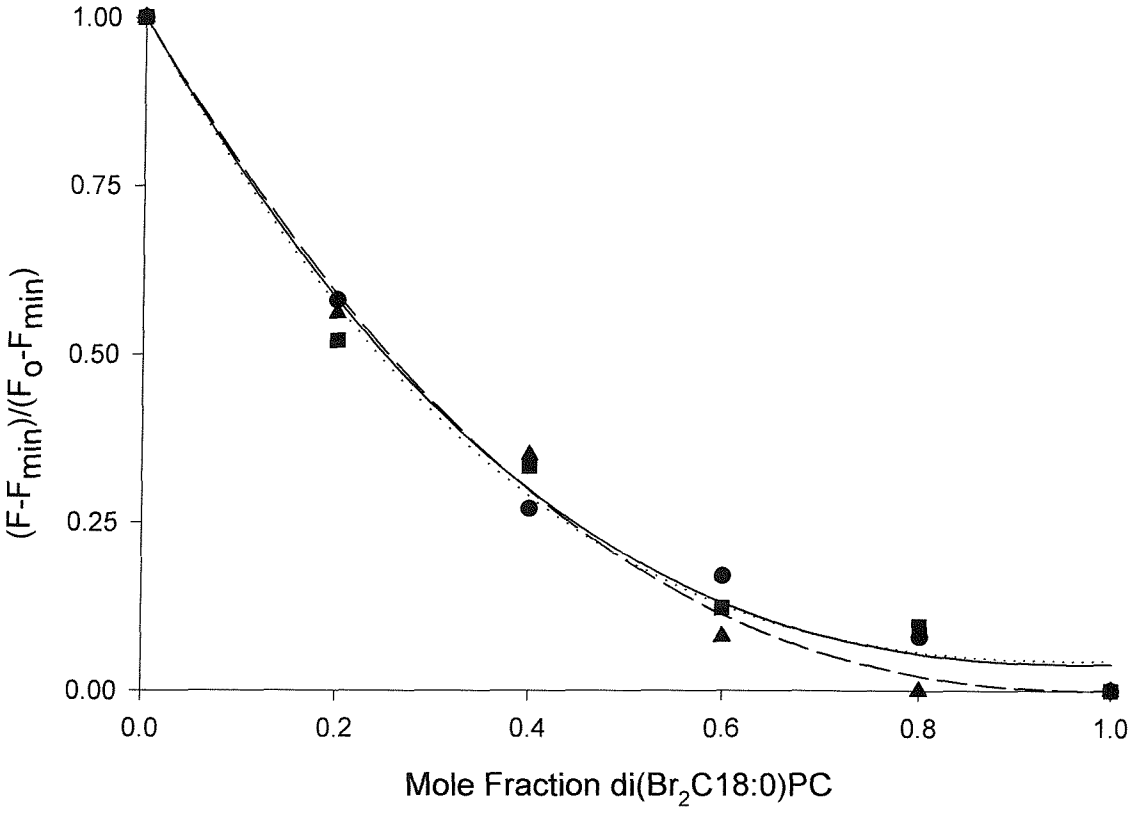

Figure 5.13: Relative fluorescence intensities for OmpF in mixtures of di(C16:1)PC and di(Br_2C18:0)PC.

OmpF was reconstituted in mixtures of di(C16:1)PC and di(Br_2C18:0)PC at the given mole fraction of brominated lipid. For experimental conditions see Figure 5.10. The symbols represent fluorescence results presented in triplicate, and the lines are fitted using an n value of 2.54 to give K values of 1.29 ± 0.37 (—●—), 1.42 ± 0.39 (—▲—), and 1.44 ± 0.11 (—■—).

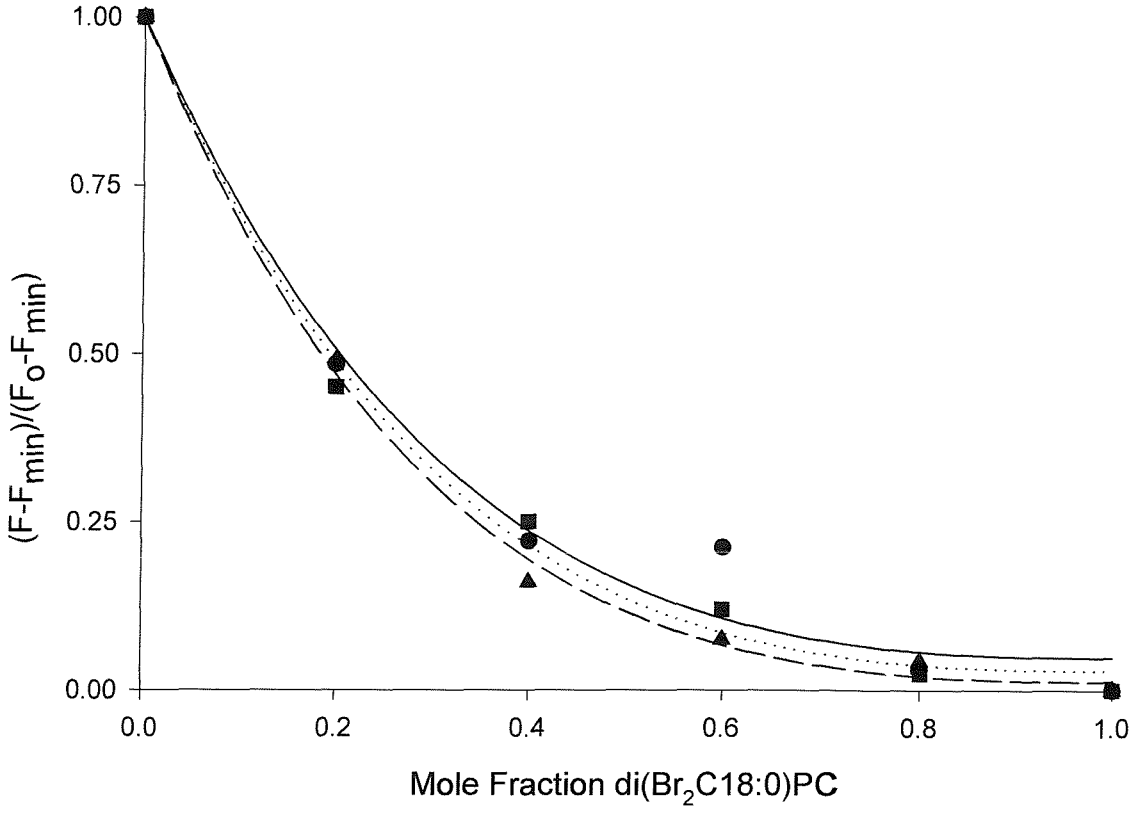

Figure 5.14: Relative fluorescence intensities for OmpF in mixtures of di(C20:1)PC and di(Br_2C18:0)PC.

OmpF was reconstituted in mixtures of di(C20:1)PC and di(Br_2C18:0)PC at the given mole fraction of brominated lipid. For experimental conditions see Figure 5.10. The symbols represent fluorescence results presented in triplicate, and the lines are fitted using an n value of 2.54 to give K values of 0.76 ± 0.15 (—●—), 0.71 ± 0.0.05 (—▲—), and 0.73 ± 0.08 (—■—).

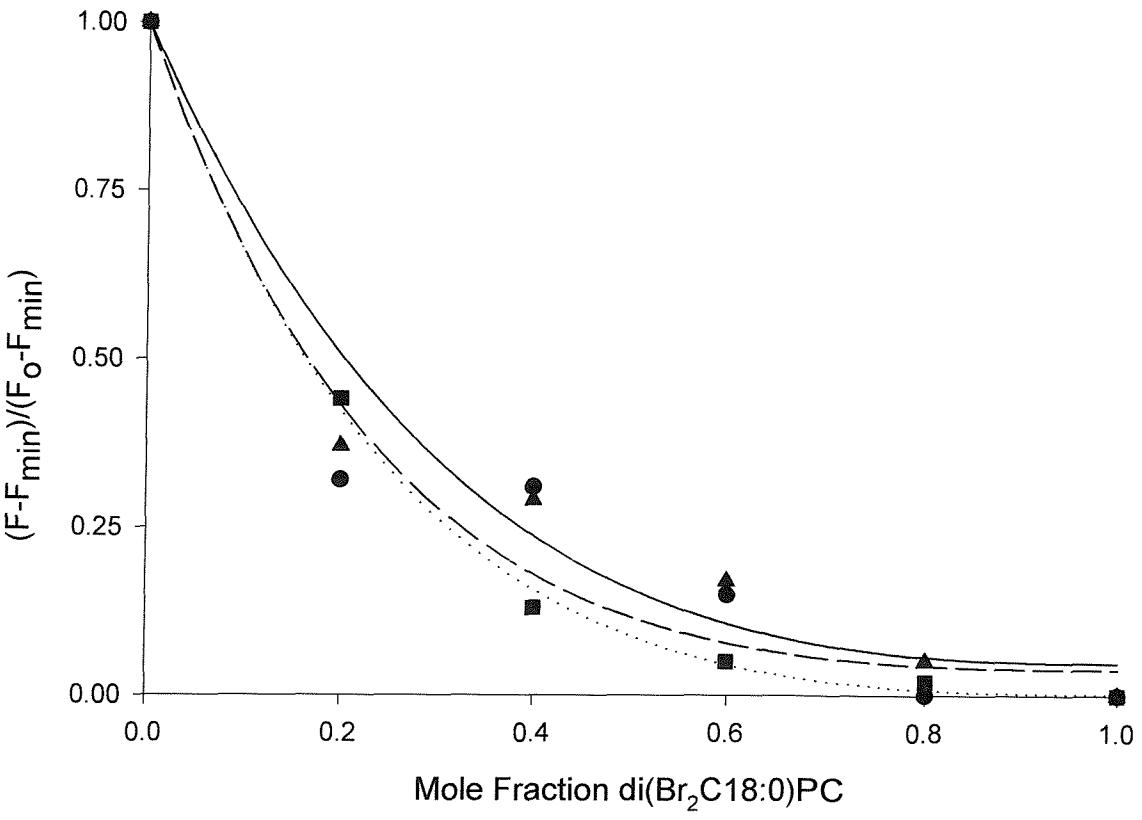

Figure 5.15: Relative fluorescence intensities for OmpF in mixtures of di(C22:1)PC and di(Br_2C18:0)PC.

OmpF was reconstituted in mixtures of di(C22:1)PC and di(Br_2C18:0)PC at the given mole fraction of brominated lipid. For experimental conditions see Figure 5.10. The symbols represent fluorescence results presented in triplicate, and the lines are fitted using an n value of 2.54 to give K values of 0.53 ± 0.18 (—●—), 0.57 ± 0.16 (—▲—), and 0.6 ± 0.06 (—■—).

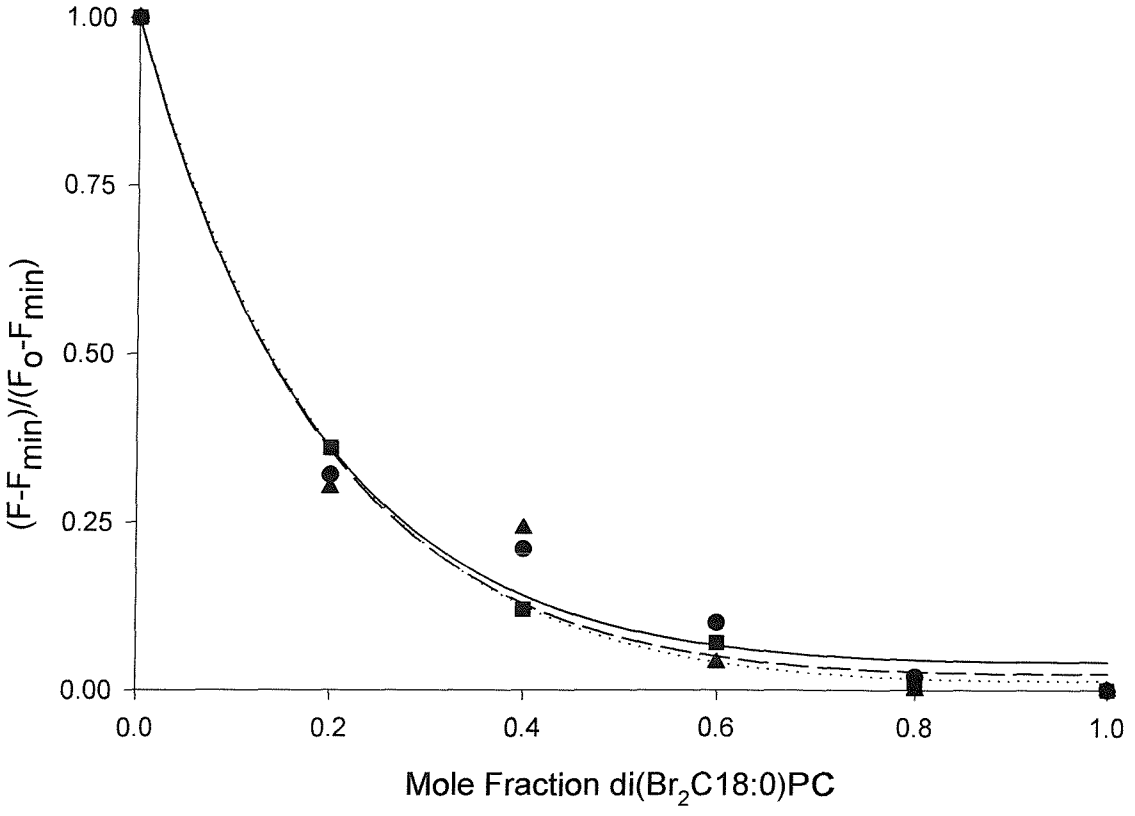

Figure 5.16: Relative fluorescence intensities for OmpF in mixtures of di(C24:1)PC and di(Br_2C18:0)PC.

OmpF was reconstituted in mixtures of di(C24:1)PC and di(Br_2C18:0)PC at the given mole fraction of brominated lipid. For experimental conditions see Figure 5.10. The symbols represent fluorescence results presented in triplicate, and the lines are fitted using an n value of 2.54 to give K values of 0.47 ± 0.09 (—●—), 0.48 ± 0.11 (—▲—), and 0.50 ± 0.03 (—■—).

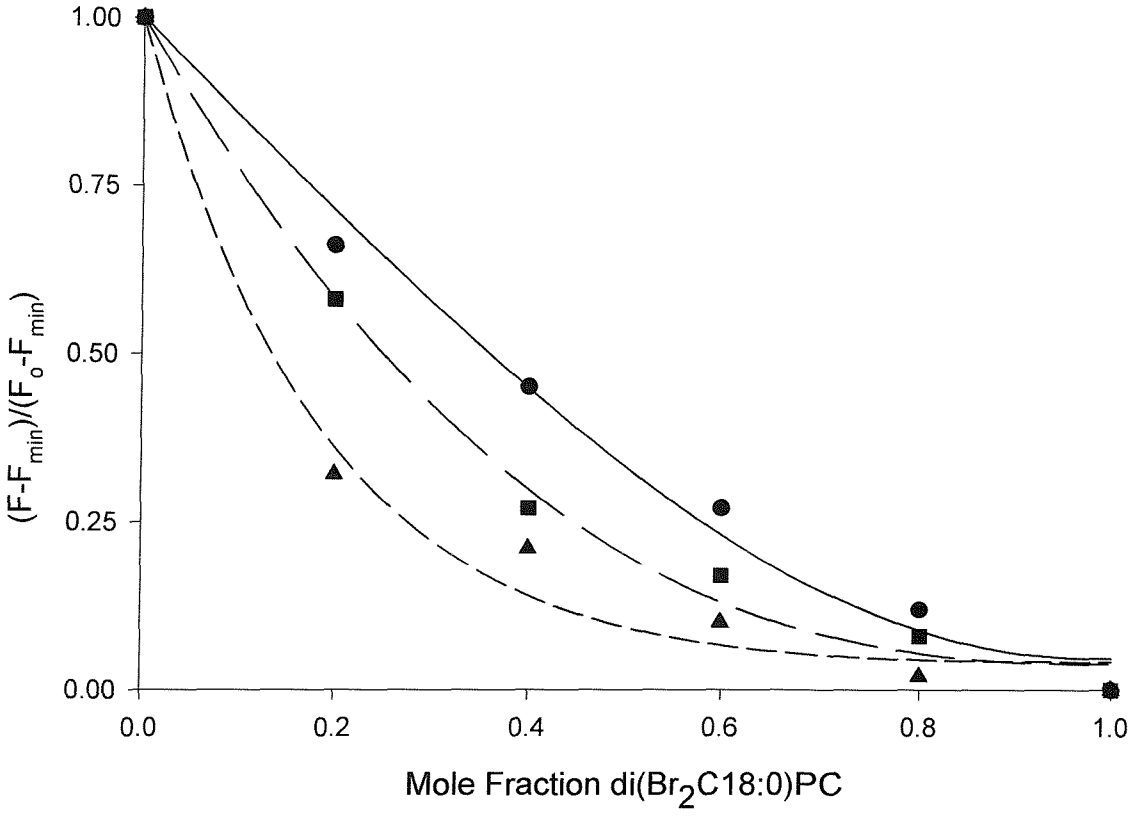

Figure 5.17: Comparison of the relative fluorescence intensities for OmpF in mixtures of di(C14:1)PC, di(C18;1)PC, or di(C24:1)PC and di(Br_2C18:0)PC. OmpF was reconstituted in mixtures of di(C14:1)PC, (—●—), di(C18:1)PC (—▲—), or di(C24:1)PC (—■—) and di(Br_2C18:0)PC at the given mole fraction of brominated lipid. For experimental conditions see Figure 5.10. The relative binding affinities for the lipids shown are 1.66 ± 0.22 for di(C14:1)PC, and 0.47 ± 0.09 for di(C24:0)PC. The number of lattice sites for the di(C18:1)PC data shown are 2.56 ± 0.23.

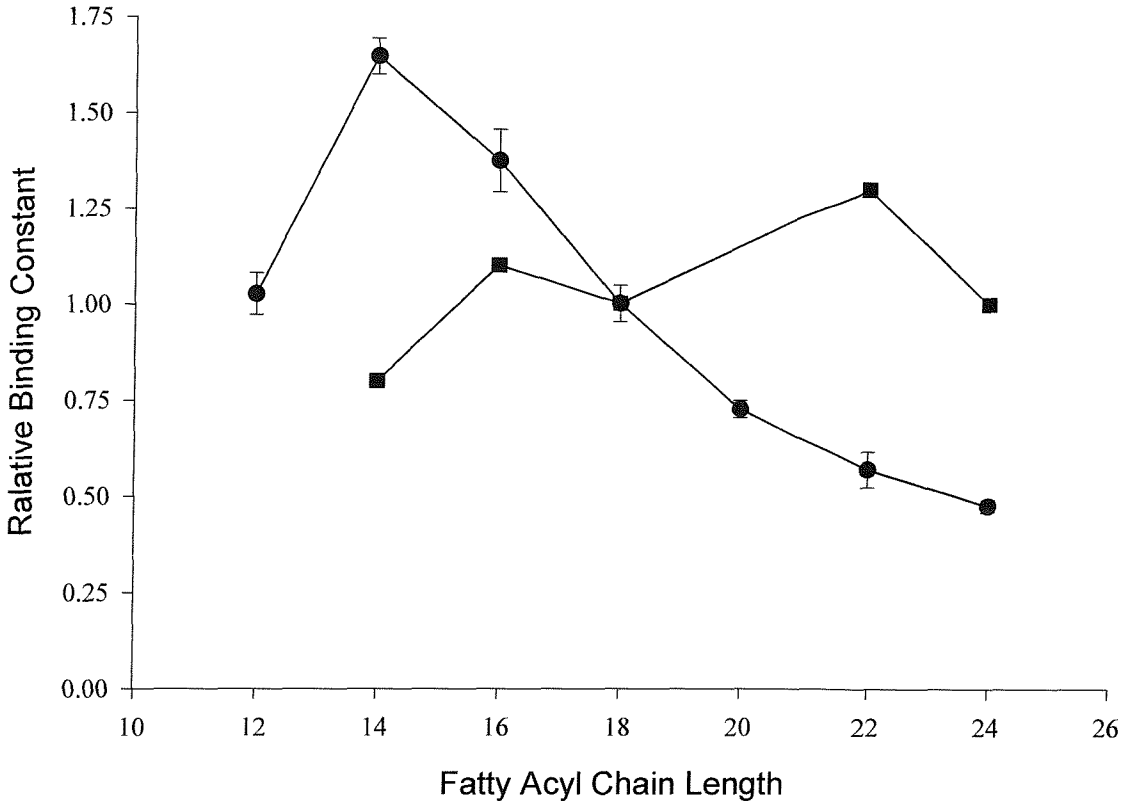

Figure 5.18: Relative binding affinities of OmpF for different chain length phosphatidylcholines compared to those obtained for the Ca^{2+}-ATPase, a typical α-helical membrane protein (East & Lee, 1982).

The binding constants of OmpF for different fatty acyl chain length phosphatidylcholines was measured relative to di(C18:1)PC in fluorescence quenching studies with di(Br_2C18:0)PC. The relative binding affinities obtained for OmpF (–●–) were compared to published values (East & Lee, 1982) for the Ca^{2+}-ATPase (–■–) as a function of the fatty acyl chain length.

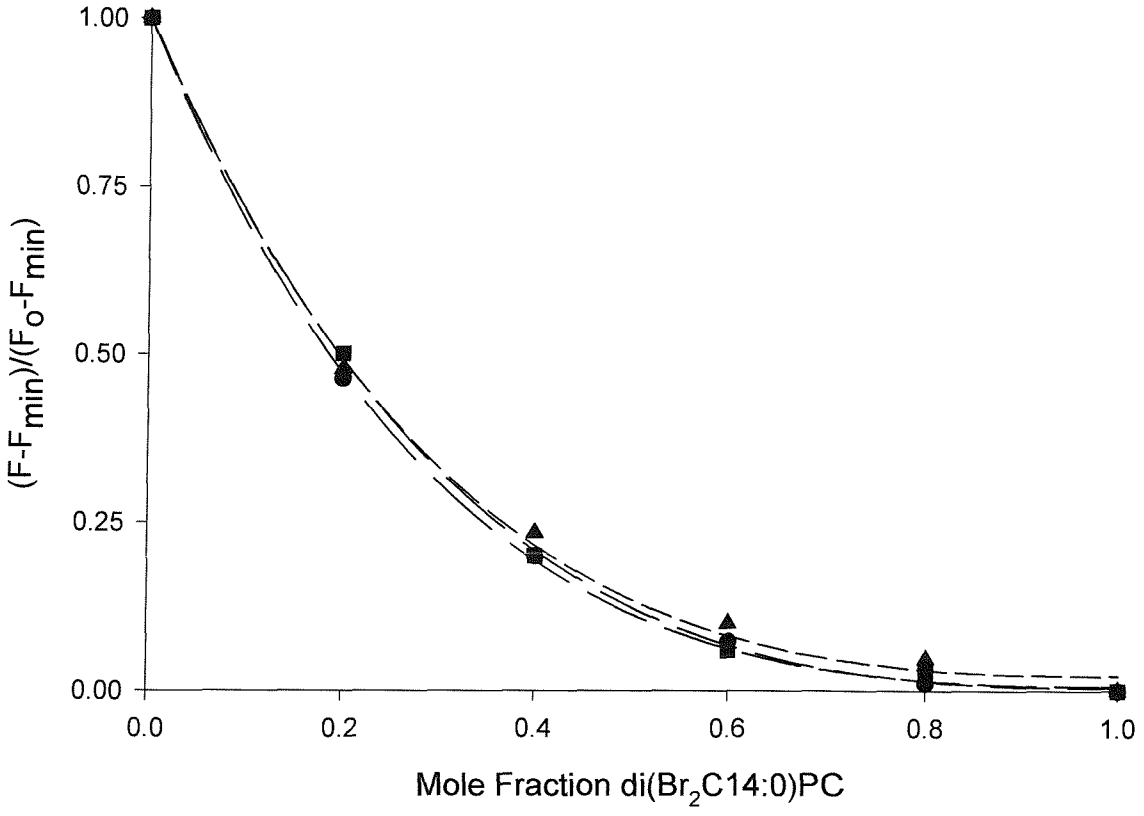

Figure 5.19: Relative fluorescence intensities for OmpF in mixtures of di(C18:1)PC and di(Br_2C14:0)PC.

OmpF was reconstituted in mixtures of di(C18:1)PC and di(Br_2C14:0)PC at the given molar ratio of brominated lipid. For experimental conditions see Figure 5.10. The symbols represent fluorescence results presented in triplicate, and the lines are fitted using an n value of 2.54 to give K values of 0.75 ± 0.05 (—●—), 0.72 ± 0.0.02 (—▲—),and 0.78 ± 0.03 (—■—)

.

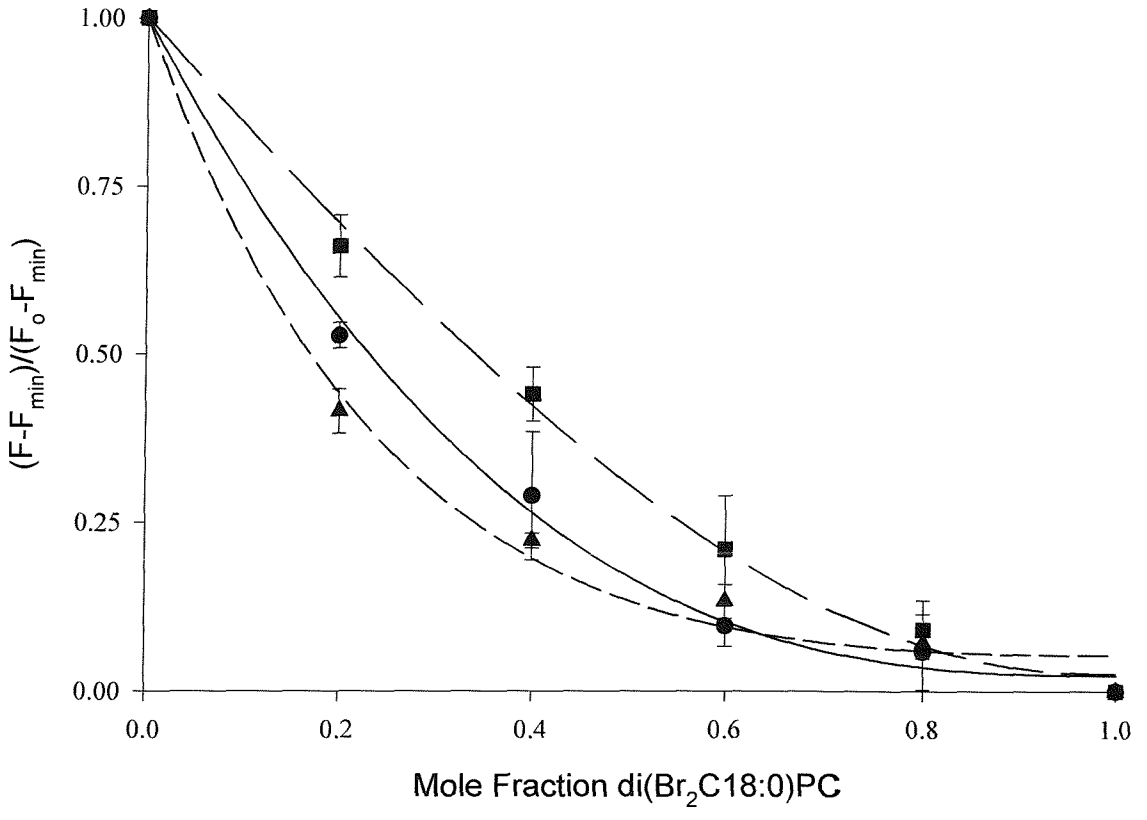

Figure 5.20: Relative fluorescence intensities for W61F in mixtures of di(Br_2C18:0)PC and di(C14:1)PC, di(C18:1)PC or di(C24:1)PC.

The OmpF mutant W61F was reconstituted in mixtures of di(C14:1)PC, di(C18:1)PC or di(C24:1)PC with di(Br_2C18:0)PC at the given mole fraction of brominated lipid. For experimental conditions see Figure 5.10. The symbols represent mean fluorescence results, and the lines are fitted to give K values of 1.62 ± 0.18 for di(C14:1)PC (—●—), 0.61 ± 0.09 for di(C24:1)PC (—▲—), using an n value of 2.61 ± 0.26 obtained from the di(C18:1)PC data (—■—).

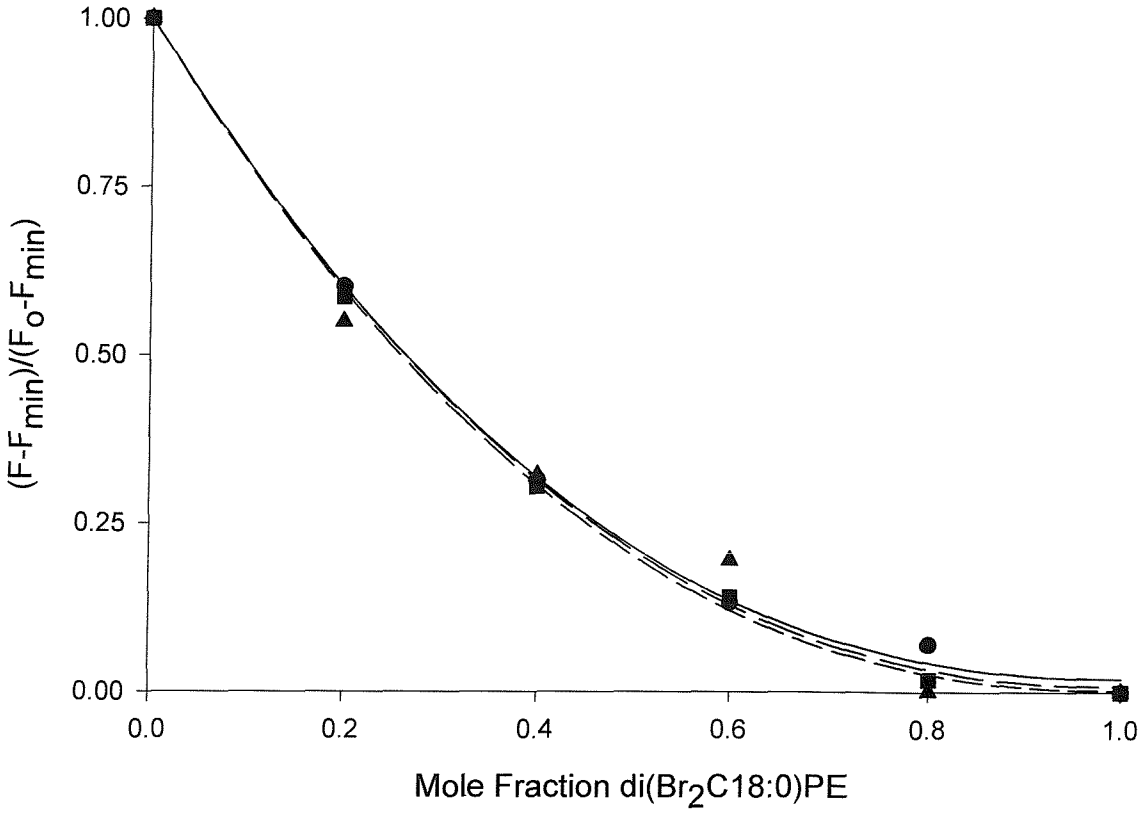

Figure 5.21: Relative fluorescence intensities for OmpF in mixtures of di(C18:1)PE and di(Br_2C18:0)PE.

OmpF was reconstituted in mixtures of di(C18:1)PE and di(Br_2C18:0)PE at the given mole fraction of brominated lipid. For experimental conditions see Figure 5.10. The symbols represent the fluorescence results presented in triplicate, and the lines are fitted assuming a K value of 1.0 for di(C18:1)PE relative to di(Br_2C18:0)PE. The n values obtained from the data were 2.33 ± 0.10 (—●—), 2.30 ± 0.27 (—▲—), and 2.33 ± 0.07 (—■—).

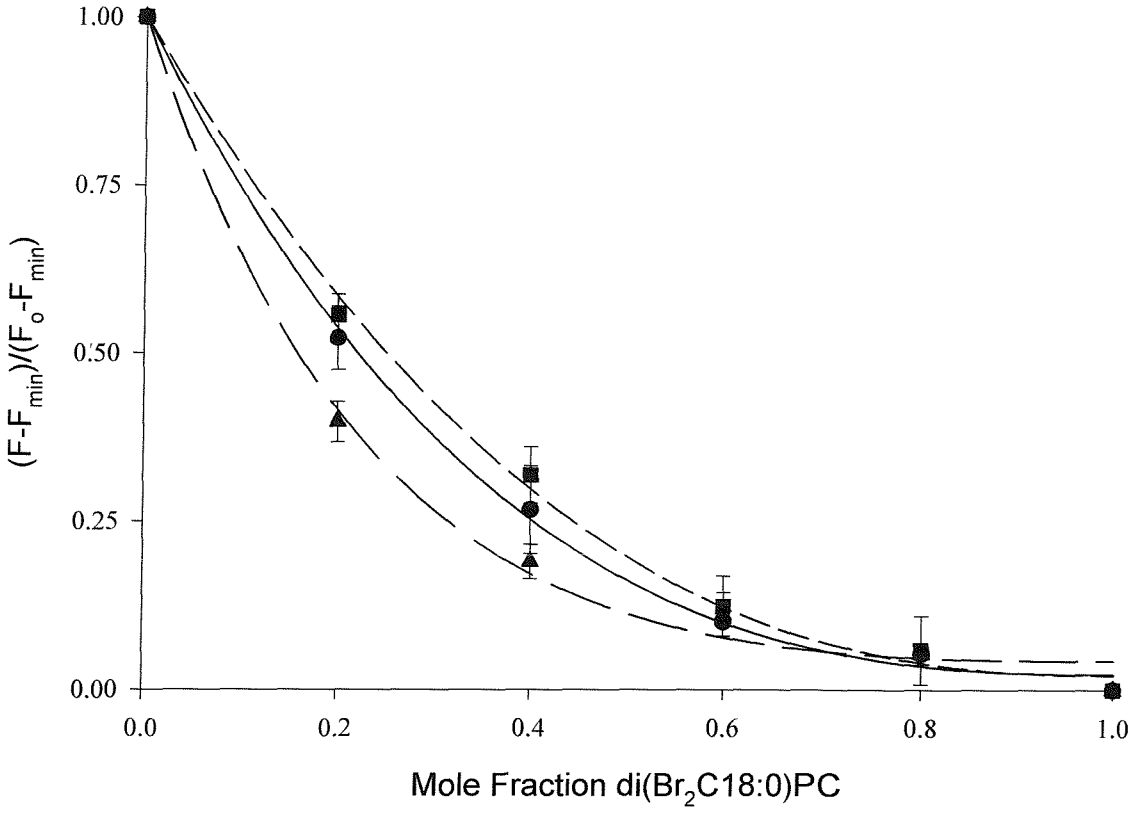

Figure 5.22: Relative fluorescence intensities for OmpF in mixtures of di(C18:1)PE, di(C18:1)PG or di(C18:1)PC and di(Br_2C18:0)PC.

OmpF was reconstituted in mixtures of di(C18:1)PC, di(C18:1)PE or di(C18:1)PG and di(Br_2C18:0)PC at the given mole fraction of brominated lipid. For experimental conditions see Figure 5.10. The symbols represent mean fluorescence results, and the lines are fitted to give K values of 0.87 ± 0.09 for di(C18:1)PE .(—●—), 0.56 ± 0.07 for di(C18:1)PG (—▲—), using an n value of 2.54 ± 0.25 obtained from the di(C18:1)PC data (—■—)

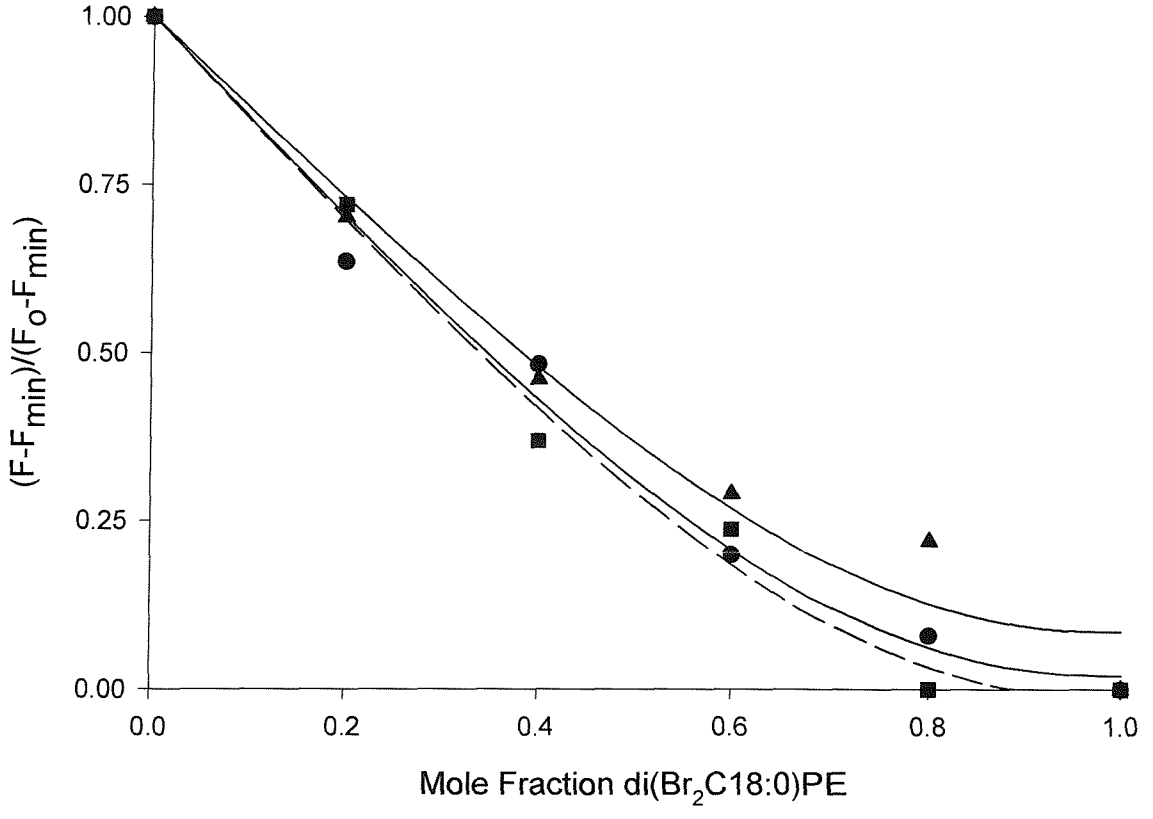

Figure 5.23: Relative fluorescence intensities for OmpF in mixtures of di(C14:1)PE and di(Br_2C18:0)PE.

OmpF was reconstituted in mixtures of di(C14:1)PE and di(Br_2C18:0)PE at the given mole fraction of brominated lipid. For experimental conditions see Figure 5.10. The symbols represent the fluorescence results presented in triplicate, and the lines are fitted using an n value of 2.54 to give K values of 1.65 ± 0.22 (—●—), 1.71 ± 0.35 (—▲—), and 1.67 ± 0.19 (—■—)

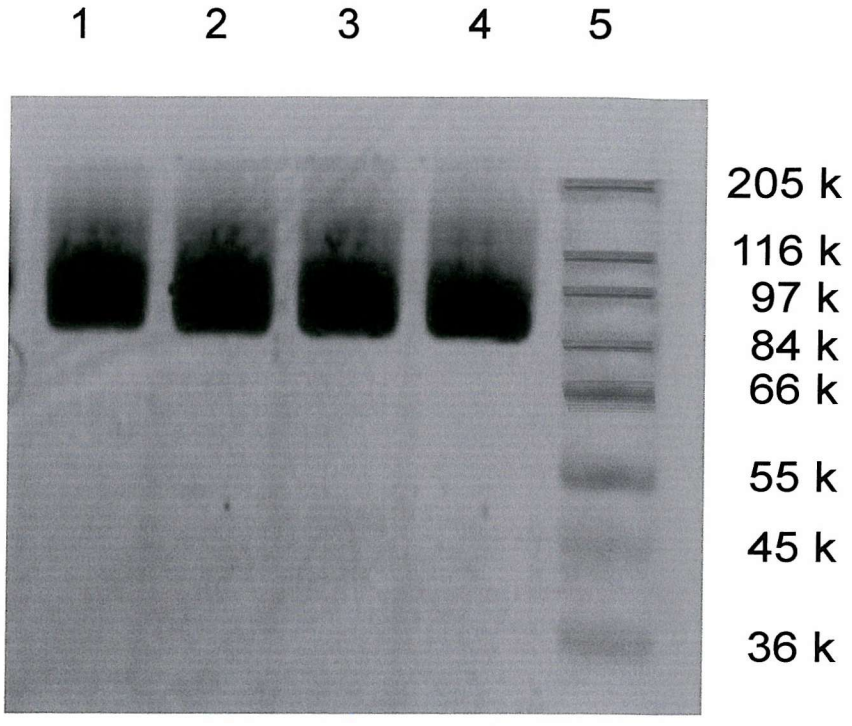

Figure 5.24: 15 % SDS-polyacrylamide gel stained with Coomassie brilliant blue showing OmpF reconstituted by the dialysis method.

Lane 5 contains high M_r Sigma marker. Lane 1 to 4 show 8.0 μg OmpF that has been reconstituted in di(C14:1)PC, di(C24:1)PC, di(C18:1)PE and di(C18:1)PG respectively. All samples have a lipid-to-protein molar ratio of 600:1 and were reconstituted using the detergent octyl-POE, which was subsequently removed by dialysis.

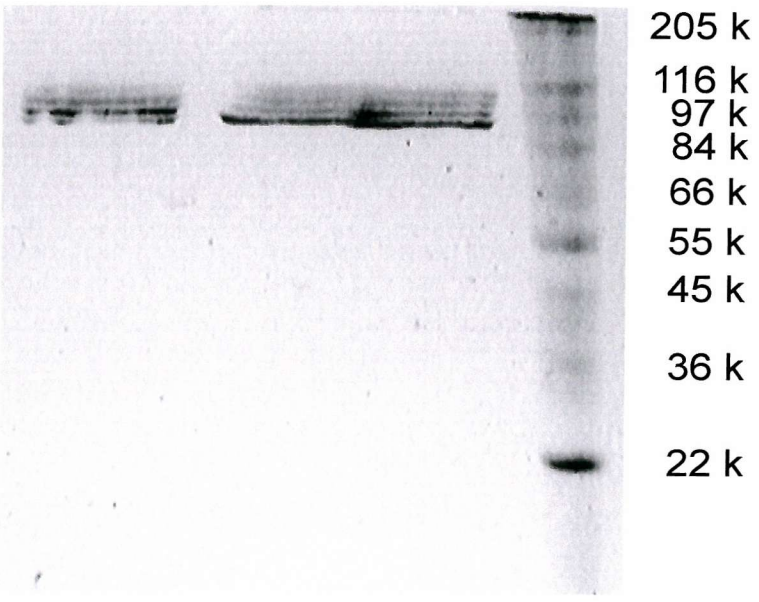

Figure 5.25: Analysis of LPS binding to reconstituted OmpF by SDS-PAGE

Lanes 1 contains high M_r Sigma marker. Lane 2 contains 6.0 μg of native OmpF showing the trimer at 90 k. Lane 3 contains 6.0 μg of OmpF that has been reconstituted into di(C18:1)PC. The reconstituted OmpF was purified by sucrose density centrifugation and the lipid-to-protein molar ratio in the fraction was 700:1 (Figure 3.15).

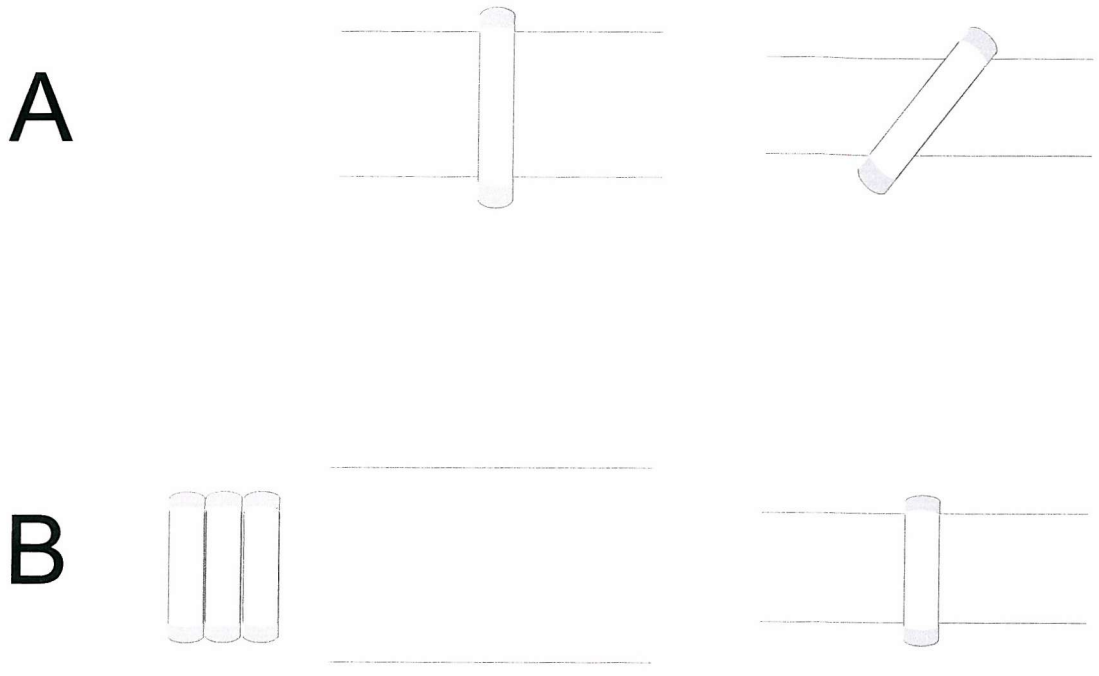

Figure 5.26: Effect of hydrophobic mismatch on the orientation of a transmembrane α-helix.

A) A long peptide can tilt in a bilayer to ensure that hydrophobic matching between the hydrophobic region in the protein and the fatty acyl chains is achieved.

B) A short peptide is unable to stretch to fit in bilayer that is too thick, and will instead aggregate. A short peptide can, however, fit in a thin bilayer.

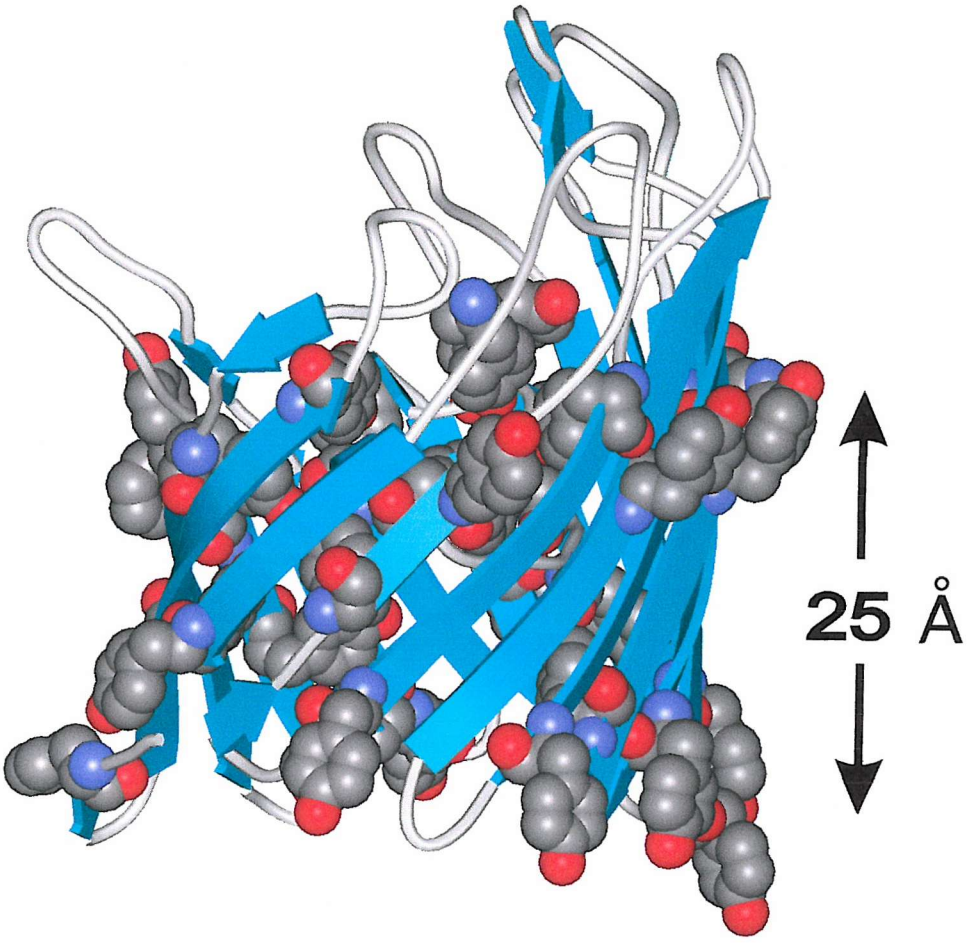

Figure 5.27: Structure of the non-polar membrane-spanning region of OmpF, defined by rings of aromatic residues.

The structure of an OmpF monomer is shown with the boundary of Tyr residues represented in spacefill. The distance between the two rings is 25 Å.

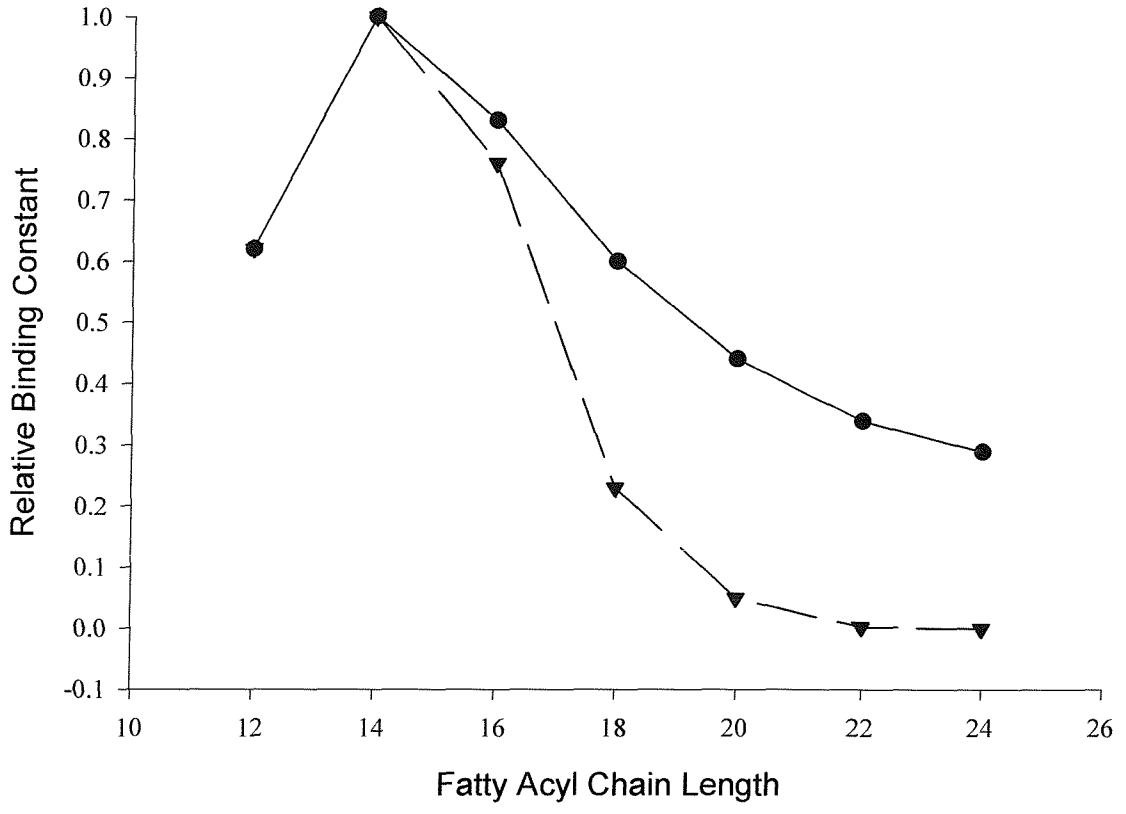

Figure 5.28: Comparison of lipid binding constants of OmpF obtained from fluorescence quenching studies with di(Br_2C18:0)PC (—●—) and from theoretical models of Fattal and Ben-Shaul (—▲—) (Fattal & Ben-Shaul, 1993, 1995).

Phospholipid	Relative Binding Constant
Di(C12:0)PC	1.04
Di(C14:1)PC	1.67
Di(C16:1)PC	1.38
Di(C18:1)PC	1.00
Di(C20:1)PC	0.73
Di(C22:1)PC	0.57
Di(C24:1)PC	0.48
Di(C18:1)PG	0.55
Di(C18:1)PE	0.87
Di(C14:1)PE	1.67

Table 5.1: Relative binding constants of OmpF for various phospholipids.
The relative binding affinities of the wild type OmpF for various phospholipids were determined relative to di(C18:1)PC, using n = 2.54, from data presented if Figures 5.10 to 5.16 for different phosphatidylcholine fatty acyl chain lengths, and Figure 5.22 for different head groups.

5.4 Discussion

5.4.1 Hydrophobic Matching

The energetic cost of exposing hydrophobic residues to water is high so that the thickness of the hydrophobic region of a membrane protein should match the hydrophobic thickness of the lipid bilayer (White & Wimley, 1999). The response of a membrane system in the event of a hydrophobic mismatch can involve deforming the lipid bilayer in the vicinity of the membrane protein to match the hydrophobic thickness of the protein or altering the lipid-exposed surface of the protein. Most models of hydrophobic mismatch assume that the lipid chains will adjust their length to provide a bilayer with a matching hydrophobic thickness (Mouritsen & Bloom, 1984; Fattal & Ben-Shaul, 1993; Nielson *et al.*, 1998).

Looking at the binding constants of OmpF for phosphatidylcholine with different fatty acyl chain lengths, strongest binding was observed with di(C14:1)PC (Table 5.1). Similarly strong binding was seen to di(C14:1)PE (Table 5.1). Phosphatidylcholine with fatty acyl chains longer or shorter than C14 had lower relative binding constants, particularly between C20 and C24. In contrast, binding studies with the Ca^{2+}-ATPase, a typical α-helical membrane protein, revealed that the binding constant remains fairly similar between fatty acyl chain lengths of C14 and C24 (Figure 5.18) (East & Lee, 1982). Thus it appears from these results that the Ca^{2+}-ATPase binds equally well to phosphatidylcholines that have different fatty acyl chain lengths, whereas OmpF binds best to a phospholipid giving a hydrophobic thickness of 23 Å in di(C14:1)PC (Equation 5.2) and binds less well to thicker or thinner membranes. These findings may be attributed to differences in the secondary structures of these proteins. The Ca^{2+}-ATPase is an α-helical protein, in which each α-helix is stabilised by hydrogen bonding between NH and CO groups within individual peptide chains. OmpF, however, is a β-sheet protein and is therefore stabilised by hydrogen bonds between NH and CO groups in different β-strands. The closed β-barrel structure of OmpF is presumed to provide a very rigid structure, which may not adapt easily to changes in the membrane thickness. The α-helical structure of the Ca^{2+}-ATPase is less rigid and may

therefore be able to adapt to different bilayer thickness by tilting in the membrane, as illustrated in Figure 2.26 (Lee, 1998).

The binding constant of OmpF for phosphatidylcholine with fatty acyl chains between C14 and C24 can also be compared to results from the predictive models of Fattal and Ben-Shaul (1993) and Mouritsen and Bloom (1984, 1993). Table 5.2 shows how the changes in the relative binding constants for phosphatidylcholines with fatty acyl chain lengths between C14 and C18 are comparable. However above C20, where the theoretical models predict a continuing decrease in the interaction energy, the actual changes in binding constant are very small (Figure 5.18). The theoretical models assume that the protein structure acts as a rigid entity in the membrane and that the lipid bilayer distorts around the protein to achieve hydrophobic matching between the hydrocarbon chains and the hydrophobic region of the protein (Mouritsen & Bloom, 1984; Fattal & Ben-Shaul, 1993; Nielson *et al.*, 1998). The results suggest that on increasing the fatty acyl chain length from C14 to C20, the lipid bilayer compresses around the OmpF to match the thickness of the hydrophobic region of OmpF. However, at fatty acyl chain lengths of greater than C20 the β-barrel may in addition deform to help maximise the interaction with the bilayer.

Membrane proteins may alter their state of aggregation or fail to insert at all into a bilayer if the hydrophobic matching requirements are not met (Killian, 1998). OmpF forms stable trimers in the native *E. coli* membrane that requires boiling for several minutes for denaturation to occur (Garavito & Rosenbusch, 1985). OmpF is also extremely stable in the highly denaturing detergent, SDS. Analysis of OmpF after reconstitution into lipid bilayers of varying hydrophobic thickness by SDS-PAGE suggests that the trimeric structure of OmpF is maintained upon reconstitution, and that altering the state of aggregation of the β-barrel is therefore not an action taken by this protein when hydrophobic mismatch occurs.

The hydrophobic thickness of OmpF, defined by the belts of aromatic residues, is 25 Å, as can be seen in Figure 5.27 (Cowan *et al.*, 1992). This would match

the hydrophobic thickness of a bilayer with C14 fatty acyl chains (Lewis & Engelman, 1983). This is consistent with the result that OmpF shows strongest binding to di(C14:1)PC and di(C14:1)PE. Molecular dynamic simulation studies have been used to study the effects of different degrees of hydrophobic mismatch between OmpF and phospholipids (Tielman *et al.*, 1998). In di(C16:1)PE bilayers, with a thickness of 26 Å, OmpF caused a decrease in the local thickness of the bilayer near the protein of approximately 4 Å less than the bulk lipid. This would be equivalent to the bilayer thickness with C14 fatty acyl chains (Equation 5.2). A decrease in the order parameters of the lipid close to the porin was also observed and was postulated to be due to a tilt in the lipid chains (Tielman *et al.*, 1998).

5.4.2 OmpF in the *E. coli* Outer Membrane

The outer membrane of Gram negative cells, where porins are found, has an asymmetric lipid distribution with the outer leaflet containing LPS exclusively and the inner membrane containing phospholipids only (Nikaido & Vaara, 1985). The fatty acids esterified to the lipid moieties of LPS are short, and generally between 8 and 14 carbon atoms, with C14 being the most predominant (Lugtenberg & Peters, 1976; Raetz, 1978). Most of the fatty acyl chains are saturated. The predominant phospholipid species in the *E. coli* outer membrane is phosphatidylethanolamine, with some phosphatidylglycerol and cardiolipin. The major fatty acids found attached to these phospholipids include palmitic acid (C16:0), palmitoleic acid (C16:1) and cis-vaccenic acid (C18:1) or their cyclopropane derivatives. The outer membrane phospholipids have a higher proportion of saturated fatty acyl chains than the inner cytoplasmic membrane.

No significant alteration in the binding constant was observed between the zwitterionic phospholipids phosphatidylcholine and phosphatidylethanolamine, with C14 or C18 fatty acyl chains (Table 5.1). The binding constant of OmpF for the anionic lipid phosphatidylglycerol, however, was approximately half that of phosphatidylcholine (Table 5.1). Reasons for the observed lower binding affinity of phosphatidylglycerol are

unclear as the structure of OmpF shows no apparent segregation of positive and negative charge in the transmembranous regions.

SDS-PAGE analysis of OmpF before and after reconstitution shows that LPS remains associated with OmpF, and is therefore not easily displaced by phospholipids (Figure 5.25). The crystal structure of FhuA, an iron transporter found in the outer membrane of E. coli cells, that has a β-barrel structure composed of 22 β-strands, is the only known high resolution structure of a protein-LPS complex (Ferguson *et al.*, 1998, 2000). Like porins, the hydrophobic region of FhuA is defined by two bands of aromatic residues that delineate the interface between the fatty acyl chains and polar head groups of the surrounding membrane lipid. FhuA is however mononomeric in contrast to the native trimeric structure of porins (Ferguson *et al.*, 1998). An LPS binding motif has been identified from the crystal structure of FhuA, consisting of several positively charged residues that hydrogen bond to phosphate residues on LPS. The motif was found in several other proteins by sequence analysis (Ferguson *et al.*, 2000). Biochemical studies (Yamade & Mizushima, 1980; Rocque *et al.*, 1987; Hoenger *et al.*, 1990) have inferred the possibility of there being a similar LPS binding site in the OmpF trimer interface, but the structure of a LPS molecule was not defined in the high resolution crystal structure of OmpF (Cowan *et al.*, 1992). Although porins were not among the group of proteins found to possess this LPS binding motif, these studies support proposals that LPS binding is required for insertion and folding of membrane proteins into the outer membrane (De Cock & Tomassen, 1996; De Cock *et al.*, 1999).

CHAPTER 6
LIPOSOME SWELLING ASSAYS

6.1 Introduction

Biological membranes are generally impermeable to hydrophilic solutes due to the hydrophobic nature of the membrane interior, unless they are taken up by a specific, active transport system or facilitated diffusion process. The cell envelope of Gram negative cells consists of a dual membrane structure, a typical inner membrane and an outer membrane, which has a rather nonspecific permeability to a wide range of solutes (Nikaido, 1983). The permeability profile of the outer membrane is due to the presence of the porins. The general porins of *E. coli* allow the passive diffusion of solute molecules with a molecular weight up to 600 Da. Diffusion of solute molecules that are larger than the molecular weight cut-off of the general porins is facilitated by a group of specific porins. The permeability of each particular species of porin differs. The *E. coli* general porins OmpF and OmpC, for example, have a preference for cationic solutes whereas the other *E. coli* general porin PhoE is anion-selective. The diameter of the transmembrane pores can also differ between porin species to provide pores with different molecular weight cut-off limits. Organisms can, therefore, alter the permeability of their outer membranes in response to changes in the environmental conditions by varying the types of porin expressed (Nikaido & Rosenberg, 1983). Many porins of other Gram negative bacteria have properties similar to the *E. coli* porins. The largest known exclusion limit is seen in *Pseudomonas aeruginosa*, which is permeable to hydrophilic substrates up to 5000 Da.

6.1.1 Functional Studies of Porins

Early investigations into the function of porin *in vivo* involved measuring the uptake of radiolabelled solutes into Gram negative cells (Steven *et al.*, 1977;

Sonntag *et al.*, 1978; Korteland *et al.*, 1984; Heine *et al.*, 1987). Another method employed was to measure the diffusion of solutes through the outer membrane by coupling the diffusion process with enzymatic hydrolysis of the solute (Nikaido & Rosenberg, 1983; Korteland *et al.*, 1984). These studies provided insight into the hydrophilicity of the pores and the solute preference shown by several porins, such as PhoE, which has a preference for negatively charged solutes. *In vitro* studies into porin function provided further information regarding the pore-forming properties of these proteins.

In the vesicle permeability method purified protein was reconstituted into lipid vesicles in which radiolabelled solutes were entrapped (Nakae, 1975, 1976). After passage of the proteoliposomes through a gel filtration column those solutes, which are permeable through the porins, will leave the liposomes and be retained on the column. The molecular weight exclusion limit of various porins were measured using this method. Using planar lipid bilayers the conductance of a single porin channel can be determined and used to calculate the effective diameter of the pore (Lakey *et al.*, 1985).

The liposome swelling method was established to measure the relative kinetics of the permeation of different substrates. These assays were based on the methods used by Bangham and coworkers to measure the permeability of phospholipid bilayers of liposomes (De Gier *et al.*, 1968; Bangham *et al.*, 1974). Proteoliposomes are formed within which a large impermeable sugar is entrapped, to maintain a given osmolarity. The permeability rates of various soutes can then be tested by diluting the proteoliposomes into an isotonic solution of a test solute. Influx of the test solute into the liposomes will be followed by an influx of water, which causes the liposomes to swell. This can be detected by measuring the optical density, which will decrease upon swelling of the liposomes as the refractive index of the liposome is reduced. The relative permeabilities of various solutes can be calculated from the initial rates of swelling of the liposomes.

Several insights into the properties of porins have been made through these functional studies (Nikaido, 1983):

1) There is a decrease in diffusion rate with larger solutes even when they are well within the exclusion limit of the pore. Reasons proposed for this phenomenon include solute collision with the rims of the pore and viscous drag exerted by the pore walls.
2) Diffusion through the pore is retarded by the hydrophobicity of the solute.
3) The *E. coli* porins OmpF and OmpC show a preference for cations and the PhoE porin shows an anion preference.
4) Channel closure is seen when non-physiological electrical potentials are applied across the bilayer.

6.1.2 Liposomes

Liposomes are composed of a bilayer of lipid molecules enclosing an aqueous volume. They are usually characterised on the basis of size and the number of bilayers encompassing any one liposome (Figure 6.1):

1) Multi-lamellar vesicles (MLVs) – these form spontaneously when dried lipid films are suspended and shaken in an aqueous buffer. They are composed of concentric lamellae and their size can vary between 50 and 10,000 nm.
2) Small unilamellar vesicles (SUVs) – these can be formed by mechanical dispersion of mlvs, usually sonication. They consist of a single lipid bilayer and are approximately 20-50 nm in diameter.
3) Large unilamellar vesicles (LUVs) – can be formed by freeze-thawing of SUVs. They are also composed of single lamellae but their diameter can be anything up to 10,000 nm.

6.1.3 Liposome Sizing

Liposomes can be sized using quasi-elastic light scattering or more directly using electron microscopy. The latter is more precise and has the advantage of being able to view each individual liposome (New, 1990). It is, however, a time-consuming method and is limited also by the availability of specialized equipment. Light scatter is a more amenable method, and is simple and rapid to perform. Its main drawback is that it measures an average property of the bulk liposome sample and will not represent any small deviations from a mean value.

Many of the instruments currently employed in particle sizing are based on the principles of Brownian motion and photon correlation spectroscopy (PCS). Such instruments will measure the size of particles by measuring their rate of diffusion through a fluid. Brownian motion is a consequence of thermal agitation, causing particles in solution to randomly collide with the solvent molecules. Such collisions result in random movement that causes suspended particles to diffuse through the solution. The rate of diffusion of these particle is dependent on three factors: the temperature of the fluid, the viscosity of the fluid, and the particle size. In a solution of known viscosity, whose temperature is kept constant, that rate of diffusion or diffusion coefficient (D) is inversely proportional to the particle size, according to Stokes-Einstein equation:

$$D = \frac{k_B T}{3\pi\eta d} \qquad \text{Equation 6.1}$$

where:

	k_B	=	Boltzmann constant (1.38×10^{-16} erg/ °K)
	T	=	temperature (°K)
	η	=	diluent viscosity (poise)
	d	=	equivalent spherical diameter (centimeters)

Particles undergoing Brownian motion can be studied by illuminating the sample with a laser and measuring the scattered light with a photomultiplier tube (PMT). The light scattered at any given moment will provide an interference pattern. The intensity of light detected at the PMT will depend on the interference pattern, which will depend on the pattern of particles in the laser beam. The positions of the particles in solution will move relative to one another as they move through the solution. This will be reflected in a constantly changing interference pattern and varying light intensity at the detector. Large particles will change positions more slowly relative to small, quick-moving particles. PCS can size particles by analysing the exact time scale of the random fluctuations caused by the diffusing particles.

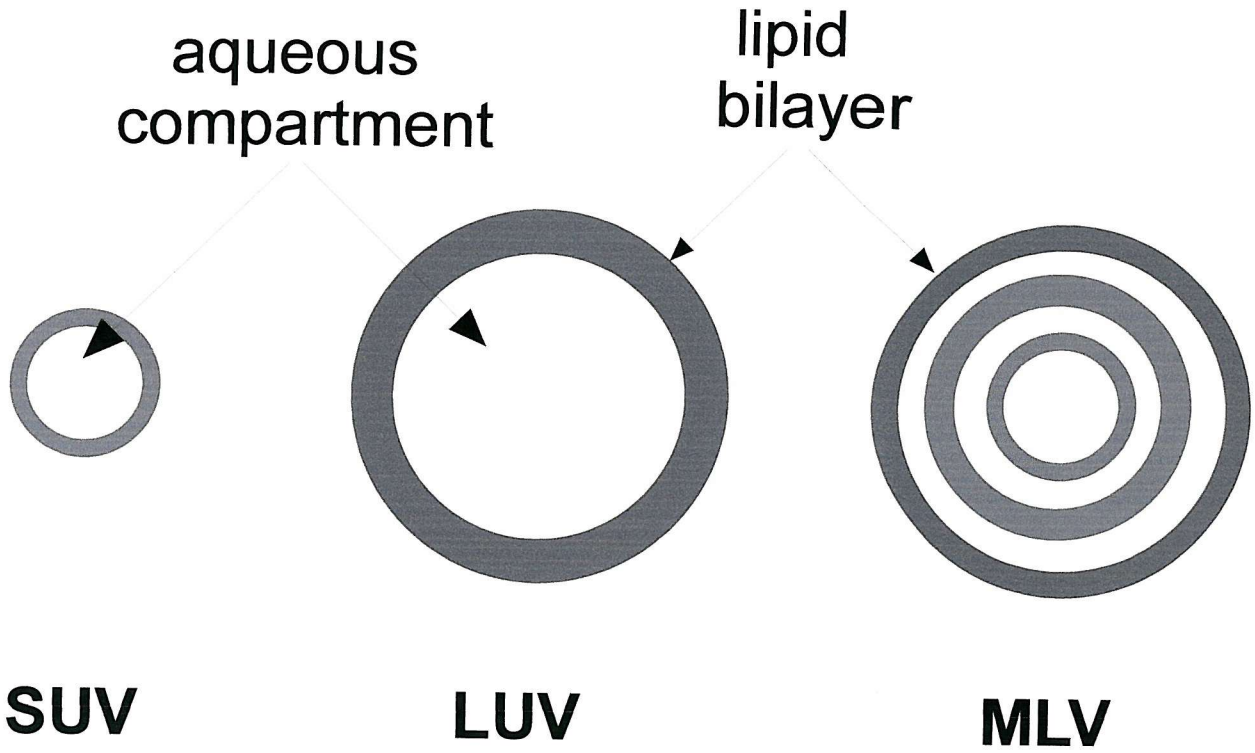

Figure 6.1: **Types of Lipid Vesicles**

6.2 MATERIALS AND METHODS

6.2.1 Materials

Amersham Pharmacia biotech

Dextran T-40 average M_W = 35000 - 45000

6.2.2 Methods

6.2.2.1 Liposome Swelling Assay

OmpF was reconstituted into MLVs using the method of Nikaido et al. (Nikaido & Rosenberg, 1983; Nikaido *et al.*, 1991). Previous studies by this group have shown that up to 100 μg of non-ionic detergent can be introduced per μmol of phospholipid without adversely affecting the permeability of the liposomes. The OmpF stocks used for these studies were stored in 1 % of the non-ionic detergent octyl-POE at a final protein concentration of 1 mg/ml. The amount of OmpF incorporated into the MLVs was 0.025 μg per μmol of lipid for liposome swelling assays with monosaccharide sugars and 0.4 μg of OmpF per μmol of lipid for liposome swelling assays with the larger sugars. These are equivalent to 0.25 and 4 μg of octyl-POE per μmol of lipid, respectively, concentrations which will not affect the liposome permeability. Therefore it was not necessary to remove the detergent prior to assaying the permeability of the proteoliposomes.

4 μmols of the lipid to be studied and 1 μmol of di(C18:1)PG were dried onto the walls of a 10 ml round-bottom flask. The lipid was resuspended in 200 μl of water containing either 0.125 μg or 2 μg OmpF. The flasks were sealed under nitrogen and vortex-mixed before being sonicated for 30 seconds in a Ultrawave bath sonicator. The round-bottom flasks were warmed at 45 °C and connected to a vessel containing desiccant beads that was attached to a water-vacuum pump. The samples were dried for a further 2 hours in a vacuum dessiccator before resuspending in 0.6 ml of 5 mM Tris-HCl, pH 8.0 containing 15 % (w/v) dextran T-40. Resuspension was achieved by gentle

swirling of the samples in the sugar solution, then leaving to incubate at room temperature for 30 minutes and subsequent hand shaking of the flasks. The assays were performed by using a Shimadzu UV 3000 at 25 °C, measuring the reduction in the light scatter upon dilution of 20 µl of sample into 0.63 ml of test solute. The absorbance at 400 nm was recorded for 2 minutes after rapid mixing of the sample into the test solute. The isoosmotic concentration of the test solutes was determined by diluting liposomes into solutions containing various concentrations of the OmpF-impermeable solute stachyose, and finding the concentration of stachyose that caused neither shrinking nor swelling of the liposomes. The concentrations of stachyose used for this determination were 25, 30 and 37 mM in 5 mM Tris-HCl, pH 8.0. The test solutes employed were arabinose, galactose, glucose, sucrose, maltose and lactose. The structures of these sugars and their molecular weights are illustrated in Figure 6.2.

6.2.2.2 Fluorescence Quenching by di(Br_2C18:0)PC using the Liposome Swelling Reconstitution Method

To examine the mixing of OmpF with lipid when the samples were reconstituted using the procedure described in Section 6.2.2.1, but the reconstitution was performed using brominated lipid. The conditions were the same as those described in Section 6.2.2.1 except the concentration of OmpF was increased to a level detectable by fluorescence spectroscopy and the samples were finally suspended in 10 mM Hepes, pH 7.2, 1 mM EGTA for fluorescence measurements instead of 5 mM Tris-HCl, pH 8.0 containing 15 % (w/v) dextran T-40.

In brief 5 µmols of di(Br_2C18:0)PC or 5 µmols of di(C18:1)PC were dried onto the walls of a 10 ml round-bottom flask. The lipid was resuspended in 300 µl of a 1 mg/ml OmpF solution in 20 mM NaH_2PO_4, pH 7.2. The samples were then sonicated and dried as in Section 6.2.2.1 but the dried protein-lipid samples were resuspended in 0.6 ml of 10 mM Hepes, pH 7.2, 1 mM EGTA buffer. 8.9 µl of each sample (equivalent to 0.12 nmols of OmpF) were diluted into a final volume of 3 ml of 10 mM Hepes, pH

7.2, 1 mM EGTA. The fluorescence was recorded between 300 and 380 nm using an excitation wavelength of 280 nm. All spectra were corrected for light scatter by subtracting the emission of protein-free control liposomes.

The samples prepared for fluorescence analysis were also analysed by SDS-PAGE to determine whether the trimeric structure was maintained during the reconstitution procedure. 8.0 μg of the reconstituted OmpF was analysed on 15 % polyacrylamide gels as described in Section 3.2.2.6

6.2.2.3 Liposome Swelling Assay using the Bio-Beads Method

To look at the effect of using a detergent-mediated reconstitution method on the liposome swelling assay, reconstitutions were performed using octyl-POE. As mentioned in Section 6.2.2.1 up to 100 μg of non-ionic detergent can be introduced per μmol of phospholipid without adversely affecting the permeability of the liposomes. Using higher concentrations of octyl-POE necessitates incorporating a step to remove the excess detergent. The method employed to remove the octyl-POE prior to measuring the permeability of the liposomes, utilising detergent-absorbing Biobeads-SM2. The concentrations of octyl-POE used were similar to those used in the fluorescence reconstitutions, described in Section 3.2.2.2. The detergent was removed at either of two stages in the experiment as detailed below.

a) 4 μmols of di(C14:1)PC and 1 μmol of di(C18:1)PG were dried onto the walls of a 10 ml glass vial, to which was added 0.125 μg of OmpF and 5.4 mg of octyl-POE in a final volume made up to 0.6 ml with 5 mM Tris-HCl, pH 8.0 containing 15 % (w/v) dextran T-40. The sample was mixed well and then sonicated for 30 seconds. 114 mg of Biobeads-SM2 was added to the sample. A further 114 mg of Biobeads-SM2 were added after 1, 2 and 3 hour periods. The sample was separated from the Biobeads-SM2 5 minutes after the final Biobead addition by pipetting into a clean vial. The swelling assay was then performed with the vesicles as described in Section 6.2.2.1.

b) A second method was used that involved incorporating the Biobeads-SM2 at a later stage in the experiment. The lipid was dried as before and then 0.125 μg of OmpF and 5.4 mg of octyl-POE were added in a final volume made up to 0.2 ml with 5 mM Tris-HCl, pH 8.0. The flasks were sealed under nitrogen and vortex-mixed before being sonicated for 30 seconds in an Ultrawave bath sonicator. 4 x 114 mg Biobead additions were made to the sample as described above. The sample was separated from the Biobeads-SM2 5 minutes after the final Biobead addition by pipetting into a clean 10 ml round-bottom flask. The samples were then dried by warming the round-bottom flasks at 45 °C and connecting them to a vessel containing desiccant beads that was attached to a water-vacuum pump. All further steps were carried out identically to Section 6.2.2.1.

6.2.2.4 Liposome Sizing

All of the liposome samples prepared were sized using a Coulter N4 particle sizer. 20 μl of liposome suspension was diluted into 2.5 mls of 0.2 μm filtered distilled water. Each sample was allowed to equilibrate for 15 minutes before the light scatter was measured 12 times for 5 minutes at an angle of 90 °.

6.3 Results

6.3.1 Liposome Swelling Assays

Phosphatidylglycerol was chosen as a component of all of the liposomes used as it has a negative charge (see Figure 1.2) and will therefore cause charge repulsion between adjacent lamellae in MLVs.

The isoosmotic concentration of the dextran-containing liposomes was determined by diluting the samples into solutions of stachyose, which is impermeable to the OmpF pore. The concentration of stachyose that caused neither shrinking nor swelling of the liposome solution, i.e., the concentration that causes no change in the optical density of the liposome solution was taken to be the isoosmotic concentration (Nikaido *et al.*, 1991). As can be seen from the example shown in Figure 6.3 the isoosmotic concentration was 30 mM. All the control and sample liposomes assayed had an isoosmotic concentration of 30 mM.

To measure the permeability rates of various sugars through OmpF by the liposome swelling assay, the influx of water through the membrane must be a lot faster than the rate of influx of the test solutes. The extent of the light scatter changes for protein-free liposomes was seen to vary according to the lipid chain length (Figure 6.4), with the greatest change seen for those liposomes prepared with short lipid chain lengths (di(C14:1)PC). The rates of water permeability were calculated by fitting the data to a single exponential

$$f = a \times \exp(-b * t) + \text{residue} \qquad \text{Equation 6.2}$$

where b is equal to the diffusion rate of the test solute, a is the amplitude of the light scatter change, t is the time in seconds and the residue is the light scatter remaining at long time.

It can be seen from Table 6.1 that the rate of water permeability does not vary significantly between liposomes made from phosphatidylcholines with different fatty acyl chain lengths. In contrast the fatty acyl chain length of the lipid has a large effect on the amplitude of the light scatter decrease. This situation is mimicked in proteoliposomes (Figure 6.5), where the largest changes are seen in the di(C14:1)PC liposomes. Further the presence of OmpF has no significant effect on the rate of the movement (Table 6.2). This effect of chain length presumably results from interactions between the fatty acyl chains, where an increase in the cohesiveness of the chains would be expected with an increased chain length. Since swelling of the liposomes results in an increase in the surface area occupied by each lipid molecule, the extent of swelling for a given osmotic shock will decrease with increasing chain length.

The flux of all of the sugars through protein-free control liposomes was negligible as can be seen from the optical density data for liposomes made from different chain length phosphatidylcholines (Figure 6.6), showing that the presence of protein tranporters are required for transport of the sugars into the liposomes.

Light scatter changes for the proteoliposomes in various test solutes were also determined as a function of time, and then fitted to a first order rate equation (Equation 6.2). In those cases where the rate of sugar influx into the proteoliposomes is fast, the decrease in light scatter at long time is close to the maximum decrease seen in the Tris experiments. For example, the maximum observed decrease in light scatter for OmpF in di(C14:1)PC with arabinose was 22 % (Figure 6.7), very close to the maximum observed decrease for liposomes of di(C14:1)PC in Tris, which was 27 % (Figure 6.4). However for sugars where the rate is slower, the maximum decrease in the light scatter is very small, e.g., the light scatter for OmpF in di(C24:1)PC liposomes in arabinose decreased by only 5 % (Figure 6.7) whereas in Tris the maximum drop was 13 % (Figure 6.4). In those cases where the decrease in light scatter at long time is close to the maximum change, fitting to Equation 6.2 gives good estimates for the rates of maximum amplitude of change. However, when the decrease in light scatter at long time represents only a small fraction of the expected total change, fitting to Equation 6.2

does not give reliable values for rate and amplitude; any underestimate of the maximum amplitude of the changes leads to an overestimate for the rate of change. For consistency, therefore, it was decided to fix the amplitudes in all of the experiments to the amplitude of change seen in Tris experiments, which were repeated for each batch of liposomes.

Figure 6.7 shows the results obtained for the different lipid chain lengths in arabinose. The rate of change with arabinose is seen to be fastest in liposomes made with di(C18:1)PC, with the slowest rate being seen with di(C24:1)PC. The rates are presented in Table 6.3. The results obtained for proteoliposomes in galactose show a similar pattern with the highest rate seen in di(C18:1)PC (Figure 6.8 and Table 6.4). As can be seen in Figure 6.9 the results obtained for di(C18:1)PC and di(C24:1)PC in glucose do not fit very well to a single exponential, and were therefore also fitted to a double exponential

$$f = a * \exp(-b * t) + (c - a) * \exp(-d * t) \qquad \text{Equation 6.3}$$

where a is the amplitude of the light scatter change described by the rate b, t is the time in seconds, c is the total amplitude of the light scatter change, and d is the rate of the second component of the change.

As shown in Figure 6.10, a good fit is obtained to the double exponential. The data fit a major component, corresponding to 74 – 80 % of the total amplitude, that has a permeability rate (b = 0.0028 in di(C18:1)PC, and b = 0.0019 in di(C24:1)PC) similar to that obtained by fitting the same data to a single exponential (e.g., b = 0.0019 for di(C24:1)PC) and a small component with a faster rate (Table 6.6)

For all of the proteoliposomes assayed, the fastest diffusing sugar was the pentose sugar arabinose, followed by the hexose sugars galactose and then glucose (Table 6.7). The influx of the disaccharide sugars appeared very slow and did not provide any discernible information on differences in the permeability rates of these

sugars, e.g., Figure 6.11 shows the light scatter data when proteoliposomes made with different lipid chain lengths are diluted into sucrose. The light scatter results for di(C14:1)PC in various disaccharides tested is shown in Figure 6.12.

6.3.2 Fluorescence Quenching by di(Br_2C18:1)PC when OmpF is Reconstituted using the Liposome Swelling Method

Figure 6.13 shows the level of quenching seen when OmpF is reconstituted into di(Br_2C18:1)PC liposomes, by the liposome swelling method. The fluorescence intensity is quenched approximately 50 % by the bromine-containing molecules, which is comparable to other reconstitution methods investigated in Chapter 3 (Table 3.2).

6.3.3 SDS-PAGE Analysis of OmpF Reconstituted by the Swelling Method

SDS-PAGE analysis of OmpF reconstituted by the swelling method showed a band corresponding to the trimer at approximately 90 k (Figure 6.14).

6.3.4 Liposome Swelling using the Biobead Method.

Two methods of reconstitution were investigated, that involved the use of Biobeads-SM2. When Biobeads-SM2 were added to the detergent-containing sample of di(C14:1)PC liposomes in dextran (see Section 6.2.3(a)), the light scatter from the liposomes was very low and no change in the light scatter was observed after dilution of the proteoliposomes into permeable sugars. When the Biobeads-SM2 were added at a later point in the experiment (see Section 6.2.3(b)), the light scatter changes in the proteoliposomes after dilution into arabinose were similar to those seen for di(C14:1)PC in Figure 6.7 (Figure 6.15). The rates calculated were 0.0071 ± 0.0003 for the

proteoliposomes reconstituted as normal, and 0.0065 ± 0.0002 for the proteoliposomes reconstituted using Biobeads-SM2.

6.3.5 Liposome Sizing

The size of the vesicles was examined using a Coulter N4 Plus particle sizer. An example of a typical result is shown in Figure 6.16A and 6.16B shows the sizes of liposomes obtained after incorporating Biobeads-SM2 into the reconstitution. Table 6.8 shows the results obtained for vesicles prepared from phosphatidylcholine with different fatty acyl chain lengths and for vesicles containing different amounts of protein. The effect of the varying reconstitution methods employed on the vesicle size was also examined. The sizes were examined using unimodal analysis, which provides a measure of the mean particle size of the sample and a measure of the polydispersity or breadth of the particle-size distribution. As can be seen in Table 6.8 the size of the vesicles was very similar between liposomes prepared using different fatty acyl chain lengths and also for vesicles with different amounts of OmpF. Variations in the vesicle size were however seen when the use of Bio-Beads was introduced into the reconstitution method. When the Bio-Beads were added to the liposome suspension in dextran, small vesicles with a mean diameter of 90 nm were seen. When the Bio-Beads were added at an earlier stage in the experiment, prior to the lipids being dried and swollen in the dextran solution, larger vesicles were seen. These vesicles were, however, smaller than those prepared without the use of Bio-Beads (approximately 500 nm as opposed to approximately 650 nm).

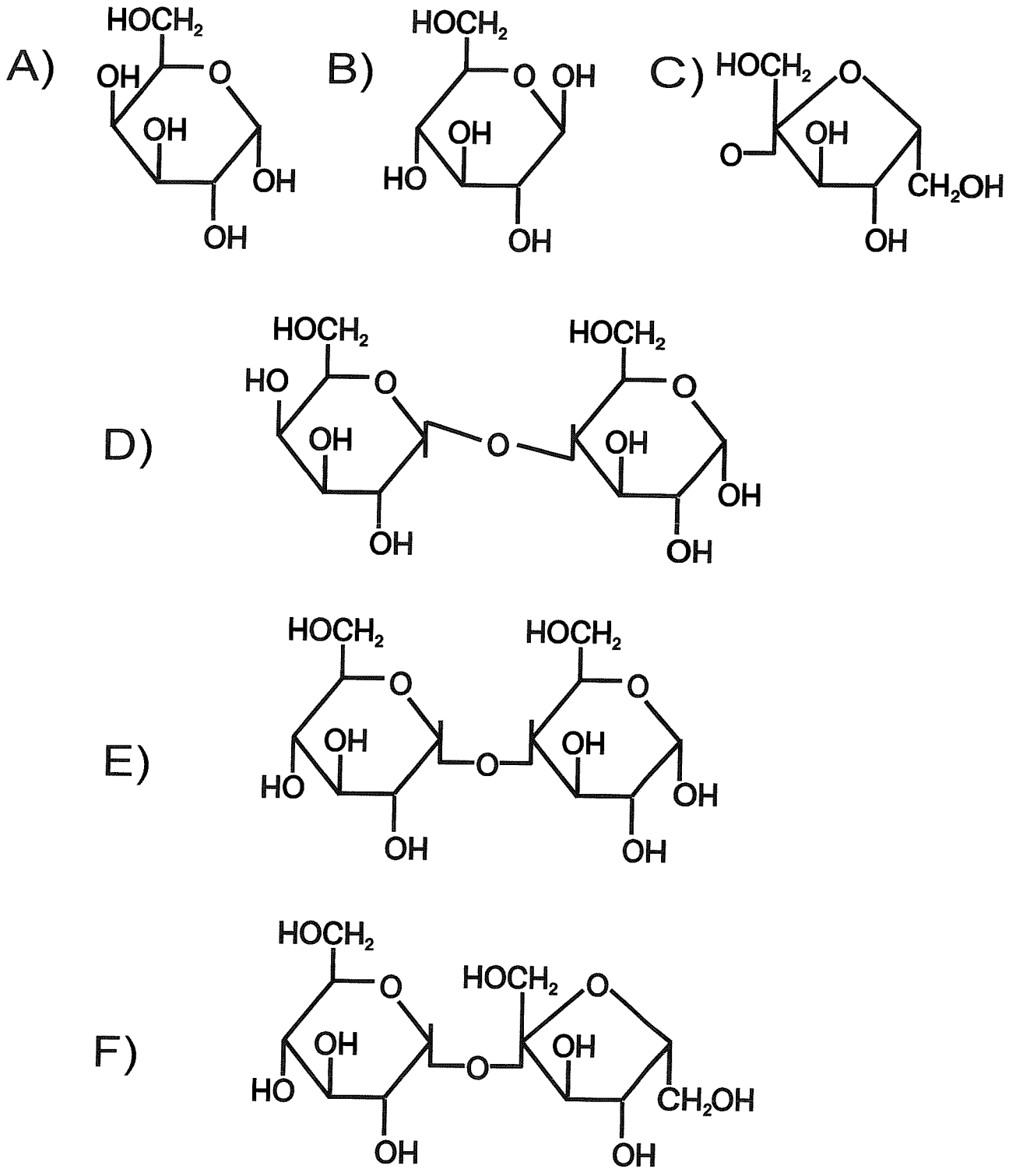

Figure 6.2: Structure and molecular weight of the sugars used as test solutes in the liposome swelling assays.

A) glucose, B) galactose, C) arabinose, D) lactose, E) maltose, and F) sucrose.

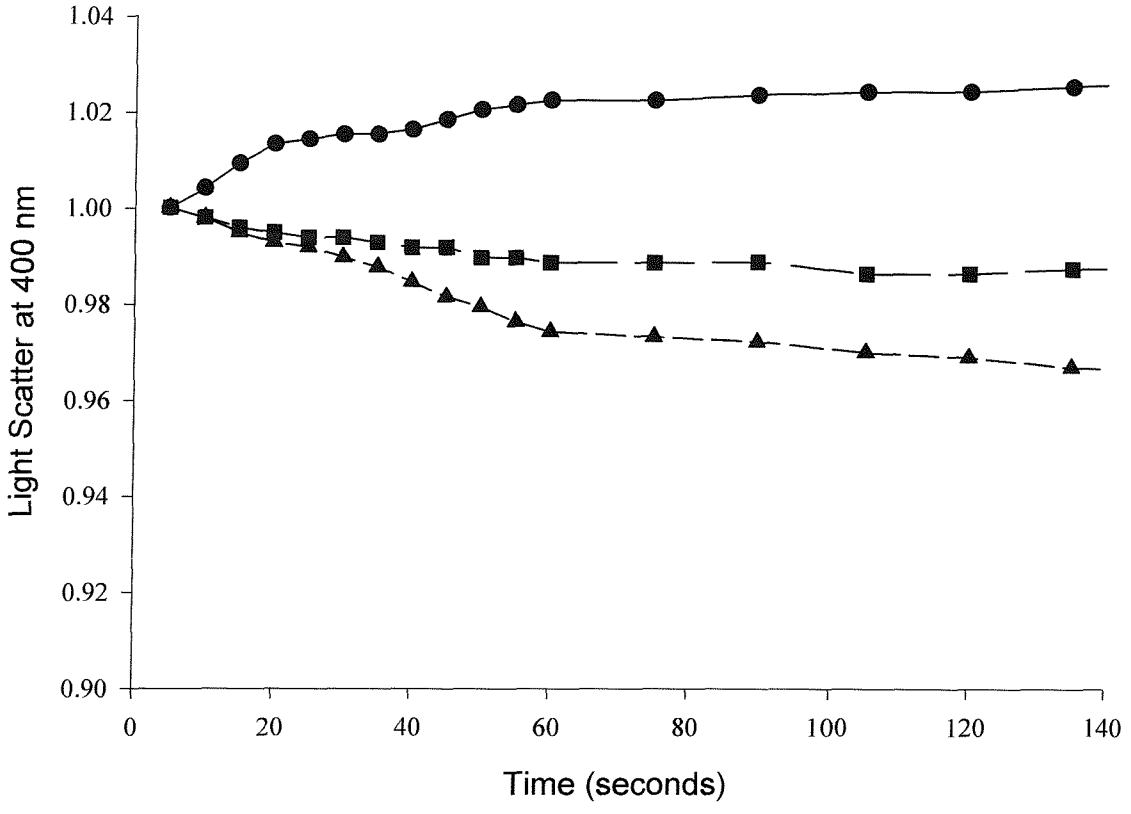

Figure 6.3: Optical density changes in proteoliposomes diluted into stachyose solutions.

20 µl of liposomes containing 0.025 µg of OmpF/µmol of phospholipid were diluted into 0.63 ml of stachyose solutions at 25, 30 or 37 mM concentrations, the diluents always contained 5 mM Tris-HCl, pH 8.0. The light scatter was measured at 400 nm at 25 °C. The stachyose concentrations used were 37 mM (top curve), 30 mM (middle curve) and 25 mM (bottom curve), and showed that liposomes were isoosmotic with 30 mM stachyose.

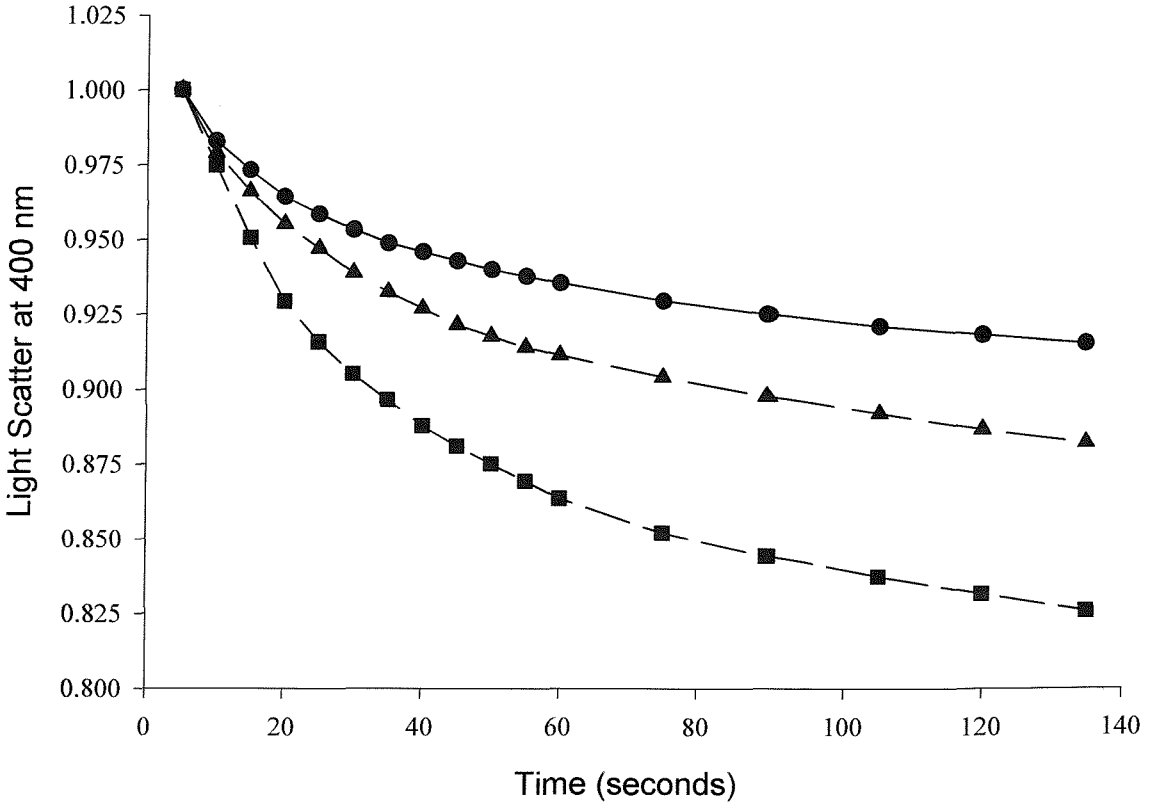

Figure 6.4: Optical density changes in control liposomes diluted into 5 mM Tris, pH 8.0.

20 µl of protein-free control liposomes made from di(C18:1)PG and either di(C14:1)PC (—●—), di(C18:1)PC (—▲—) or di(C24:1)PC (—■—) at molar ratios of 1:4, were diluted into 0.63 ml of 5 mM Tris-HCl, pH 8.0. The light scatter was measured at 400 nm at 25 °C. The data were fitted to a single exponential to give rates and amplitudes shown in Table 6.1.

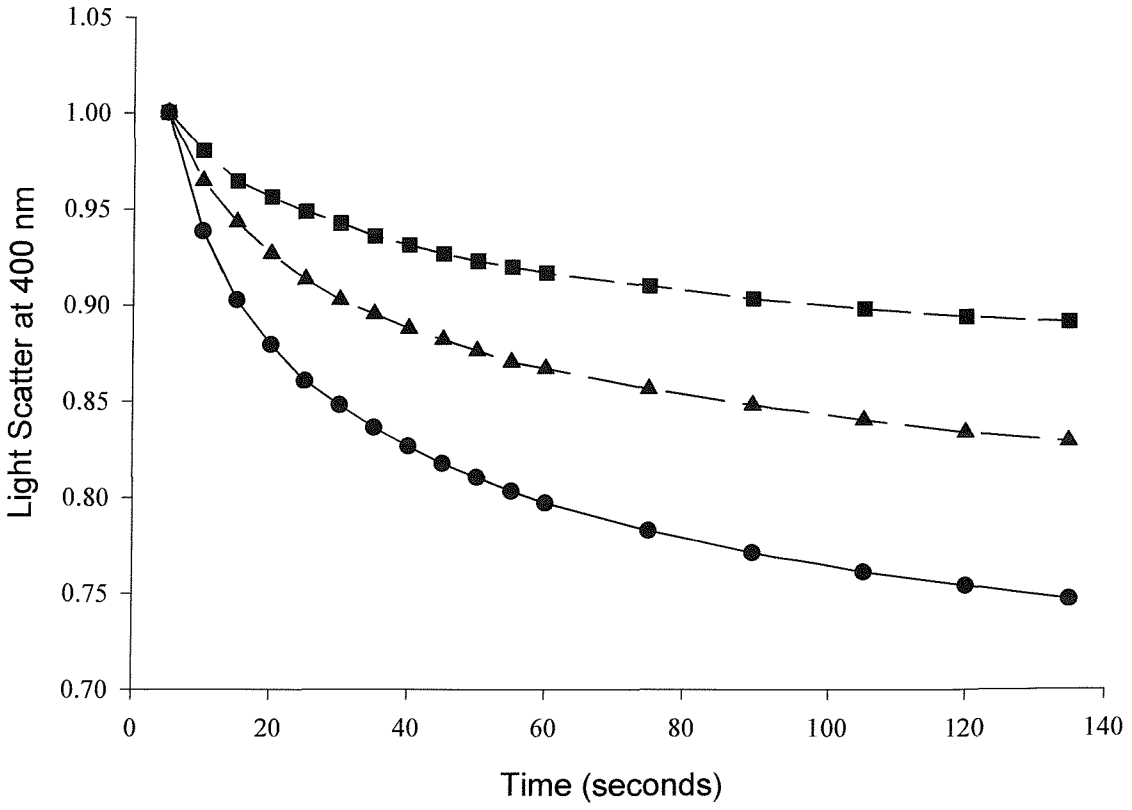

Figure 6.5: Optical density changes in proteoliposomes diluted into 5 mM Tris, pH 8.0.

20 µl of liposomes made from di(C18:1)PG and either di(C14:1)PC (—●—), di(C18:1)PC (—▲—) or di(C24:1)PC (—■—) at molar ratios of 1:4, containing 0.025 µg of OmpF/µmol of phospholipid were diluted into 0.63 ml of 5 mM Tris-HCl, pH 8.0. The light scatter was measured at 400 nm at 25 °C. The light scatter was measured at 400 nm at 25 °C. The data were fitted to a single exponential to give rates and amplitudes shown in Table 6.2.

Figure 6.6: Optical density changes in control liposomes in test solutes.

20 μl of protein-free control liposomes made from di(C18:1)PG and A) di(C14:1)PC, B) di(C18:1)PC or C) di(C24:1)PC at molar ratios of 1:4, were diluted into 0.63 ml of 5 mM Tris-HCl, pH 8.0 containing 30 mM of the test sugar. The monosaccharide sugars assayed were arabinose (—●—), glucose (—▲—) and galactose (—■—). The light scatter was measured at 400 nm at 25 °C.

A)

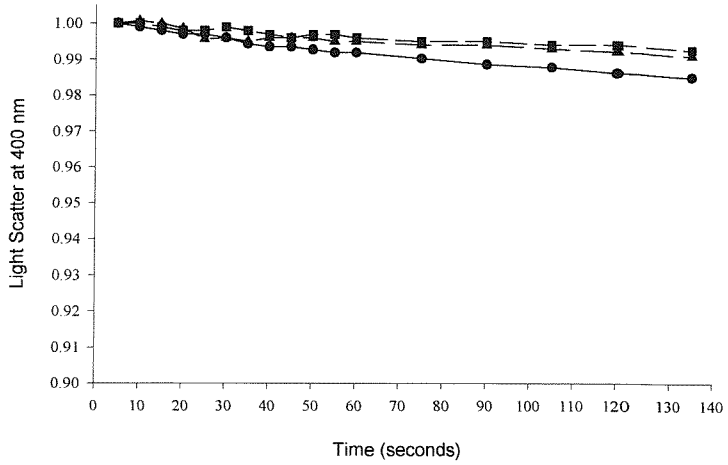
Light Scatter at 400 nm
1.00
0.99
0.98
0.97
0.96
0.95
0.94
0.93
0.92
0.91
0.90
0 10 20 30 40 50 60 70 80 90 100 110 120 130 140
Time (seconds)

B)

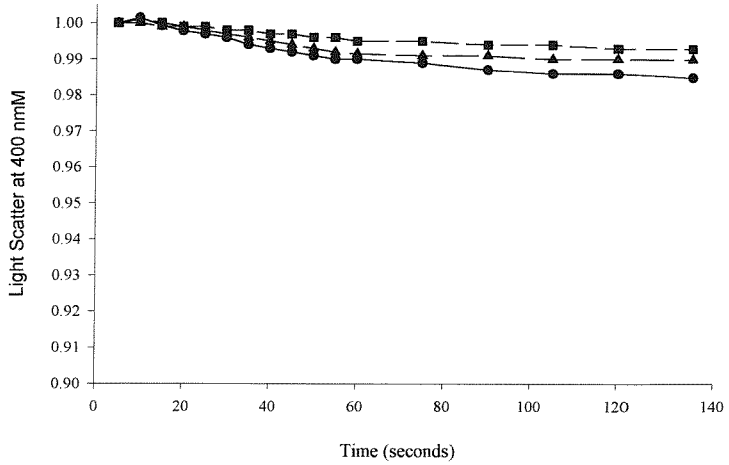
Light Scatter at 400 nmM
1.00
0.99
0.98
0.97
0.96
0.95
0.94
0.93
0.92
0.91
0.90
0 20 40 60 80 100 120 140
Time (seconds)

C)

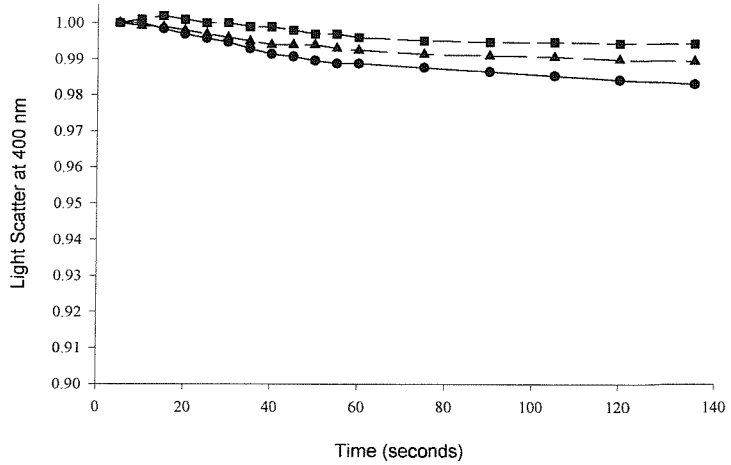
Light Scatter at 400 nm
1.00
0.99
0.98
0.97
0.96
0.95
0.94
0.93
0.92
0.91
0.90
0 20 40 60 80 100 120 140
Time (seconds)

A)

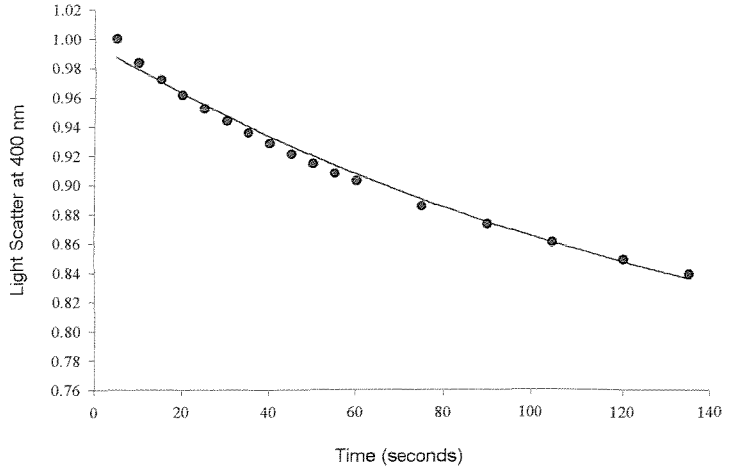

B)

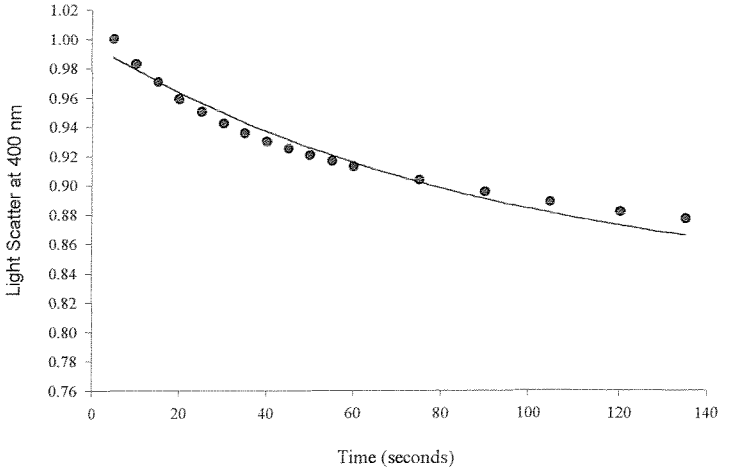

Figure 6.7: Optical density changes in proteoliposomes in 30 mM arabinose.

20 µl of proteoliposomes made from di(C18:1)PG and A) di(C14:1)PC, B) di(C18:1)PC or C) di(C24:1)PC containing 0.025 µg of OmpF/µmol of phospholipid were diluted into 0.63 ml of 5 mM Tris-HCl, pH 8.0 containing 30 mM arabinose. The light scatter was measured at 400 nm at 25 °C. The data were fitted to a single exponential to give rates and amplitudes shown in Table 6.3.

C)

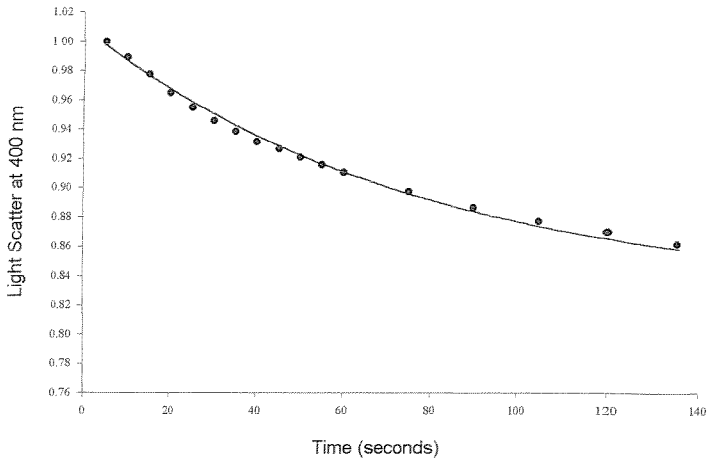
Light Scatter at 400 nm
1.02
1.00
0.98
0.96
0.94
0.92
0.90
0.88
0.86
0.84
0.82
0.80
0.78
0.76
0
20
40
60
80
100
120
140
Time (seconds)

D)

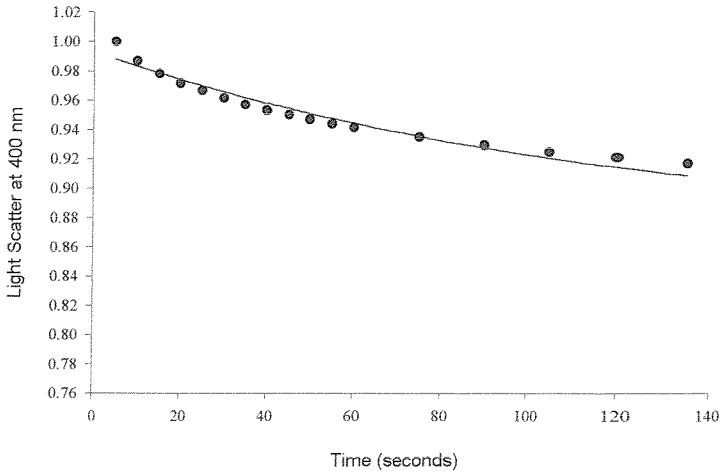
Light Scatter at 400 nm
1.02
1.00
0.98
0.96
0.94
0.92
0.90
0.88
0.86
0.84
0.82
0.80
0.78
0.76
0
20
40
60
80
100
120
140
Time (seconds)

E)

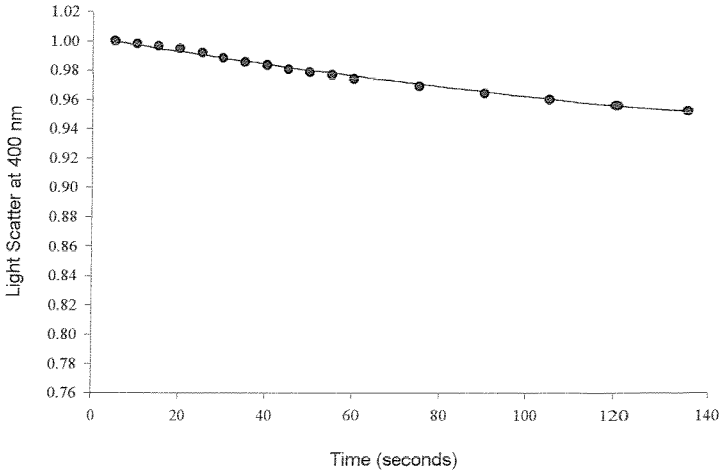
Light Scatter at 400 nm
1.02
1.00
0.98
0.96
0.94
0.92
0.90
0.88
0.86
0.84
0.82
0.80
0.78
0.76
0
20
40
60
80
100
120
140
Time (seconds)

Figure 6.8: Optical density changes in proteoliposomes in 30 mM galactose.
20 μl of proteoliposomes made from di(C18:1)PG and A) di(C14:1)PC, B) di(C18:1)PC or C) di(C24:1)PC at molar ratios of 1:4, containing 0.025 μg of OmpF/μmol of phospholipid were diluted into 0.63 ml of 5 mM Tris-HCl, pH 8.0 containing 30 mM galactose. The light scatter was measured at 400 nm at 25 °C. The data were fitted to a single exponential to give rates and amplitudes shown in Table 6.4,

A)

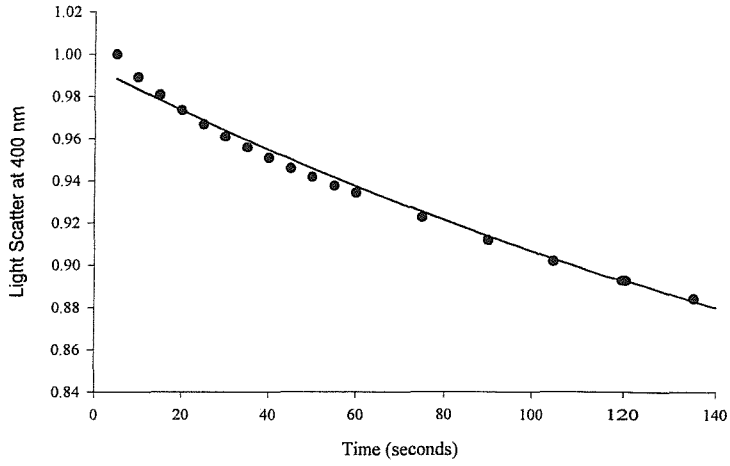
Light Scatter at 400 nm
1.02
1.00
0.98
0.96
0.94
0.92
0.90
0.88
0.86
0.84
0
20
40
60
80
100
120
140
Time (seconds)

B)

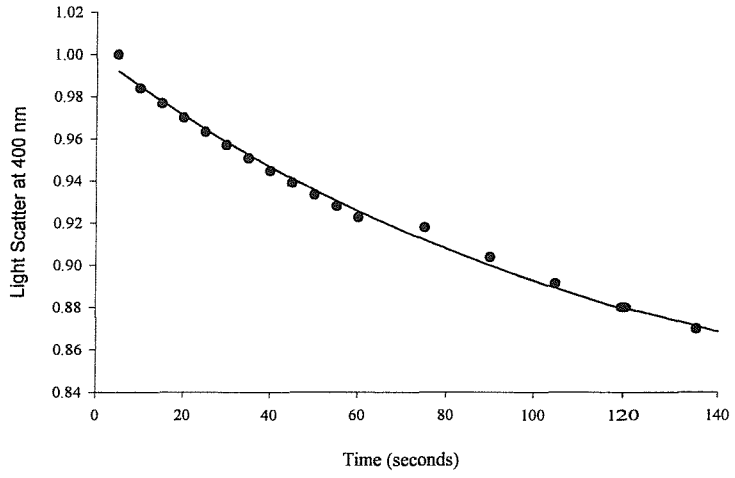
Light Scatter at 400 nm
1.02
1.00
0.98
0.96
0.94
0.92
0.90
0.88
0.86
0.84
0
20
40
60
80
100
120
140
Time (seconds)

C)

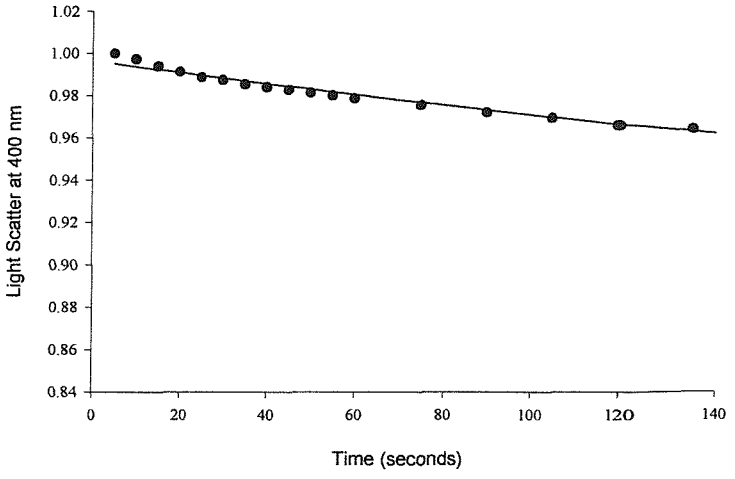
Light Scatter at 400 nm
1.02
1.00
0.98
0.96
0.94
0.92
0.90
0.88
0.86
0.84
0
20
40
60
80
100
120
140
Time (seconds)

Figure 6.9: Optical density changes in proteoliposomes in 30 mM glucose.
20 μl of proteoliposomes made from di(C18:1)PG and A) di(C14:1)PC, B) di(C18:1)PC or C) di(C24:1)PC at a molar ratio of 1:4, containing 0.025 μg of OmpF/μmol of phospholipid were diluted into 0.63 ml of 5 mM Tris-HCl, pH 8.0 containing 30 mM glucose. The light scatter was measured at 400 nm at 25 °C. The data were fitted to a single exponential to give rates and amplitudes shown in Table 6.5.

A)

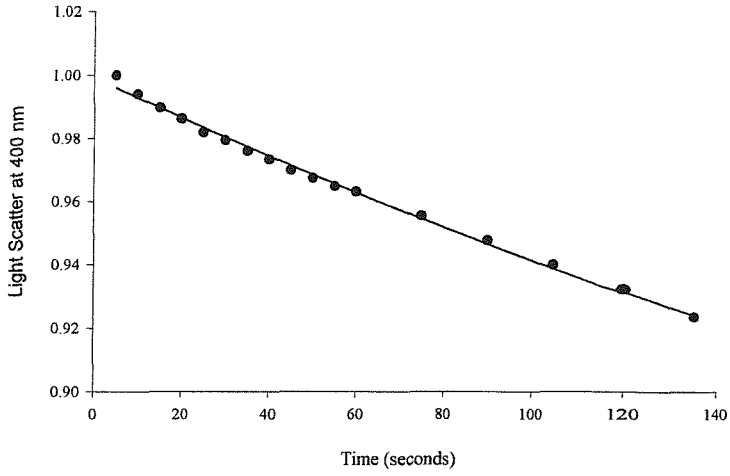
Light Scatter at 400 nm
1.02
1.00
0.98
0.96
0.94
0.92
0.90
0
20
40
60
80
100
120
140
Time (seconds)

B)

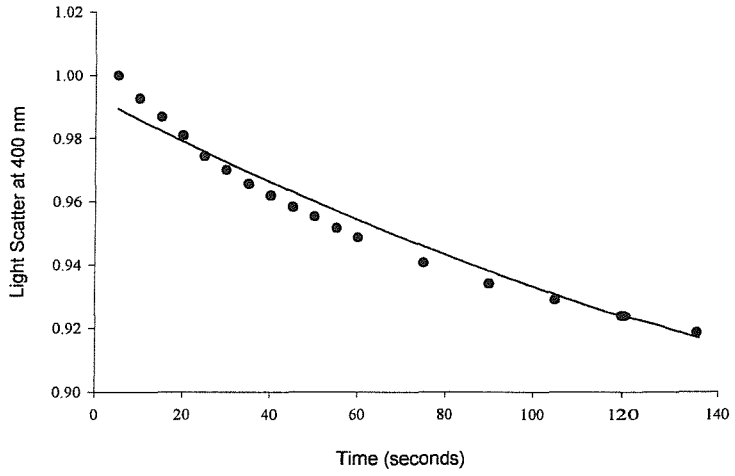
Light Scatter at 400 nm
1.02
1.00
0.98
0.96
0.94
0.92
0.90
0
20
40
60
80
100
120
140
Time (seconds)

C)

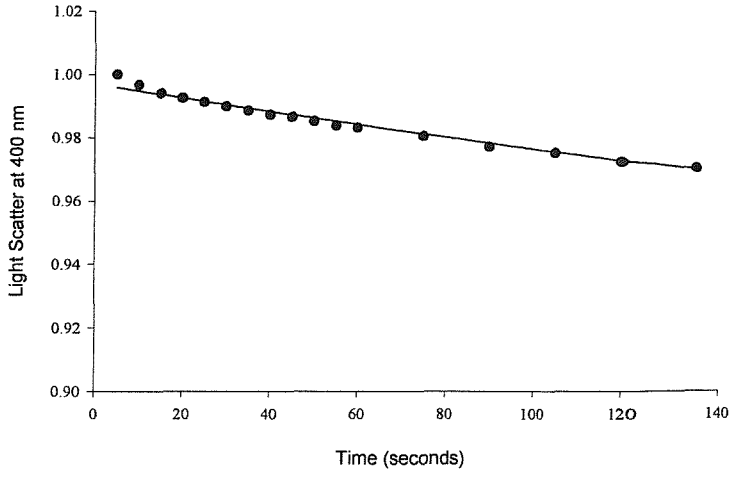
Light Scatter at 400 nm
1.02
1.00
0.98
0.96
0.94
0.92
0.90
0
20
40
60
80
100
120
140
Time (seconds)

A)

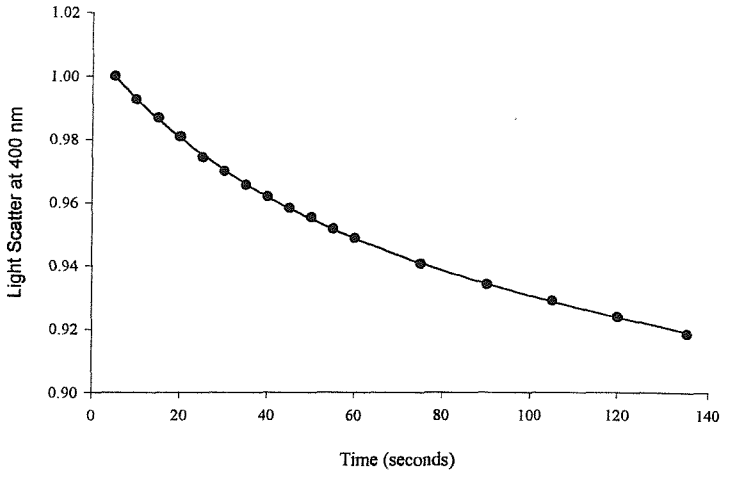

B)

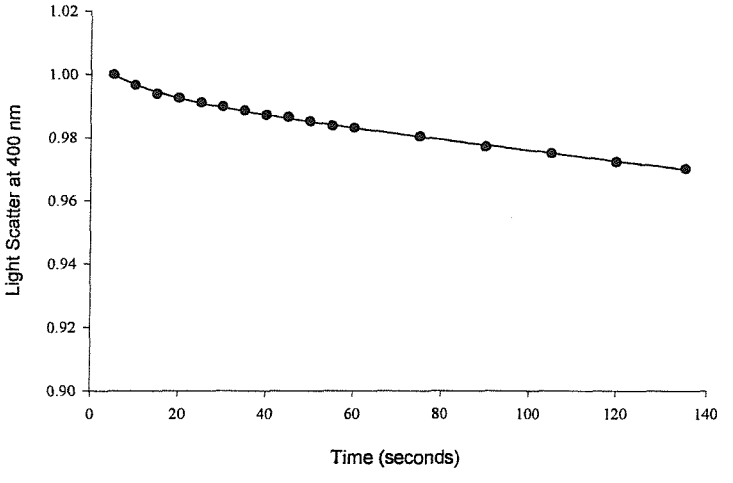

Figure 6.10: Optical density changes in di(C18:1) and di(C24:1) proteoliposomes in 30 mM glucose.

20 µl of proteoliposomes made from di(C18:1)PG and A) di(C18:1)PC or B) di(C24:1)PC at a molar ratio of 1:4, containing 0.025 µg of OmpF/µmol of phospholipid were diluted into 0.63 ml of 5 mM Tris-HCl, pH 8.0 containing 30 mM glucose. The light scatter was measured at 400 nm at 25 °C. The data were fitted to a double exponential to give rates and amplitudes shown in Table 6.6.

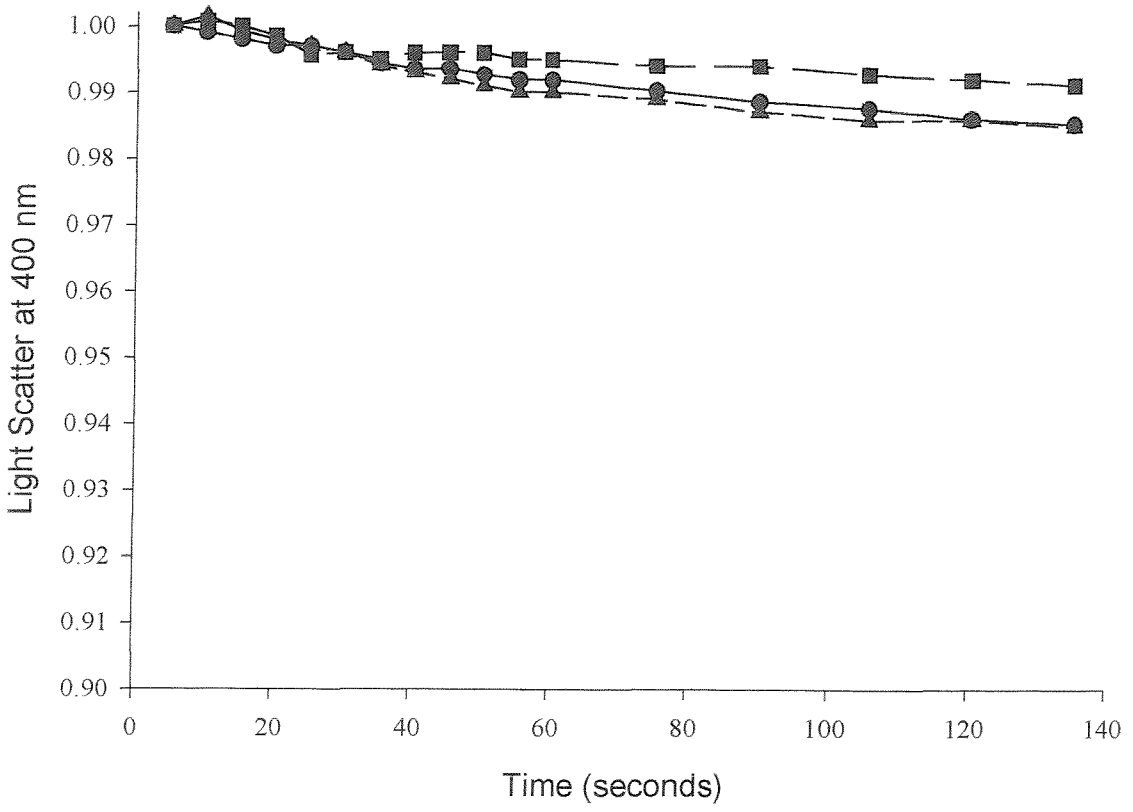

Figure 6.11: Optical density changes in proteoliposomes in 30 mM sucrose.

20 µl of proteoliposomes made from di(C18:1)PG and di(C14:1)PC (—●—, di(C18:1)PC (—▲—) or di(C24:1)PC (—■—), at a molar ratio of 1:4, containing 0.40 µg of OmpF/µmol of phospholipid were diluted into 0.63 ml of 5 mM Tris-HCl, pH 8.0 containing 30 mM sucrose. The light scatter was measured at 400 nm at 25 °C.

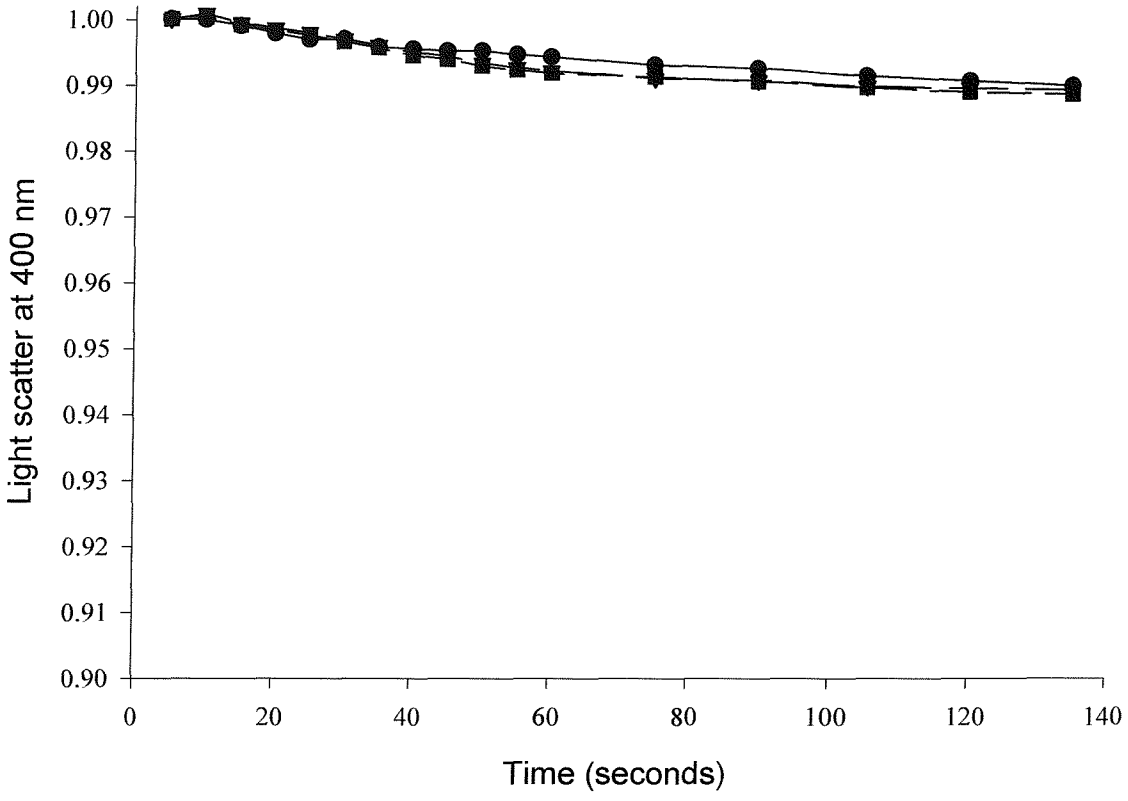

Figure 6.12: Optical density changes in di(C18:1)PC proteoliposomes in disaccharide sugars.

20 µl of proteoliposomes made from di(C18:1)PG and di(C18:1)PC at a molar ratio of 1:4 respectively, containing 0.40 µg of OmpF/µmol of phospholipid were diluted into 0.63 ml of 5 mM Tris-HCl, pH 8.0 containing 30 mM sucrose (—●—), maltose (—▲—) and lactose (—■—). The light scatter was measured at 400 nm at 25 °C.

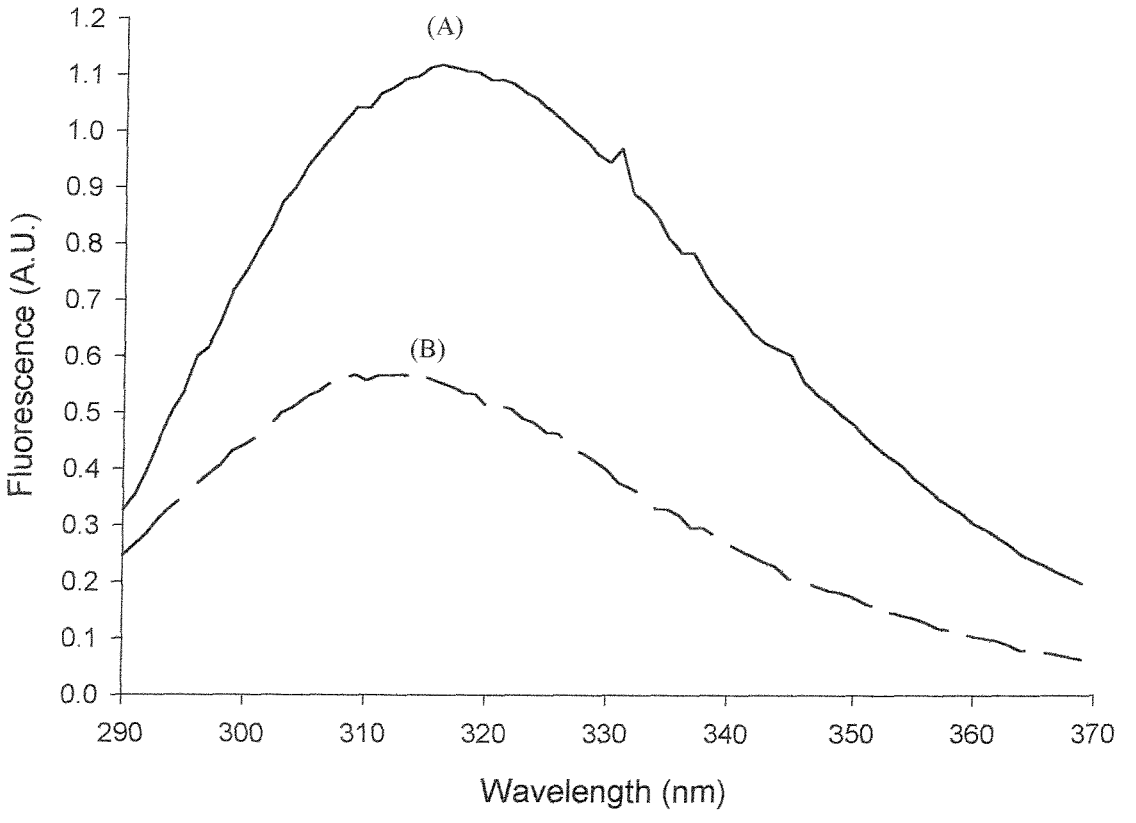

Figure 6.13: Fluorescence spectra of OmpF in bilayers of di(C18:1)PC or di(Br_2C18:0)PC reconstituted by the liposome swelling method.

The fluorescence spectra of OmpF reconstituted by the liposome swelling method into bilayers of A) di(C18:1)PC or B) di(Br_2C18:0)PC. The fluorescence of 0.125 nmols of OmpF was excited at 280 nm in 20 mM Hepes, pH 7.2, 1 mM EGTA.

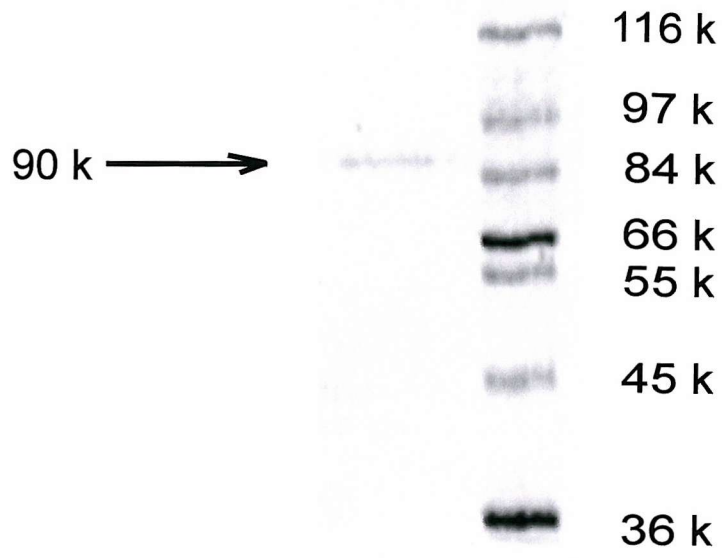

Figure 6.14: SDS-PAGE of OmpF reconstituted by the liposome swelling method.

Lane 1 contains 8.0 μg of OmpF that was reconstituted by the swelling method. Lane 2 contains high M_r Sigma markers.

A)

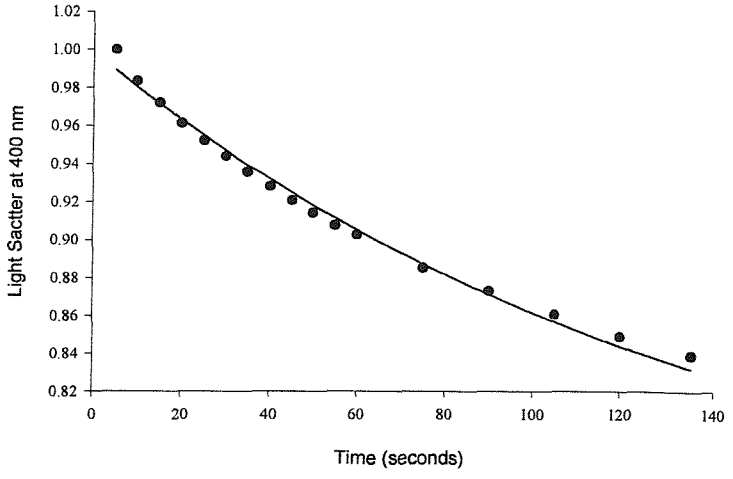

B)

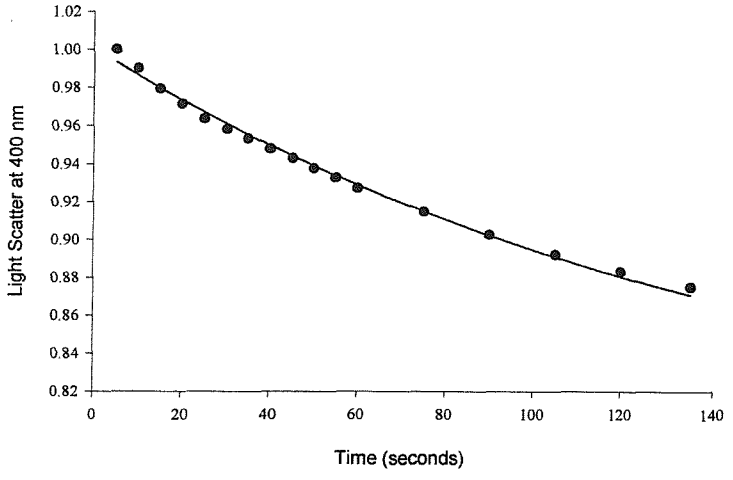

Figure 6.15: Liposome swelling assay using Biobeads-SM2.

20 µl of proteoliposomes made from di(C18:1)PG and di(C14:1)PC at a molar ratio of 1:4, containing 0.025 µg of OmpF/µmol of phospholipid were diluted into 0.63 ml of 5 mM Tris, pH 8.0 containing 30 mM arabinose. The samples were reconstituted by the swelling method with (A) or without (B) the use of Biobeads-SM2. The light scatter was measured at 400 nm at 25 °C. The data were fitted to a single exponential to give rates, b = 0.0071 ± 0.0003, with an amplitude of 0.271 ± (A), and b = 0.0065 ± 0.0002, with an amplitude of 0.221 ± (B).

a.)

b.)

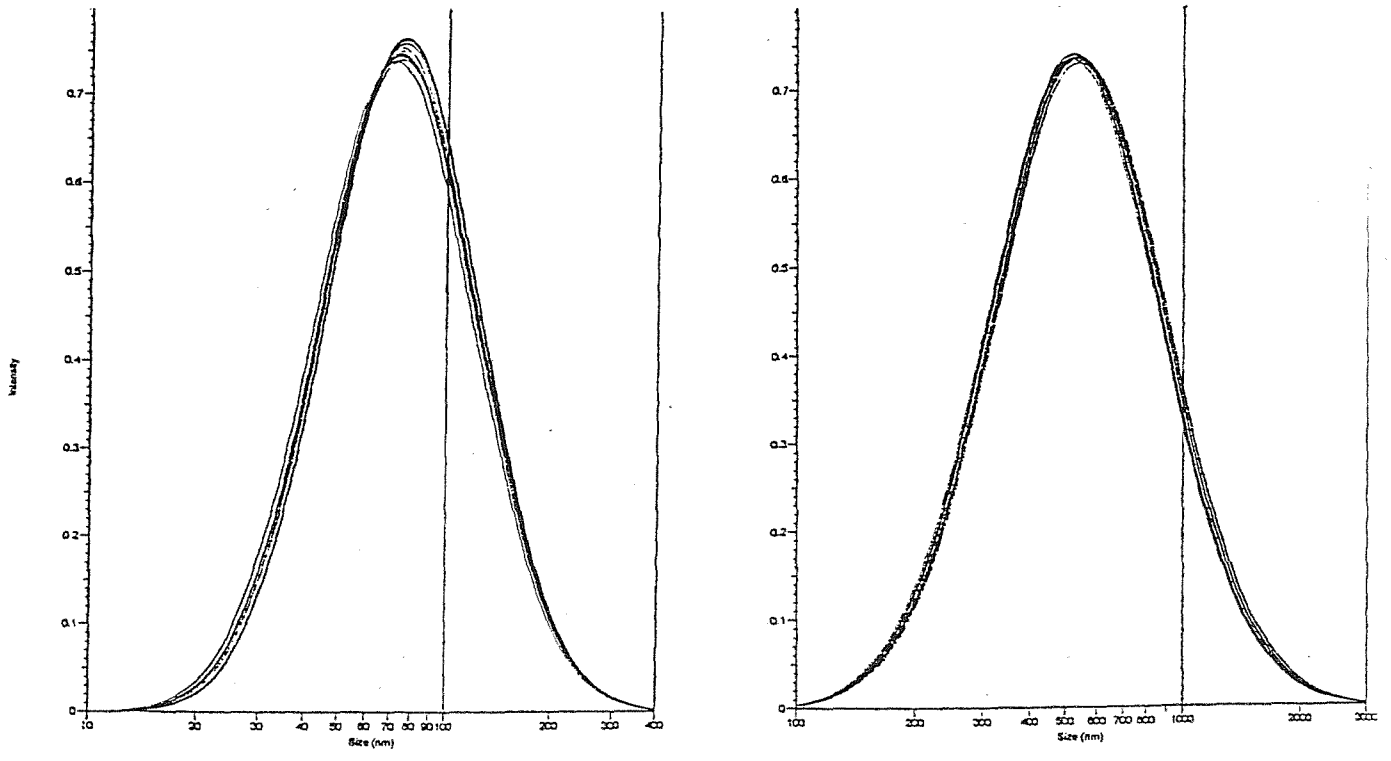

Figure 6.16: Determination of the sizes of vesicles reconstituted by the liposome swelling method.

Proteoliposomes were sized using a Coulter N4 Plus particles sizer.

a.) Proteoliposomes of di(C18:1)PG and di(C18:1)PC, containing 0.25 μg of OmpF/μmol of phospholipid, prepared using Biobeads-SM2 (Section 6.2.2.3(b)).

b.) Proteoliposomes of di(C18:1)PG and di(C18:1)PC, containing 0.25 μg of OmpF/μmol of phospholipid, prepared by the standard swelling method (Section 6.2.2.3(a)).

	Amplitude	Rate
Di(C14:1)PC	0.188 ± 0.004*	0.025 ± 0.0014
	0.211 ± 0.005	0.024 ± 0.0015
Di(C18:1)PC	0.130 ± 0.003*	0.022 ± 0.0014
	0.144 ± 0.004	0.024 ± 0.0013
Di(C24:1)PC	0.090 ± 0.004*	0.025 ± 0.0015
	0.096 ± 0.003	0.024 ± 0.0014

Table 6.1: Amplitude and rate of permeability of control liposomes to water. The reduction in light scatter was measured after dilution of control liposomes into 0.63 ml of 5 mM Tris-HCl, pH 8.0. The data were obtained using two different samples of liposomes. Example data are shown in Figure 6.4, and are indicated in the table by the *.

	Amplitude	Rate
Di(C14:1)PC	0.269 ± 0.007*	0.029 ± 0.002
	0.219 ± 0.006	0.026 ± 0.002
Di(C18:1)PC	0.182 ± 0.004*	0.026 ± 0.002
	0.162 ± 0.005	0.027 ± 0.002
	0.211 ± 0.006	0.025 ± 0.001
Di(C24:1)PC	0.119 ± 0.003*	0.025 ± 0.001
	0.130 ± 0.003	0.023 ± 0.001

Table 6.2: Amplitude and rate of permeability of proteoliposomes to water.
The reduction in light scatter was measured after dilution of proteoliposomes into 0.63 ml of 5 mM Tris-HCl, pH7.2. The data were obtained using two different samples of liposomes. Example data are shown in Figure 6.5, and are indicated in the table by the *.

Lipid	Permeability Rate	Amplitude
Di(C14:1)PC	0.0067 ± 0.0003*	0.269 ± 0.007
	0.0066 ± 0.0002	0.219 ± 0.006
Di(C16:1)PC	0.01057 ± 0.001078	0.172 ± 0.005*
	0.00997 ± 0.000727	0.166 ± 0.006
Di(C18:1)PC	0.0131 ± 0.00068	0.182 ± 0.004
	0 0113 ± 0.0006	0.162 ± 0.005
	0.0124 ± 0.0002	0.211 ± 0.006
Di(C20:1)PC	0.00814 ± 0.0008	0.126 ± 0.006*
	0.01028 ± 0.0006	0.135 ± 0.005
Di(C24:1)PC	0.0041 ± 0.0006*	0.119 ± 0.003
	0.0038 ± 0.0003	0.130 ± 0.003

Table 6.3: Permeability Rates for arabinose, calculated by fitting to single exponentials.

Permeability rates were obtained by fitting light scatter data to single exponentials. Example data are shown in Figure 6.7, and are indicated in the table by the *.

Lipid	Permeability Rate	Amplitude
Di(C14:1)PC	0.0039 ± 0.0001*	0.269 ± 0.007
	0.0037 ± 0.0001	0.219 ± 0.006
Di(C18:1)PC	0.0071 ± 0.0005*	0.182 ± 0.004
	0 0080 ± 0.0002	0.162 ± 0.005
	0.0092 ± 0.0003	0.211 ± 0.006
DI(C24:1)PC	0.0024 ± 0.0001*	0.119 ± 0.003
	0.0025 ± 0.0002	0.130 ± 0.003

Table 6.4: Permeability Rates for galactose, calculated by fitting to single exponentials.

Permeability rates were obtained by fitting light scatter data to single exponentials. Example data are shown in Figure 6.8, and are indicated in the table by the *.

Lipid	Permeability Rate	Amplitude
Di(C14:1)PC	0.0028 ± 0.0001*	0.219 ± 0.006
	0.0024 ± 0.0001	0.269 ± 0.007
Di(C18:1)PC	0.0040 ± 0.0002*	0.182 ± 0.002
	0 0060 ± 0.0003	0.162 ± 0.002
	0.0040 ± 0.0002	0.211 ± 0.001
DI(C24:1)PC	0.0019 ± 0.0001*	0.119 ± 0.003
	0.0018 ± 0.0002	0.130 ± 0.003

Table 6.6: Permeability Rates for glucose, calculated by fitting to single exponentials.

Permeability rates were obtained by fitting light scatter data to a single exponential. Example data are shown in Figure 6.9.

Lipid	Total Amplitude	Rate (b)	a	Rate (d)	c-a
Di(C18:1)PC	0.182 ± 0.004	0.0028 ± 0.0004	0.134 ± 0.002	0 027 ± 0.0103	0.048
	0.162 ± 0.005	0.0027 ± 0.0001	0.123 ± 0.002	0.018 ± 0.0030	0.039
	0.211 ± 0.006	0.0030 ± 0.0001	0.168 ± 0.001	0.078 ± 0.0071	0.043
Di(C24:1)PC	0.119 ± 0.003	0.0019 ± 0.0001	0.110 ± 0.001	0.079± 0.0103	0.009
	0.130 ± 0.003	0.0014 ± 0.0006	0.107 ± 0.001	0.048 ± 0.0041	0.023

Table 6.6: Permeability Rates for glucose, calculated by fitting to double exponentials.

Permeability rates were obtained by fitting light scatter data to double exponentials. Example data are shown in Figure 6.10.

	Di(C14:1)PC	DI(C18:1)PC	DI(C24:1)PC
Arabinose	0.0067 ± 0.00007	0.0123 ± 0.00091	0.0039 ± 0.00021
Galactose	0.0038 ± 0.00014	0.00810 ± 0.0010	0.0022 ± 0.00007*
Glucose	0.0026 ± 0.00028	0.0028 ± 0.00016*	0.0017 ± 0.00033*

Table 6.7: Mean permeability rates for monosaccharide sugars through OmpF.

	Mean Diameter (nm)	Standard Deviation (nm)
Di(C14:1)PC	621.7	276.8
	648.6	288.9
Di(C18:1)PC	653.2	290.6
	628.9	283.9
Di(C24:1)PC	633.0	282.6
	685.3	304.9
Di(C14:1)PC (a. Biobeads-SM2)	532.8	235.7
Di(C14:1)PC (b. Biobeads-SM2)	94.5	40.6

Table 6.8: Sizes of liposome vesicles.

All of the liposome samples prepared were sized using a Coulter N4 particle sizer. 20 μl of liposome suspension was diluted into 2.5 mls of 0.2 μm filtered distilled water. Each sample was allowed to equilibrate for 15 minutes before the light scatter was measured 12 times for 5 minutes at an angle of 90 °.

6.4 Discussion

The function of porins can be studied by reconstitution into sealed lipid vesicles. To establish whether varying the lipid bilayer thickness had an effect on the functioning of OmpF, the function was determined after reconstitution into vesicles prepared with phosphatidylcholine with different fatty acyl chain lengths. To measure the function of porins by the swelling method, the extent of water influx into the liposomes was first established. The extent of the water permeability was seen to differ between liposomes made from different chain length phosphatidylcholine, with the amplitude of the drop in the light scatter being highest in di(C14:1)PC and decreasing with increasing lipid chain lengths (Figures 6.4 and 6.5, and Tables 6.1 and 6.2). The different magnitudes of the light scatter changes were not related to changes in the vesicle size, since, as shown in Table 6.8, these data did not change significantly with chain length. The rates of water influx were found to be independent of the fatty acyl chain length. Rather it is likely that the differences follow from changes in the cohesiveness of the lipids due to interaction between the lipid fatty acyl chains.

The rates calculated for the monosaccharide sugars showed, as anticipated, that the highest permeability is seen with the pentose sugar, arabinose, followed by the hexose sugars galactose and glucose, respectively (Figures 6.7 – 6.11). The light scatter changes observed for proteoliposomes in the disaccharide sugars tested were so small that rates could not be accurately measured (Figures 6.12 - 6.13). The permeability rates for the monosaccharides were seen to be dependent on the fatty acyl chain length of the phosphatidylcholine. Highest rates were observed with di(C18:1)PC, which were two- and three-fold higher with arabinose than in di(C14:1)PC and di(C24:1)PC, respectively (Table 6.3). The differences in the rates were two- and four-fold higher in di(C18:1)PC in galactose than with di(C14:1)PC and di(C24:1)PC, respectively (Tables 6.4 – 6.5). The rates in glucose were also highest for di(C18:1)PC proteoliposomes, but the differences in the rates between the three phosphatidylcholine chain lengths assayed were less than the rate differences seen in arabinose and galactose (Tables 6.6 - 6.8). In calculating the permeability rates for the sugars, the data did not always fit well to a

single exponential (Figures 6.8 and 6.10). These data were instead fitted to a double exponential, where two components – a slow component, that accounted for a large fraction of the amplitude (approximately 75 %), and a fast component that corresponded to a very small part of the total light scatter change. The rate of the slow component was very similar to rates calculated from a single exponential equation for the same data (Tables 6.5 and 6.7). The rate of the slow component was therefore assumed to represent the permeability of the test sugar. The source of the fast rate was not determined in the experiments. Comparison of the fast rates obtained from different batches of proteoliposomes and from different lipid chain lengths did not reveal any similarities, and so these minor components were presumed to be artefacts and were not investigated further.

It has been shown that the activity of the Ca^{2+}-ATPase is dependent on the chain length of the lipids surrounding it in the membrane (Caffrey & Feignson, 1981; Starling *et al.*, 1993). Optimal activity was seen in di(C18:1)PC, with lower activities in shorter or longer chain lipids. A similar bell-shaped activity profile was seen for the melibiose permease transporter, found in *E. coli* (Dumas *et al.*, 2000), and the human erythrocyte hexose transporter (Carruthers & Melchior, 1984). Highest activity for melibiose permease was seen in di(C16:1)PC, which provides a bilayer with a hydrophobic thickness of 26 Å. It was concluded from this study that the highest protein activity is seen when the hydrophobic matching condition is met (Dumas *et al.*, 2000). The hydrophobic thickness of OmpF has been estimated by measuring the distance between the rings of aromatic residues found at the membrane interfaces. At 25 Å, this distance would best match a bilayer of di(C14:1)PC, which has a hydrophobic bilayer thickness of 23 Å and thus would meet the hydrophobic matching conditions. Although this condition gives the strongest binding of lipid (see Chapter 4) it does not correspond to the highest permeability rate (Table 6.7). This result is somewhat unexpected. As described in Chapter 1 the most common chain length in the outer membrane is C14, and thus it would have been expected that the greatest permeability would be seen in di(C14:1)PC. It is possible that permeabilities of OmpF to other solutes show a different chain length dependence although there is no direct evidence

for this. However, it is notable that the activity of the Ca^{2+}-ATPase in di(C18:1)PC is about 20 % higher than in the native SR membrane (Lee, 1998). It is possible therefore that biological membranes are not optimised to give maximum activity for any particular membrane protein, perhaps because the membrane contains a large number of different proteins, each of which might have its own requirement for maximum activity.

The observation that permeability changes with chain length shows that the structure of the porin must change with changes in bilayer thickness. These changes are likely to be small. For example, the porins remain trimeric in the bilayers (Figure 6.14). Thus it appears that even β-barrel proteins cannot be considered to be rigid, undistortable structures in the membrane.

Major alterations to the secondary structure of OmpF could be detected by circular dichroism. This method would however only detect gross conformational changes from a β-sheet to an α-helical structure, which is an unlikely event to occur within the lipid bilayer. Analysis of proteolysis patterns is an alternative approach, which could be used to investigate changes in the outer loop regions of OmpF. Resonance energy transfer could also be used as a molecular ruler to detect changes in intermolecular distances between particular amino acid residues or the distance between a particular amino acid residue and a lipid headgroup. This method requires labelling of the groups with fluorophores which will act as donors or acceptors in energy transfer. Combined, these methods may establish whether distortion of OmpF occurs in lipid bilayers that do not match its hydrophobic membrane-spanning region.

CHAPTER 7
GENERAL CONCLUSIONS

Porins are a family of β-barrel proteins found in the outer membrane of Gram negative cells. The structure of these proteins is extremely stable and requires boiling for several minutes for complete denaturation to occur (Garavito & Rosenbusch, 1985). The solubility of the OmpF porin in several detergents was compared to the Ca^{2+}-ATPase, a typical α-helical membrane protein, in Chapter 3. These studies show that the effectiveness of a detergent in solubilising a particular membrane protein is strongly dependent on the structure of the membrane protein in question. Two suitable detergents for reconstitution of OmpF were identified – octyl-POE and OG. Detergent-mediated reconstitution of membrane proteins into bilayers of exogenous lipid depend on solubilisation of the lipid and protein components without irreversible loss of protein function, and then removal of the detergent so that lipid bilayers can reform with the protein incorporated. The relative ease with which a detergent can be removed is strongly dependent on the cmc value of the detergent, with those detergents with a high cmc value being relatively easy to remove compared to a detergent with a low cmc value. Methods of removal for the former can include dilution, dialysis, or gel filtration. Detergents with a low cmc can be exchanged by dialysis for a detergent with a high cmc or alternatively can be removed using detergent absorbing beads, such as Biobeads SM-2, which are also effective in removing detergents with a high cmc. The effect of the method of detergent removal on the reconstitution process was investigated and found to have little influence in fluorescence quenching experiments with di(Br_2C18:0)PC.

Binding of lipids to OmpF was shown to be selective. The highest binding constant was seen for phospholipids with C14 fatty acyl chains (Figure 7.1). The hydrophobic thickness of lipid bilayers consisting of C14 fatty acyl chains is approximately 23 Å (Lewis & Engelman, 1983). This is comparable to the thickness of the hydrophobic region of OmpF (25 Å), measured as the distance between the two aromatic rings found at the membrane interfaces (Cowan *et al.*, 1992). The native

environment of OmpF contains both lipopolysaccharide and phospholipids, with fatty acyl chain lengths of C14 predominately esterified to LPS and C16 and C18 chain lengths being the predominant phospholipid species. This selectivity in binding means that if the outer membrane contains a variety of lipids with different fatty acyl chains, those with C14 chains will preferentially accumulate around the OmpF. Some selectivity was also seen with respect to lipid headgroup: binding of phosphatidylethanolamine was comparable to phosphatidylcholine, but the binding constant determined for phosphatidylglycerol was approximately half that of phosphatidylcholine.

Studies of the effect of varying bilayer thickness on the function of OmpF were reported in Chapter 6. Unexpectedly the highest permeability rates of OmpF with monosaccharide sugars were found in bilayers of di(C18:1)PC. The results from Chapters 5 and 6 are compared in Figure 7.1. It shows that OmpF has the highest binding constant for di(C14:1)PC, but that the permeability rate of OmpF is highest in di(C18:1)PC. Similar observations were recently made with the melibiose transporter. Maximum rates were observed in di(C16:1)PC, whereas the thickness of the hydrophobic region of the protein matches bilayers of di(C18:1)PC (Dumas *et al.*, 2000). In the case of the Ca^{2+}-ATPase, however, both the highest activity and binding constant were found in di(C18:1)PC. Thus it might be that for some membrane proteins hydrophobic matching is required for highest activity, whereas for others a degree of hydrophobic mismatch gives the highest activity. For OmpF it is, of course, possible that optimal chain lengths for permeability are different for different chain solutes. Thus although the permeability to sugars is highest in di(C18:1)PC the permeability of cations for example might be higher in other lipids. It is also possible that a degree of mismatch between the lipid and the protein is required to provide the optimal pore diameter in the porin. The observation that permeability is highest in di(C18:1)PC could imply that the thickness of the outer membrane of E. coli is more like that of di(C18:1)PC than of di(C14:1)PC although, as already described, the hydrophobic thickness of OmpF is the same as that of a bilayer of di(C14:1)PC. Alternatively, if the thickness of the outer membrane is comparable to a bilayer of di(C14:1)PC, then OmpF operates at less than

its maximum possible rate in the outer membrane. Again a parallel can be drawn with the Ca^{2+}-ATPase, which shows a higher rate of activity in bilayers of di(C18:1)PC than in the native SR membrane (Caffrey & Feignson, 1981; Starling *et al.*, 1993). It may be that a cell cannot optimise the outer membrane for the function of all the proteins in the membrane simply because of the large number of different species of proteins.

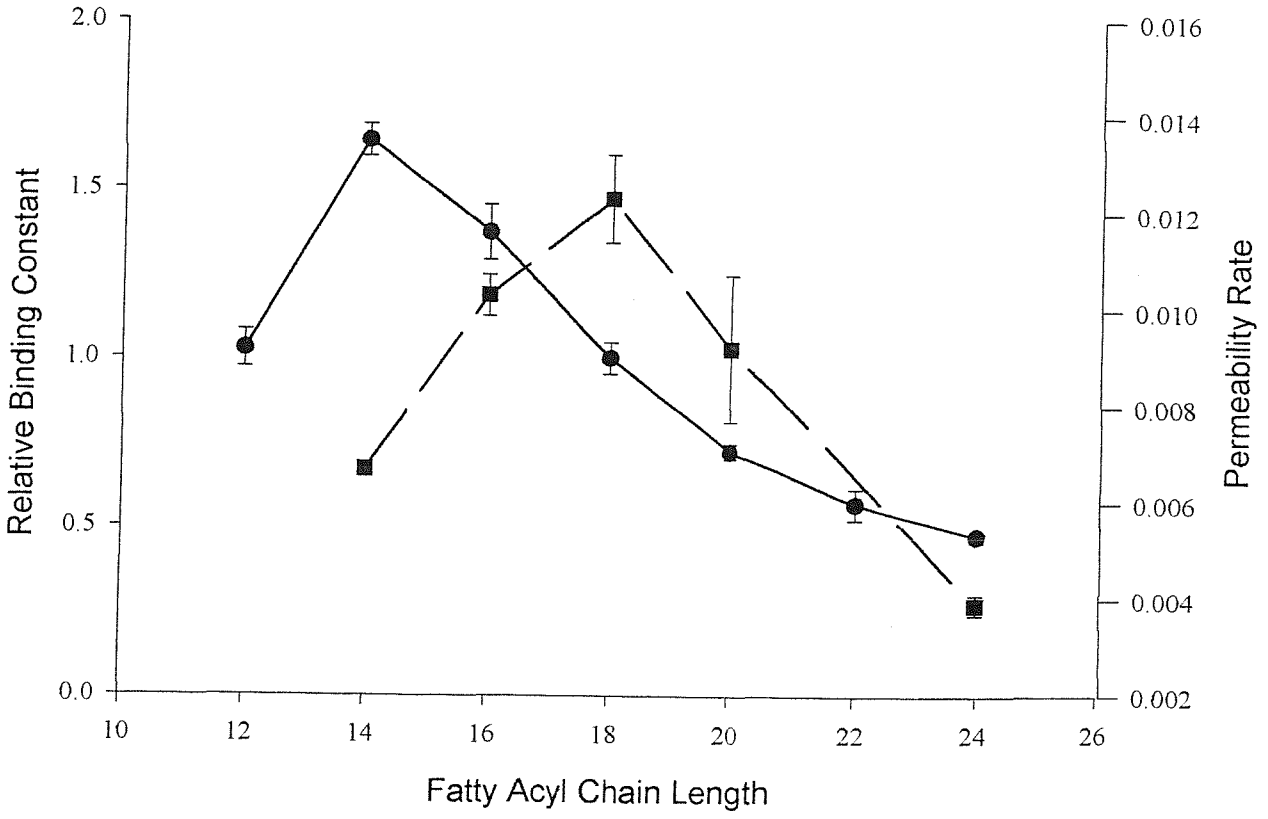

Figure 7.1: Comparison of the effects of different chain length phosphatidylcholine on the lipid binding constant and function of OmpF.

Results from binding studies (—●—) are compared to results of functional assays (—▲—).

REFERENCES

Allen, T.M., Romans, A.Y., Kercret, H. & Segrest, J.P. (1980) Biochim.Biophys.Acta **601**, 328-342

Bainbridge, G., Gokce, I. & Lakey, J.H. (1998) FEBS Lett. **431**, 305-308

Bainbridge, G., Mobasheri, H., Armstrong, G.A., Lea, E.J.A. & Lakey, J.H. (1998) J.Mol.Biol. **275**, 171-176

Bangham, A.D., Hill, M.W. & Miller, N.G.A. (1974) Methods in Membrane Biology (Korn, E.D., ed.), Preparation and Use of Liposomes as Models of Biological Membranes. pp. 1-68,

Bauer, K., Struyve, M., Bosch, D., Benz, R. & Tomassen, J. (1989) J.Biol.Chem. **264**, 16393-16398

Benz, R. (1988) Ann.Rev.Microbiol. **42**, 359-393

Bernstein, H.D. (2000) C.Opin.Microbiol. **3**, 203-209

Bogdanov, M. & Dowhan, W. (2000) J.Biol.Chem. **274**, 36827-36830

Booth, P.J. & Curran, A.R. (1999) C.Opin.Struc.Biol. **9**, 115-121

Booth, P.J., Riley, M.L., Flitsch, S.L., Templer, R.H., Farooq, A. & Curran, A.R. (1997) Biochemistry **36**, 197-203

Braun, P. & von Heijne, G. (1999) Biochemistry **38**, 9778-9782

Buchanan, S.K. (1999) C.Opin.Struc.Biol. **9**, 455-461

Buckland, A.G. & Wilton, D.C. (2000) Biochim.Biophys.Acta **1483**, 199-216

Buehler, L.K., Kusumoto, S., Zhang, H. & Rosenbusch, J.P. (1991) J.Biol.Chem. **266**, 2446-24450

Caffrey, M. & Feignson, G.W. (1981) Biochemistry **20**, 1949-1961

Carruthers, A. & Melchior, D.L. (1984) Biochemistry **23**, 6901-6911

Cowan, S.W., Schirmer, T., Rummel, G., Steiert, M., Ghosh, S., Pauptit, R.A., Jamsomius, J.N. & Rosenbusch, J.P. (1992) Nature **358**, 727-733

Creighton, T.E. (1993) Proteins. Structures & Molecular Properties. Conformational Properties of Polypeptide Chains. pp. 171-200, W.H. Freeman & Company, New York

Cronan, J.E. (1978) Ann.Rev.Biochem. **47**, 163-189

Cullis, P.R., Fenske, D.B. & Hope, M.J. (1996) Biochemistry of Lipids, Lipoproteins and Membranes. New Comprehensive Biochemistry Volume 31 (Vance, D.E. & Vance, J., eds.), Physical and functional roles of lipids in membranes. pp. 1-33, Elsevier, Amsterdam, Lamsanne, New York, Oxford, Shannon, Toyko

Dawidowicz, E.A. & Rothman, J.E. (1976) Biochim.Biophys.Acta **455**, 621-630

Dawson, R.M.C. (1967) Biochem.J. **102**, 205-210

De Cock, H., Brandenburg, K., Wiese, A., Holst, O. & Seydel, U. (1999) J.Biol.Chem. **274,** 5114-5119

De Cock, H. & Tomassen, J. (1996) EMBO J. **15,** 5567-5573

De Gier, J., Mandersloot, J.G. & Van Deenen, L.L.M. (1968) Biochim.Biophys.Acta **150**, 666-675

de Kruijff, B. (1987) Nature **329**, 587-588

Delcour, A.H., Alder, J., Kung, C. & Martinac, B. (1992) FEBS **304**, 216-220

Dowhan, W. (1998) Biochim.Biophys.Acta **1376**, 455-466

Doyle, D.A., Cabral, J.M., Pfuetzner, R.A., Kuo, A., Gulbis, M., Cohen, S.L., Chait, B.T. & MacKinnon, R. (1998) Sccience **280**, 69-77

Dumas, F., Lebrun, M.C. & Tocanne, J.F. (1999) FEBS Lett. **458**, 271-277

Dumas, F., Tocanne, J.F., Leblanc, G. & Lebrun, M.C. (2000) Biochemistry **39**, 4846-4854

East, J.M. & Lee, A.G. (1982) Biochemistry **21**, 4144-4151

Epand, R.M. (1998) Biochim.Biophys.Acta **1376**, 353-368

Eppens, E.F., Nouwen, N. & Tomassen, J. (1997) EMBO J. **16**, 4295-4301

Eppens, E.F., Saint, A., Van Gelder, P., Van Boxtel, R. & Tomassen, J. (1997) FEBS Lett. **415**, 317-320

Fattal, D.R. & Ben-Shaul, A. (1993) Biophys.J. **65**, 1795-1809

Fattal, D.R. & Ben-Shaul, A. (1995) Physica A **220**, 192-216

Ferguson, A.D., Hofmann, E., Coulton, J.W., Diederichs, K. & Welte, W. (1998) Science **282**, 2215-2227

Ferguson, A.D., Welte, W., Hofmann, E., Lindner, B., Holst, O., Coulton, J.W. & Diederichs, K. (2000) Structure **8**, 585-592

Forst, D., Schulein, K., Wacker, T., Diederichs, K., Kreutz, W., Benz, R. & Welte, W. (1993) J.Mol.Biol **229**, 258-262

Forst, D., Welte, W., Wacker, T. & Diederichs, K.(1998) Nature Struc.Biol. **5**, 37-46

Fourel, D., Bernadec, A. & Pages, J.M. (1994) Eur. J. Biochem. **222**, 625-630

Freudl, R., MacIntyre, M., Degan, M. & Henning, U.(1988) J.Biol.Chem. **263**, 344-349

Galanos, C., Luderitz, O. & Westphal, O.(1969) Eur.J.Biochem. **9**, 245-249

Garavito, R.M. & Rosenbusch, J.P.(1985) Meth.Enzymol. **125**, 309-328

Gutman, M., Tsfadia, Y., Masad, A. & Nachliel, E. (1992) Biochim.Biophys.Acta **1109**, 141-148

Hancock, R.E., Karunaralne, D.N. & Beregger-Egli, C. (1994) Bacterial Cell Wall (Gluysen, J.M. & Hanenbeck, R., eds.), Molecular Organisation and Structural Role of Outer Membrane Macromolecules. New Comprehensive Biochemistry Volume 27. pp. 263-276, Elsevier, Amsterdam, Lamsanne, New York, Oxford, Shannon, Toyko

Harroun, T.A., Heller, W.T., Weiss, T.M., Yang, L. & Huang, H.W.(1999) Biophys.J. **76**, 937-945

Harwood, J.L. & Russel, N.J. (1984) Lipids in plants and microbes George Allen and Unwin, London

Heine, H.G., Kyngdon, J. & Ferenci, T. (1987) Gene **53**, 287-292

Helenius, A., McCaslic, D.R., Fries, E. & Tanford, C.(1979) Meth.Enzymol. **LVI**, 734-749

Helenius, A. & Simons, K. (1975) Biochim.Biophys.Acta **415**, 29-79

Hirata, H. (1986) Techniques for the Analysis of Membrane Proteins (Ragan, C.I. & Cherry, R.J., eds.), Reconstitution of membrane proteins into vesicular membranes. pp. 77-96, Chapman and Hall, London, New York

Hoenger, A., Gross, H., Aebi, U. & Engel, A. (1990) J.Struc.Biol. **103**, 185-195

Huijbregts, R.P.H., de Kroon, A.I.P.M. & de Kruijff, B. (2000) Biochim.Biophys.Acta **1469**, 43-61

Jap, B.K. & Walian, P.J.(1996) Physiol.Rev. **76**, 1073-1088

Jap, B.K. & Walian, P.J.(1998) Nature Struc.Biol. **5**, 6-8

Jeanteur, D., Schirmer, T., Fourel, D., Simonet, V., Rummel, G., Widmer, C., Rosenbusch, J.P. & Pages, J.M.(1994) Proc.Natl.Acad.Sci. **91**, 10675-10679

Johnson, J.E. & Cornell, R.B.(1999) Mol.Membrane Biol. **16**, 217-235

Jones, G.R. & Cossins, A.R. (1990) Liposomes, A Practical Approach. (Rickwood, D. and Hames, B.D., eds.) Physical Methods of Study pp. 183-220, IRL Press, Oxford, New York, Tokyo

Karshikoff, A.(1994) J.Mol.Biol. **240**, 372-384

Killian, J.A. (1998) Biochim.Biophys.Acta **1376**, 401-416

Killian, J.A., Salemink, I., de Planque, M.R.R., Lindblom, G., Koeppe, R.E. & Greathouse, D.V. (1996) Biochemistry **35**, 1037-1045

Killian, J.A. & von Heijne, G. (2000) Trends Biochem.Sci. **25**, 429-434

Klebba, P.E. & Newton, S.M.C. (1998) C.Opin.Microbiol. **1**, 238-248

Knowles, P.F., Marsch, D. & Rattle, H.W.E. (1976) Magnetic Resonance of Biomolecules (John Wiley & Sons, eds.), Wiley Interscience London, New York, Sydney, Toronto

Koeppe, R.E., Killian, J.A., Greathouse, D.V. & Anderson, O.S.(1998) Biol.Skr.Vid.Selsk. **49**, 93-98

Korteland, J., De Graaff, P. & Lugtenberg, B. (1984) Biochim.Biophys.Acta **778**, 311-316

Kreusch, A. & Schulz, G.E. (1994) J.Mol.Biol **243**, 891-905

Laemmli, U.K. (1970) Nature **227**, 680-685

Lakey, J.H., Lea, E.J.A. & Pattus, F. (1991) FEBS Lett. **278**, 31-34

Lakey, J.H., Watts, A. & Lea, E.J.A. (1985) Biochim.Biophys.Acta **817**, 208-216

Lakowicz, J.R. (1983) Principles of Fluorescence Spectroscopy. Plenum Press, New York & London

Lambeth, J.D. & Ryu, S.H. (1996) Biochemistry of Lipids, Lipoproteins and Membranes. New Comprehensive Biochemistry Volume 31 (Vance, D.E. & Vance, J., eds.), Glycerolipids in signal transduction. pp. 237-254, Elsevier, Amsterdam, Lamsanne, New York, Oxford, Shannon, Toyko

Landolt-Marticorena, C., Williams, K.A., Deber, C.M. & Reithmeier, A.F. (1993) J.Mol.Biol **229**, 602-608

Le Dain, A.C., Hase, C.C., Tomassen, J. & Martinac, B. (1996) EMBO J. **15**, 3524-3528

Lee, A.G. (1983) Membrane Fluidity in Biology. Volume 2 (Aloria, R.C., ed.), Lipid phase transitions and mixtures. pp. 43-88, Academic Press, Inc., New York

Lee, A.G. (1998) Biochim.Biophys.Acta **1376**, 381-390

Lehninger, A.L. (1982) Principles of Biochemistry (Anderson, S. and Fox, J., eds.), Worth Publishers Ltd. New York

Levy, D., Gulik, A., Bluzatt, A. & Rigaud, J.L. (1992) Biochim.Biophys.Acta **1107**, 283-298

Lewis, B.A. & Engelman, D.M. (1983) J.Mol.Biol **166**, 211-217

Lichtenberg, D., Robson, R.J. & Dennis, E.A. (1983) Biochim.Biophys.Acta **737**, 285-304

London, E. & Feigenson, G.W. (1981) Biochemistry **20**, 1939-1948

Luecke, H., Schobert, B., Richter, H.T., Cartailler, J.P. & Lanyi, J.K. (1999) J.Mol.Biol **29**, 899-911

Lugtenberg, B., Meijers, J., Peters, R., Van de Hoek, P. & Van Alphen, L. (1975) FEBS Lett. **58**, 254-258

Lugtenberg, B. & Peters, R. (1976) Biochim.Biophys.Acta **441**, 38-47

Lugtenberg, B. & Van Alphen, L. (1983) Biochim.Biophys.Acta **737**, 51-115

Mall, S., Broadbridge, R., Sharma, R.P., Lee, A.G. & East, J.M. (2000) Biochemistry **39,** 2071-2078

Martin, D.W. (1983) Biochemistry **22**, 2276-2282

Moller, J.V., Le Maire, M. & Anderson, J.P. (1986) Progress in Protein-Lipid Interactions 2 (A.Watts and De Pont, J.J.H.M., eds.), Uses of non-ionic and bile salt detergents in the study of membrane proteins. pp. 147-196, Elsevier, Amsterdam, New York, Oxford

Mouritsen, O.G. & Bloom, M. (1984) Biophys.J. **46**, 141-153

Nakae, T. (1975) J.Biol.Chem. **251,** 2176-2178

Nakae, T. (1976) Biochem.Biophys.Res.Comm. **71**, 877-884

Nakamura, K. & Mizushima, S. (1976) J.Biochem. **80**, 1411-1422

New, R.R.C. (1990) Liposomes A Practical Approach (Rickwood, D. and Hames, B.D., eds.), Characterisation pf Liposomes pp. 105-162 IRL Press Oxford, New York, Tokyo

Nielson, C., Goulian, M. & Anderson, O.S. (1998) Biophys.J. **74**, 1966-1983

Nikaido, H. (1994) J.Biol.Chem. **269**, 3905-3908

Nikaido, H., Nikaido, K. & Harayama, S. (1991) J.Biol.Chem. **266**, 770-779

Nikaido, H. & Rosenberg, E.Y. (1983) J.Bacteriol. **153**, 241-252

Nikaido, H. (1983) Meth.Enzymol. **97**, 85-100

Nikaido, H. & Vaara, M. (1985) Microbiol.Rev. **49**, 1-32

Op den Kamp, J.A.F. (1979) Ann.Rev.Biochem. **48**, 47-71

Paternostre, M.T., Roux, M. & Rigaud, J.L. (1988) Biochemistry **27**, 2668-2677

Pattnaik, B.R., Ghosh, S. & Rajeswari, M. (1997) Biochem.Molec.Biol.Int. **42**, 173-181

Phale, P.S., Schirmer, T., Prilipov, A., Kuo-Long, L., Hardmeyer, A. & Rosenbusch, J.P. (1997) Proc.Natl.Acad.Sci.USA **94**, 6741-6745

Piknova, B., Marsch, D. & Thomson, T.E. (1997) Biophys.J. **72**, 2660-2668

Piknova, B., Perochon, E. & Tocanne, J.F. (1993) Eur.J.Biochem. **218**, 385-396

Prilipov, A., Phale, P.S., Van Gelder, P., Rosenbusch, J.P. & Koebnik, R. (1998) FEMS Microbiol.Lett. **163**, 65-72

Raetz, C.R.H. (1978) Microbiol.Rev. **42**, 614-659

Rigaud, J.L., Pitard, B. & Levy, D. (1995) Biochem.Biophys.Res.Comm. **1231**, 223-246

Rocque, W.J., Coughlin, R.T. & McGroarty, E.J. (1987) J.Bacteriol. **169**, 4003-4010

Roseman, M.A. (1988) J.Mol.Biol **201**, 621-623

Rosenbusch, J.P. (1974) J.Biol.Chem. **249**, 8019-8029

Saint, N., Lou, K.-L., Widmer, C., Luckey, M., Schirmer, T. & Rosenbusch, J.P. (1996) J.Biol.Chem. **271**, 20676-20680

Saint, N., Prilipov, A., Hardmeyer, A., Lou, K.L., Schirmer, T. & Rosenbusch, J.P. (1996) Biochem.Biophys.Res.Comm. **223**, 118-122

Schindler, M., Osborn, M.J. & Koppel, D.E. (1980) Nature **283**, 346-350

Schirmer, T. (1998) J.Struc.Biol. **121**, 101-109

Schirmer, T., Keller, T.A., Wang, Y.F. & Rosenbusch, J.P. (1995) Science **267**, 512-514

Schmid, B., Maveyraud, L., Kromer, M. & Schultz, G.E. (1998) Prot.Sci. **7**, 1603-1611

Schulz, G.E. (1993) C.Opin.Cell Biol. **5**, 701-707

Seshadri, K., Garemyr, R., Wallin, E., von Heijne, G. & Elofsson, A. (1998) Prot.Sci. **7**, 2026-2032

Silvius, J.R. (1992) Ann.Rev.Biophys.Biomol.Struct. **21**, 323-348

Simons, K. & Ilkonen, E. (1997) Nature **387**, 569-572

Singer, S.J. & Nicholson, G.L. (1972) Science **175**, 720-731

Smith, P.K., Krohn, R.I., Hermanson, G.T., Mallia, A.K., Gartner, F.H., Provenzano, M.D., Fujimoto, E.K., Goeke, N.K., Olsen, B.J. & Klenk, D.C. (1985) Anal.Biochem. **150**, 76-85

Sonntag, I., Schwarz, H., Hirota, Y. & Henning, U. (1978) J.Bacteriol. **136**, 280-285

Starling, A.P., East, J.M. & Lee, A.G. (1993) Biochemistry **32**, 1593-1600

Steven, A.C., Heggeler, B., Muller, R., Kistler, J. & Rosenbusch, J.P. (1977) J.Cell Biol. **72**, 292-301

Stryer, L. (1995) Biochemistry, Fourth Edition, WH Freeman & Company, San Francisco

Stubbs, C.D. (1983) Essays in Biochem. **19**, 1-39

Tielman, D.P., Forrest, L.R., Sansom, M.S.P. & Berendson, H.J.C. (1998) Biochemistry **37**, 17554-17561

Todt, J.C., Rocque, W.J. & McGroarty, E.J. (1992) Biochemistry **31**, 10471-10478

Toyoshima, C., Nakasako, M., Nomura, H. & Ogawa, H. (2000) Nature **405**, 647-655

Van Gelder, P., Saint, N., Phale, P.S., Eppens, E.F., Prilipov, A., Van Boxtel, R., Rosenbusch, J.P. & Tomassen, J. (1997) J.Mol.Biol. **269**, 468-472

Van Voorst, F. & de Kruijff, B. (2000) Biochem.J. **347**, 601-612

Vogel, H. & Jahnig, F. (1986) J.Mol.Biol. **190**, 191-199

von Heijne, G. (1996) Prog.Biophys.molec.Biol. **66**, 113-139

Webb, R.J., East, J.M., Sharma, R.P. & Lee, A.G. (1998) Biochemistry **37**, 673-679

Weiss, M.S., Abele, U., Weckesser, J., Welte, W., Schiltz, E. & Schulz, G.E. (1991) Science **354**, 1627-1630

Weiss, M.S., Kreusch, A., Schiltz, G., Nestel, U., Welte, W., Weckesser, J. & Schulz, G.E. (1991) FEBS **280**, 379-382

Weiss, M.S. & Schulz, G.E. (1992) J.Mol.Biol. **227**, 493-509

Weiss, M.S., Wacker, T., Weckesser, J., Welte, W. & Schulz, G.E. (1990) FEBS **267**, 268-272

White, S.H. & Wimley, W.C. (1998) Biochim.Biophys.Acta **1376**, 339-352

White, S.H. & Wimley, W.C. (1999) Ann.Rev.Biophys.Biomol.Struct. **28**, 319-365

Yamade, H. & Mizushima, S. (1980) Eur.J.Biochem. **103**, 209-218

Yanagita, Y. & Kagawa, Y. (1986) Techniques for the Analysis of Membrane Proteins (Ragan, C.I. and Cherry, R.J., eds) Solubilisation and Purification of Membrane Proteins pp. 61-76, Chapman and Hall, London, New York

Yau, W.M., Wimley, W.C., Gawrisch, K. & White, S.H. (1998) Biochemistry **37**, 14713-14718